CONFIDENTIAL

NASA TECHNICAL MEMORANDUM

NASA TM X-2929

NASA TM X-2929

STABILITY AND CONTROL CHARACTERISTICS, INCLUDING AILERON HINGE MOMENTS, OF A MODEL OF A SUPERCRITICAL-WING RESEARCH AIRPLANE

by Richard J. Re

Langley Research Center
Hampton, Va. 23665

NATIONAL AERONAUTICS AND SPACE ADMINISTRATION • WASHINGTON, D. C. • MAY 1974

CONFIDENTIAL

[redacted]

1. Report No. NASA TM X-2929	2. Government Accession No.	3. Recipient's Catalog No.

4. Title and Subtitle

STABILITY AND CONTROL CHARACTERISTICS, INCLUDING AILERON HINGE MOMENTS, OF A MODEL OF A SUPERCRITICAL-WING RESEARCH AIRPLANE

5. Report Date: April 1974

6. Performing Organization Code:

7. Author(s)

Richard J. Re

8. Performing Organization Report No.: L-9196

9. Performing Organization Name and Address

NASA Langley Research Center
Hampton, Va. 23665

10. Work Unit No.: 766-73-60-04

11. Contract or Grant No.:

12. Sponsoring Agency Name and Address

National Aeronautics and Space Administration
Washington, D.C. 20546

13. Type of Report and Period Covered: Technical Memorandum

14. Sponsoring Agency Code:

15. Supplementary Notes

16. Abstract

Tests were made in the Langley 16-foot transonic tunnel to determine the longitudinal and lateral stability and control characteristics and aileron hinge moments of a 0.087-scale model of a supercritical-wing research airplane. Mach number was varied from 0.90 to 1.30 at a Reynolds number of approximately 2.4×10^6; angle of attack was varied from -8° to 14°; and angle of sideslip was set at about -5.5°, 0°, and 5.5°. Aileron hinge moments were obtained at deflection angles of -15° to 15°. Aileron, horizontal-tail, and rudder effectiveness parameters were determined.

17. Key Words (Suggested by Author(s))

Aileron
Hinge moments
Supercritical-wing airplane
Stability and control

21. No. of Pages: 130

22. Price:

STABILITY AND CONTROL CHARACTERISTICS, INCLUDING AILERON HINGE MOMENTS, OF A MODEL OF A SUPERCRITICAL-WING RESEARCH AIRPLANE*

By Richard J. Re
Langley Research Center

SUMMARY

An investigation has been made in the Langley 16-foot transonic tunnel to determine the longitudinal and lateral stability and control characteristics and aileron hinge moments of a 0.087-scale model of a supercritical-wing research airplane. Mach number was varied from 0.90 to 1.30 at a Reynolds number of approximately 2.4×10^6; angle of attack was varied from -8° to 14°; and angle of sideslip was set at about -5.5°, 0°, and 5.5°. Aileron hinge moments were obtained at deflection angles of -15° to 15°. Aileron, horizontal-tail, and rudder effectiveness parameters were determined.

The model was longitudinally stable up to lift coefficients about twice that required at cruise conditions, was directionally stable, and had positive effective dihedral. The model had positive rudder effectiveness with only small changes due to angle of attack. The aileron hinge-moment parameters (rate of change of hinge-moment coefficient with angle of attack or aileron deflection angle) were generally negative over the range of test variables and the ailerons produced positive roll effectiveness.

INTRODUCTION

The development of an airfoil, known as the NASA supercritical airfoil (refs. 1 to 4), has made it possible to increase substantially the drag-divergence Mach number of subsonic aircraft configurations. This increase is achieved by delaying shock-induced boundary-layer separation through proper contouring of the airfoil section to limit the shock strength on the upper surface.

In the course of development of an aircraft having a supercritical wing, it was required to verify the concept with a program of wind-tunnel and flight tests. The configuration selected for the "proof of concept" employs a U.S. Navy fighter aircraft (TF-8A) as a test-bed vehicle with the original wing replaced by a sweptback supercritical wing

*Title, Unclassified.

designed for possible application to an advanced transport aircraft having a cruise Mach number close to 1.0.

As a part of the program to obtain wind-tunnel results on the test-bed airplane configuration, a 0.087-scale controls model was tested in the Langley 16-foot transonic tunnel. The investigation was conducted to determine the longitudinal and lateral stability and control characteristics of the model and aileron hinge moments (for structural design) to aid in the assessment of the flying and handling qualities of the full-scale research airplane.

Complete-model aerodynamic forces and moments and aileron hinge moments were generally obtained at Mach numbers from 0.9 to 1.3, at angles of attack in the range from -8° to 14°, and at angles of sideslip of about -5.5°, 0°, and 5.5°. The Reynolds number of the investigation was approximately 2.4×10^{6}. The longitudinal and lateral stability and control characteristics of the model with and without the ailerons deflected and with rudder deflections from -5° to 5° are presented. The results of other wind-tunnel investigations to obtain aerodynamic force data and wing pressure distributions for a basically similar configuration are presented in references 5 and 6, respectively. Preliminary flight-test data on the test-bed airplane are contained in reference 7.

SYMBOLS

Physical quantities in this report are given in the International System of Units. The model longitudinal aerodynamic characteristics are referred to the stability-axis system and the lateral aerodynamic characteristics are referred to the body-axis system. All aerodynamic coefficients are based on the geometry of the basic wing which does not include the leading-edge glove or trailing-edge extension. (See fig. 1.) Moments are taken about the quarter-chord point of the basic-wing mean geometric chord located at fuselage station 99.45 cm. Aileron hinge moments are measured about the 75-percent local chord line of the basic-wing panel. The coefficients and symbols used herein are defined as follows:

b	wing span
c	streamwise local chord of wing (includes leading-edge glove and trailing-edge extension)
$\bar{c}$	mean geometric chord
c_a	average chord of aileron segment

$C_{A,i}$ duct internal axial-force coefficient (total two ducts), $\frac{\text{Internal axial force}}{qS}$

C_D drag coefficient (corrected for fuselage base pressure and duct internal flow), $\frac{\text{Drag}}{qS}$

$C_{D_{\delta_a}}$ effect of differential aileron deflection on drag coefficient, $\frac{\partial C_D}{\partial \delta_a}$, per deg

$C_{D_{\delta_L}}$ effect of deflection of aileron segments on left wing on drag coefficient, $\frac{\partial C_D}{\partial \delta_L}$, per deg

C_h aileron hinge-moment coefficient (positive for down load on aileron), $\frac{\text{Hinge moment}}{qS_a c_a}$

C_{h_α} effect of angle of attack on aileron hinge-moment coefficient, $\frac{\partial C_h}{\partial \alpha}$, per deg

$C_{h_{\delta_L}}$ effect of left aileron deflection on hinge-moment coefficient, $\frac{\partial C_h}{\partial \delta_L}$, per deg

C_L lift coefficient, $\frac{\text{Lift}}{qS}$

C_{L_α} slope of lift curve (measured in angle-of-attack range from 0° to 4°), per deg

$C_{L_{\delta_a}}$ effect of differential aileron deflection on lift coefficient, $\frac{\partial C_L}{\partial \delta_a}$, per deg

$C_{L_{\delta_L}}$ effect of deflection of aileron segments on left wing on lift coefficient, $\frac{\partial C_L}{\partial \delta_L}$, per deg

C_l rolling-moment coefficient, $\frac{\text{Rolling moment}}{qSb}$

C_{l_β} effective dihedral parameter, $\frac{\Delta C_l}{\Delta \beta}$ (from pitch tests at fixed sideslip angles), per deg

$C_{l_{\delta_a}}$ aileron effectiveness parameter, $\frac{\partial C_l}{\partial \delta_a}$, per deg

$C_{l_{\delta_L}}$ effect of deflection of aileron segments on left wing on rolling-moment coefficient, $\frac{\partial C_l}{\partial \delta_L}$, per deg

$C_{l_{\delta_r}}$ effect of rudder deflection on rolling-moment coefficient, $\frac{\Delta C_l}{\Delta \delta_r}$ (from pitch tests with $\delta_r = 0^o$ and $\pm 5^o$), per deg

C_m pitching-moment coefficient, $\frac{\text{Pitching moment}}{qS\bar{c}_w}$

$C_{m_{C_L}}$ longitudinal stability derivative, $\frac{\partial C_m}{\partial C_L}$ (measured in angle-of-attack range from 0^o to 4^o)

$C_{m,o}$ pitching-moment coefficient at $C_L = 0$

$C_{m_{\delta_h}}$ horizontal-tail effectiveness parameter, $\frac{\Delta C_m}{\Delta \delta_h}$, per deg

$C_{m_{\delta_a}}$ effect of differential aileron deflection on pitching-moment coefficient, $\frac{\partial C_m}{\partial \delta_a}$, per deg

$C_{m_{\delta_L}}$ effect of deflection of aileron segments on left wing on pitching-moment coefficient, $\frac{\partial C_m}{\partial \delta_L}$, per deg

C_n yawing-moment coefficient, $\frac{\text{Yawing moment}}{qSb}$

C_{n_β} directional-stability parameter, $\frac{\Delta C_n}{\Delta \beta}$ (from pitch tests at fixed sideslip angles), per deg

$C_{n_{\delta_a}}$ effect of differential aileron deflection on yawing-moment coefficient, $\frac{\partial C_n}{\partial \delta_a}$, per deg

$C_{n_{\delta_L}}$ effect of deflection of aileron segments on left wing on yawing-moment coefficient, $\frac{\partial C_n}{\partial \delta_L}$, per deg

$C_{n_{\delta_r}}$ rudder effectiveness parameter, $\frac{\Delta C_n}{\Delta \delta_r}$ (from pitch tests with $\delta_r = 0^o$ and $\pm 5^o$), per deg

C_Y side-force coefficient, $\frac{\text{Side force}}{qS}$

C_{Y_β} side-force parameter, $\frac{\Delta C_Y}{\Delta \beta}$ (from pitch tests at fixed sideslip angles), per deg

$C_{Y_{\delta_a}}$ effect of differential aileron deflection on side-force coefficient, $\frac{\partial C_Y}{\partial \delta_a}$, per deg

$C_{Y_{\delta_L}}$ effect of deflection of aileron segments on left wing on side-force coefficient, $\frac{\partial C_Y}{\partial \delta_L}$, per deg

$C_{Y_{\delta_r}}$ effect of rudder deflection on side-force coefficient, $\frac{\Delta C_Y}{\Delta \delta_r}$ (from pitch tests with $\delta_r = 0^o$ and $\pm 5^o$), per deg

$C_{p,b}$ fuselage base-pressure coefficient, $\frac{p_b - p}{q}$

M free-stream Mach number

p free-stream static pressure

p_b static pressure at fuselage base

q free-stream dynamic pressure

R free-stream Reynolds number per meter

S planform area of basic wing panels (including fuselage intercept)

S_a planform area of aileron segment

T_t test-section stagnation temperature, K

α angle of attack relative to fuselage reference line, deg

β angle of sideslip, deg

δ_a total included angle between left and right wing ailerons for differential (downward and upward) deflections, deg. δ_a is the sum of equal left (positive downward) and right (positive upward) aileron deflection angles. (In general, only the left wing aileron was deflected; however, the effects of differential deflection were derived from the aerodynamic increments obtained from downward and upward aileron deflections on the left wing.)

δ_h horizontal-tail incidence angle referred to fuselage reference line (positive trailing edge down), deg

δ_L left aileron deflection angle measured in plane perpendicular to hinge line (positive trailing edge down), deg

δ_r rudder deflection angle measured in plane perpendicular to hinge line (positive trailing edge left), deg

Subscripts:

h horizontal tail

v vertical tail

w wing

MODEL DESCRIPTION

The geometry of the 0.087-scale model is presented in figure 1 and a photograph showing the model mounted in the test section of the Langley 16-foot transonic tunnel is presented in figure 2. The variation in model cross-sectional area (including inlet capture area) with fuselage station is shown in figure 3.

The wing which was made of aluminum was mounted at a root incidence angle of 1.5° and incorporated about 5° of twist (washout) between the root and tip chords. The basic wing panel (dashed lines in fig. 1) had an aspect ratio of 6.78, a taper ratio of 0.364, and 42.24° of sweepback at the quarter-chord line. The airfoil ordinates for the wing at the development stage of this investigation are not available; however, the airfoil ordinates of a steel version of this wing are presented in table II of reference 5. The present wing had cutouts from the 75-percent-chord line to the trailing edge to allow for attachment of ailerons at various deflection angles. (See fig. 1.) The aileron on the left wing

was split into two segments, each of which was mounted with brackets strain gaged for measurement of hinge moments. The inboard aileron segment (which extended from 0.4b/2 to 0.6b/2) had an area of 48.34 cm^2 and an average chord of 4.229 cm. The outboard aileron segment (which extended from 0.6b/2 to 0.8b/2) had an area of 39.46 cm^2 and an average chord of 3.452 cm. The aileron on the right wing was not split into two segments and its mounting brackets were not instrumented. The gaps between the aileron segments and wing at the hinge line and at the ends of the aileron segments were filled with a silicone rubber sealant. After the silicone sealant had cured and was faired smooth with the wing and aileron surface, the adhesive bond between the wing and aileron was broken by cutting the sealant with a fine wire.

The model had the same fairing at the wing-fuselage leading-edge juncture, the same wing trailing-edge extension, the same area rule fairing on top of the fuselage, and the same horizontal and vertical tails as the model of reference 5. The present configuration differed from that of reference 5 in having a fairing on the fuselage at the base of the vertical tail to represent a housing for a drogue parachute (figs. 1 and 4) and smaller exits for the flowthrough ducts. The single inlet had a capture area of 28.39 cm^2 and was split internally into two ducts to pass along each side of the force balance and sting. The ducts changed in shape from circular about halfway along the model length to "D" shaped at the fuselage base. The duct exits had a total area of 21.16 cm^2 and were smaller than those of reference 5 to increase lateral clearance between the sides of the ducts and the sting for lateral stability testing.

WIND TUNNEL

The investigation was conducted in the Langley 16-foot transonic tunnel which is a single-return atmospheric wind tunnel with continuous air exchange. The test section is octagonal in shape with 4.724 meters between opposite walls (equivalent to the area of a circle 4.85 meters in diameter) and has axial slots at the wall vertices. The total width of the eight slots in the vicinity of the model is approximately 3.7 percent of the test-section perimeter. The test-section airspeed is continuously variable up to a Mach number of 1.3 and plenum suction is utilized to attain Mach numbers of 1.1 and above. At Mach numbers from 1.2 to 1.3, test-section wall-divergence angle is adjusted (based on calibration data) as a function of airstream dewpoint temperature to eliminate longitudinal static-pressure gradients that would occur on the center line because of condensation of atmospheric moisture. The ranges of stagnation temperatures and test-section Reynolds number per meter for this investigation are shown in figure 5.

The tunnel-sting support system pivots in the vertical plane in such a manner that the model remains on or near the test-section center line through the angle-of-attack

range. The model can be set at a given angle of sideslip by insertion of an angled coupling between the sting and strut support system.

TESTS

Boundary-Layer Transition

All tests were conducted with boundary-layer transition fixed on the model surfaces. Boundary-layer trips were placed on the wing as indicated in figure 6 and on the horizontal and vertical tails at the 5-percent local streamwise chord on both surfaces (No. 150 carborundum grains). Boundary-layer trips (No. 120 carborundum grains) on the fuselage were placed 2.54 cm aft of the nose, on the outer surface of the inlet 2.54 cm rearward of the lip, and on the inner surface of the inlet 1.27 cm rearward of the lip. All transition strips were 0.127 cm wide.

The boundary-layer transition strip on the lower surface of the wing was located according to the technique of references 8 and 9 to simulate full-scale Reynolds number boundary-layer characteristics at the wing trailing edge. However, the upper surface strip was located further forward than would be indicated by references 8 and 9 to prevent the occurrence of unnatural laminar boundary-layer separation ahead of the transition strip. Such separation would not occur at full-scale Reynolds numbers since turbulent boundary-layer flow is usually established close to the wing leading edge. The procedures of reference 10 were used to locate the wing upper surface boundary-layer trip as well as to size all the boundary-layer trip heights.

Measurements

Model aerodynamic forces and moments were measured with a six-component strain-gage balance internally placed in the fuselage. Aileron hinge moments (left wing only) were measured by means of strain gages mounted on the aileron attachment brackets. The strain gages were calibrated "in place" after the aileron segments were mounted on the wing and after all model preparations for testing had been completed. The aileron on the left wing was split into two segments so that hinge moments on the inboard and outboard portions were measured separately. Pressures in the balance chamber, at the base of the fuselage, and in the plane of the duct exits were measured on strain-gaged differential pressure transducers.

Corrections and Accuracy

The axial-force measurements were adjusted to the condition of free-stream static pressure acting in the balance chamber and at the fuselage base (base area 37.254 cm^2).

Examples of the pressure conditions that existed at the fuselage base are presented in figure 7 as pressure coefficients. Axial force has also been adjusted for the internal force due to the flow through the ducts. Separate tests were made with pressure rakes mounted externally on the model at the base of the fuselage to survey the duct flow in the plane of the exit. The magnitude of the correction to axial-force coefficient for duct internal flow is illustrated in figure 8.

Model attitude was calculated from the known attitude of the support system and deflection characteristics under load of the sting-balance combination. Model angle of attack and sideslip were adjusted for tunnel flow angularity. No corrections have been made to the data for test-section wall interference effects or for local condensation effects that may have occurred in the model flow field.

The accuracy of the data based on instrument error and repeatability is estimated to be within the following limits:

	M = 0.90	M = 1.30
C_L	±0.010	±0.007
C_D (at low lift)	±0.0007	±0.0005
C_m	±0.005	±0.003
C_l	±0.0006	±0.0003
C_n	±0.0004	±0.0003
C_Y	±0.002	±0.002
C_h	±0.005	±0.005
$C_{p,b}$	±0.007	±0.005
M	±0.01	±0.01
α, deg	±0.1	±0.1
β, deg	±0.1	±0.1

PRESENTATION OF RESULTS

The purpose of deflecting the control surface on the left wing was to evaluate its effectiveness as a roll-producing device; that is, as an aileron. Therefore, the treatment of the data is from that point of view. However, there has been interest in such control surfaces as high-speed maneuver flaps and with that in mind the basic aerodynamic force and moment coefficients for the model with the aileron on the left wing deflected are also presented.

The results of this investigation are presented in the following figures:

DISCUSSION

Aerodynamic Characteristics With Ailerons Undeflected

Longitudinal aerodynamic characteristics.- The longitudinal aerodynamic characteristics of the model with the ailerons undeflected and with a horizontal-tail incidence of 0^o are presented in figure 9. At a Mach number of 0.90 an abrupt pitchup is indicated (fig. 9(c)) coincident with a break in the lift curve at an angle of attack of about 8^o (fig. 9(a)). However, the pitchup occurs at a lift coefficient which is about twice that required for level flight. Further tests of this configuration (ref. 11) indicate that pitchup is further delayed with an underwing leading-edge vortex generator.

The variation with Mach number of lift-curve slope (measured at low angles of attack) and of drag coefficient at a lift coefficient of 0.44 is shown in figure 15. The lift coefficient of 0.44 with a horizontal-tail incidence of -2.5^o represents a condition near trim for the full-scale airplane. The variation with Mach number of the horizontal-tail effectiveness parameter $C_{m_{\delta_h}}$ and the longitudinal stability parameter $C_{m_{C_L}}$ (measured at low lift coefficients) is shown in figure 16. The increase in longitudinal stability $\left(\text{larger negative values of } C_{m_{C_L}}\right)$ with increasing Mach number was accompanied by a positive increase in $C_{m,o}$ with increasing Mach number so that significant trim-drag penalties near cruise-lift coefficient would be small with $\delta_h = -2.5^o$. (See fig. 21(d).)

Lateral-directional aerodynamic characteristics.- The effect of sideslip angle on the variation with angle of attack of the model lateral aerodynamic coefficients with all control surfaces at 0^o deflection is shown in figure 10. The variation of the lateral-directional stability derivatives with Mach number (fig. 17) for four angles of attack

shows that the model was directionally stable (positive C_{n_β}) and had positive effective dihedral (negative C_{l_β}). The effect of variation of sideslip angle from -6° to 11° on the model aerodynamic coefficients at angles of attack of about 0.2° and 6.4° is shown in figures 11 and 12 for Mach numbers from 0.90 to 1.02.

The variation of the model lateral aerodynamic coefficients with angle of attack with the rudder deflected is shown in figure 13. The variation of the rudder effectiveness parameter $C_{n_{\delta_r}}$ with Mach number presented in figure 18 indicates the model had positive rudder effectiveness (negative $C_{n_{\delta_r}}$) with only small effects of angle of attack.

The effect of sideslip angle on the variation with angle of attack of the model lateral aerodynamic coefficients with the rudder deflected -5° is shown in figure 14. Comparison of the data of figure 14 with that of figure 10 ($\delta_r = 0°$) indicates no significant change in the lateral stability of the model due to rudder deflection.

Aerodynamic Characteristics With Ailerons Deflected

The longitudinal and lateral aerodynamic coefficients obtained as the model was pitched through the angle-of-attack range with the aileron on the left wing deflected and with a horizontal-tail incidence of -2.5° are presented in figures 19 to 24. The variation of the aerodynamic effectiveness parameters with Mach number for aileron deflections on the left wing is shown in figure 25(a) for downward aileron deflection and in figure 25(b) for upward aileron deflection. Aileron deflection produced positive roll effectiveness ($C_{l_{\delta_L}}$) throughout the angle-of-attack and Mach number ranges with upward deflection producing about twice the effectiveness as downward deflection at Mach numbers from 0.90 to 1.02. The lift effectiveness of the aileron was positive; and, as would be expected from the roll effectiveness, upward deflection produced about twice the lift effectiveness as downward deflection at Mach numbers from 0.90 to 1.02.

All the aerodynamic characteristics discussed thus far concern aileron deflections on the left wing only. However, since upward and downward deflections were investigated, aerodynamic coefficient increments were available to determine effectiveness parameters for differential aileron deflection (upward on one wing and downward an equal amount on the opposite wing). The effectiveness parameters for differential aileron deflection δ_a (derived from the data of figs. 19 to 25) are shown in figure 26. This treatment of the data carries the reasonable assumption that deflection of the aileron on the left wing does not significantly alter the loading on the right wing. The results of figure 26 indicate that with differential aileron deflection the model had positive roll effectiveness over the Mach number range and did not encounter adverse yaw due to aileron deflection. Flight-test data on the airplane (ref. 7) which differed in some configuration details from the model tested herein, however, did indicate a small amount of adverse yaw at Mach numbers from 0.90 to 1.00.

The ailerons were differentially deflected -20° (left wing aileron -10° and right wing aileron -10°) for one series of tests with the model in sideslip to determine the effect on the lateral aerodynamic characteristics over the angle-of-attack and Mach number ranges. (See fig. 27.) Comparison of the lateral-directional stability derivatives $\left(C_{l_\beta}, C_{n_\beta}, \text{and } C_{Y_\beta}\right)$ presented in figure 28 for four angles of attack with the data of figure 17 (ailerons undeflected and $\delta_h = 0^\circ$) indicates that differential aileron deflection had little effect on lateral-directional stability.

Aileron Hinge-Moment Characteristics

Inboard aileron.- For the inboard aileron the variation of hinge-moment coefficient with angle of attack (fig. 29) increased with increasing Mach number in the angle-of-attack range from 0° to 10° and became nearly linear at the higher Mach numbers. At a Mach number of 0.90, nonlinearity in the variation of hinge-moment coefficient with angle of attack caused a change in sign of slope of the curve in the angle-of-attack range 2° to 6°. (See fig. 29(a).) The hinge-moment parameter C_{h_α} (fig. 33) was negative over the Mach number range for angles of attack -4°, 0°, and 8°. At an angle of attack of 4°, C_{h_α} was also negative except at a Mach number of 0.90 as indicated previously.

The variation of inboard aileron hinge-moment coefficient with deflection angle was negative, as can be seen in figure 31 (cross plots of the data of fig. 29), except at angles of attack from -4° to -8°. The hinge-moment parameter $C_{h_{\delta_L}}$ (fig. 32) measured at $\delta_L = -10^\circ, 0^\circ$, and 10° was negative over the Mach number range for angles of attack of -4°, 0°, 4°, and 8° and in the range from -0.002 to -0.015 for the range of variables.

Outboard aileron.- The hinge-moment coefficient variation with angle of attack for the outboard aileron (fig. 30) was similar to that of the inboard aileron. However, at Mach numbers from 0.90 to 1.02, the nonlinearity in the curves was greater, especially at negative and low positive angles of attack. The nonlinearity of the curves at a given Mach number decreased at positive angles of attack as aileron deflection angle was increased toward large positive values. At Mach numbers of 1.20 and 1.30, the variation of hinge-moment coefficient with angle of attack was nearly linear and in shape the curves closely resembled those of the inboard aileron. Comparison of the hinge-moment parameter C_{h_α} for the outboard aileron with that of the inboard aileron (fig. 33) shows similar trends over the Mach number range.

The variation of hinge-moment coefficient with deflection angle for the outboard aileron (fig. 31) was similar to that of the inboard aileron although in some cases the curves were more nonlinear at high positive deflection angles. The hinge-moment parameter $C_{h_{\delta_L}}$ (fig. 32) of the outboard aileron was in the range from 0.004 to -0.019 and reflected the nonlinearity cited for figure 31.

The similarity in the hinge-moment coefficient variation with angle of attack or deflection for the two aileron segments over the range of test parameters indicates that the flow quality on the rear part or section of the wing was good enough to insure that both the inboard and outboard aileron segments had satisfactory hinge-moment characteristics. The small negative or near-zero values of the hinge-moment parameters C_{h_α} and $C_{h_{\delta_L}}$ obtained are representative of those generally considered desirable for maintaining light control forces for aircraft handling purposes.

CONCLUSIONS

An investigation has been made to determine the longitudinal and lateral stability and control characteristics and the aileron hinge moments of a 0.087-scale model of a supercritical-wing research airplane. The model was tested at Mach numbers from 0.90 to 1.30, at angles of attack from -8° to 14°, and at angles of sideslip of about -5.5°, 0°, and 5.5°. Aileron hinge moments were obtained at deflection angles from -15° to 15°. The results include aileron, horizontal tail, and rudder effectiveness parameters. The following conclusions are indicated:

1. The model was longitudinally stable up to lift coefficients about twice that required at cruise conditions.

2. The model was directionally stable and had positive effective dihedral. Differential aileron deflection had no significant effect on lateral-directional stability.

3. The model exhibited positive rudder effectiveness over the Mach number range with only small changes due to angle of attack.

4. The aileron hinge-moment parameters (rate of change of hinge-moment coefficient with angle of attack or aileron deflection angle) were generally negative over the range of test variables.

5. The ailerons produced positive roll effectiveness throughout the angle-of-attack and Mach number ranges.

Langley Research Center,
National Aeronautics and Space Administration,
Hampton, Va., December 9, 1973.

REFERENCES

1. Whitcomb, Richard T.; and Clark, Larry R.: An Airfoil Shape for Efficient Flight at Supercritical Mach Numbers. NASA TM X-1109, 1965.

2. Whitcomb, Richard T.; and Blackwell, James A., Jr.: Status of Research on a Supercritical Wing. Conference on Aircraft Aerodynamics, NASA SP-124, 1966, pp. 367-381.

3. Harris, Charles D.: Wind-Tunnel Investigation of Effects of Trailing-Edge Geometry on a NASA Supercritical Airfoil Section. NASA TM X-2336, 1971.

4. Harris, Charles D.; and Blackwell, James A., Jr.: Wind-Tunnel Investigation of Effects of Rear Upper Surface Modification on an NASA Supercritical Airfoil. NASA TM X-2454, 1972.

5. Bartlett, Dennis W.; and Re, Richard J.: Wind-Tunnel Investigation of Basic Aerodynamic Characteristics of a Supercritical-Wing Research Airplane Configuration. NASA TM X-2470, 1972.

6. Harris, Charles D.: Wind-Tunnel Measurements of Aerodynamic Load Distribution on an NASA Supercritical-Wing Research Airplane Configuration. NASA TM X-2469, 1972.

7. Anon.: Supercritical Wing Technology – A Progress Report on Flight Evaluations. NASA SP-301, 1972.

8. Loving, Donald L.: Wind-Tunnel—Flight Correlation of Shock-Induced Separated Flow. NASA TN D-3580, 1966.

9. Blackwell, James A., Jr.: Preliminary Study of Effects of Reynolds Number and Boundary-Layer Transition Location on Shock-Induced Separation. NASA TN D-5003, 1969.

10. Braslow, Albert L.; and Knox, Eugene C.: Simplified Method for Determination of Critical Height of Distributed Roughness Particles for Boundary-Layer Transition at Mach Numbers From 0 to 5. NACA TN 4363, 1958.

11. Bartlett, Dennis W.; Harris, Charles D.; and Kelly, Thomas C.: Wind-Tunnel Development of Underwing Leading-Edge Vortex Generators on an NASA Supercritical-Wing Research Airplane Configuration. NASA TM X-2808, 1973.

Aileron geometry	Inboard segment	Outboard segment
Area, cm^2	48.34	39.46
Span, cm	11.43	11.43
Average chord, cm	4.229	3.452
Sweep at hinge line, deg	37.61	37.61

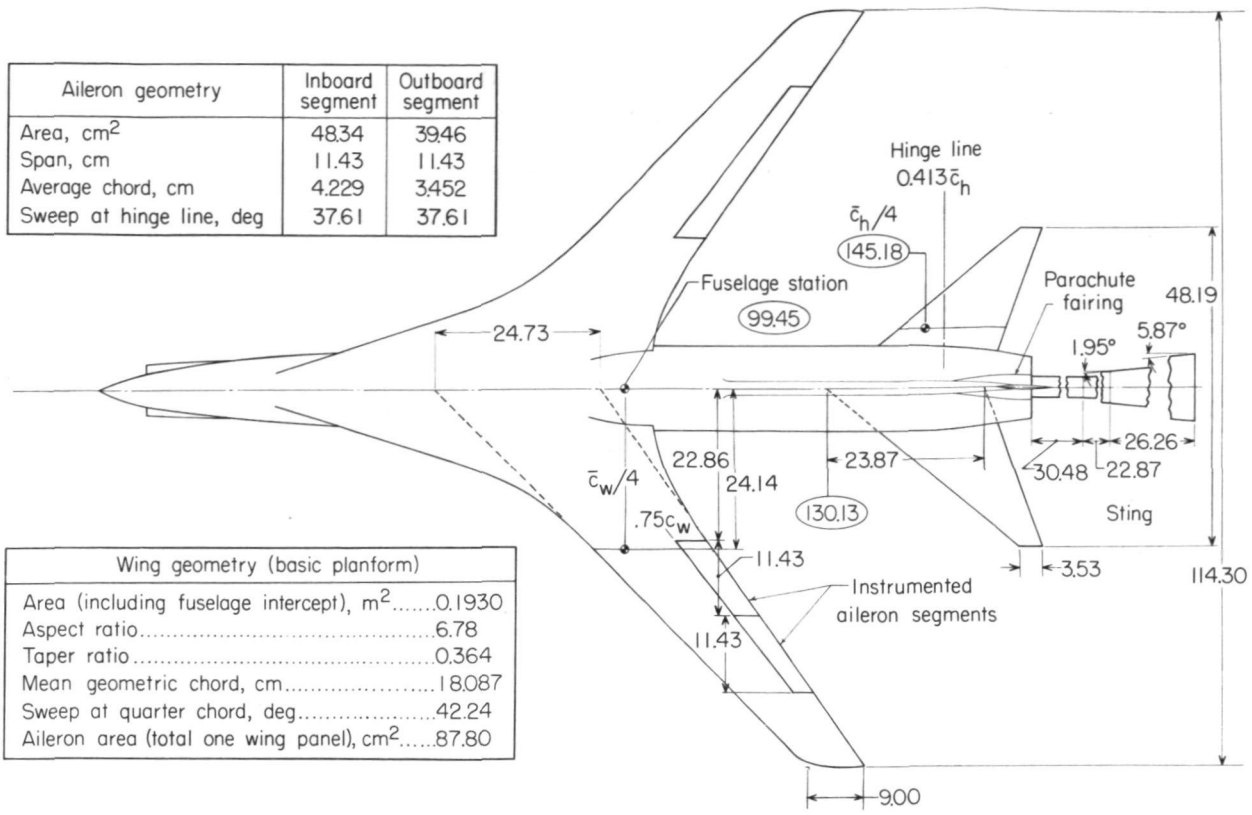

Wing geometry (basic planform)	
Area (including fuselage intercept), m^2	0.1930
Aspect ratio	6.78
Taper ratio	0.364
Mean geometric chord, cm	18.087
Sweep at quarter chord, deg	42.24
Aileron area (total one wing panel), cm^2	87.80

Vertical-tail geometry	
Area (including fuselage intercept), m^2	0.0766
Aspect ratio	1.50
Taper ratio	0.250
Mean geometric chord, cm	25.368
Sweep at quarter chord, deg	45.0
Airfoil section	
at W.L. 36.45 cm	Modified NACA 65A005.3
at tip	Modified NACA 65A004
Rudder area, cm^2	88.23

Horizontal-tail geometry	
Area (including fuselage intercept), m^2	0.0657
Aspect ratio	3.50
Taper ratio	0.148
Mean geometric chord, cm	16.220
Sweep at quarter chord, deg	45.0
Dihedral angle, deg	5.42
Airfoil section	
at span station 3.99 cm	NACA 65A006
at span station 23.66 cm	NACA 65A004

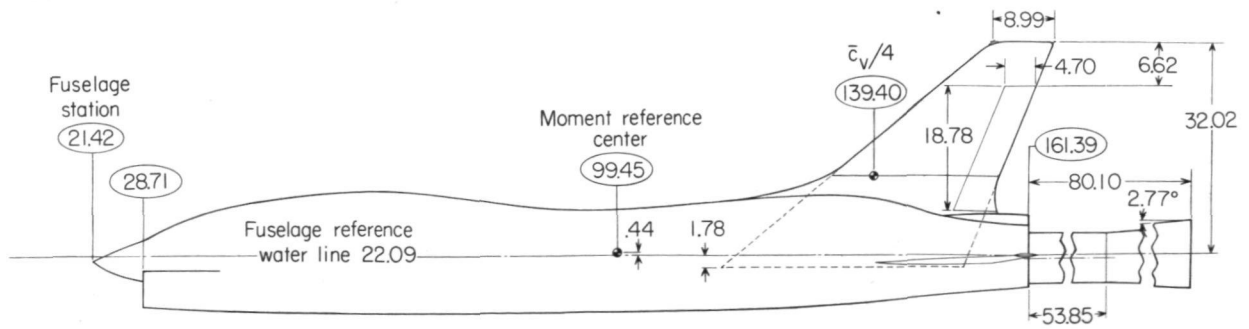

Figure 1.- Sketch of 0.087-scale model and support sting. All dimensions are in centimeters unless otherwise indicated.

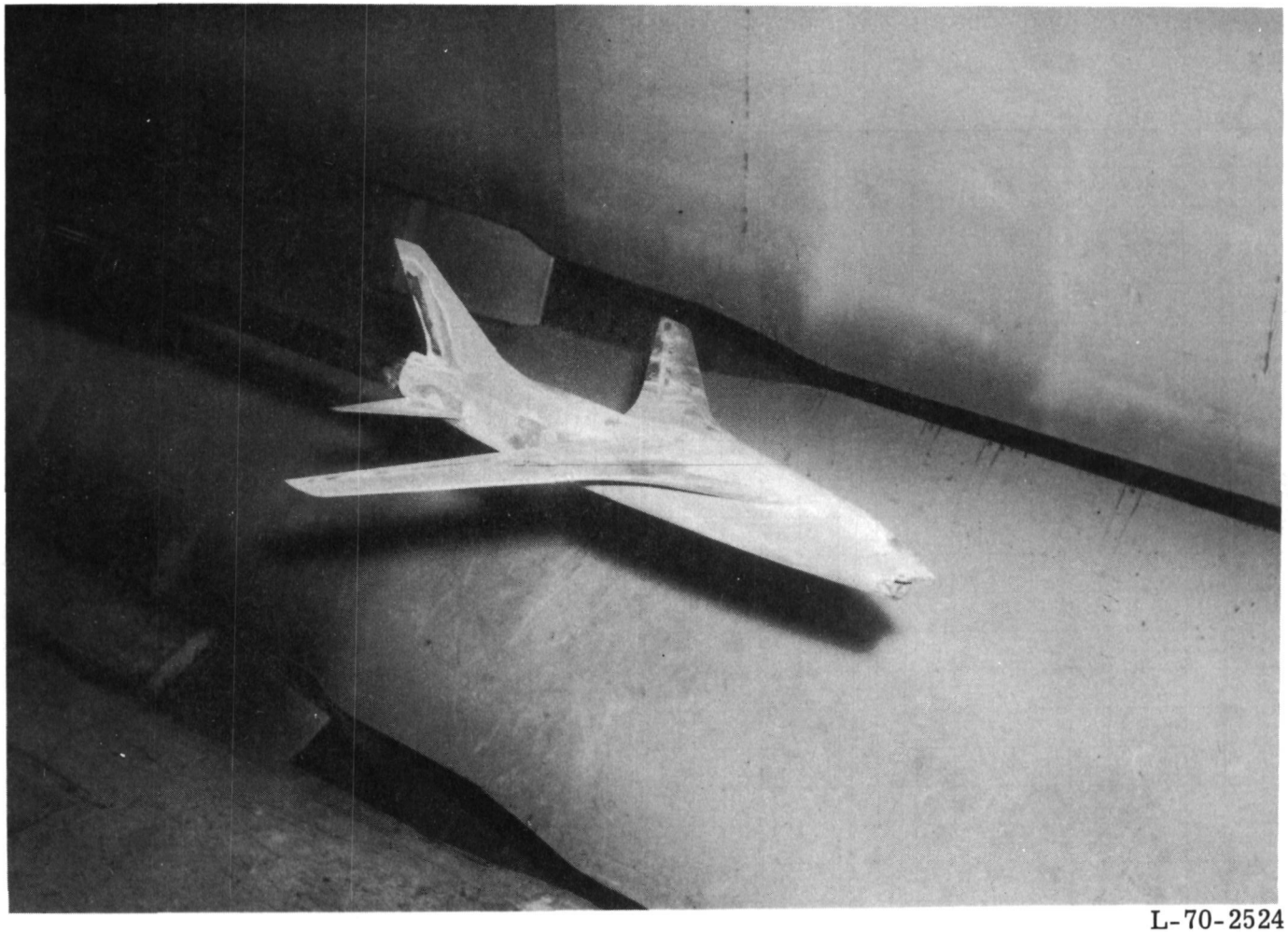

L-70-2524

Figure 2.- Photograph of 0.087-scale model in test section of Langley 16-foot transonic tunnel.

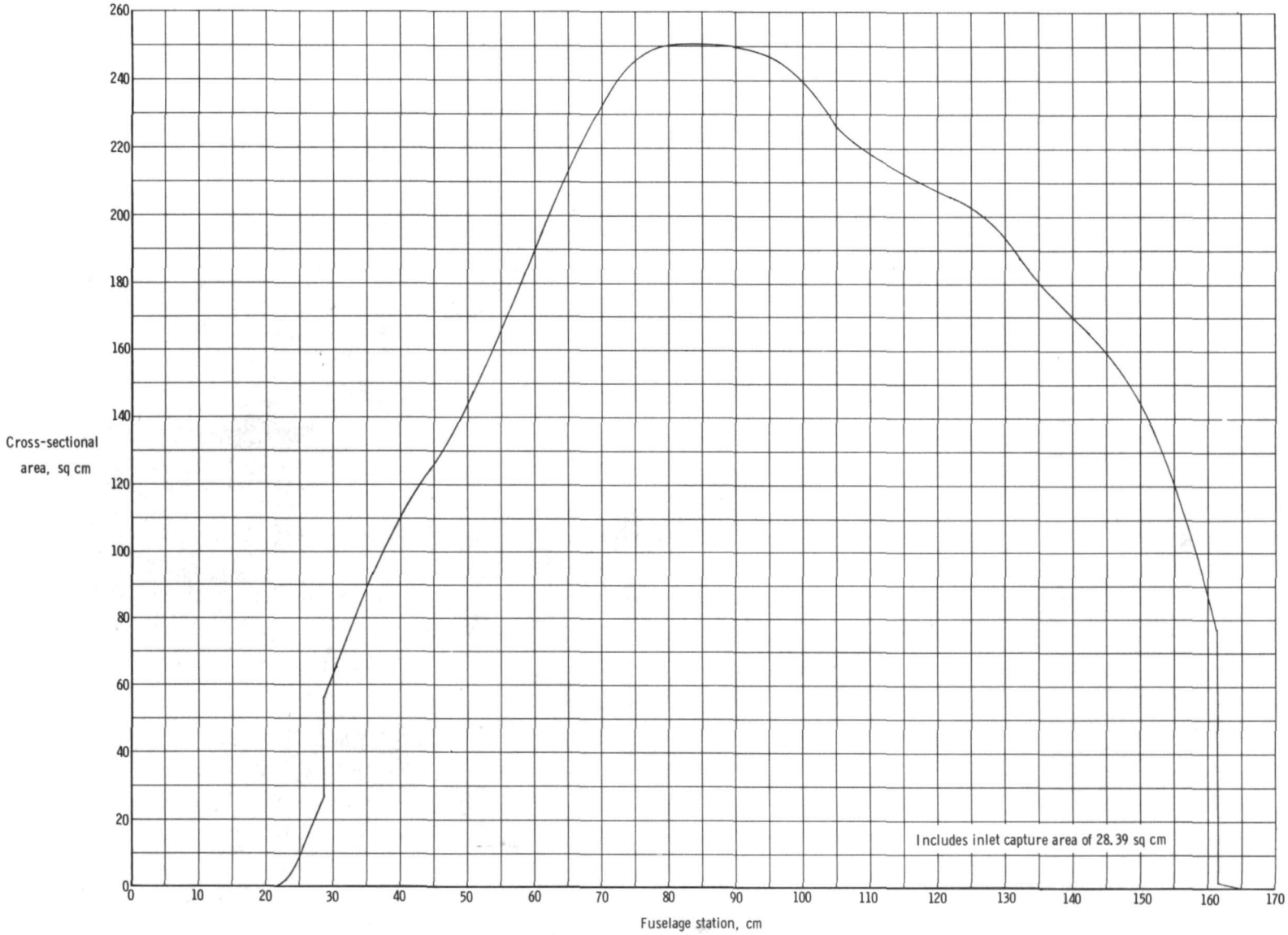

Figure 3.- Variation of model cross-sectional area (normal to fuselage reference line) with fuselage station.

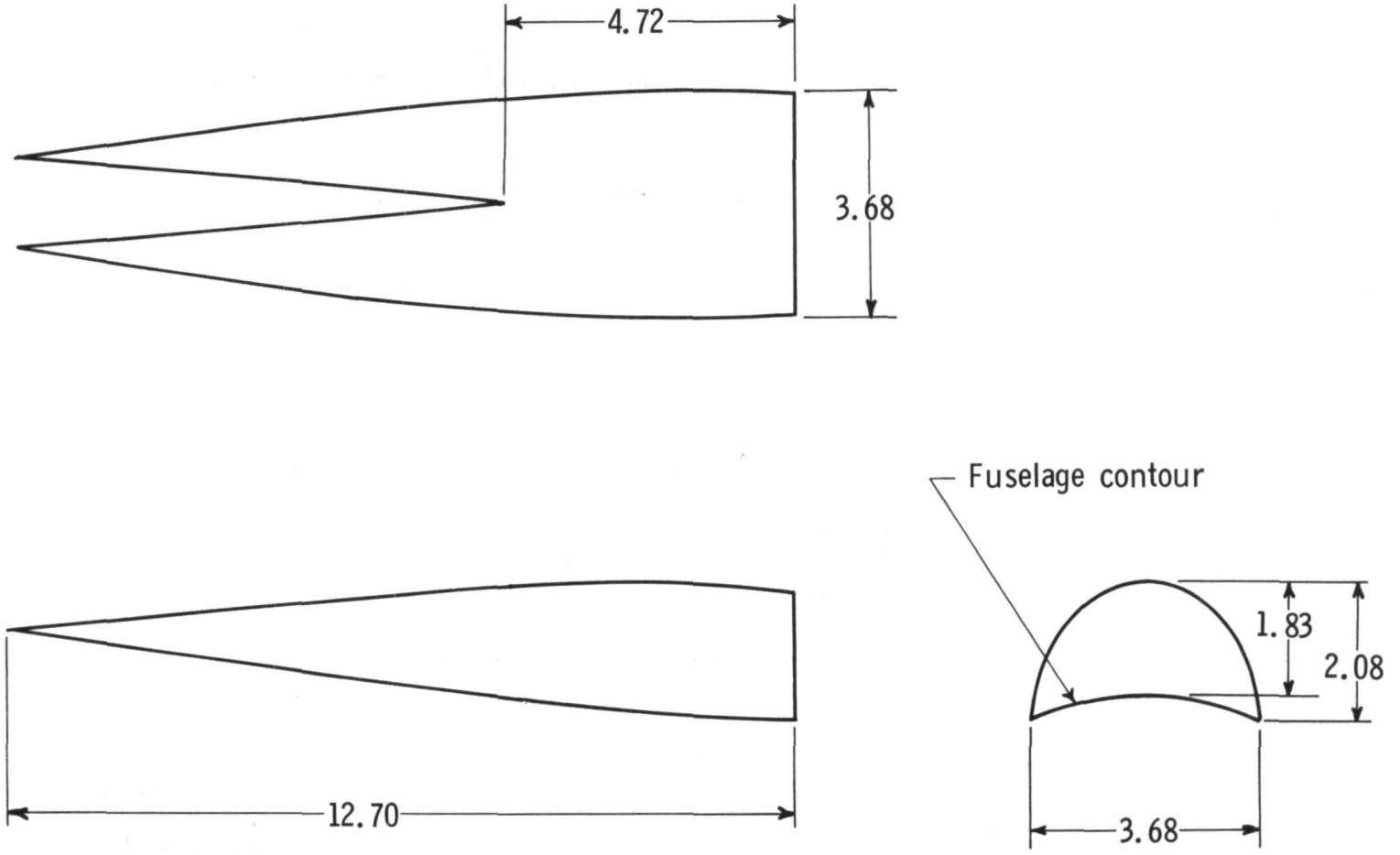

Figure 4.- Sketch of drogue parachute fairing mounted at base of vertical tail. All dimensions are in centimeters.

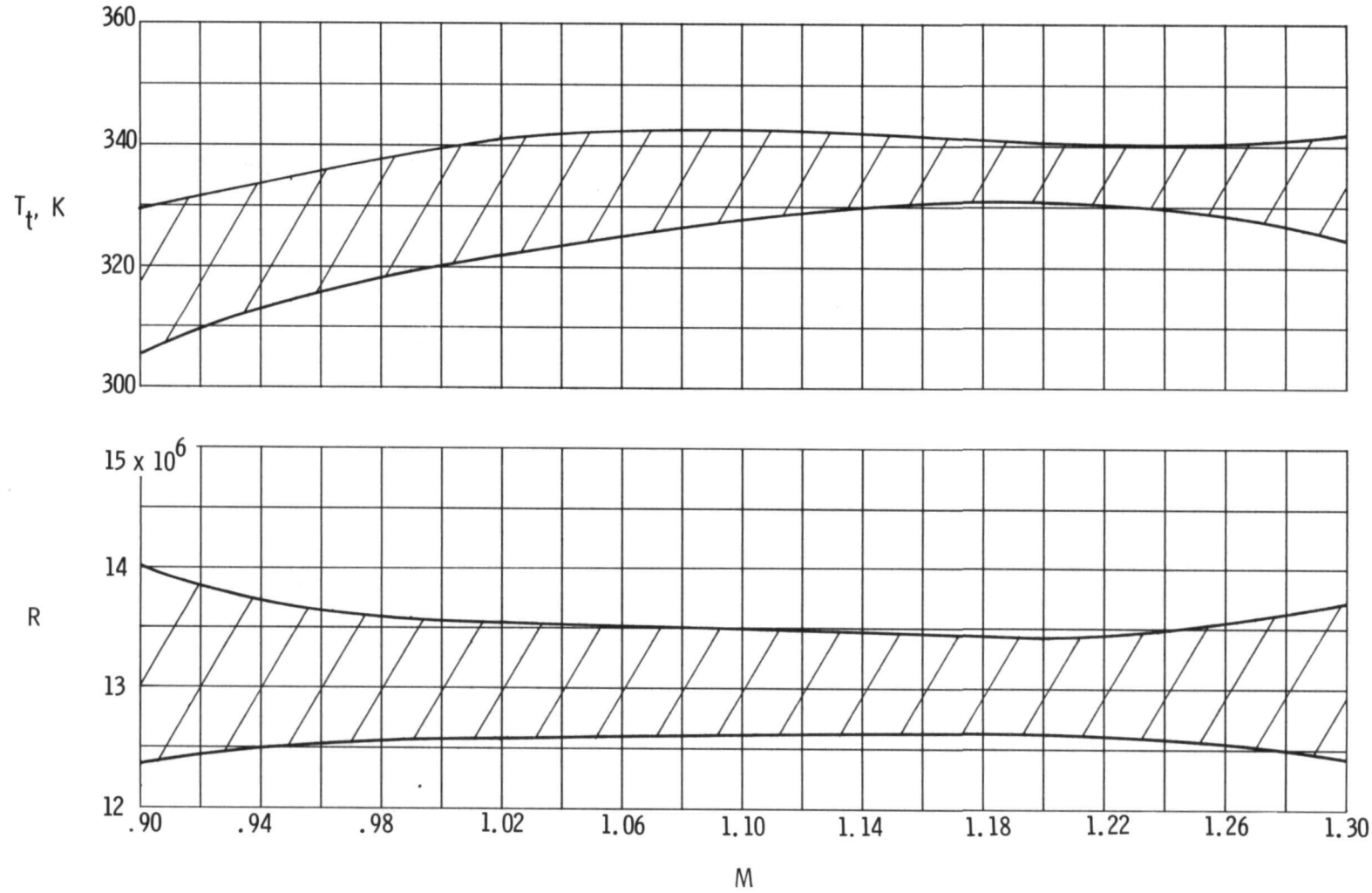

Figure 5.- Variation of test-section stagnation temperature and Reynolds number per meter with Mach number.

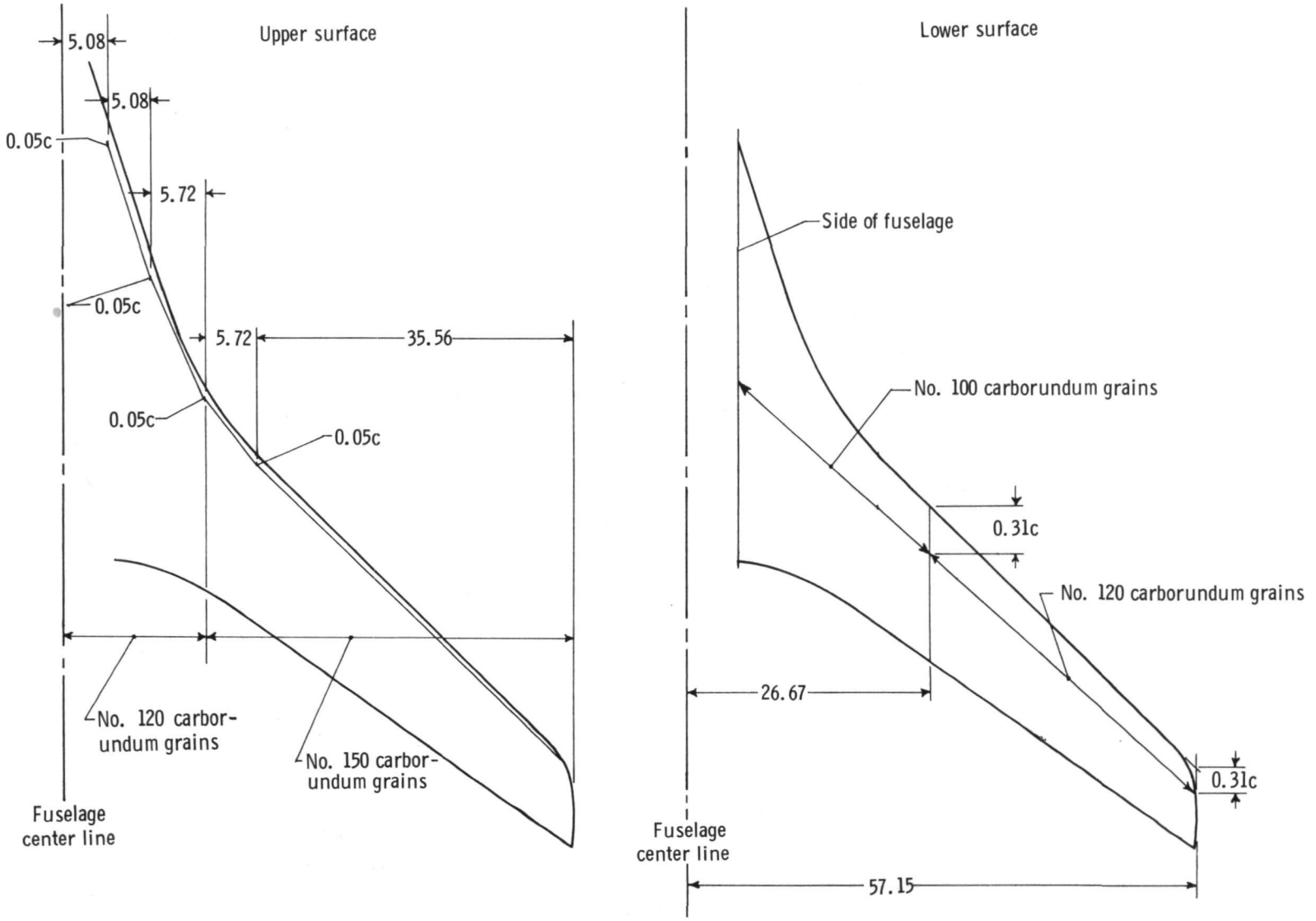

Figure 6.- Wing boundary-layer trip arrangement. All dimensions are in centimeters unless otherwise indicated.

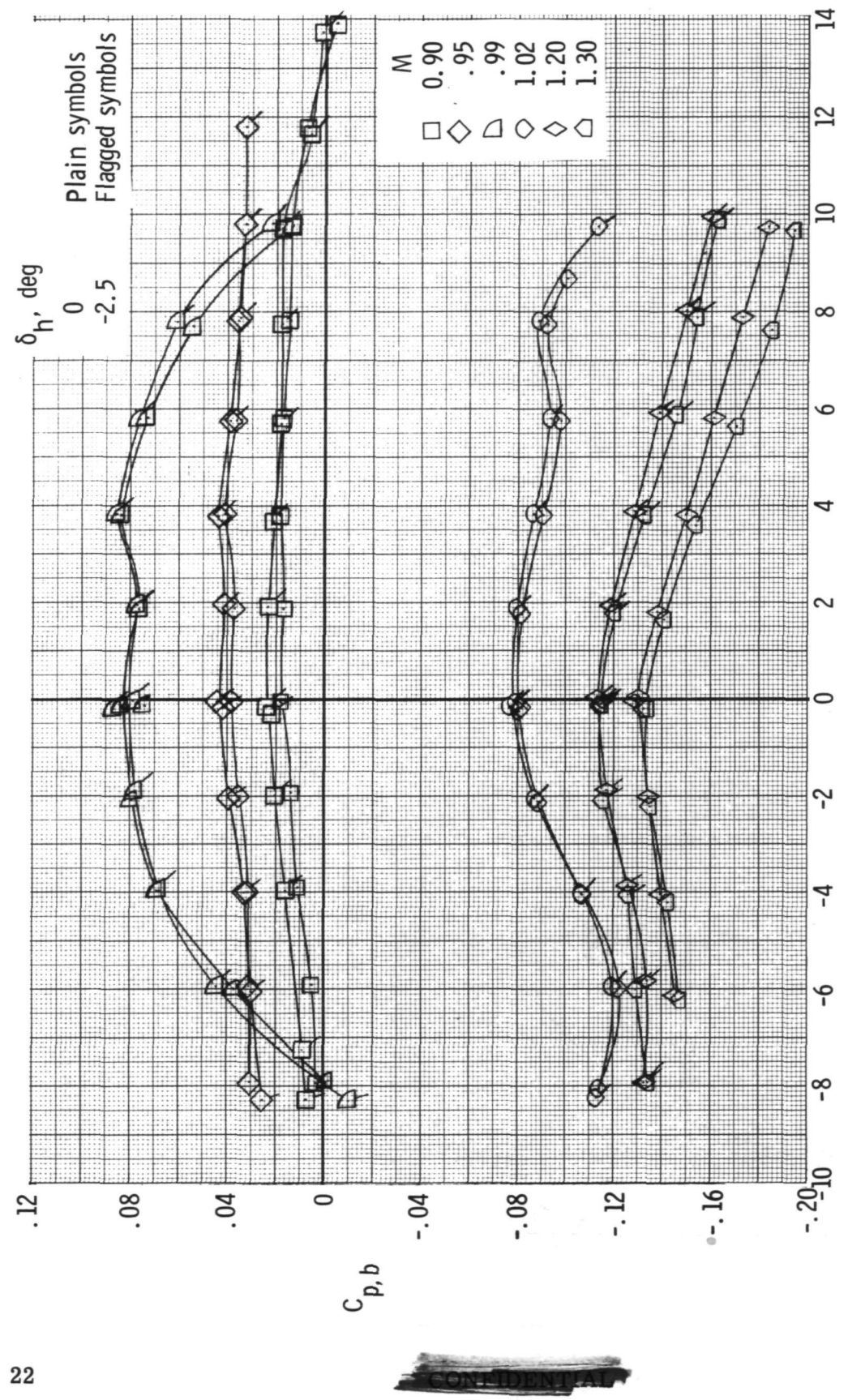

(a) Base-pressure coefficient against angle of attack for $\beta = 0^{o}$.

Figure 7.- Variation of model base-pressure coefficient with angle of attack and sideslip.

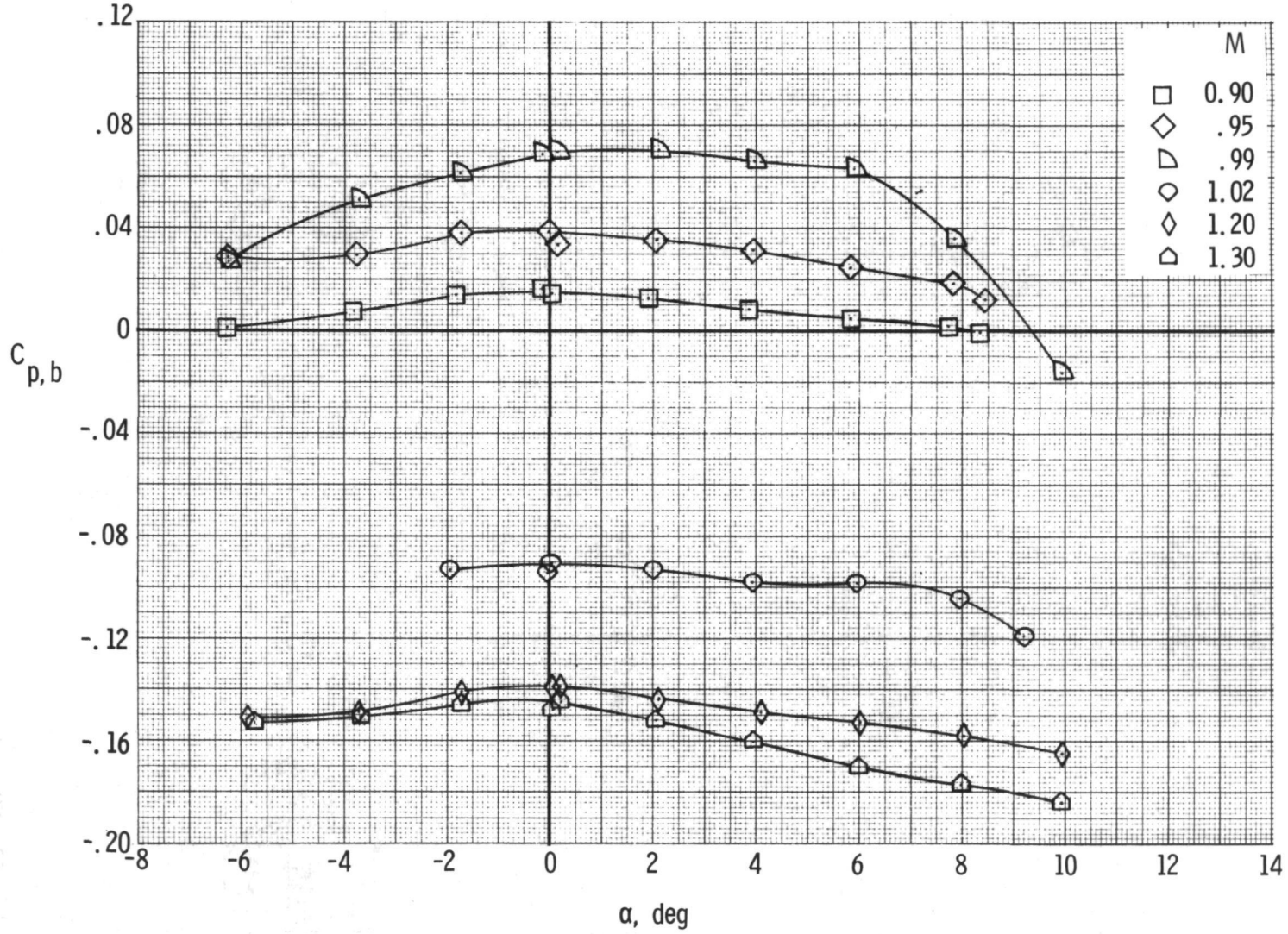

(b) Base-pressure coefficient against angle of attack for $\beta = -5.6^{o}$. $\delta_h = 0^{o}$.

Figure 7.- Continued.

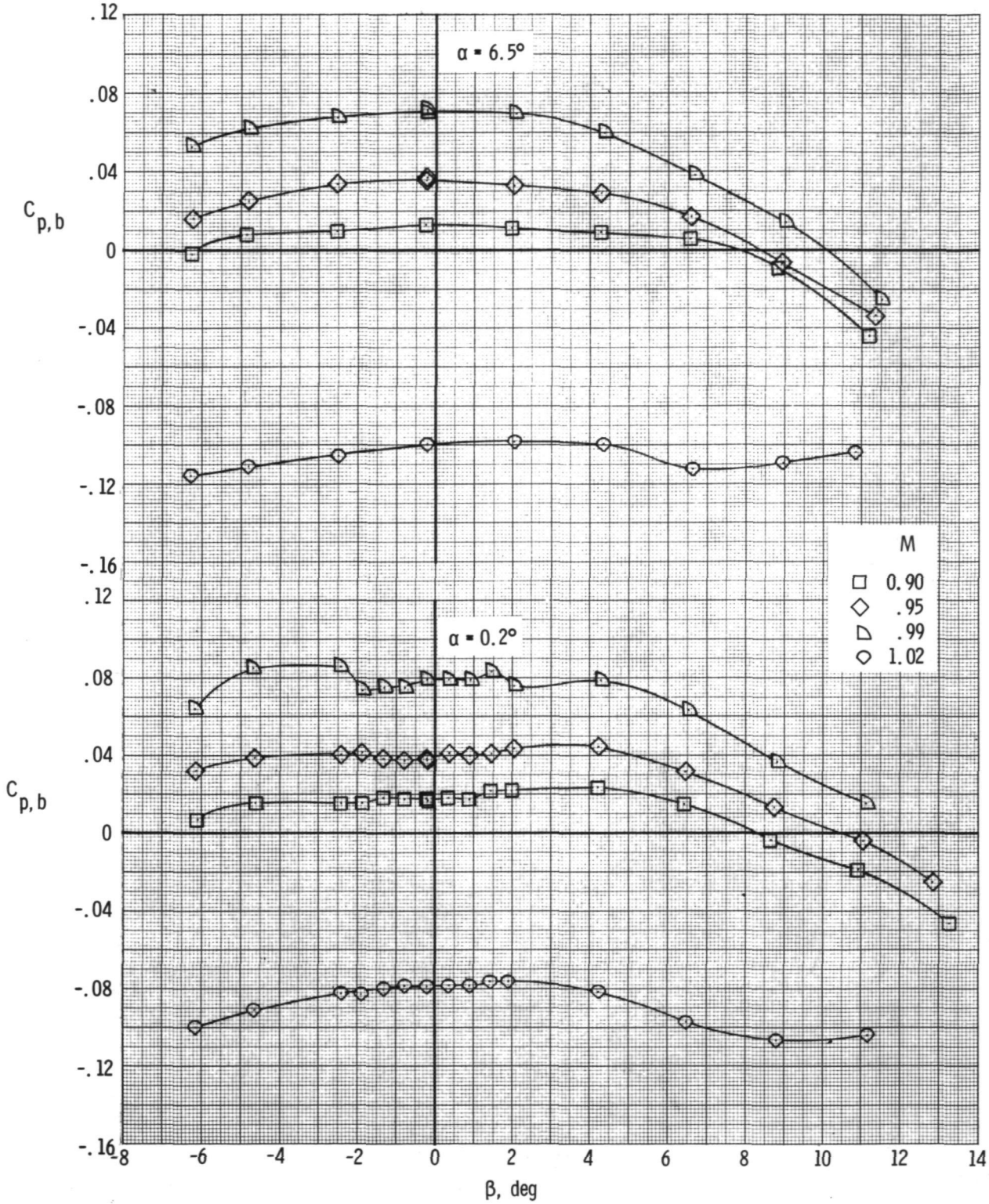

(c) Base-pressure coefficient against angle of sideslip. $\delta_h = 0^o$.

Figure 7.- Concluded.

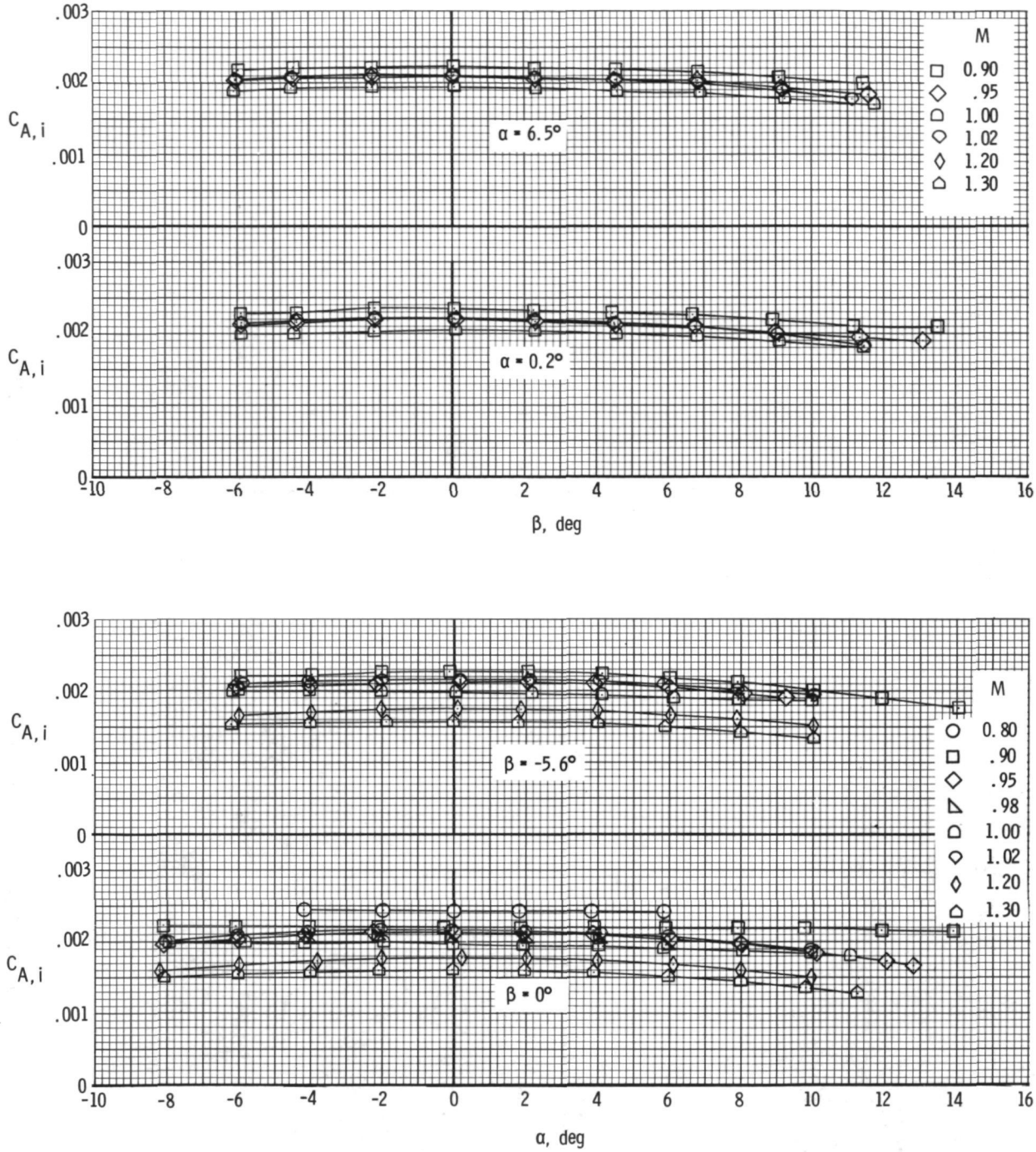

Figure 8.- Variation of internal axial-force coefficient (both ducts) with angles of attack and sideslip.

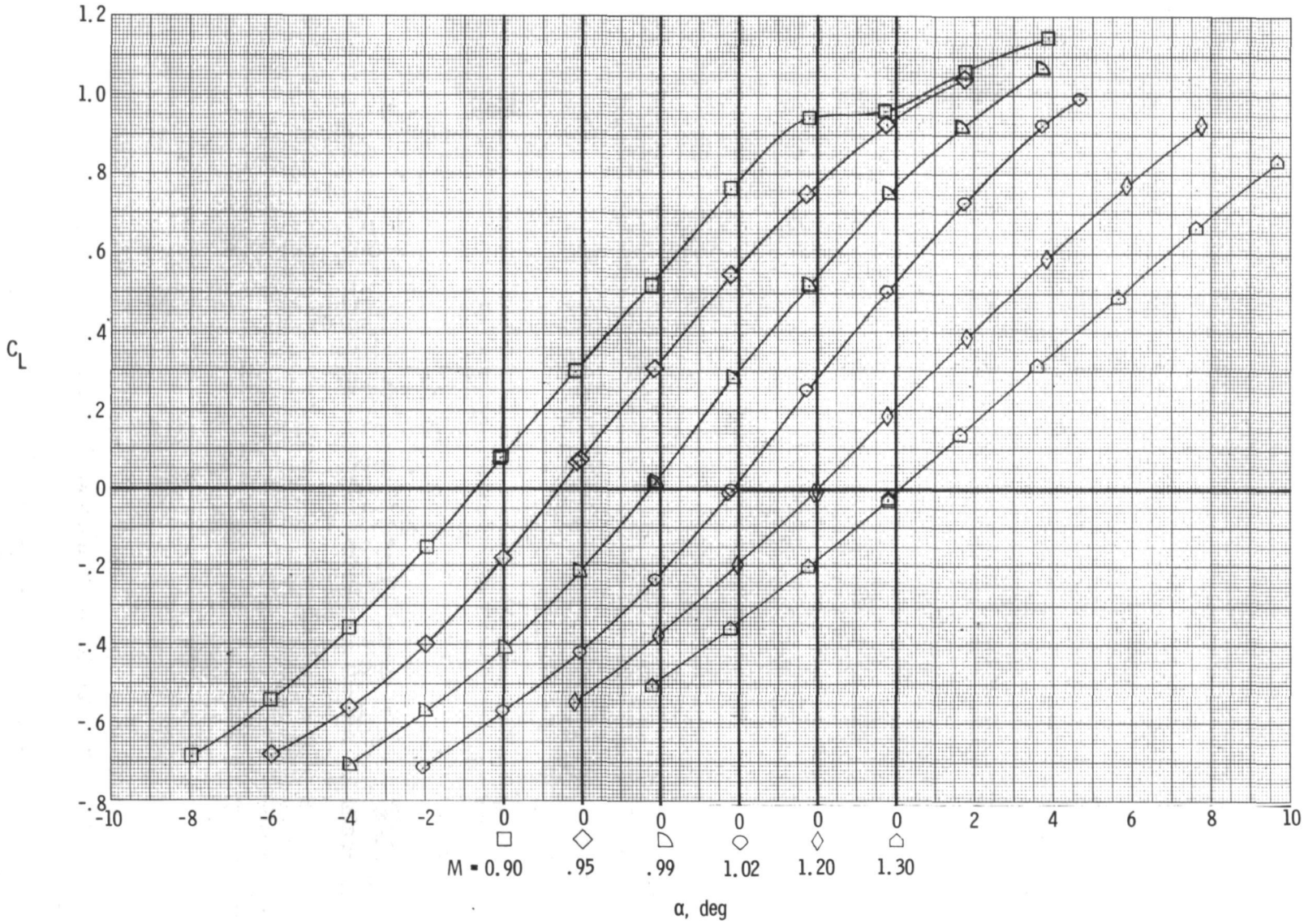

(a) Lift coefficient.

Figure 9.- Longitudinal aerodynamic characteristics of model. $\delta_h = 0^o$.

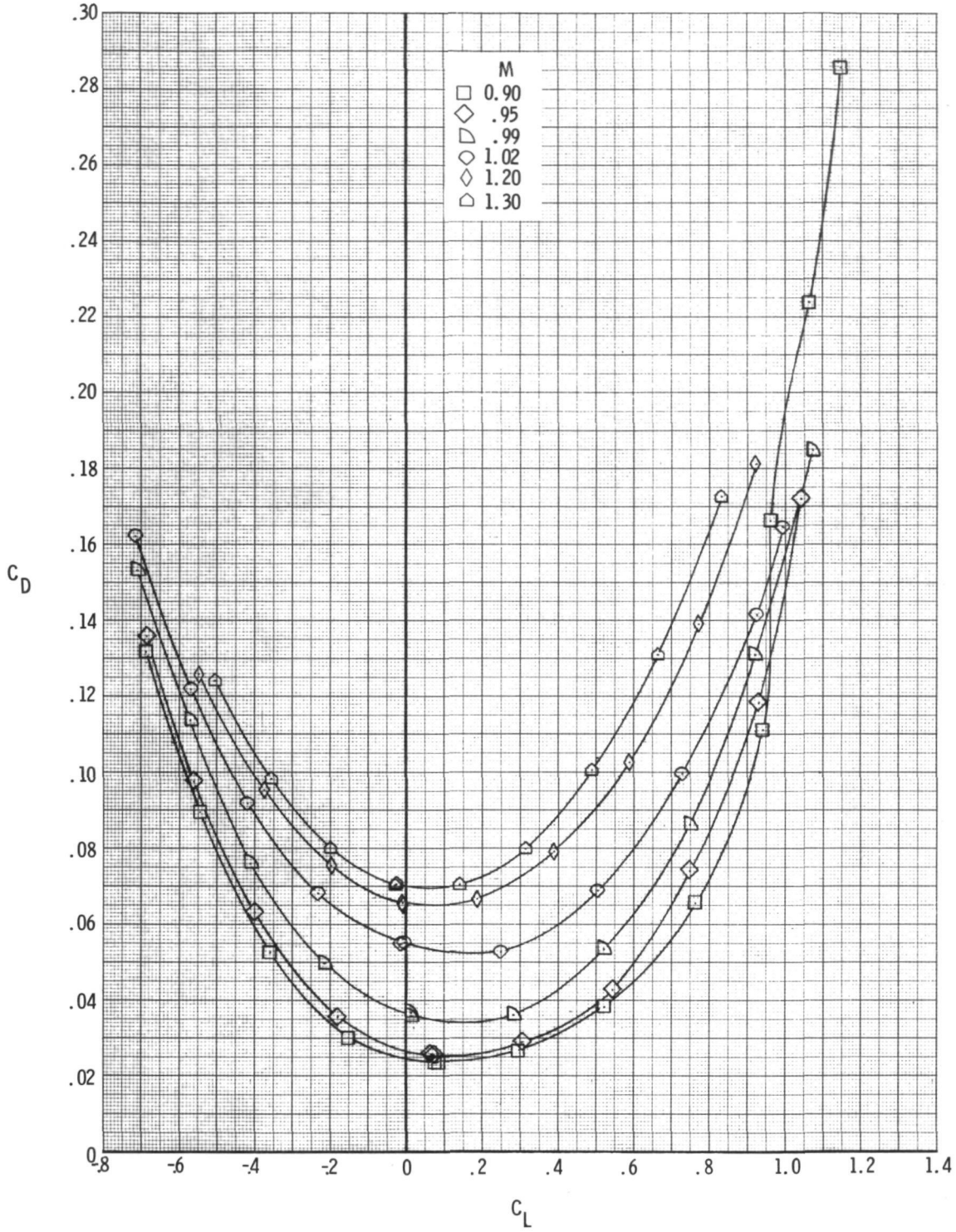

(b) Drag coefficient.

Figure 9.- Continued.

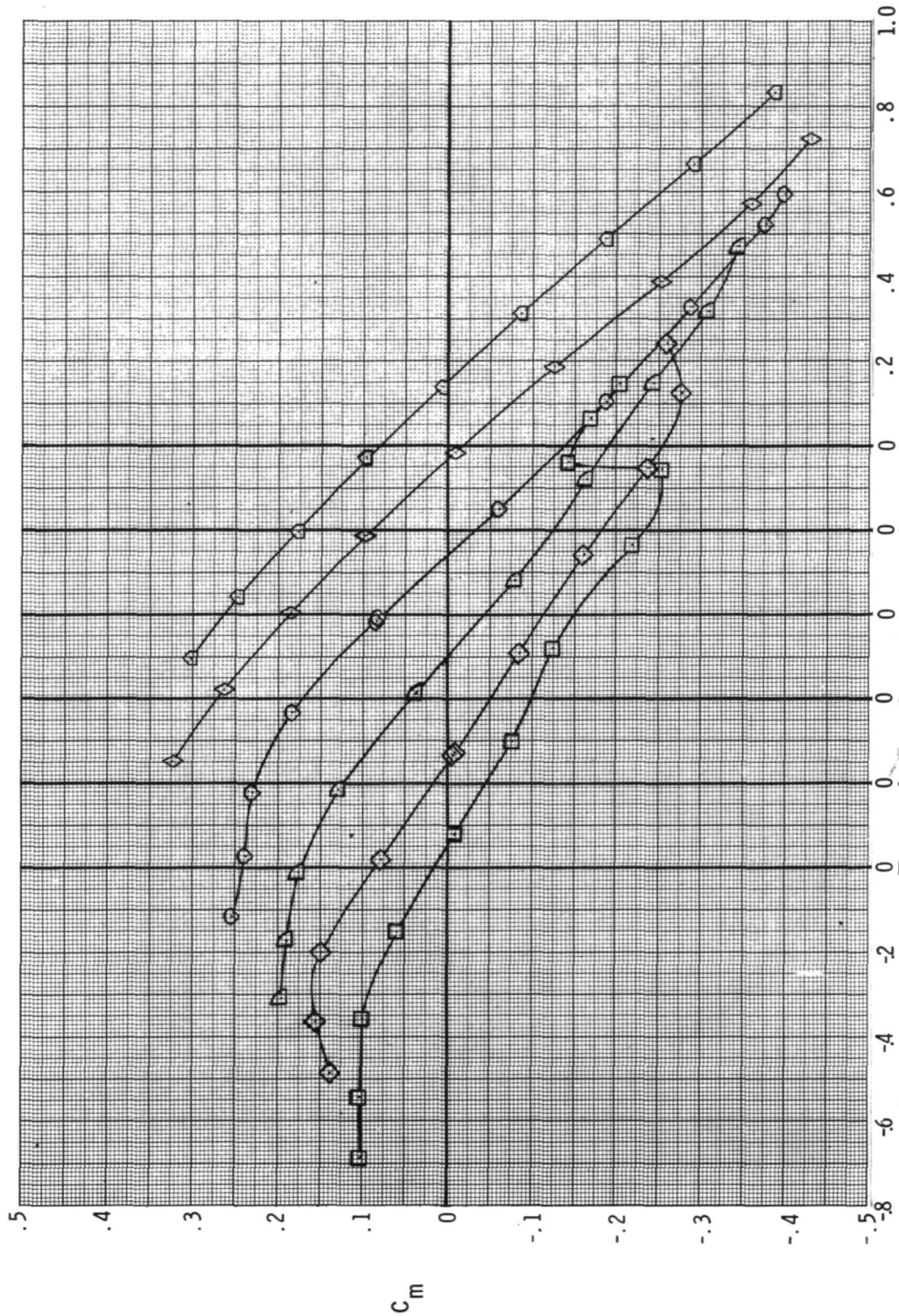

(c) Pitching-moment coefficient.

Figure 9.- Concluded.

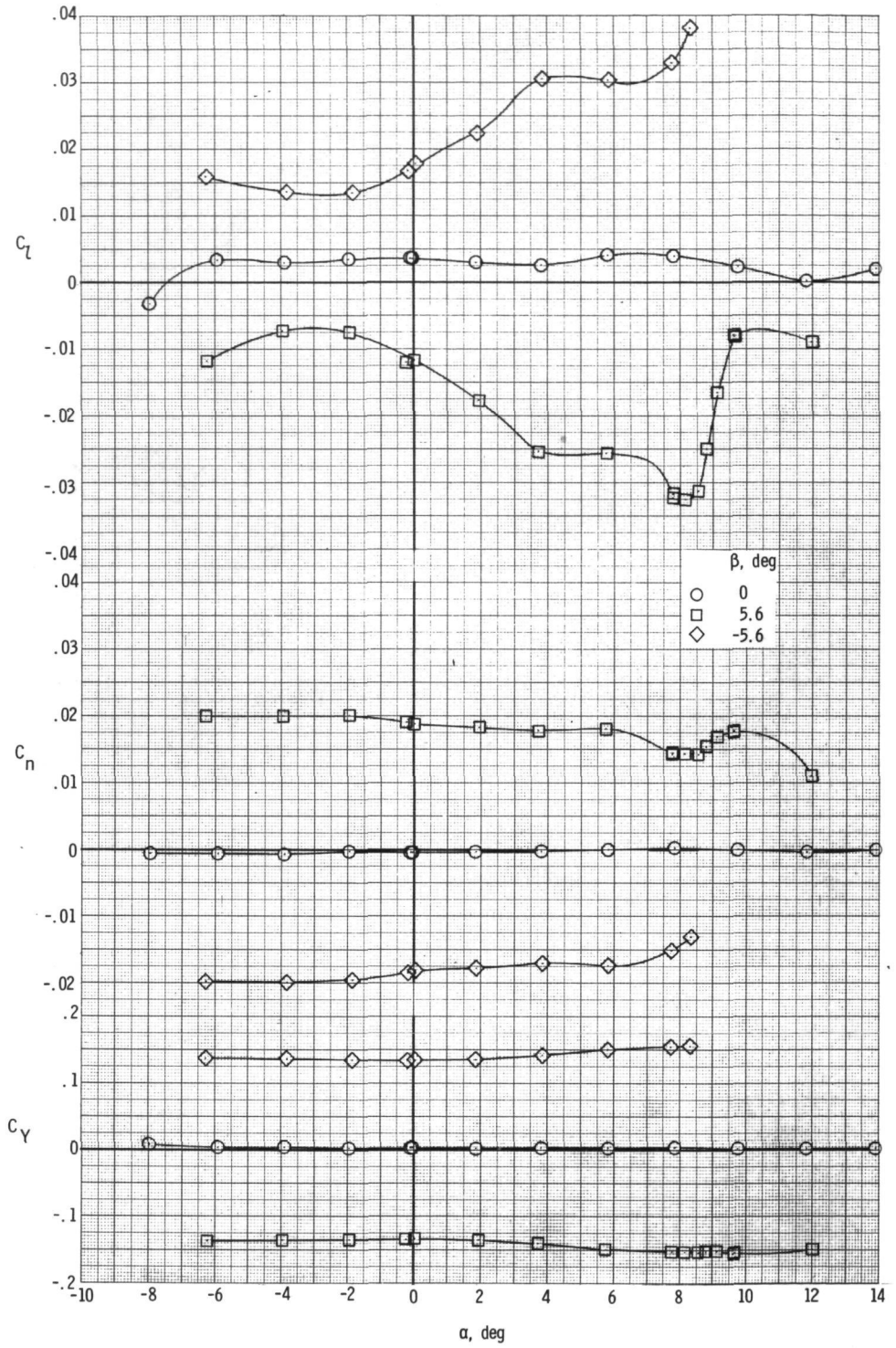

(a) M = 0.90.

Figure 10.- Variation of lateral aerodynamic coefficients with angle of attack for the model at three angles of sideslip. $\delta_h = 0^o$.

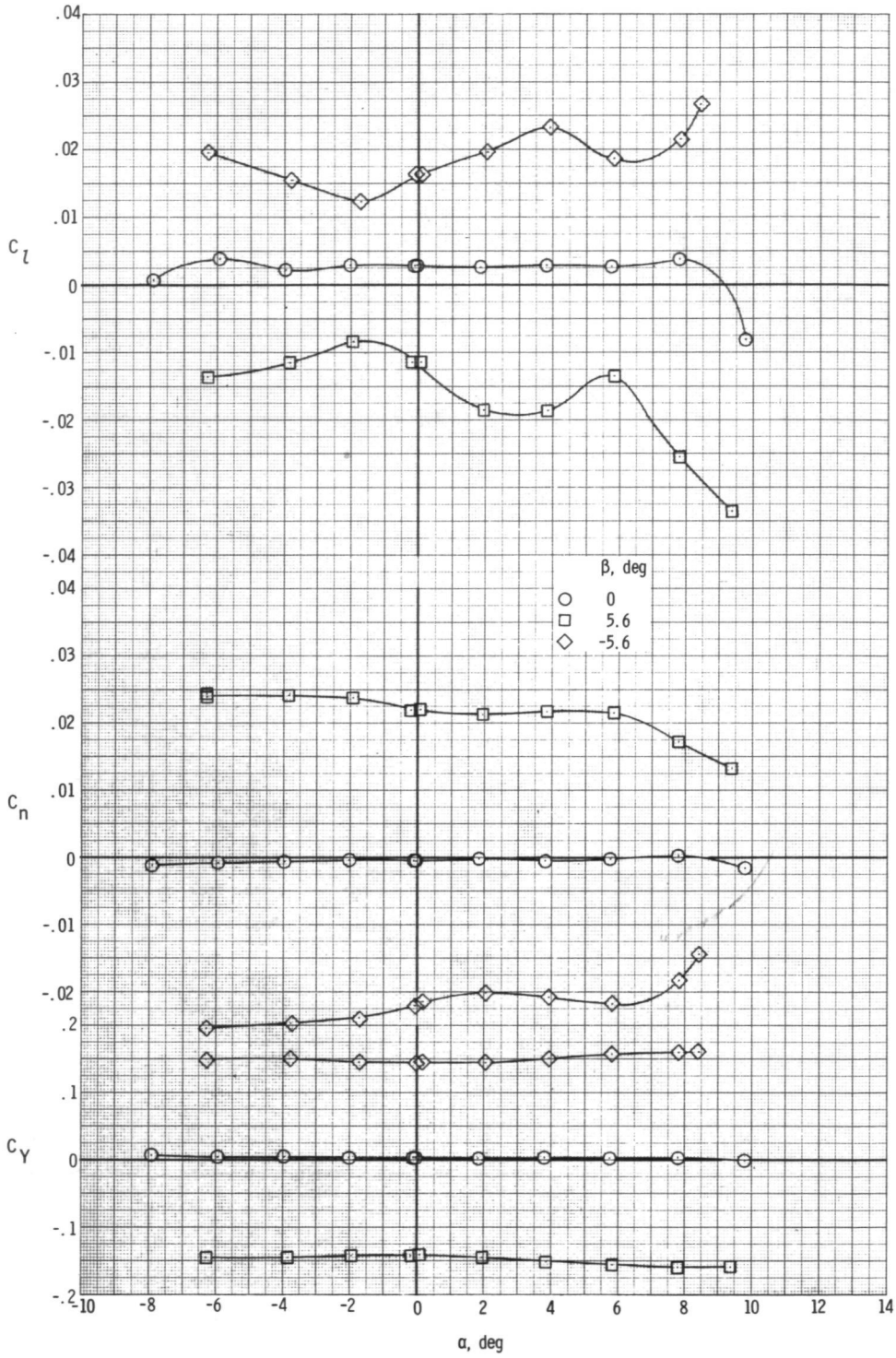

(b) M = 0.95.

Figure 10.- Continued.

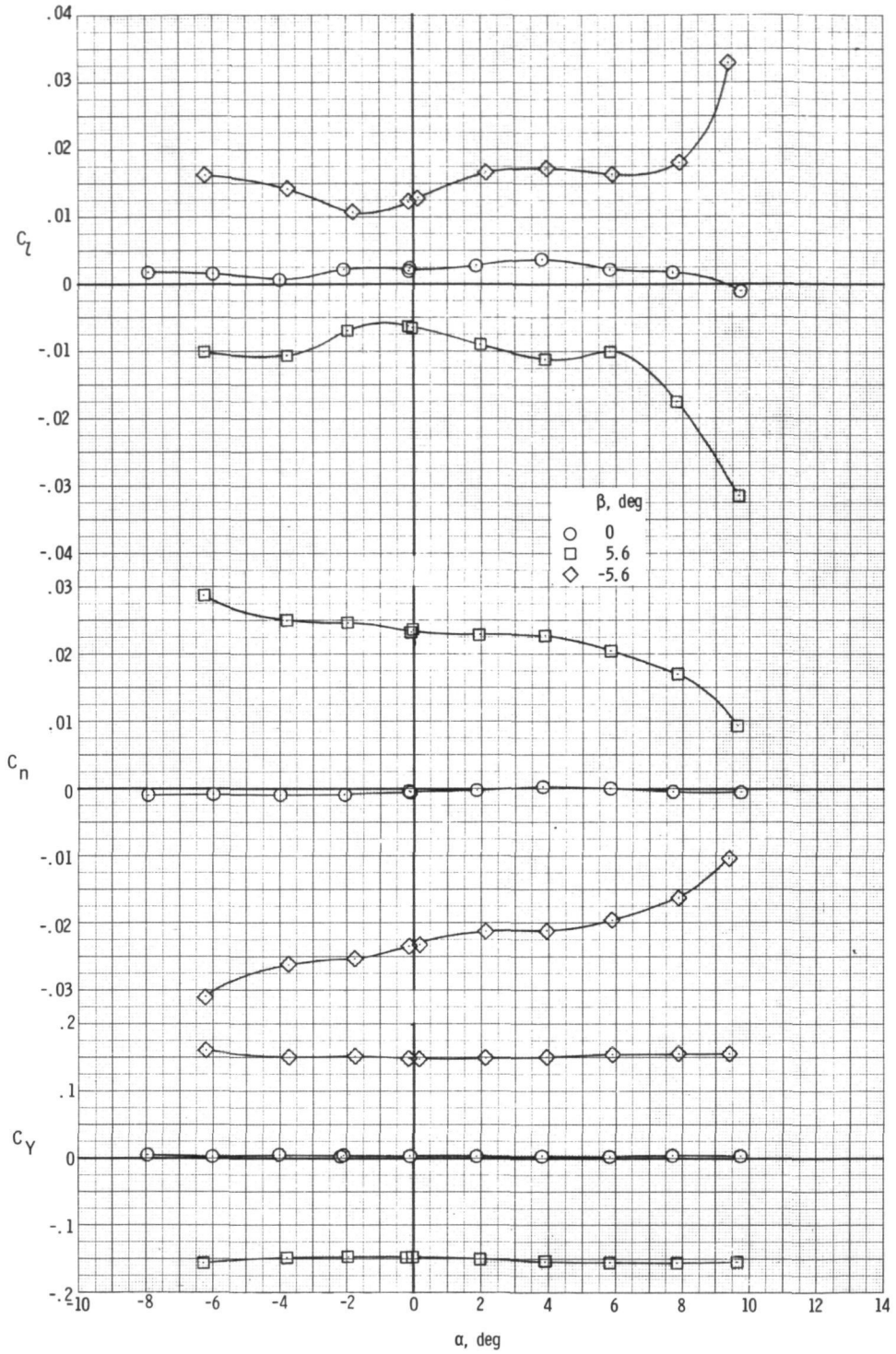

(c) M = 0.99.

Figure 10.- Continued.

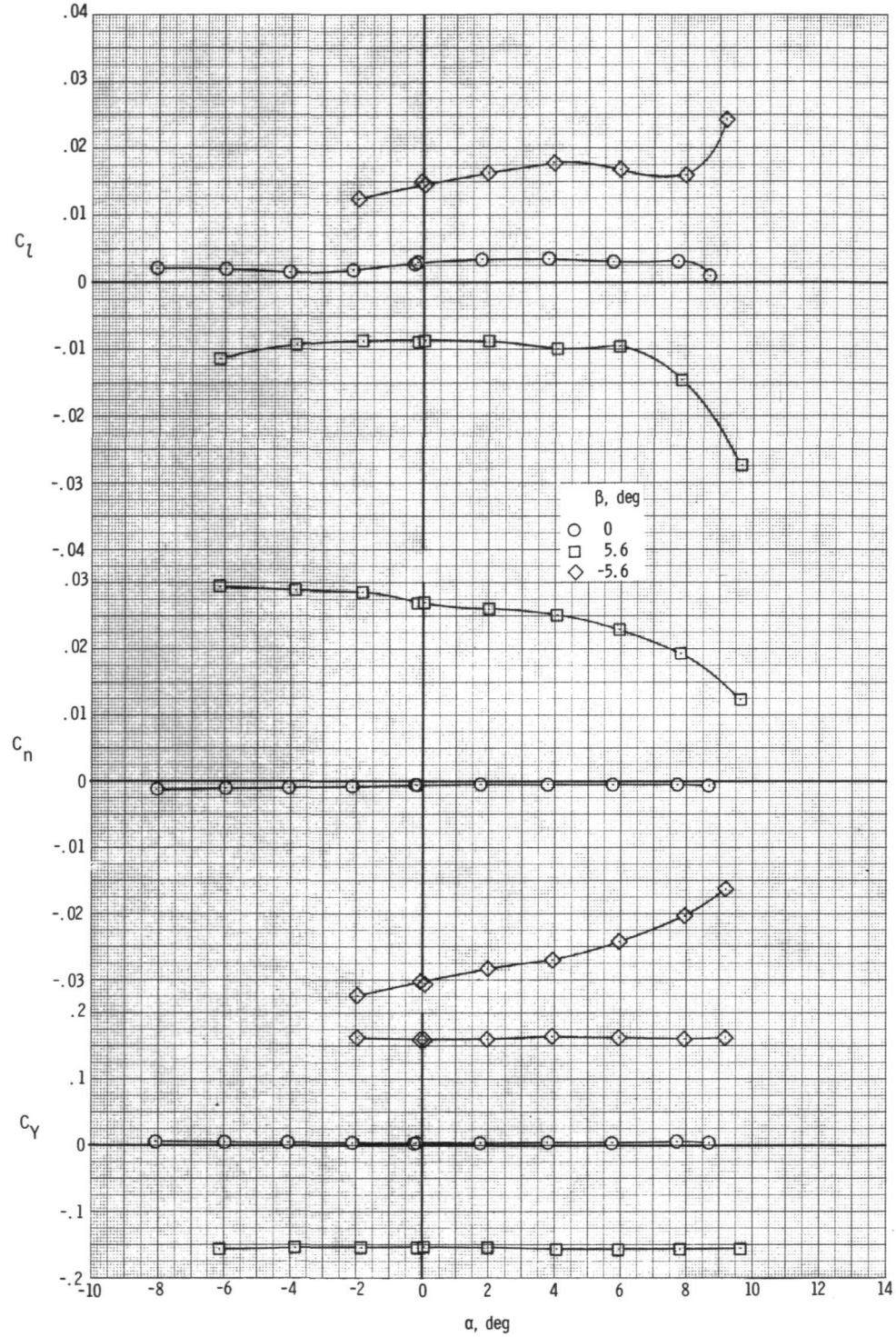

(d) M = 1.02.

Figure 10.- Continued.

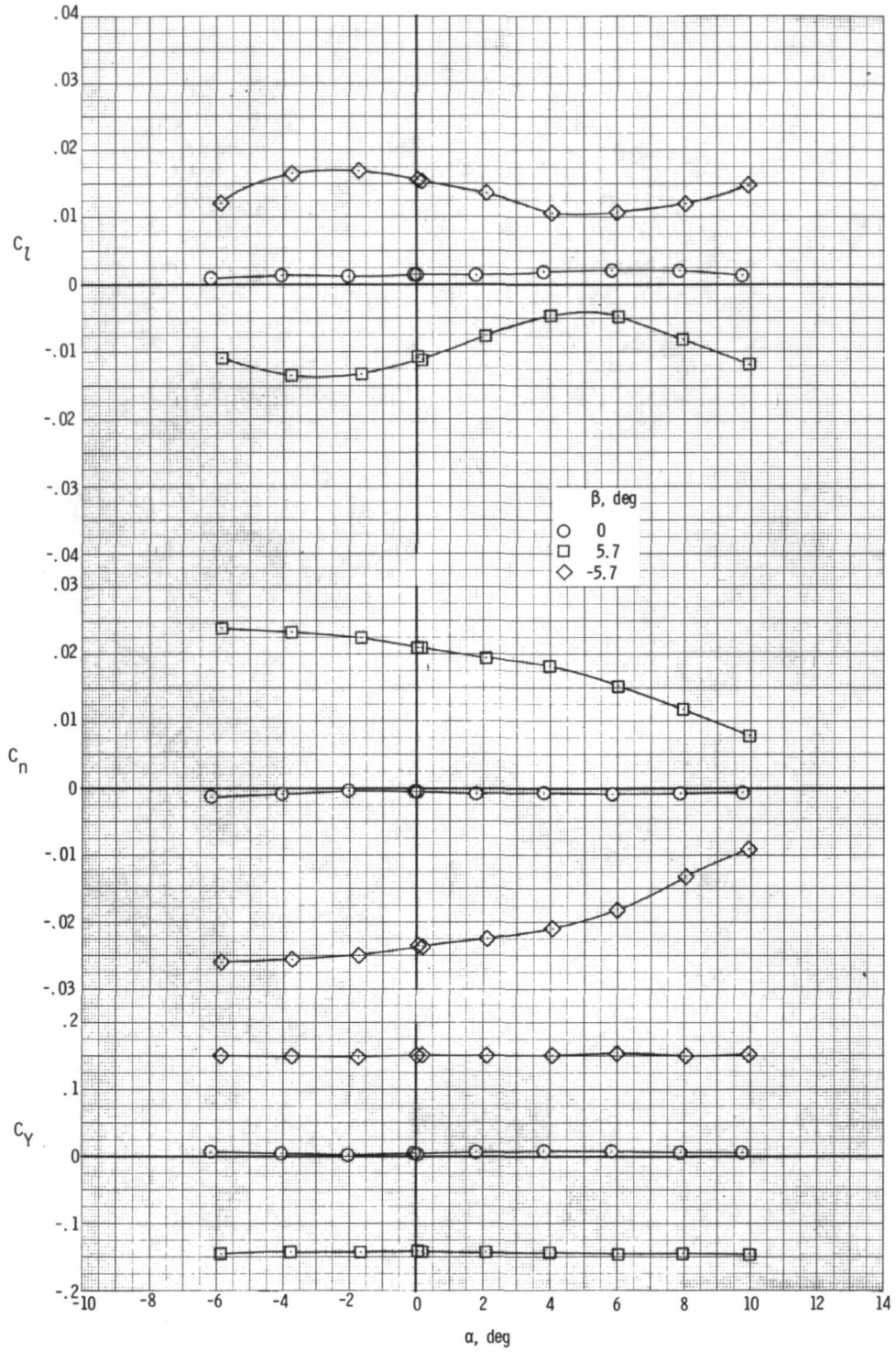

(e) M = 1.20.

Figure 10.- Continued.

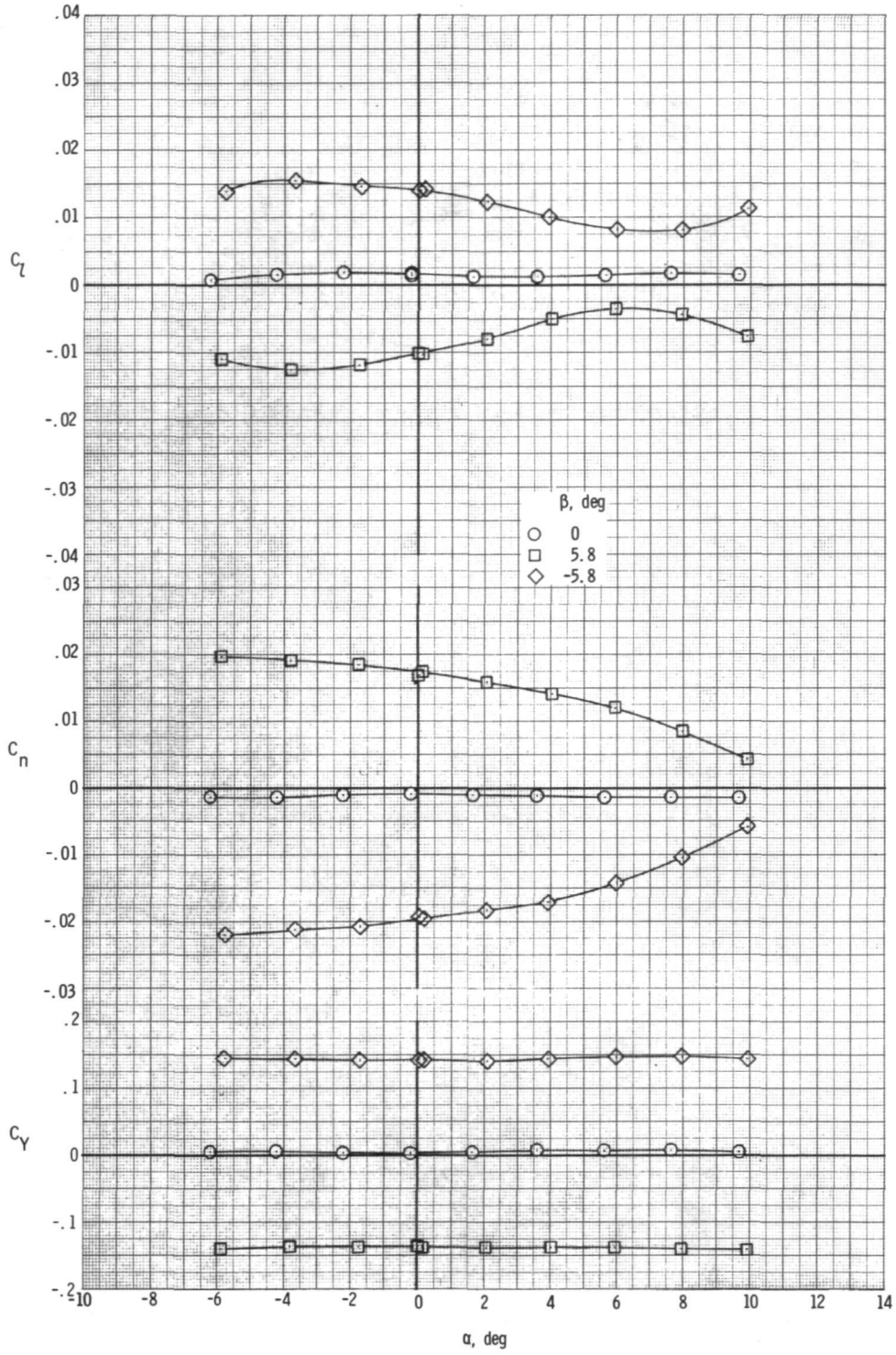

(f) M = 1.30.

Figure 10.- Concluded.

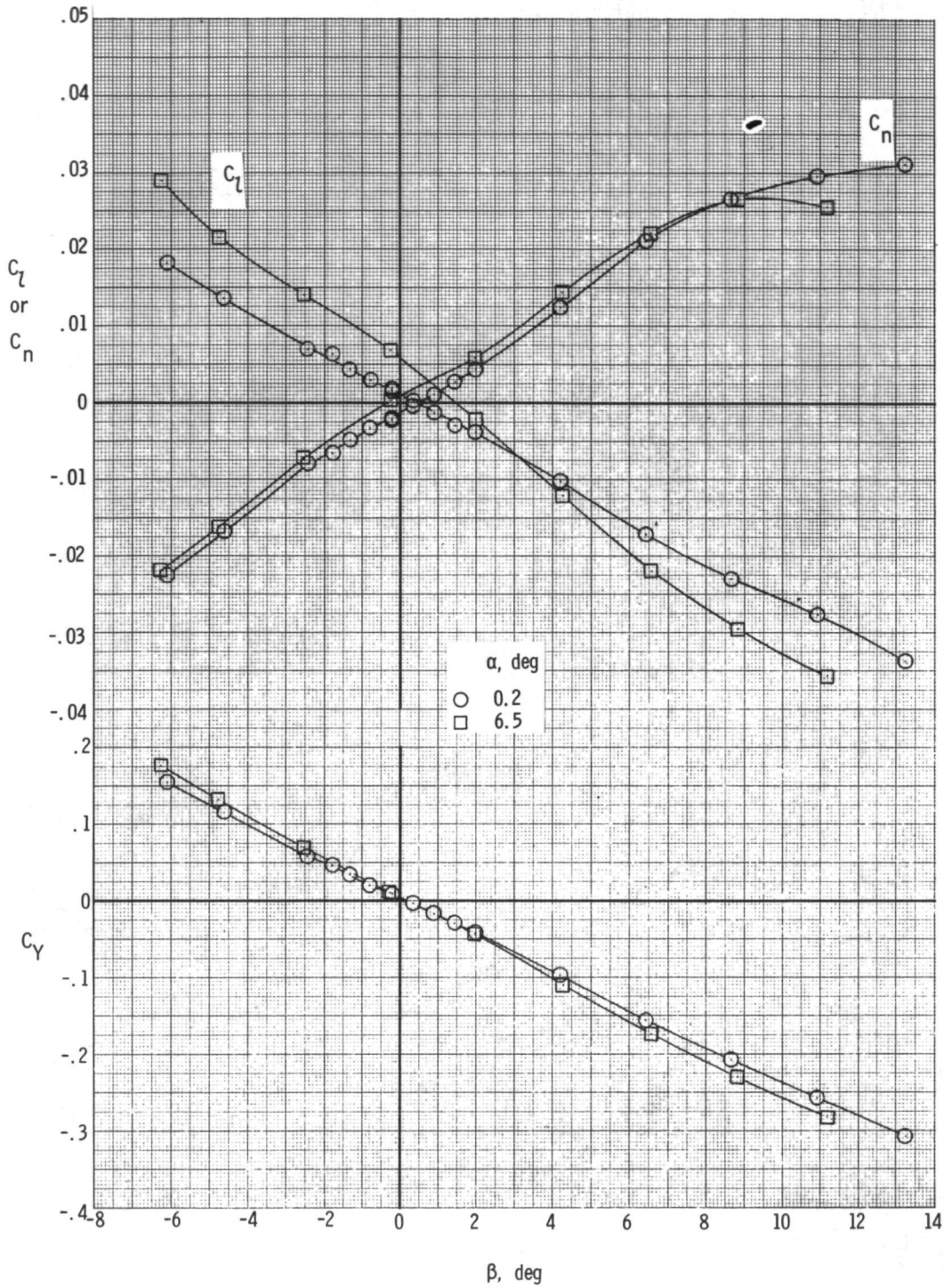

(a) M = 0.90.

Figure 11.- Variation of lateral aerodynamic coefficients with sideslip angle for the model at two angles of attack. $\delta_h = 0^o$.

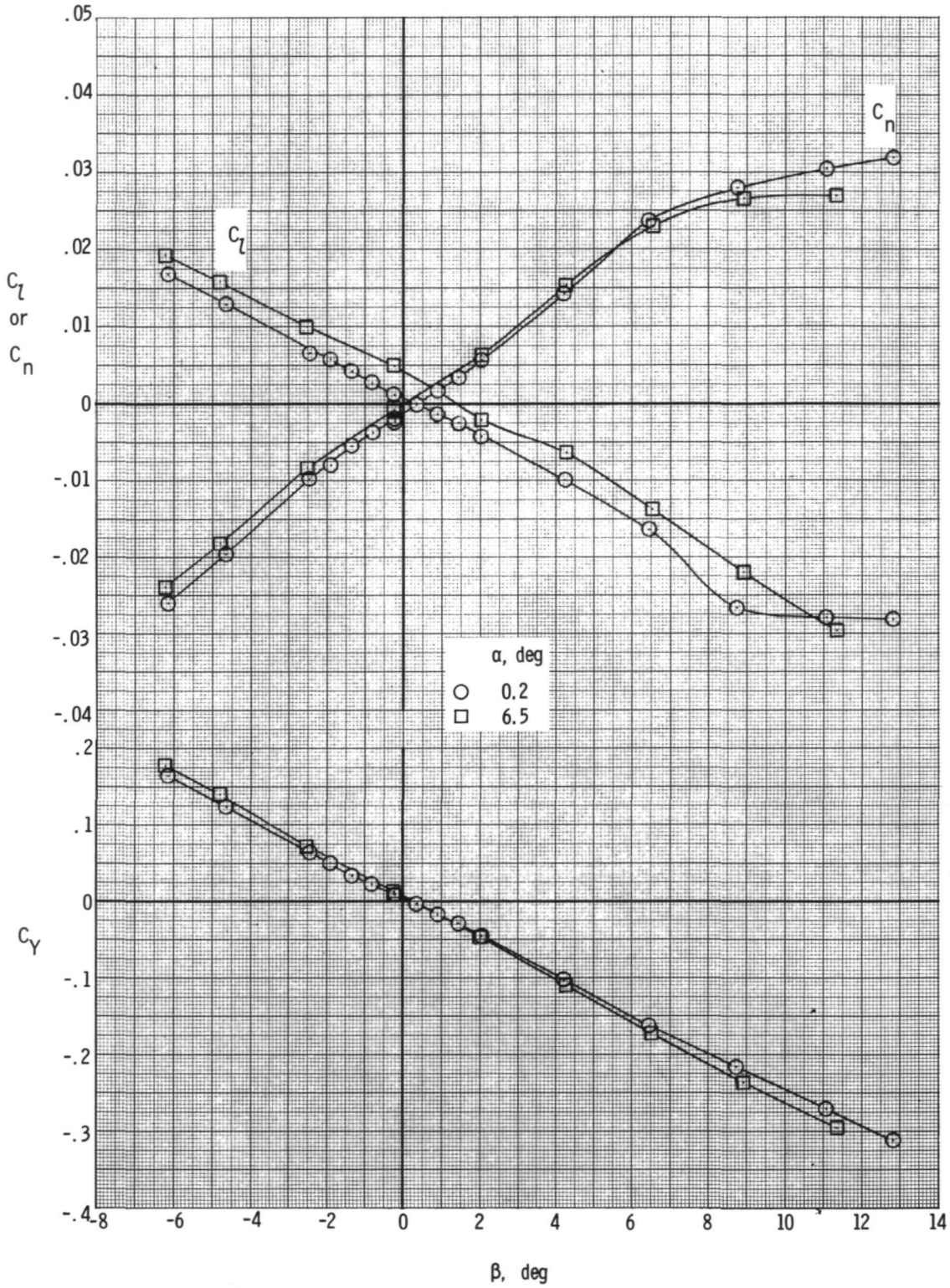

(b) M = 0.95.

Figure 11.- Continued.

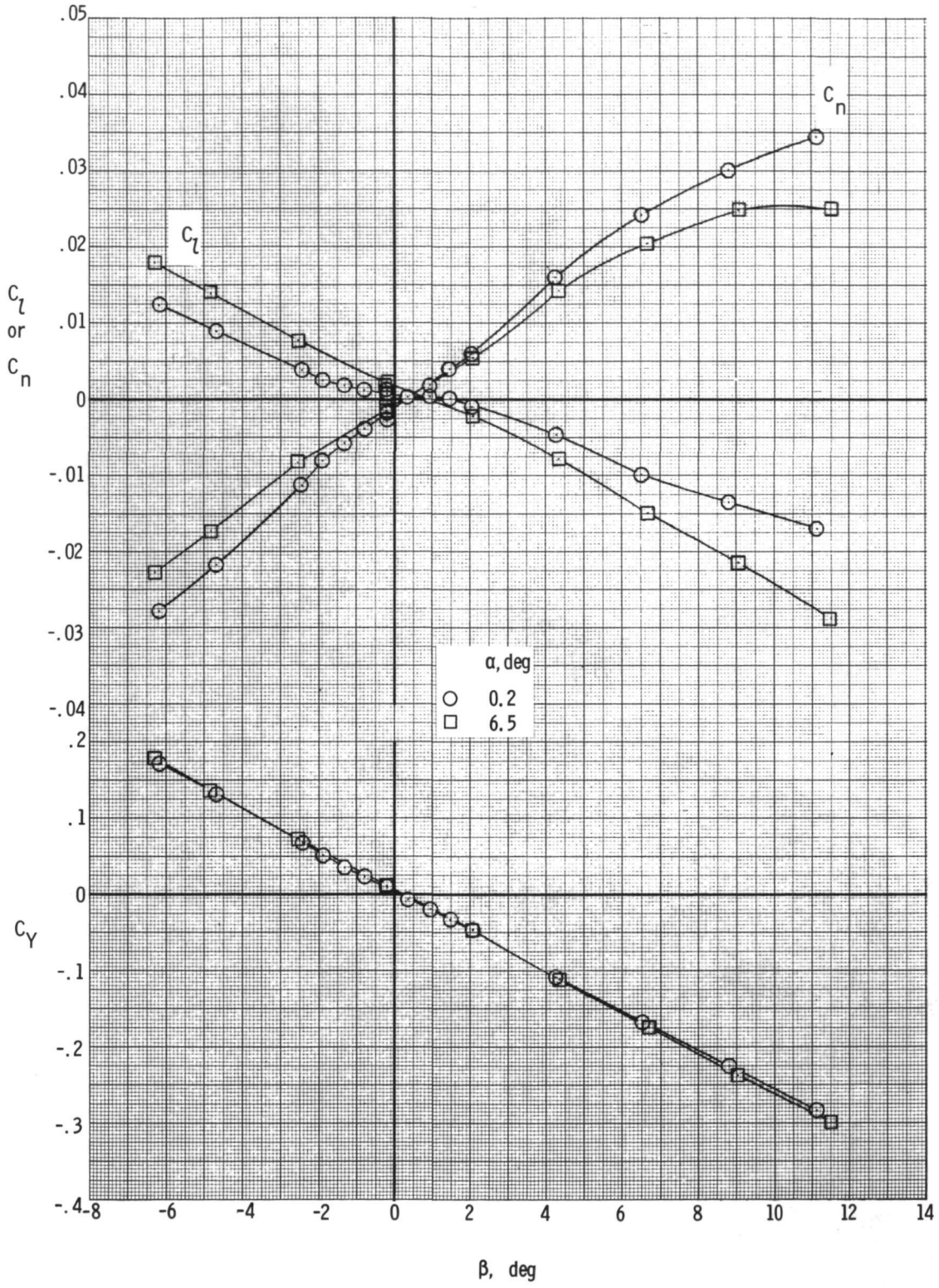

(c) M = 0.99.

Figure 11.- Continued.

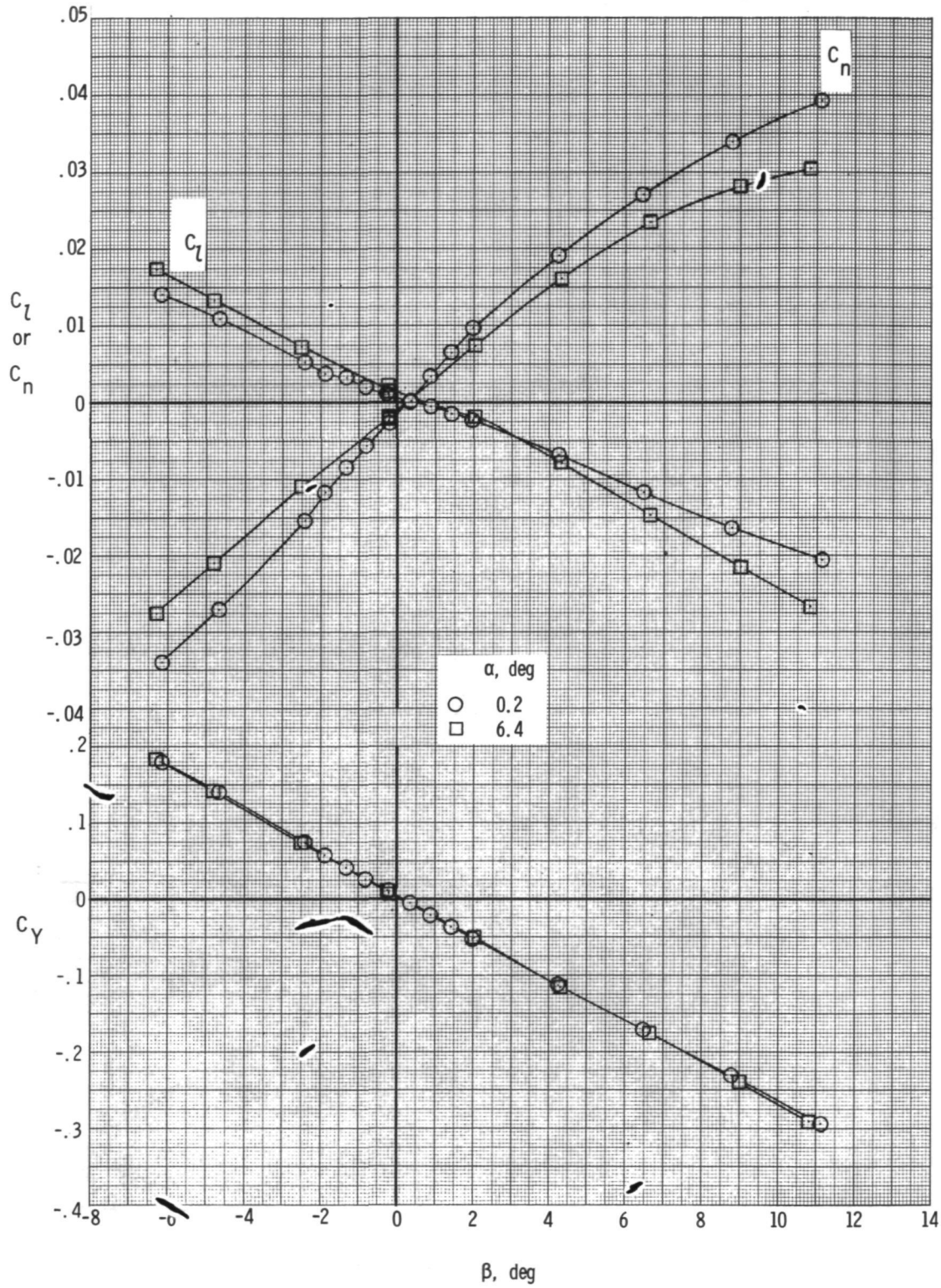

(d) M = 1.02.

Figure 11.- Concluded.

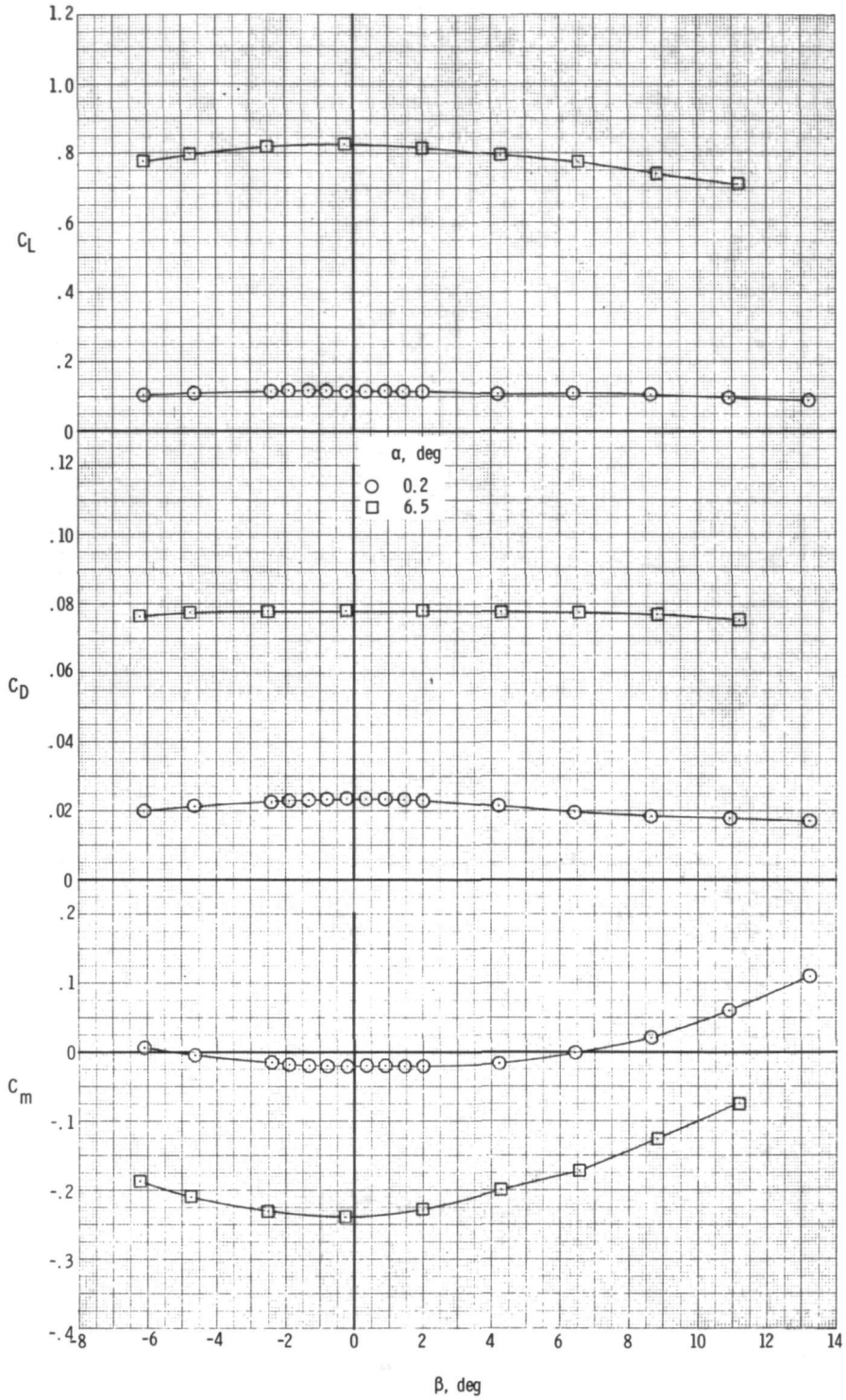

(a) M = 0.90.

Figure 12.- Variation of longitudinal aerodynamic coefficients with sideslip angle for the model at two angles of attack. $\delta_h = 0^o$.

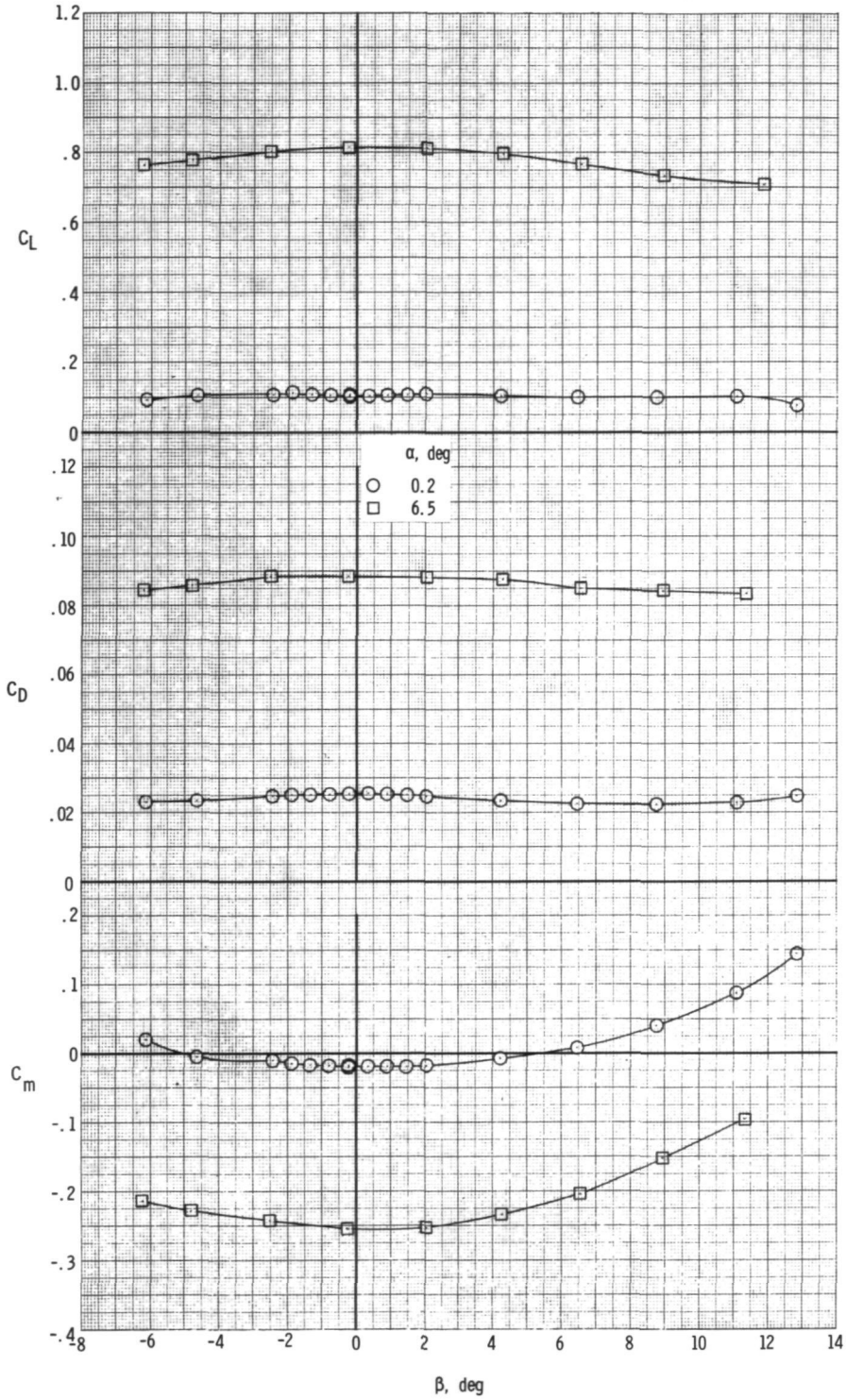

(b) M = 0.95.

Figure 12.- Continued.

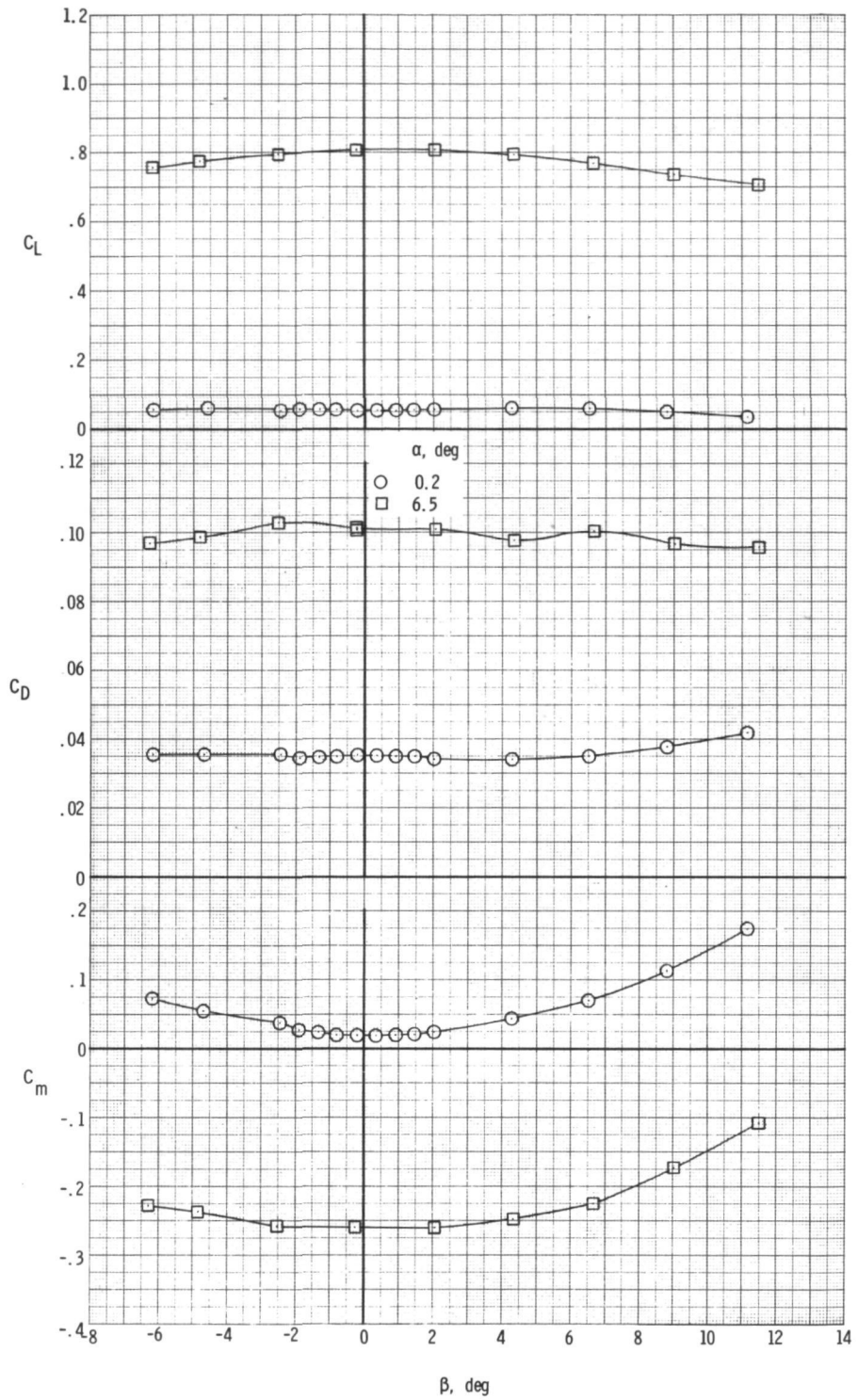

(c) M = 0.99.

Figure 12.- Continued.

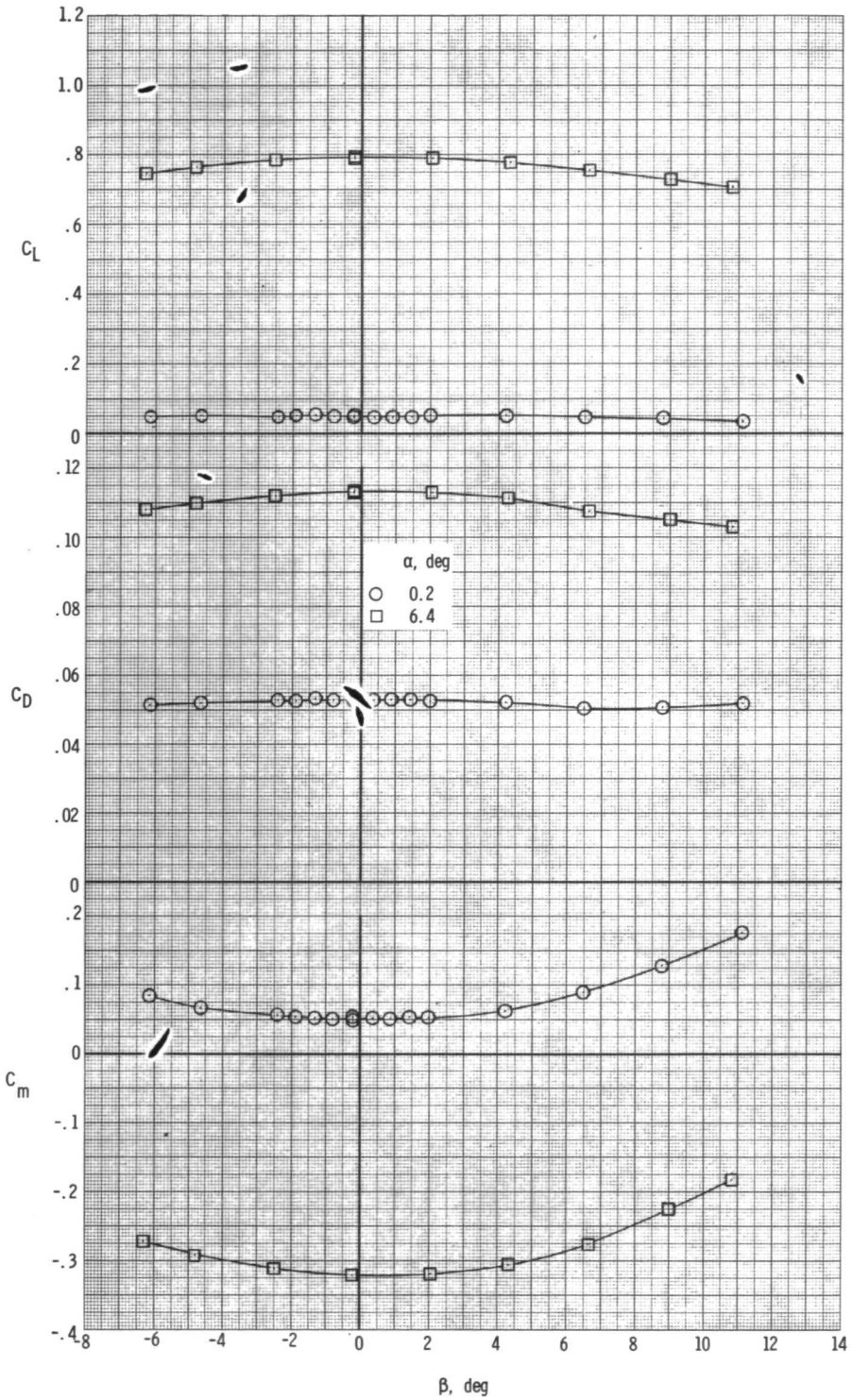

(d) M = 1.02.

Figure 12.- Concluded.

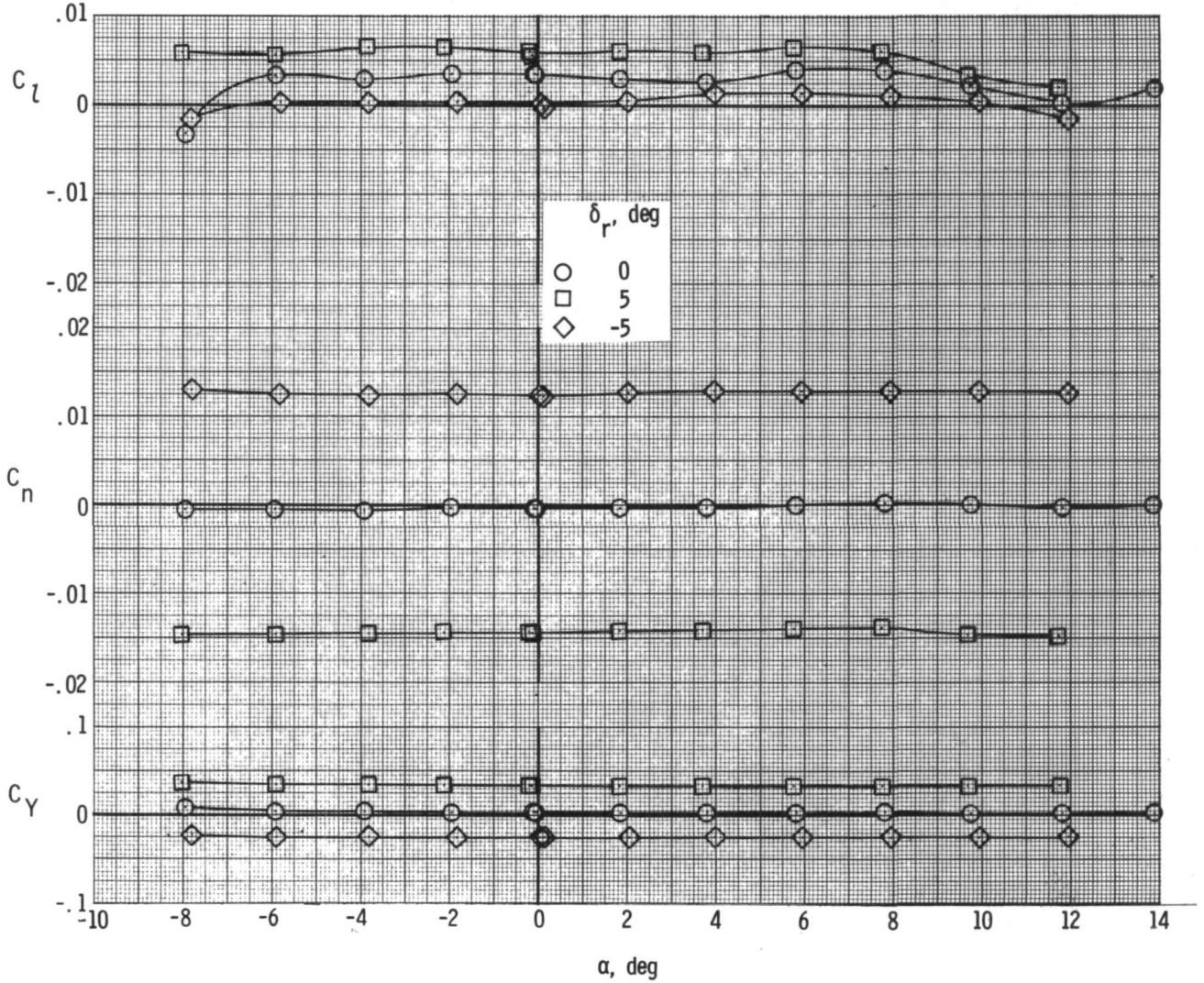

(a) M = 0.90.

Figure 13.- Variation of lateral aerodynamic coefficients with angle of attack for the model with three rudder deflection angles. $\delta_h = 0^o$ and $\beta = 0^o$.

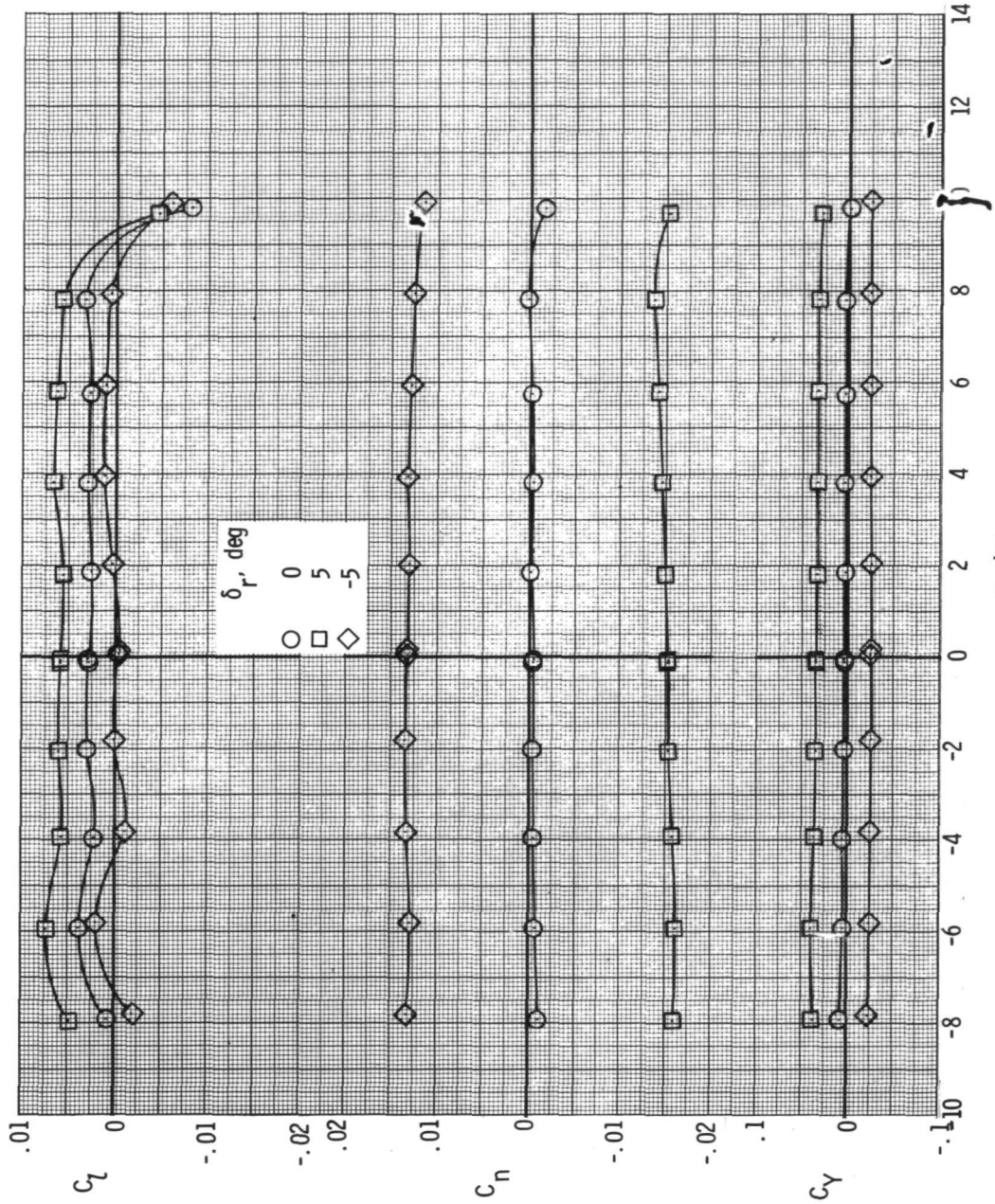

(b) $M = 0.95$.

Figure 13.- Continued.

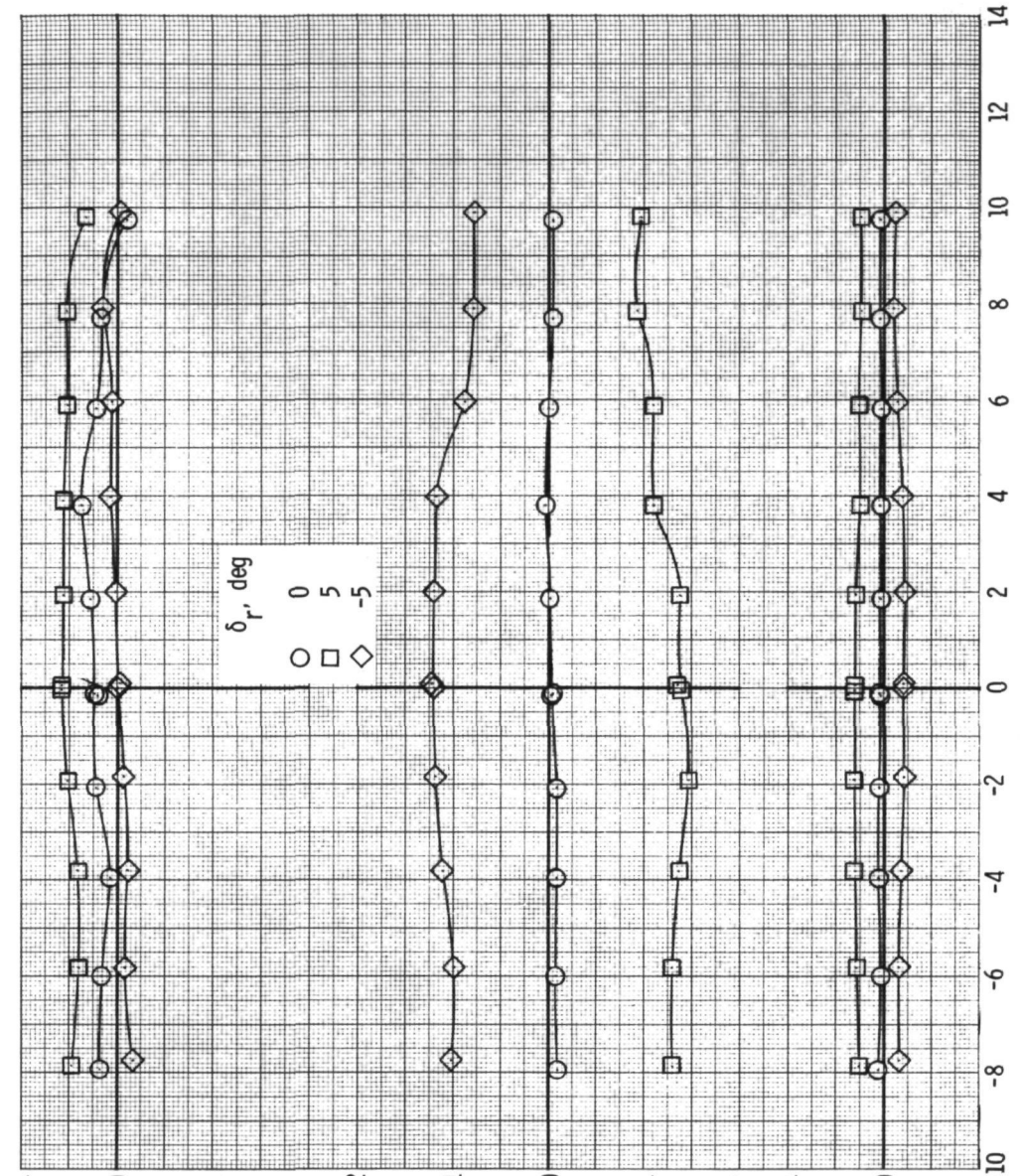

(c) M = 0.99.

Figure 13.- Continued.

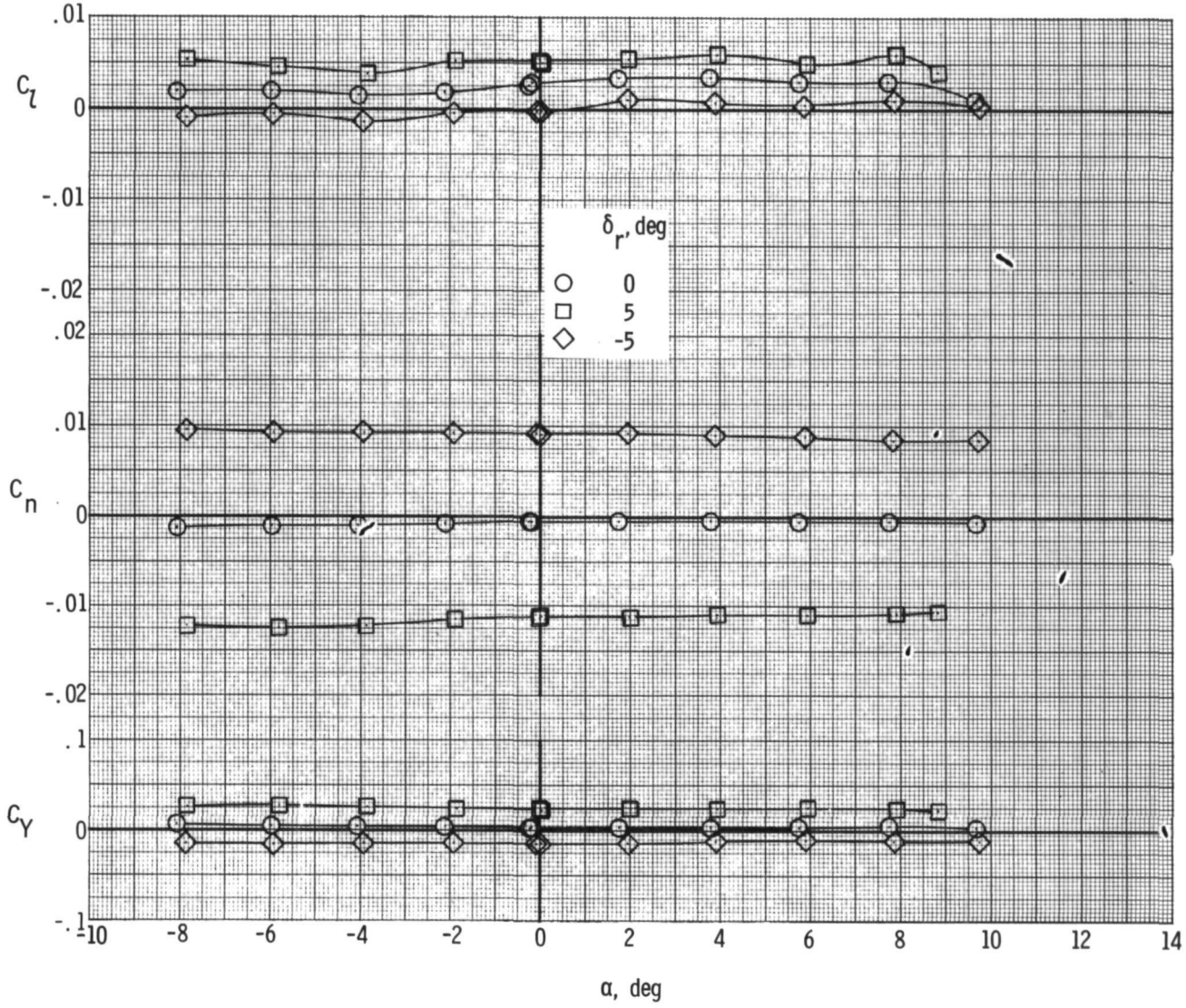

(d) M = 1.02

Figure 13.- Continued.

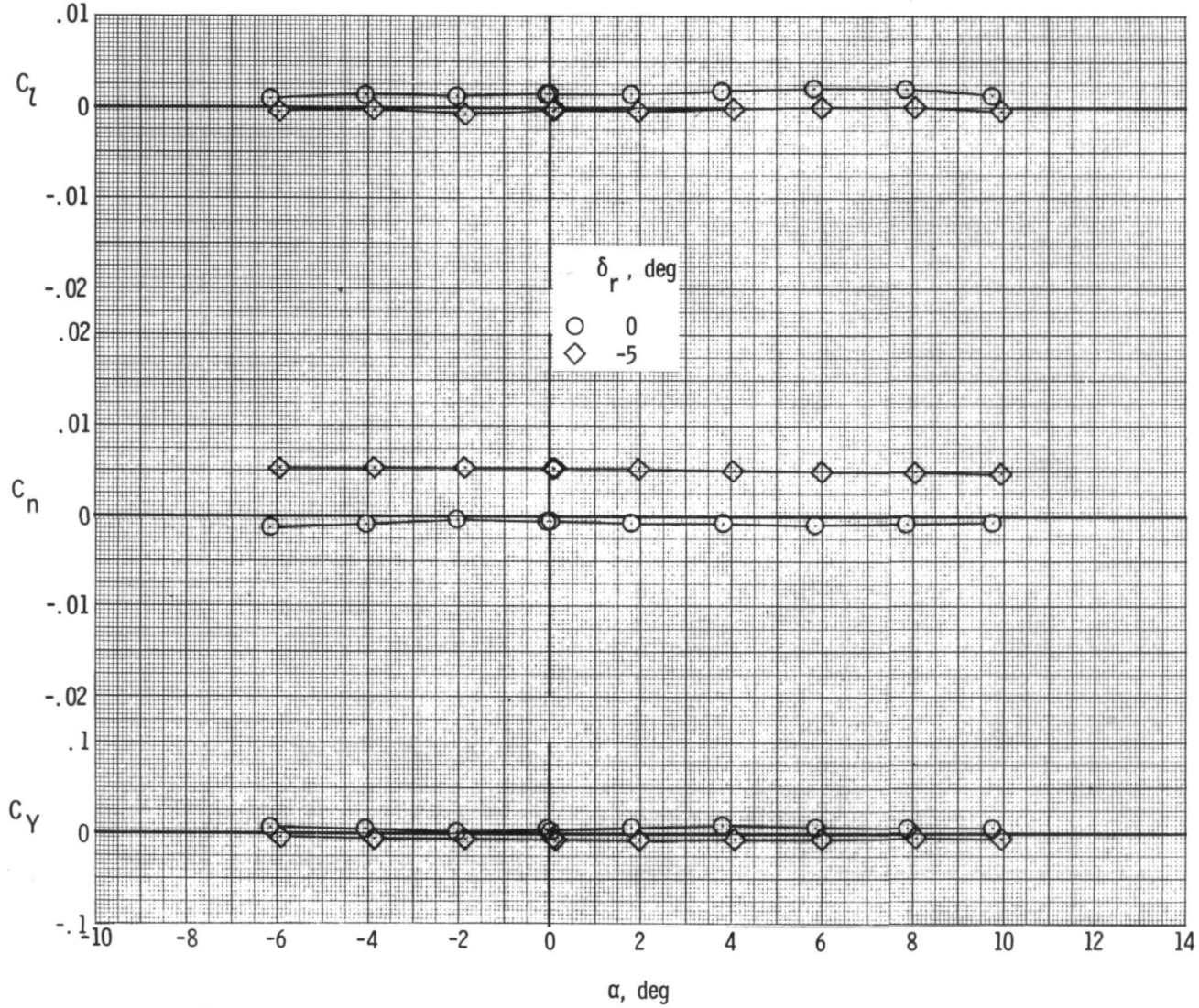

(e) M = 1.20.

Figure 13.- Continued.

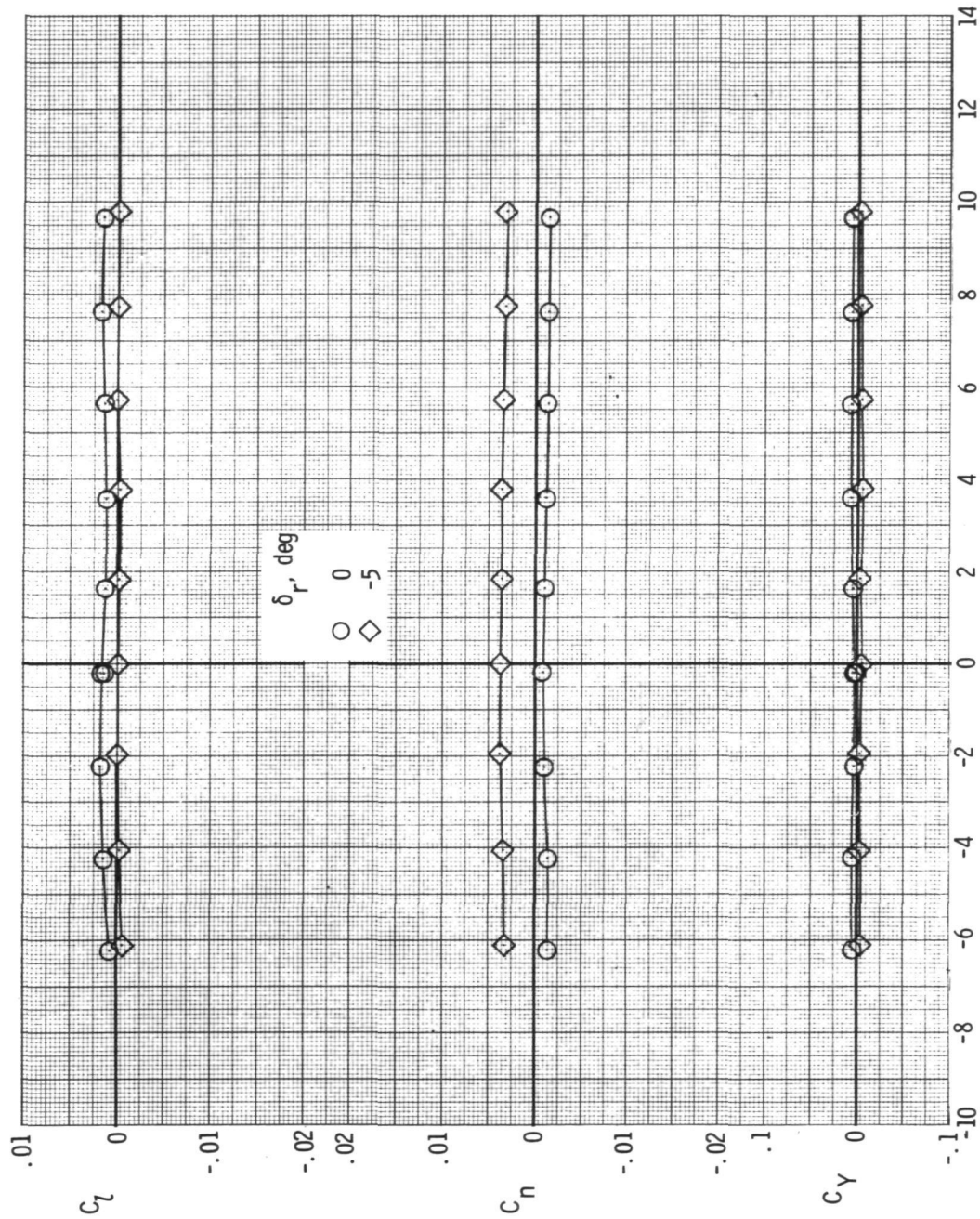

(f) M = 1.30.

Figure 13.- Concluded.

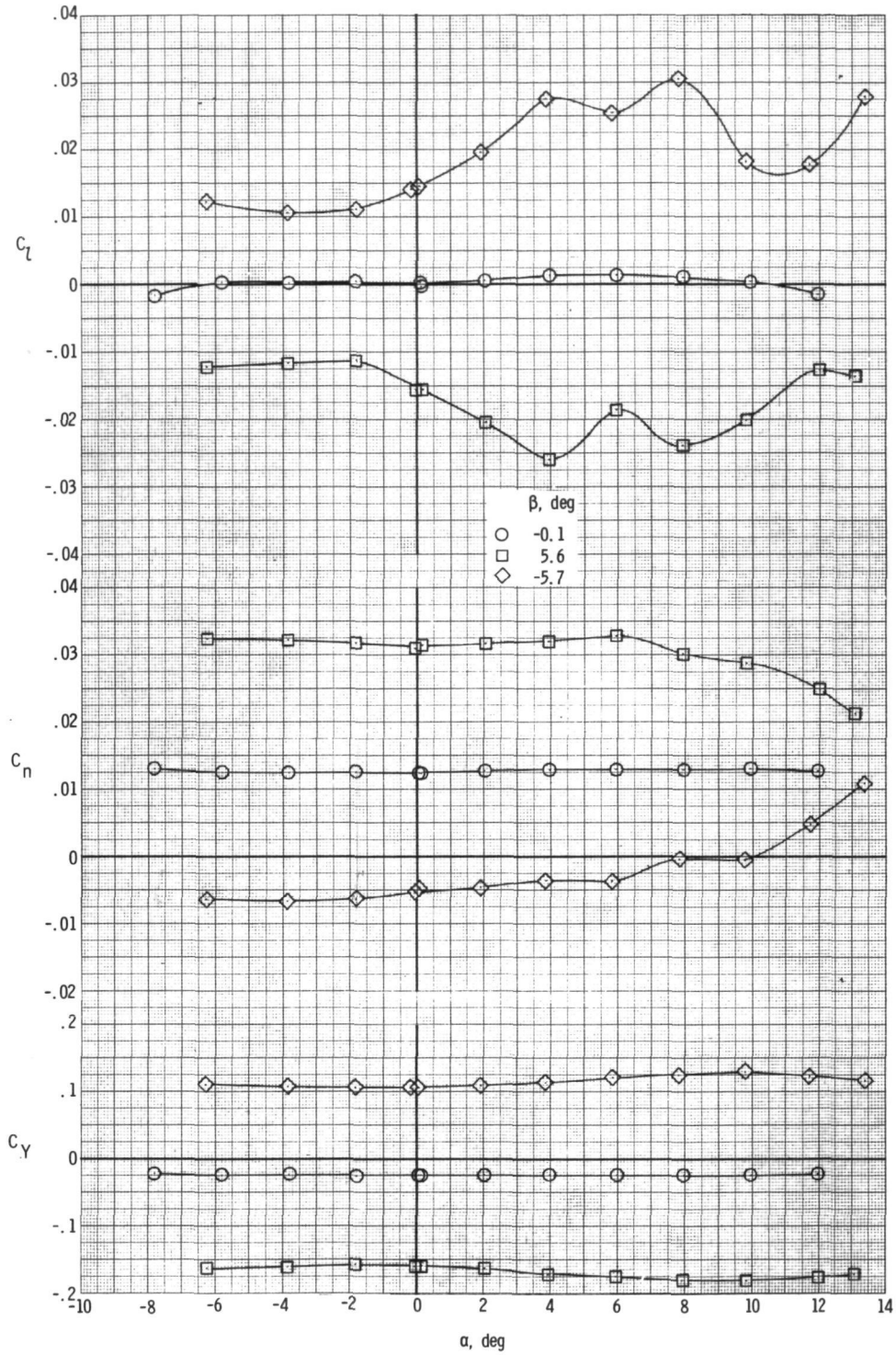

(a) M = 0.90.

Figure 14.- Variation of lateral aerodynamic coefficients with angle of attack for the model at three angles of sideslip with $\delta_r = -5^o$. $\delta_h = 0^o$.

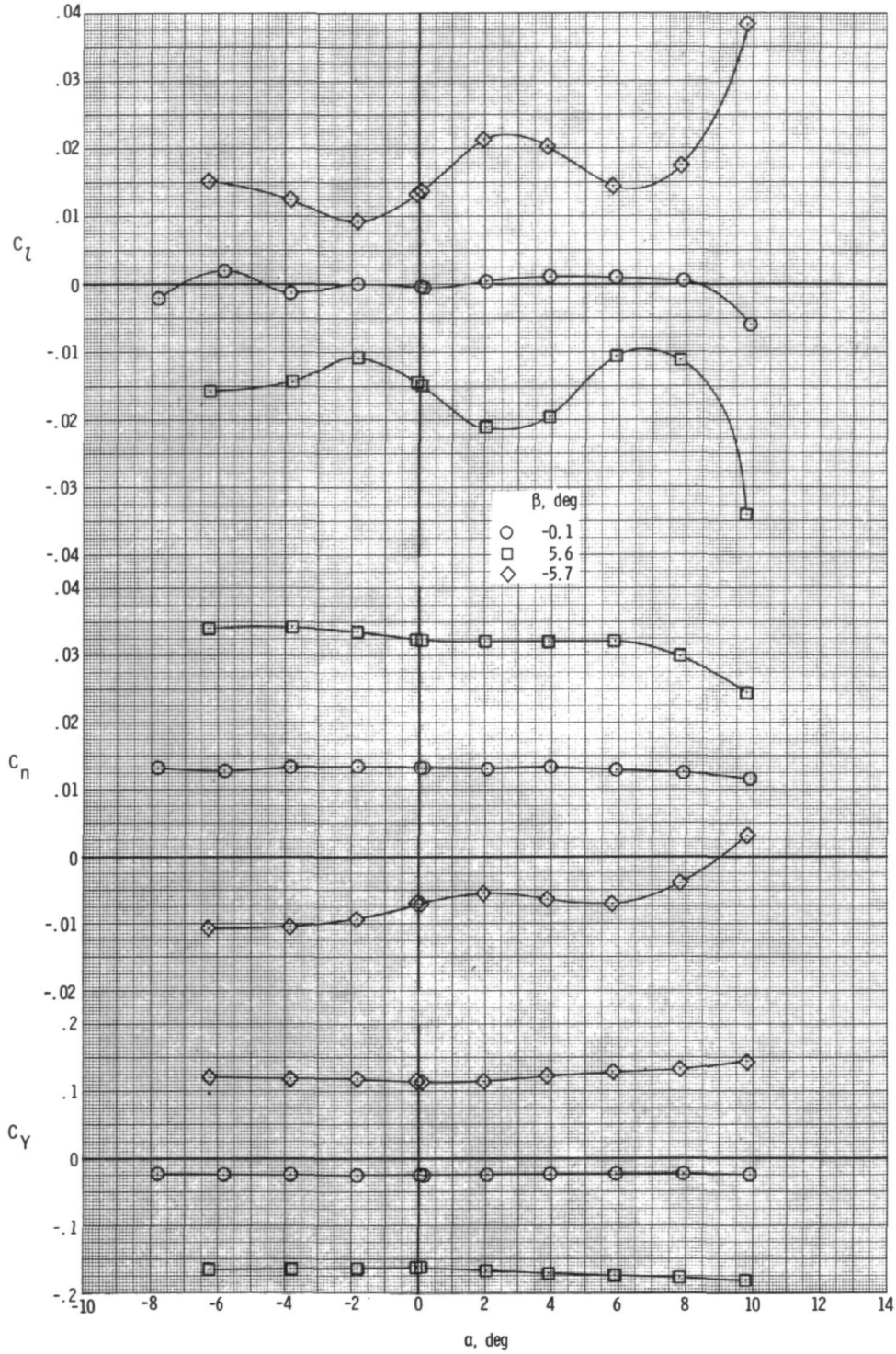

(b) M = 0.95.

Figure 14.- Continued.

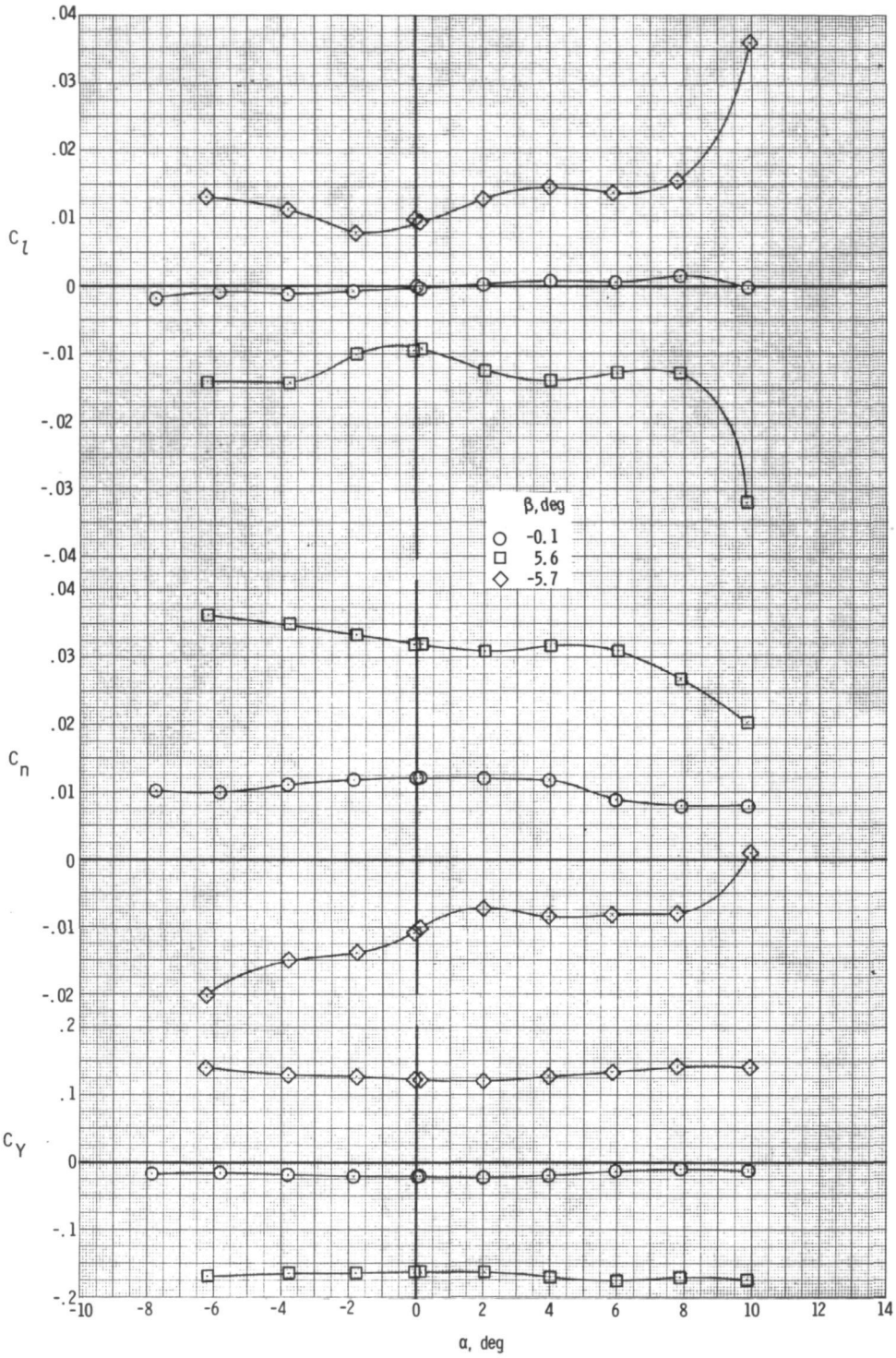

(c) M = 0.99.

Figure 14.- Continued.

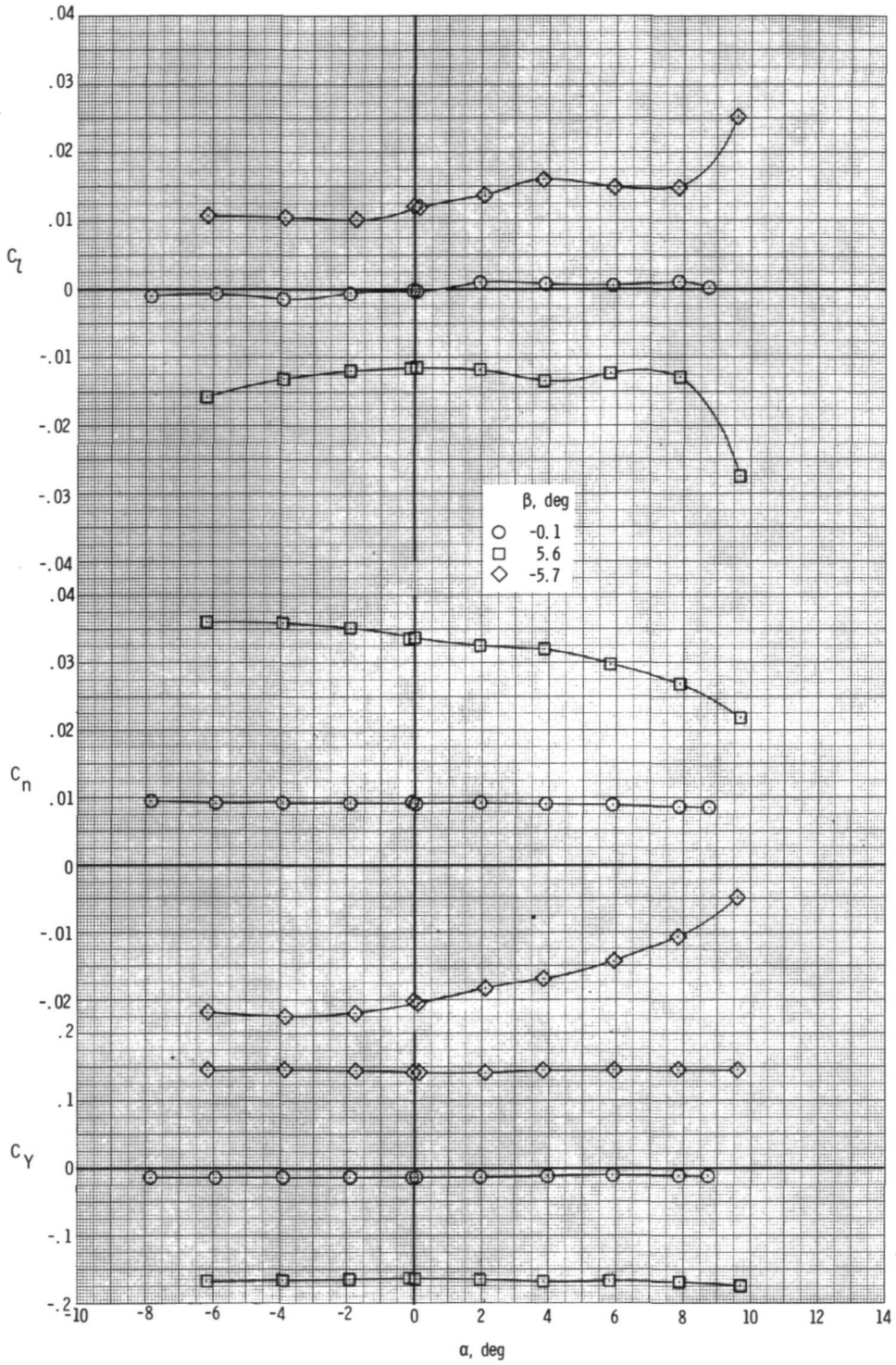

(d) M = 1.02.

Figure 14.- Continued.

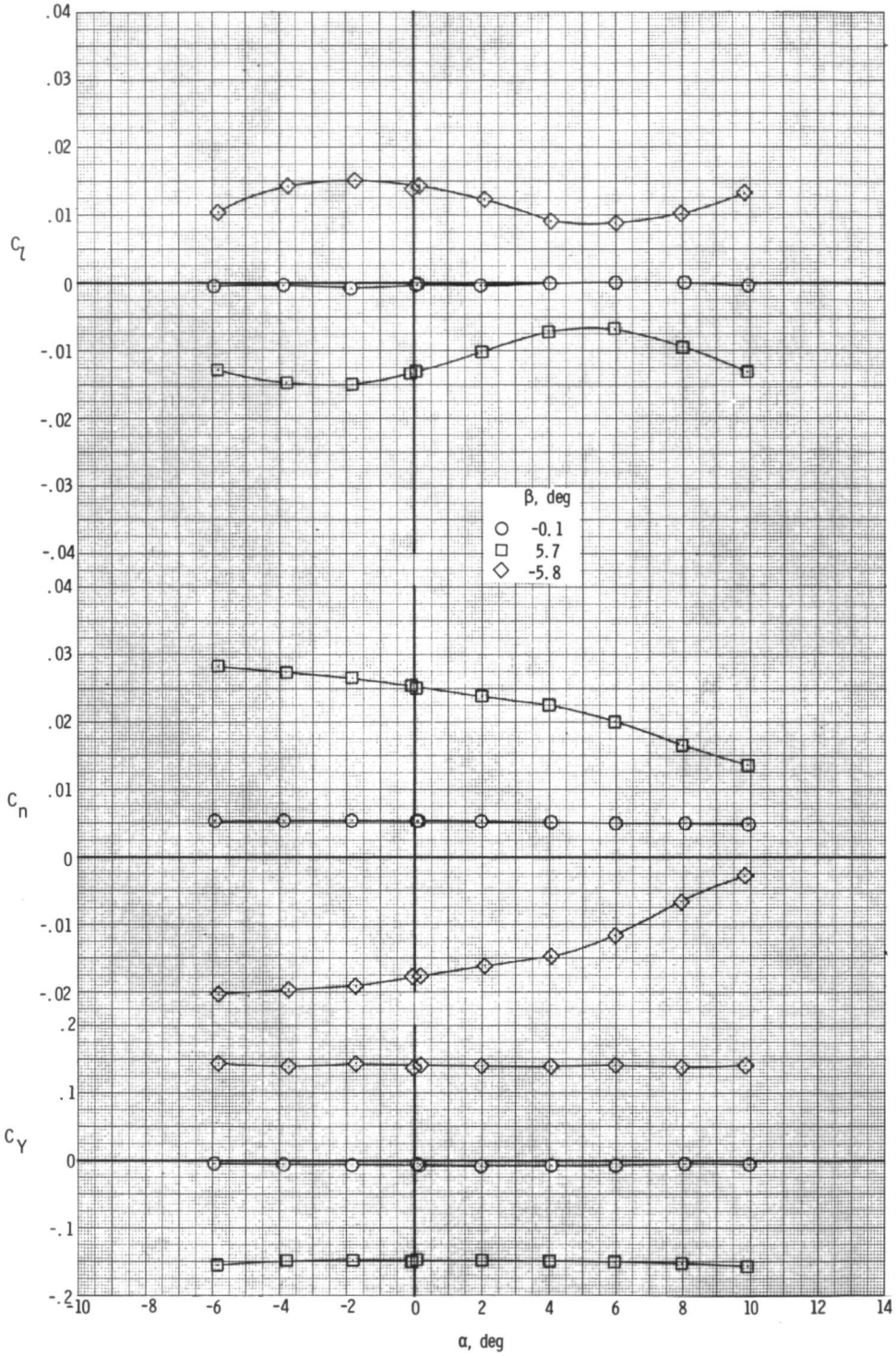

(e) M = 1.20.

Figure 14.- Continued.

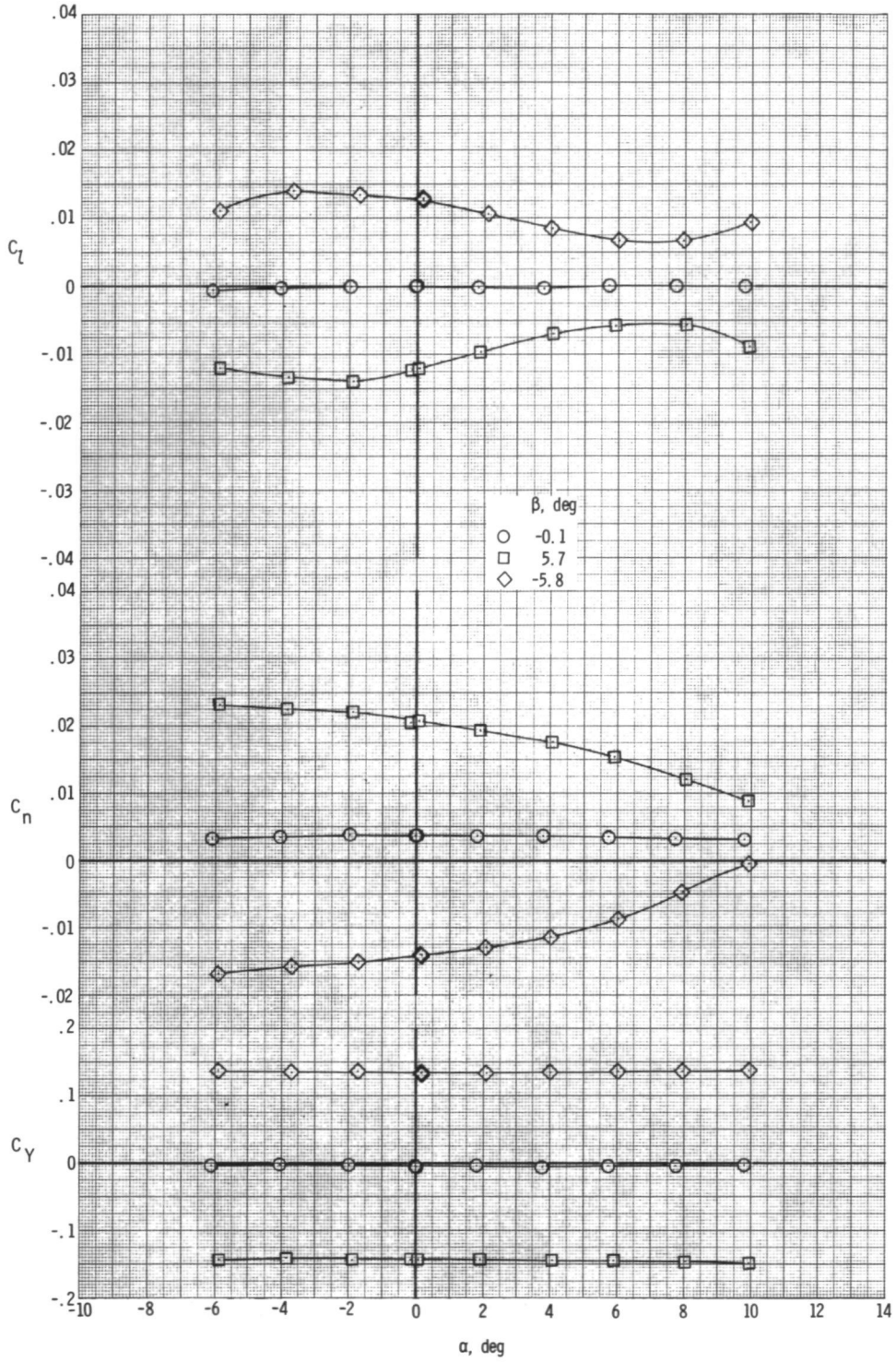

(f) M = 1.30.

Figure 14.- Concluded.

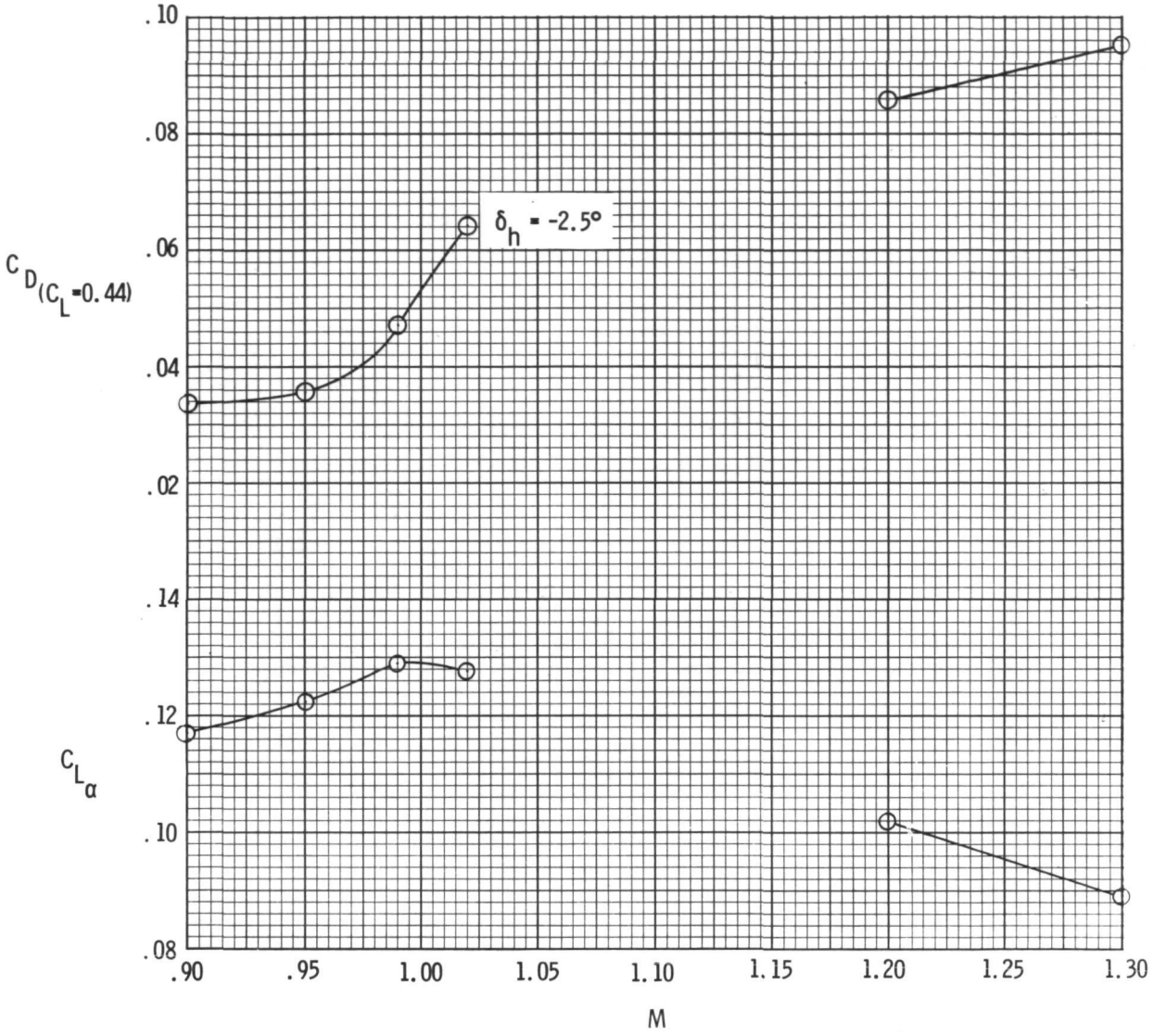

Figure 15.- Variation with Mach number of drag coefficient at a lift coefficient 0.44 and lift-curve slope.

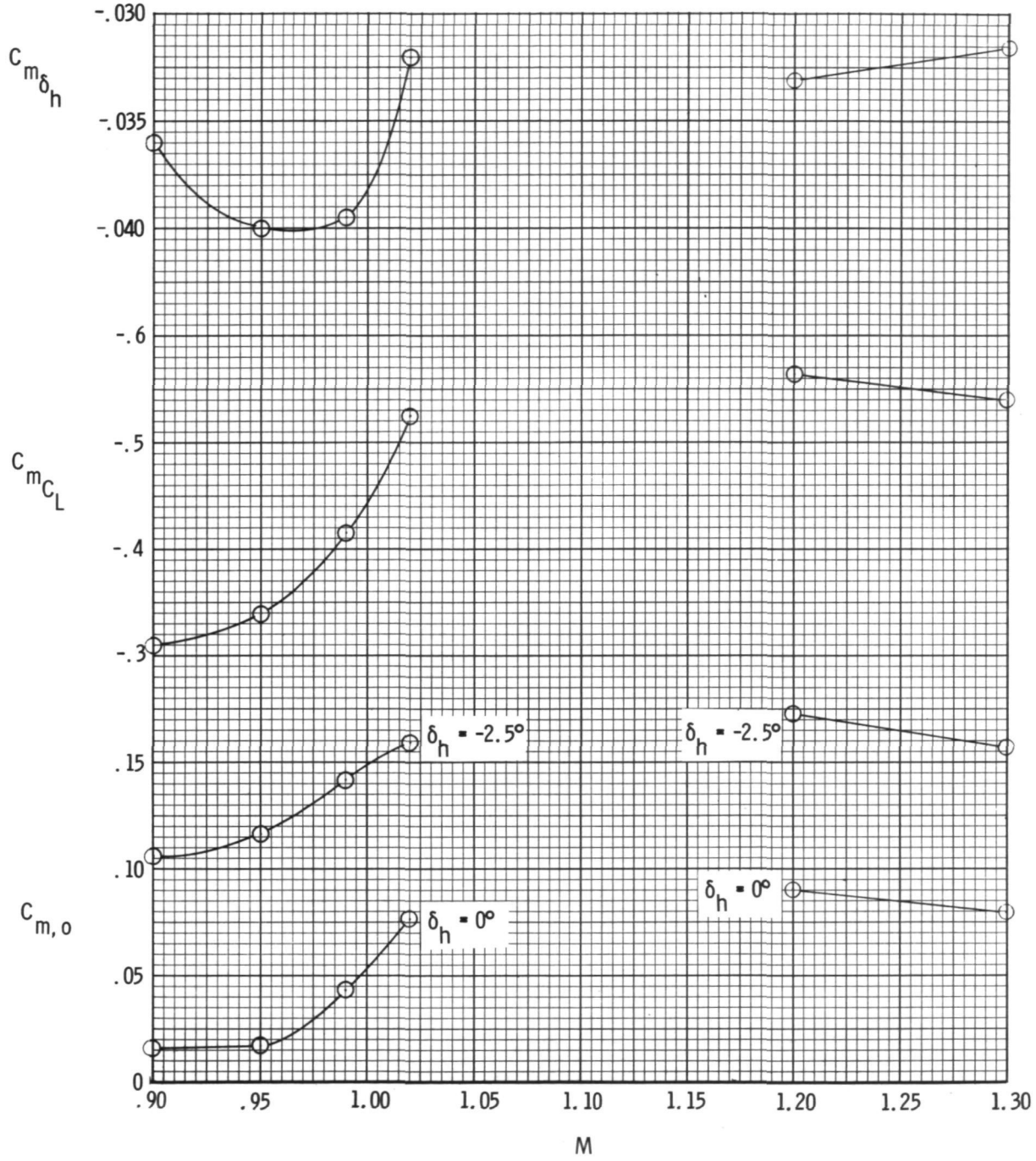

Figure 16.- Variation with Mach number of horizontal-tail effectiveness parameter, longitudinal stability derivative, and pitching-moment coefficient at zero lift.

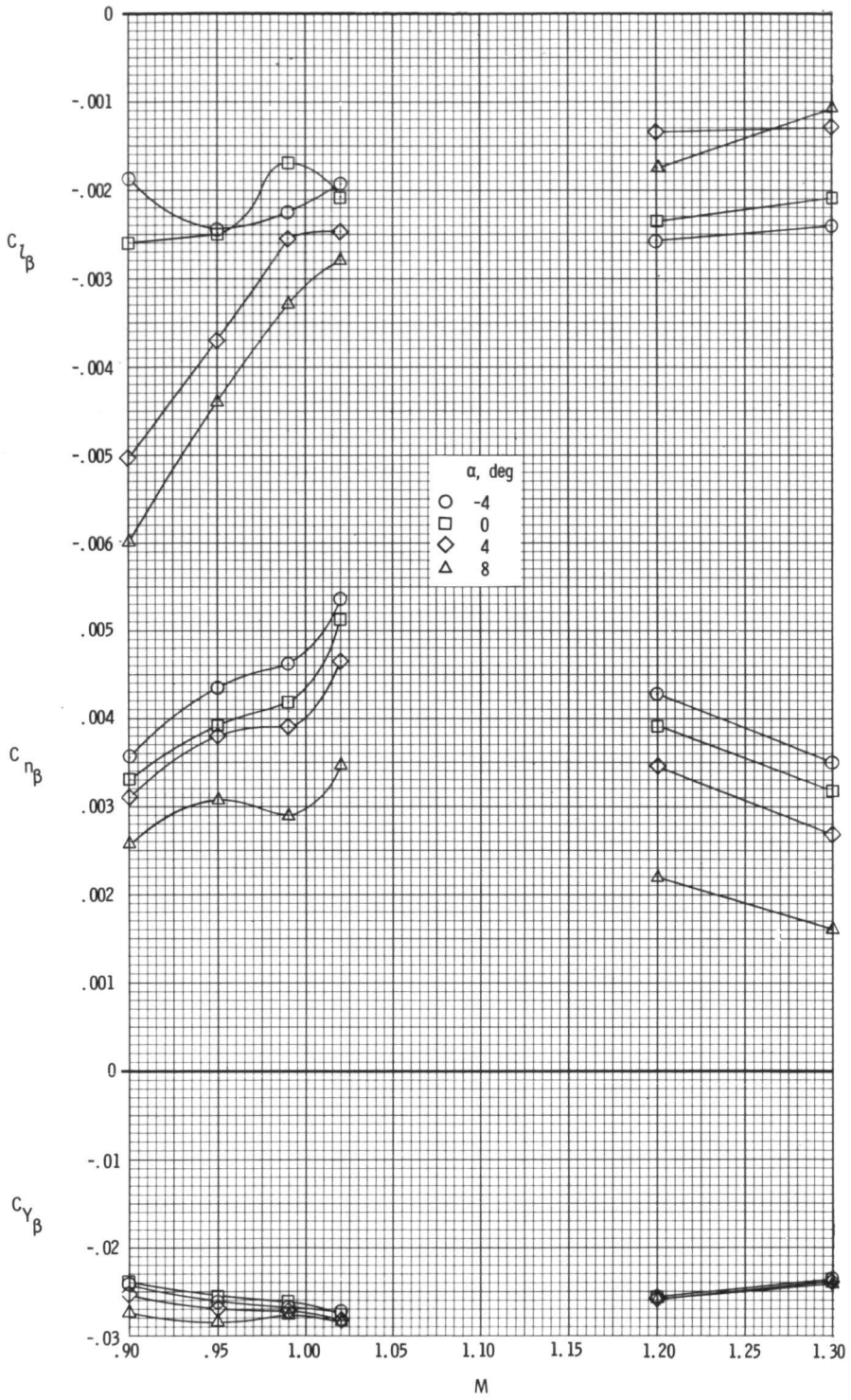

Figure 17.- Variation with Mach number of model lateral-directional stability characteristics at four angles of attack. $\delta_h = 0^o$.

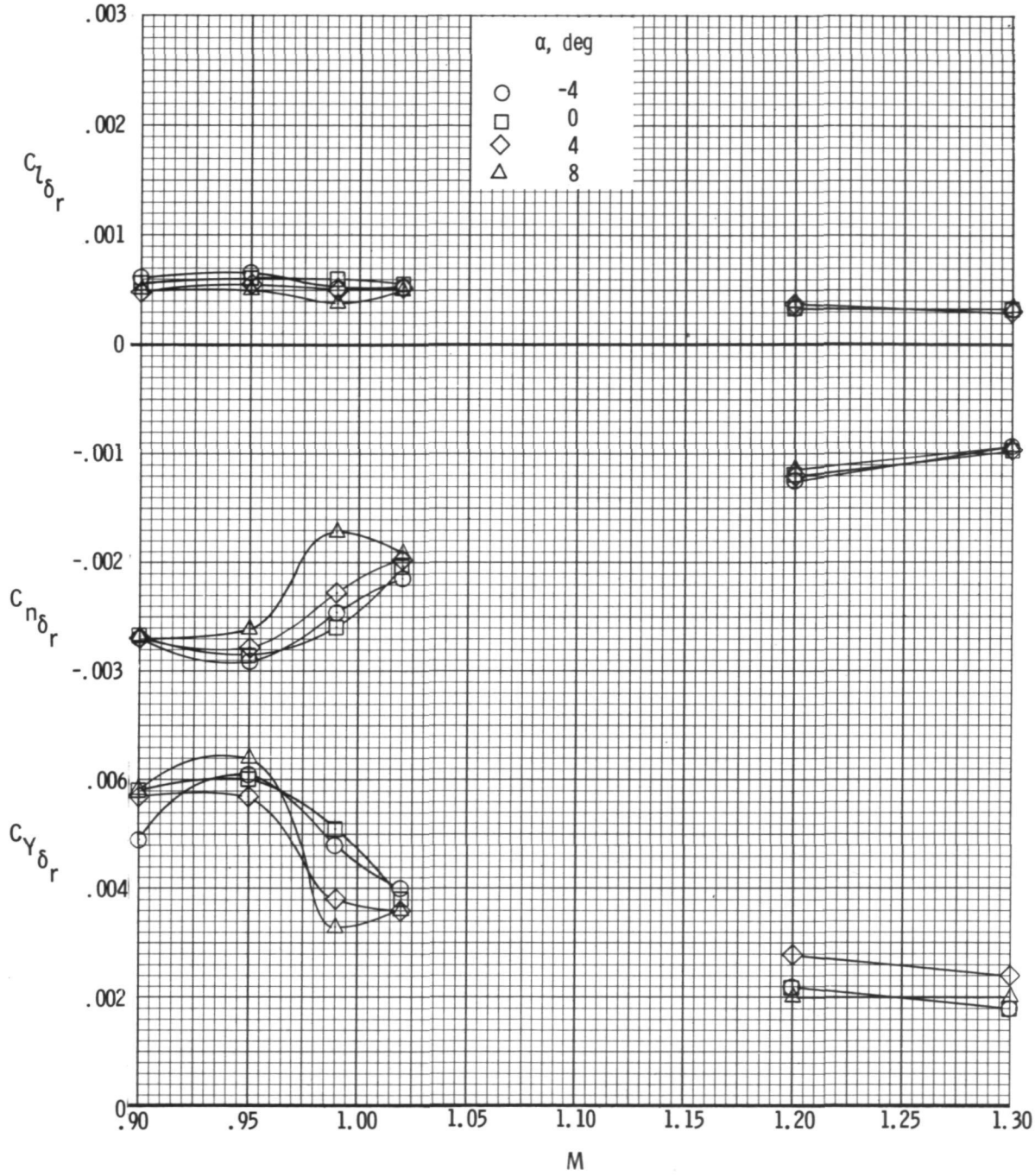

Figure 18.- Variation with Mach number of effect of rudder deflection on lateral stability characteristics. $\delta_h = 0^o$.

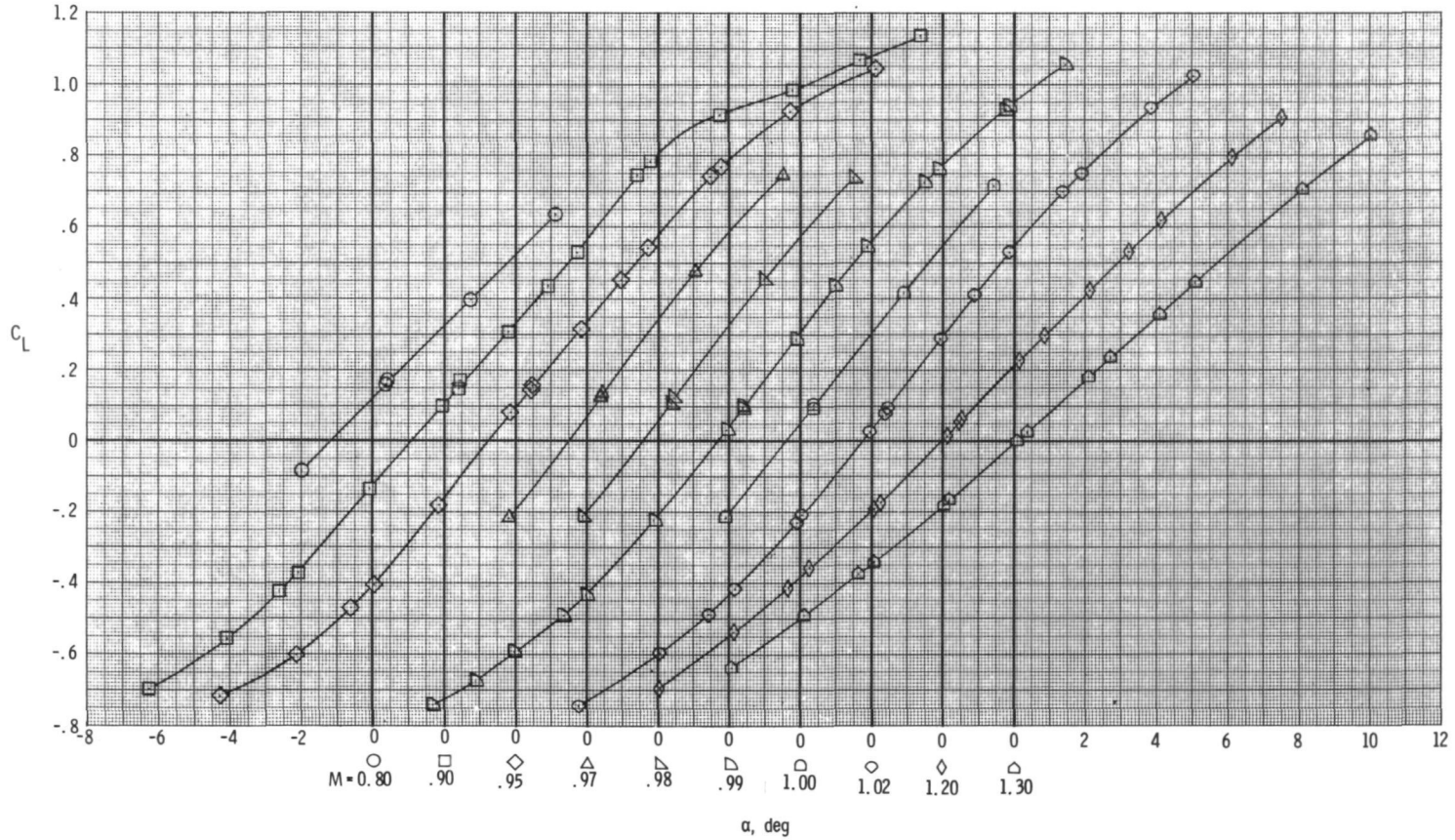

(a) $\delta_L = 15^o$.

Figure 19.- Variation of model lift coefficient with angle of attack for left aileron deflection. $\delta_h = -2.5^o$.

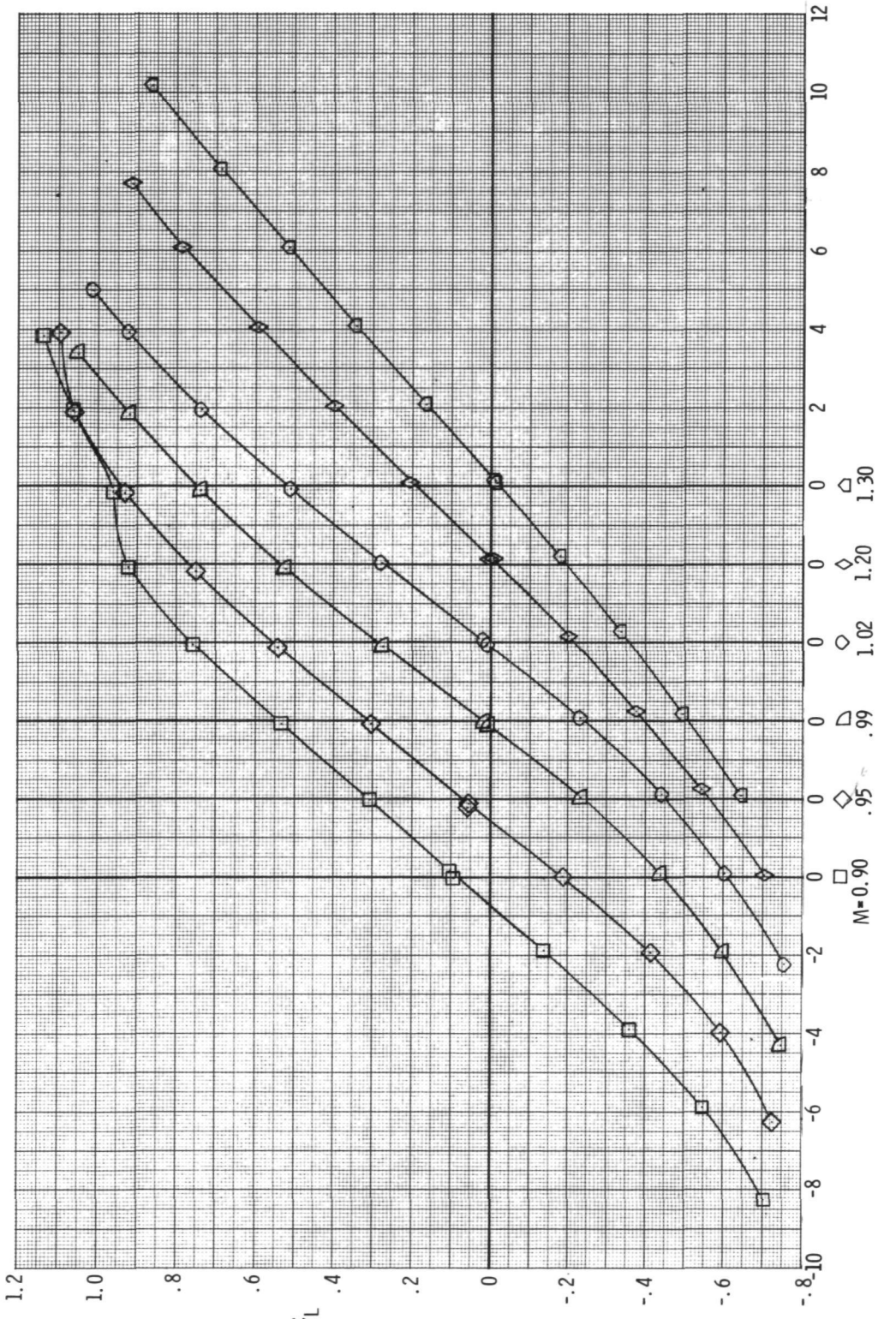

(b) $\delta_L = 10^o$.

Figure 19.- Continued.

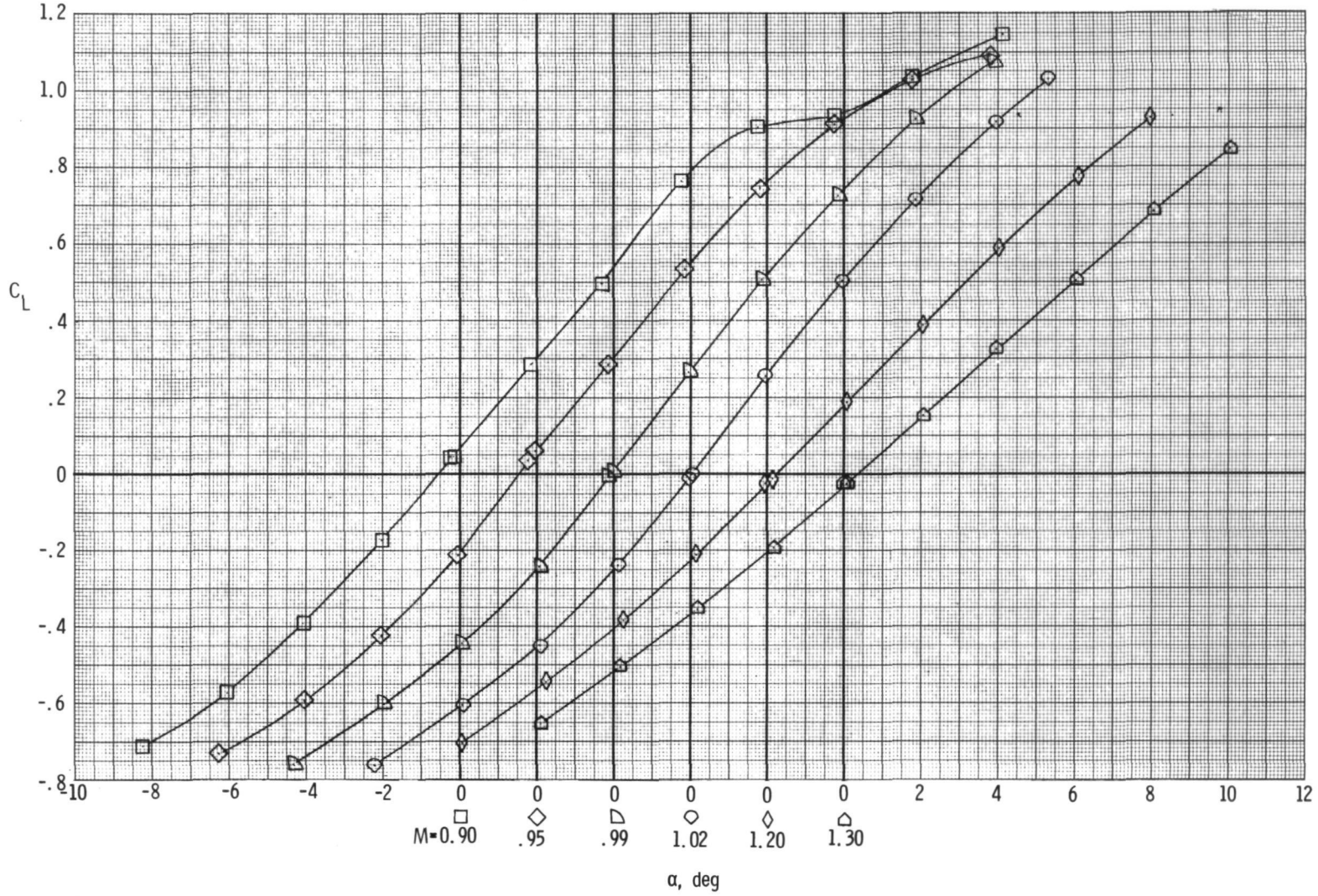

(c) $\delta_L = 5^o$.

Figure 19.- Continued.

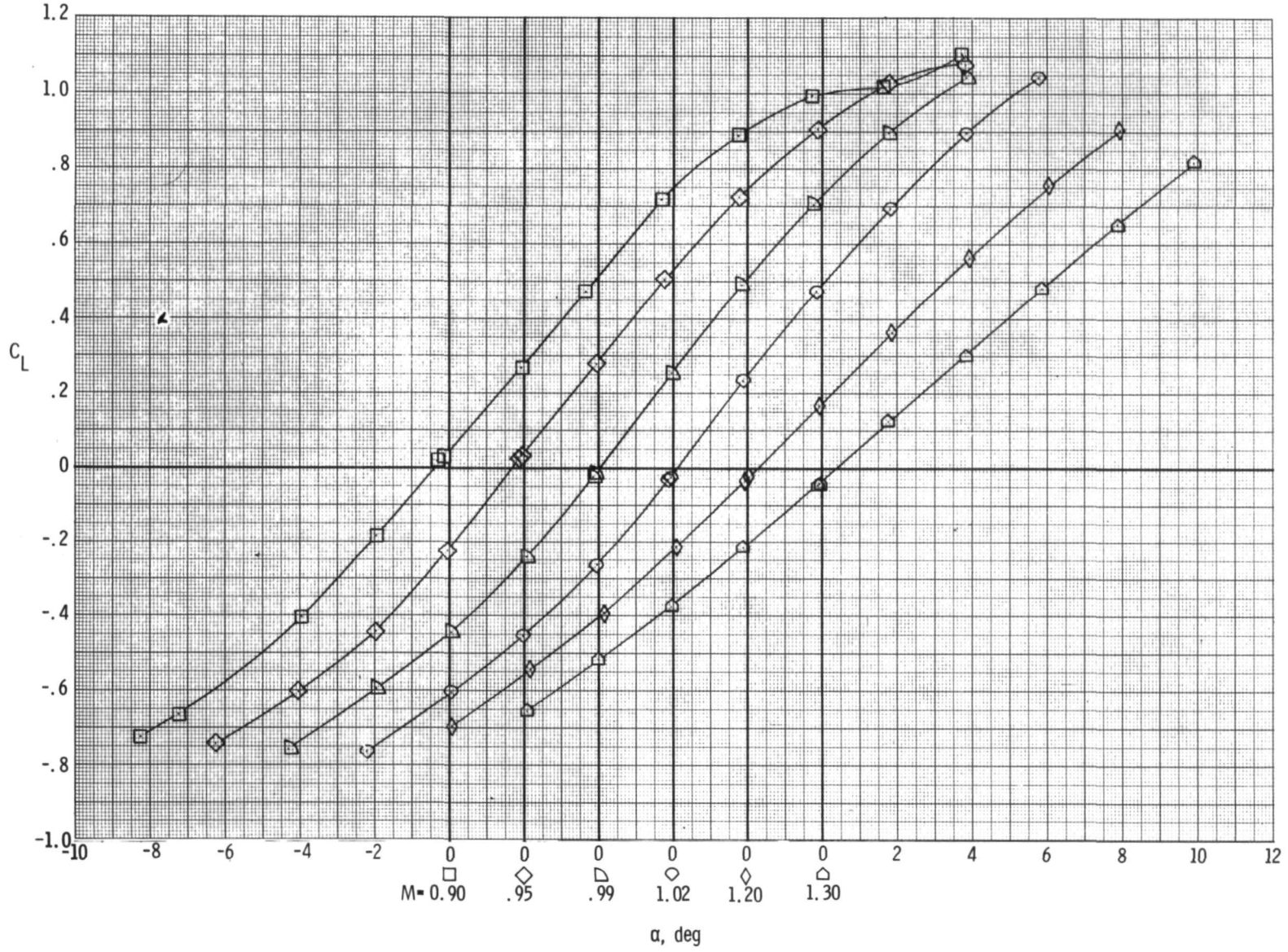

(d) $\delta_L = 0^o$.

Figure 19.- Continued.

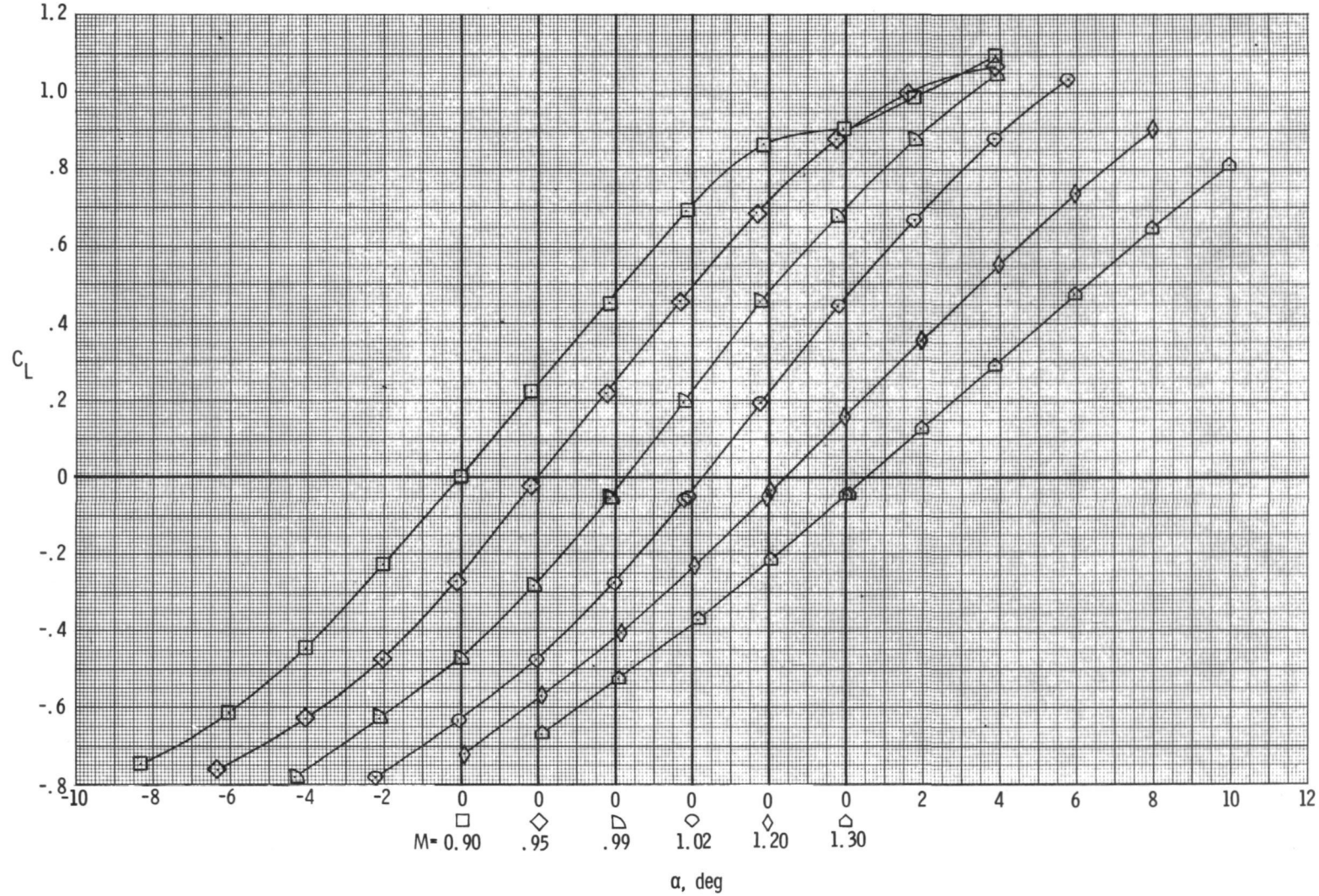

(e) $\delta_L = -5^o$.

Figure 19.- Continued.

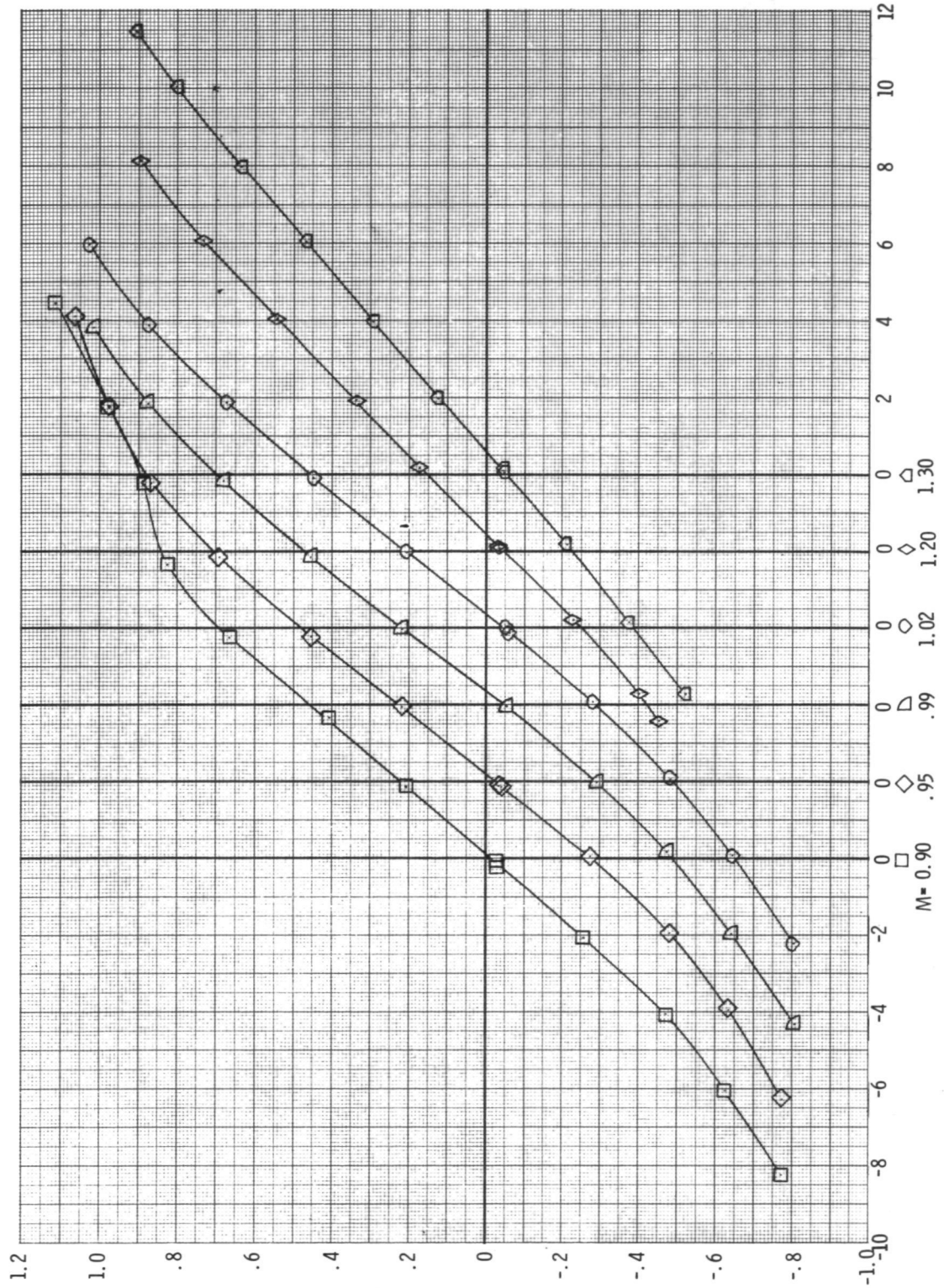

(f) $\delta_L = -10^o$.

Figure 19.- Continued.

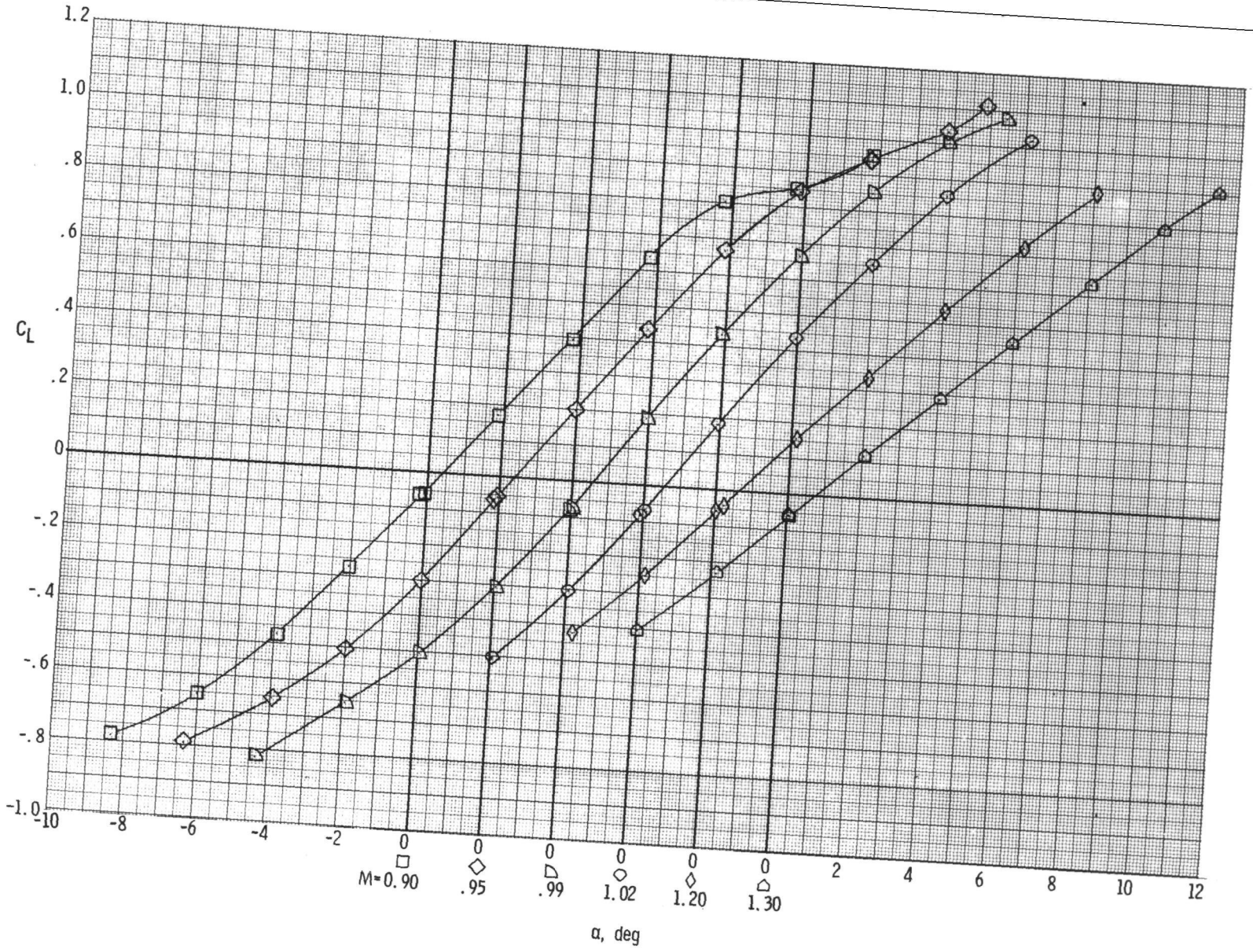

(g) $\delta_L = -15^o$.

Figure 19.- Concluded.

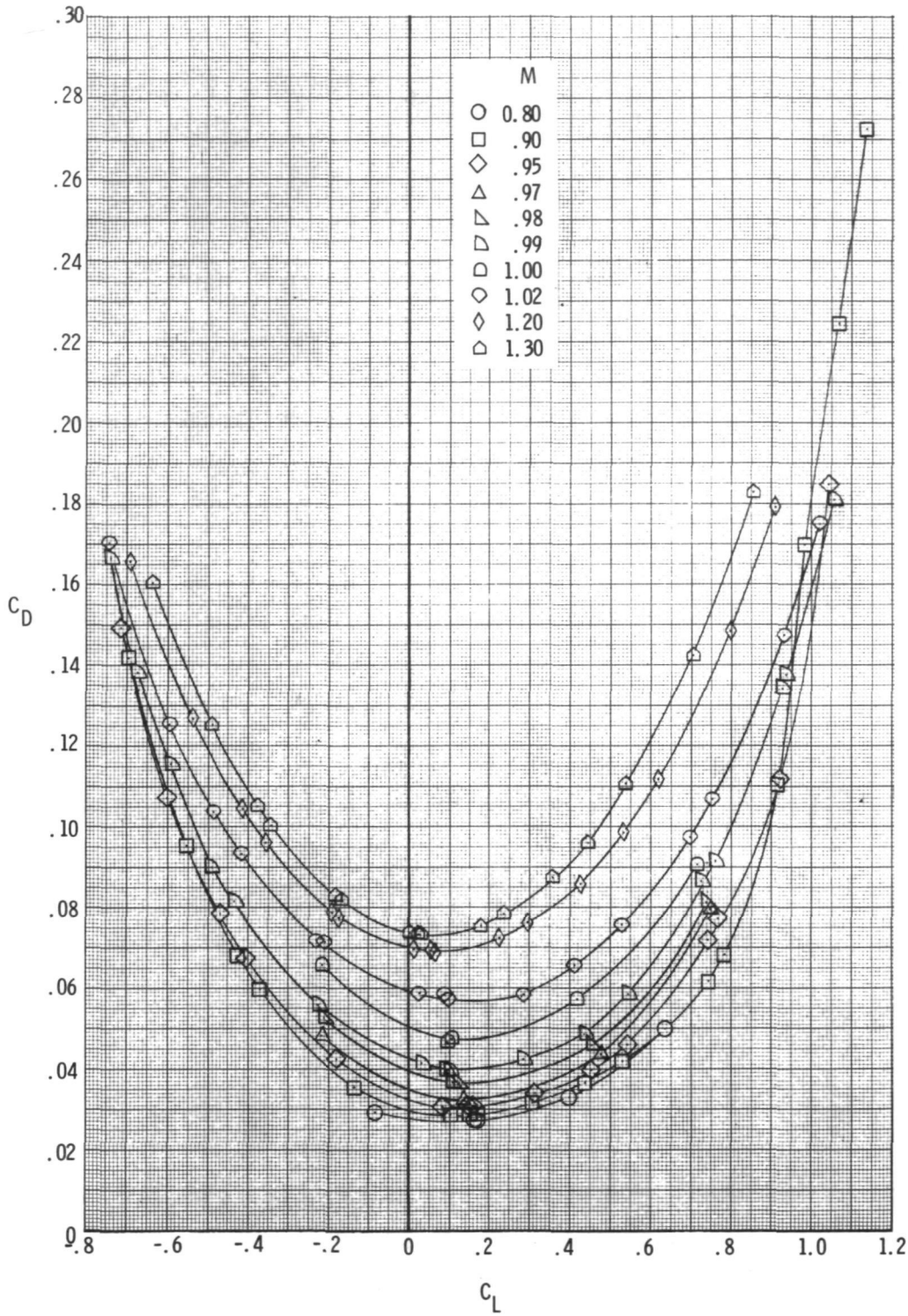

(a) $\delta_L = 15^o$.

Figure 20.- Variation of model drag coefficient with lift coefficient for left aileron deflection. $\delta_h = -2.5^o$.

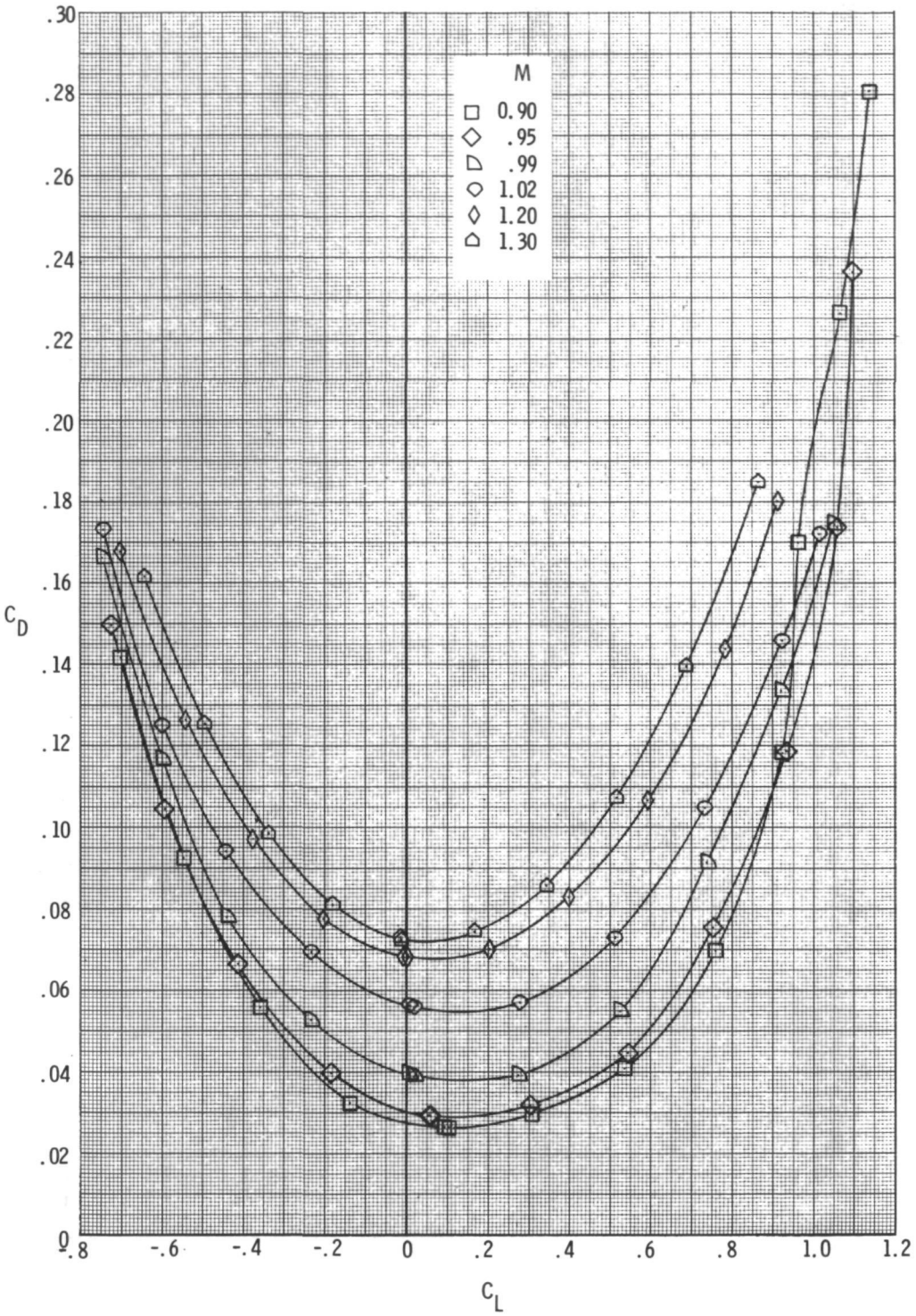

(b) $\delta_L = 10^o$.

Figure 20.- Continued.

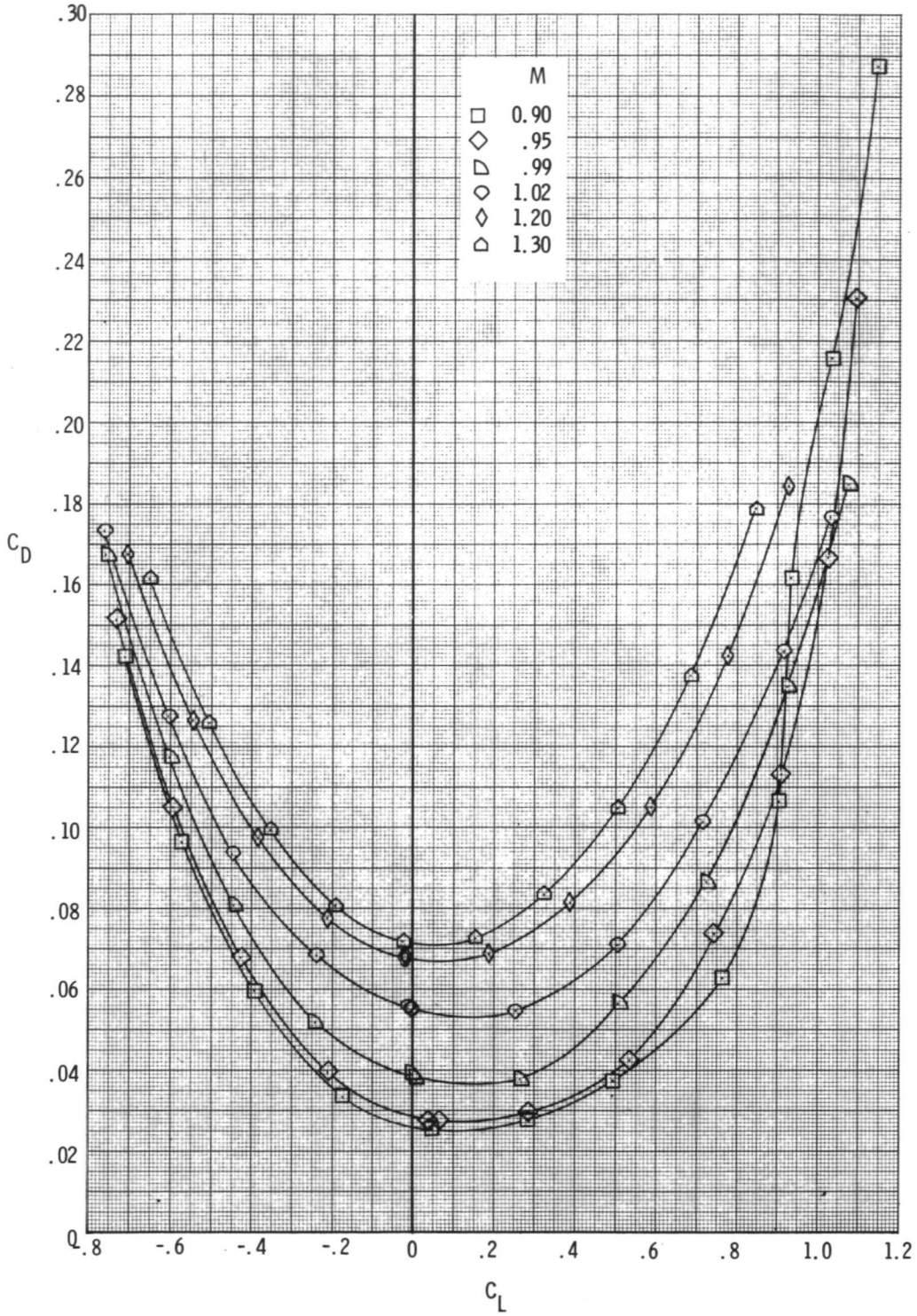

(c) $\delta_L = 5^o$.

Figure 20.- Continued.

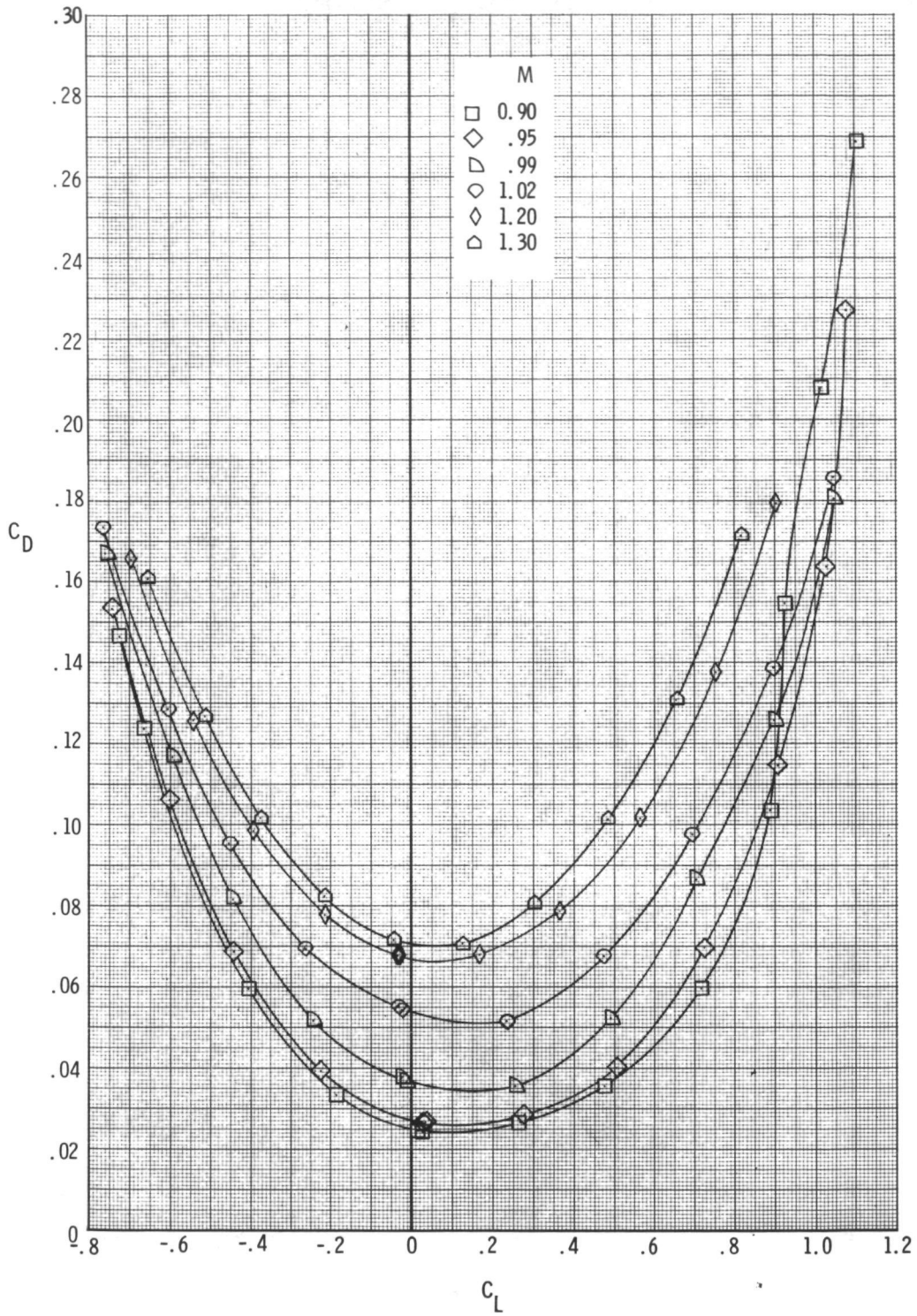

(d) $\delta_L = 0^o$.

Figure 20.- Continued.

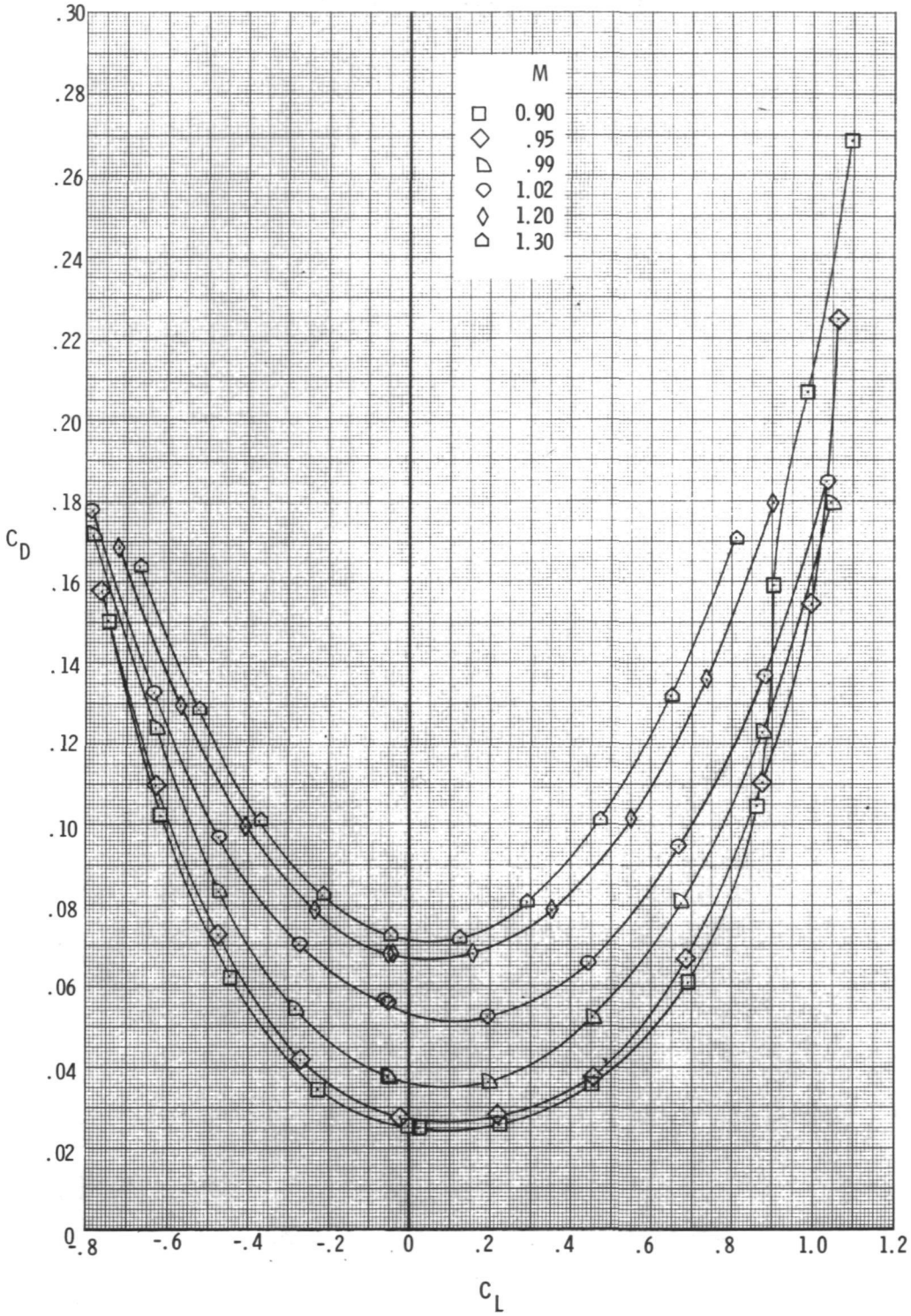

(e) $\delta_L = -5^o$.

Figure 20.- Continued.

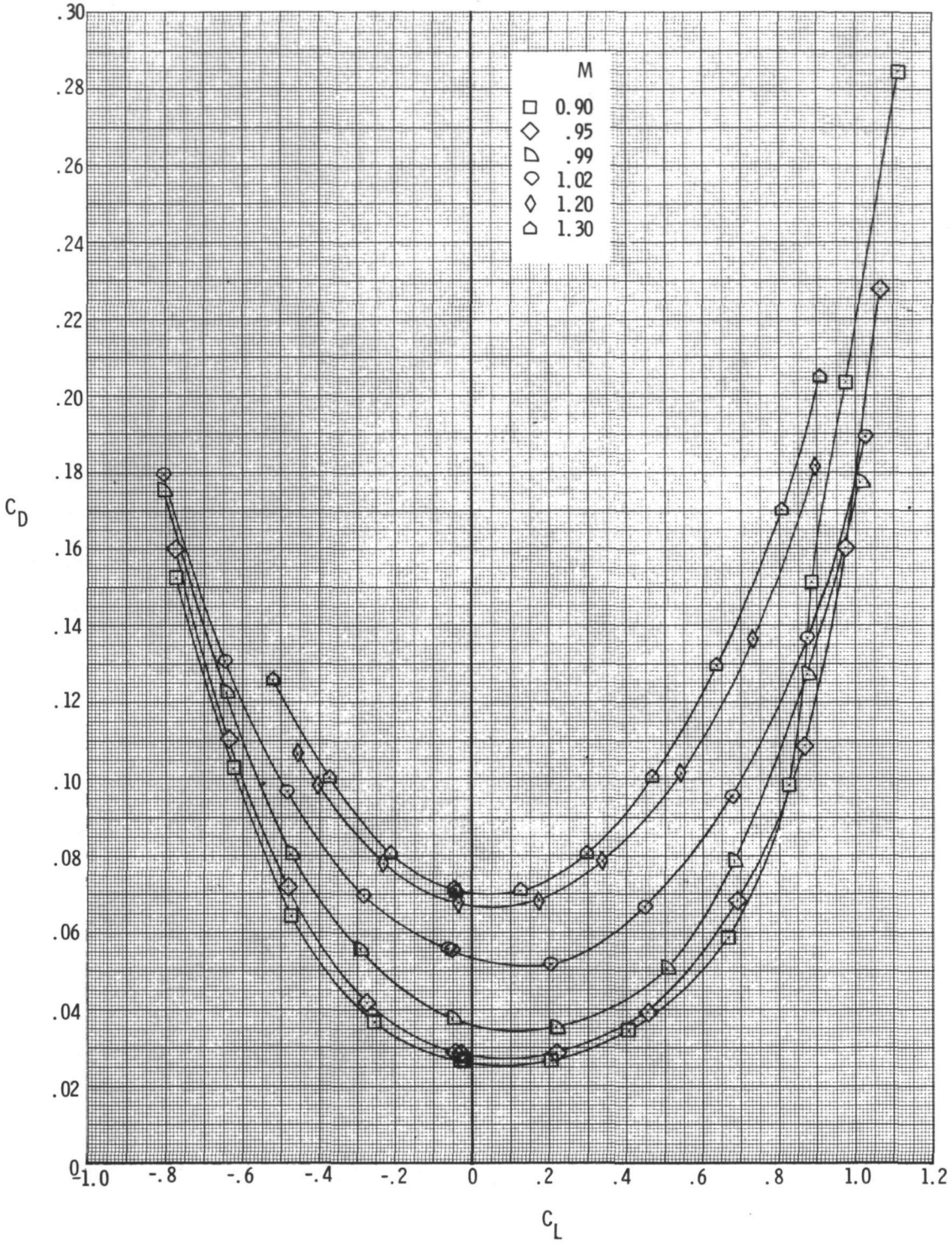

(f) $\delta_L = -10^o$.

Figure 20.- Continued.

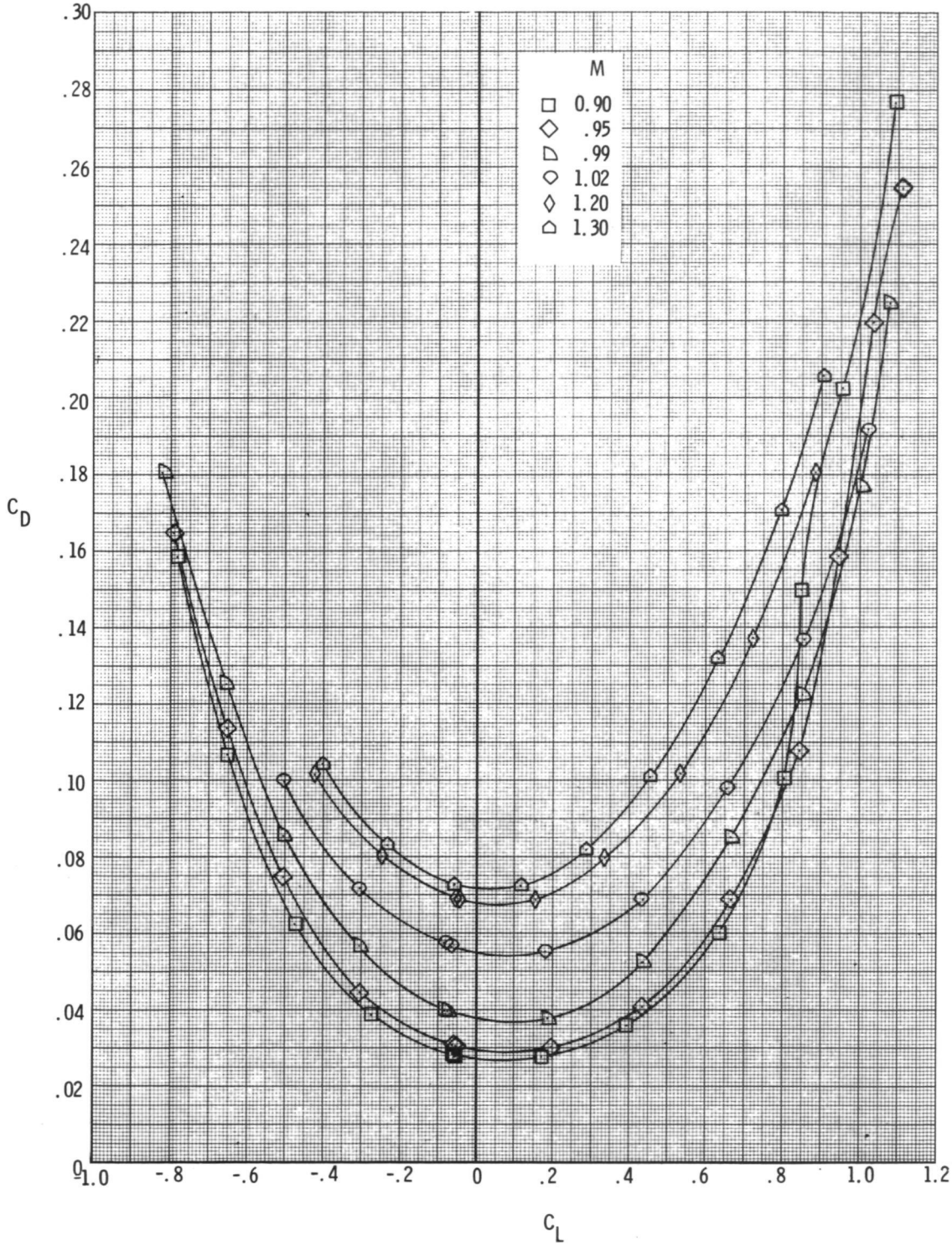

(g) $\delta_L = -15^o$.

Figure 20.- Concluded.

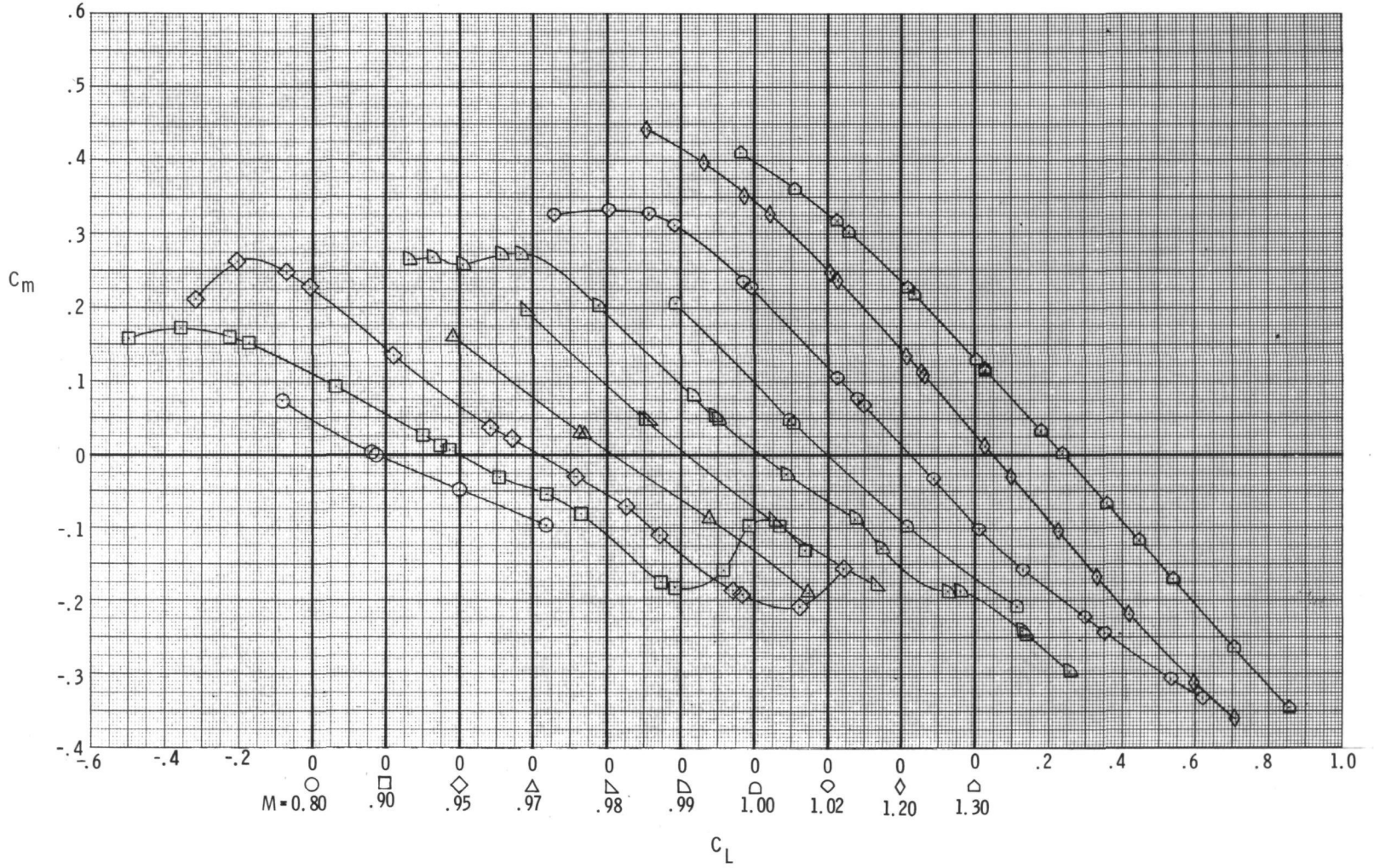

(a) $\delta_L = 15^o$.

Figure 21.- Variation of model pitching-moment coefficient with lift coefficient for left aileron deflection. $\delta_h = -2.5^o$.

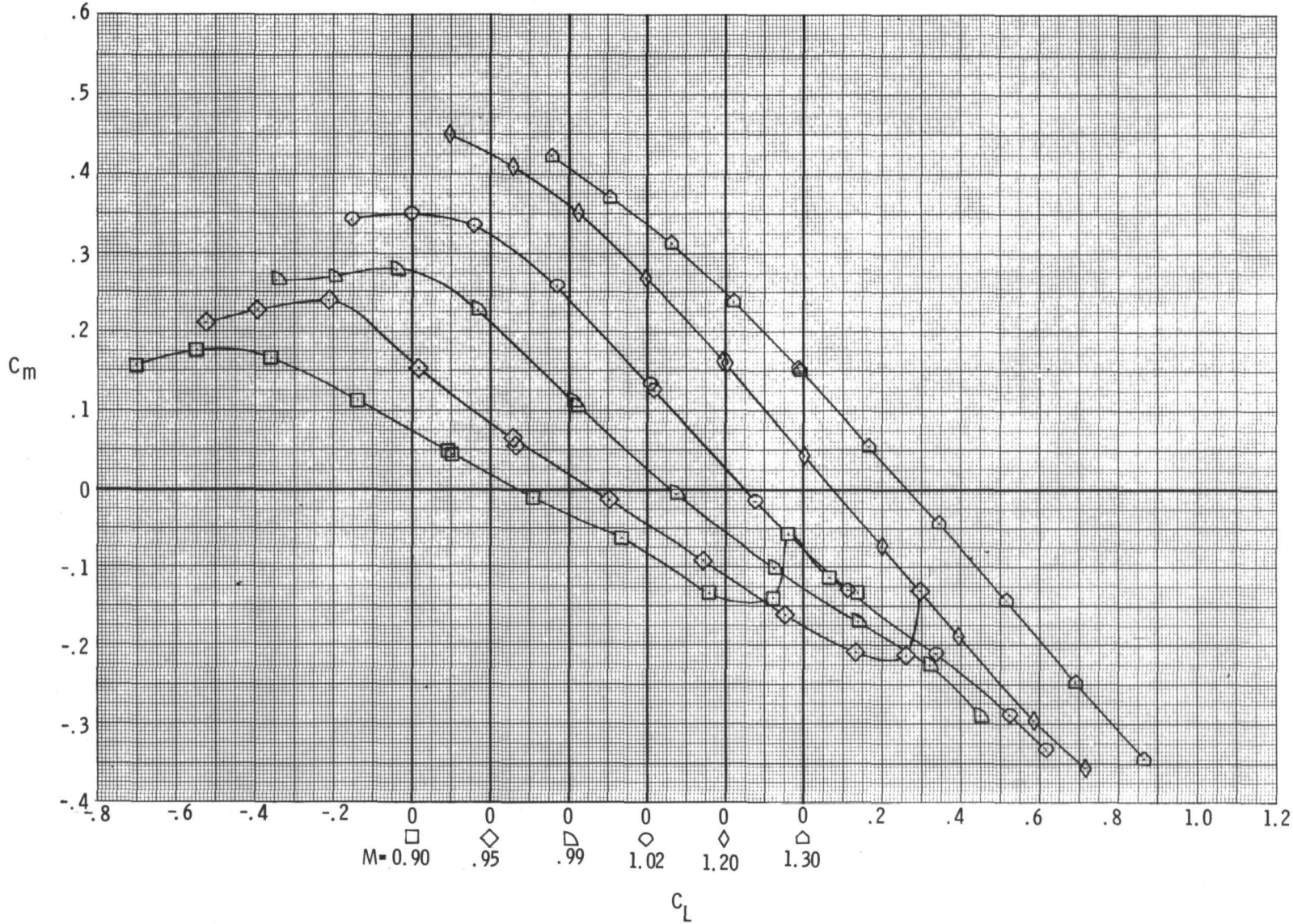

(b) $\delta_L = 10^o$.

Figure 21.- Continued.

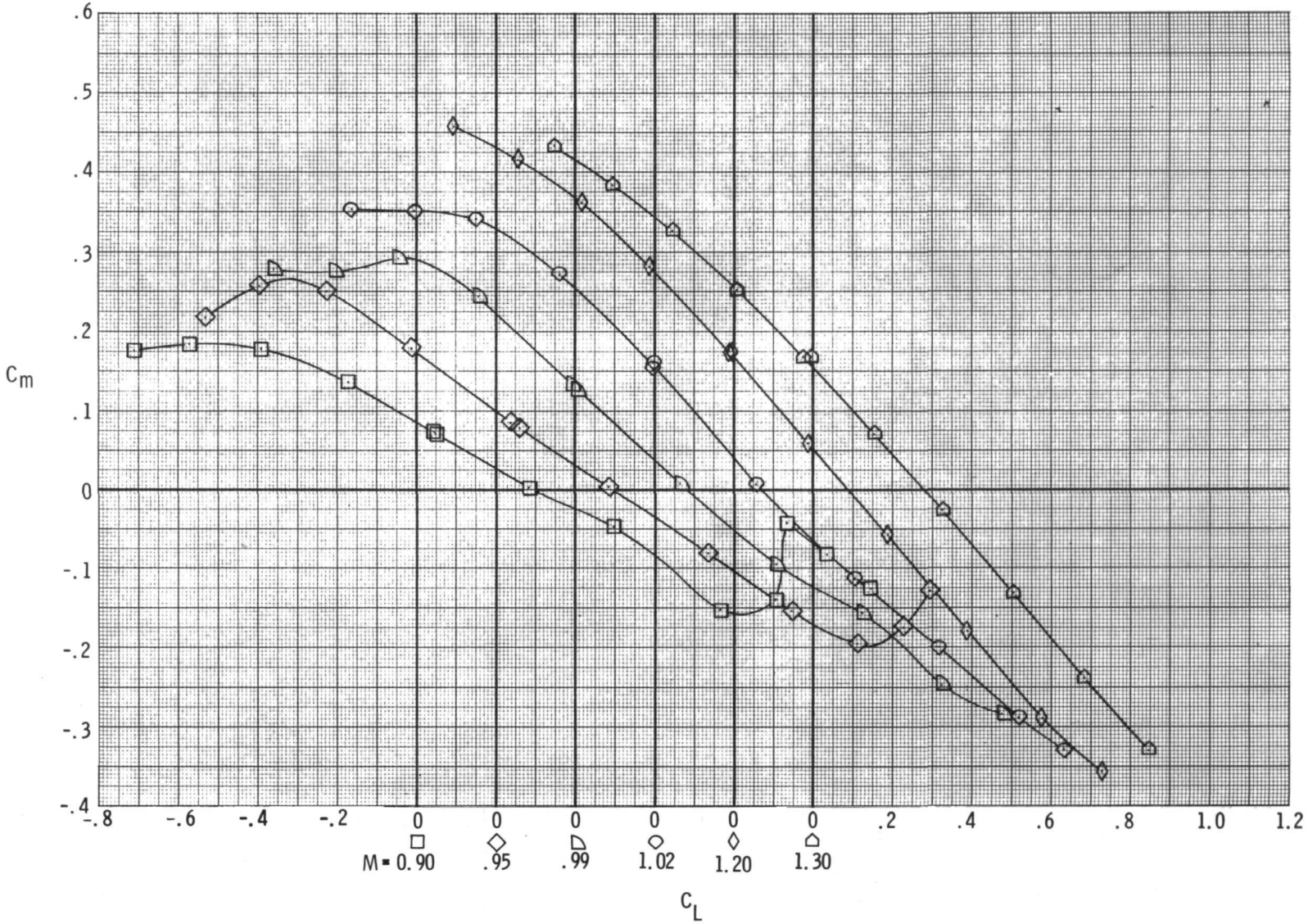

(c) $\delta_L = 5^o$.

Figure 21.- Continued.

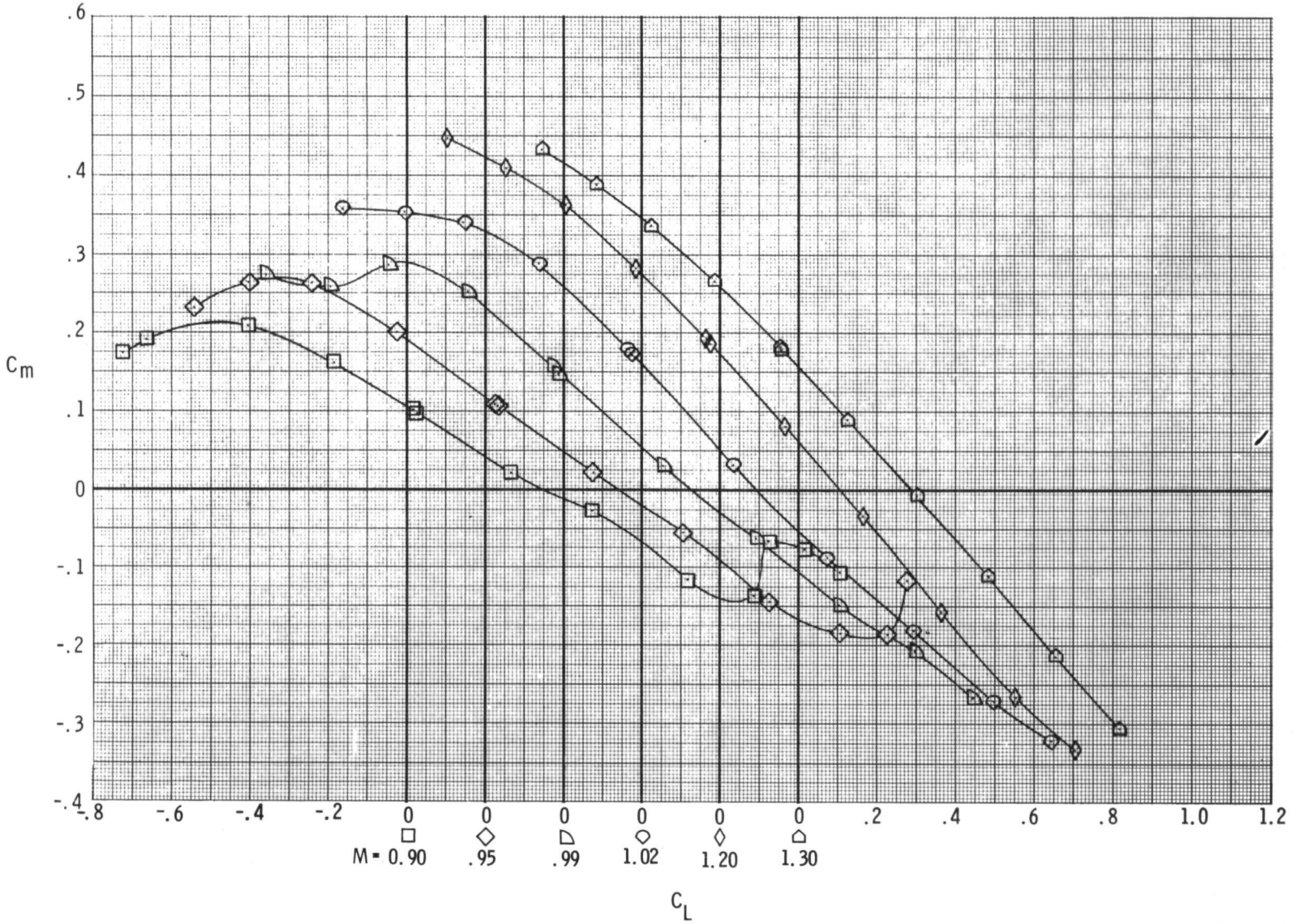

(d) $\delta_L = 0^O$

Figure 21.- Continued.

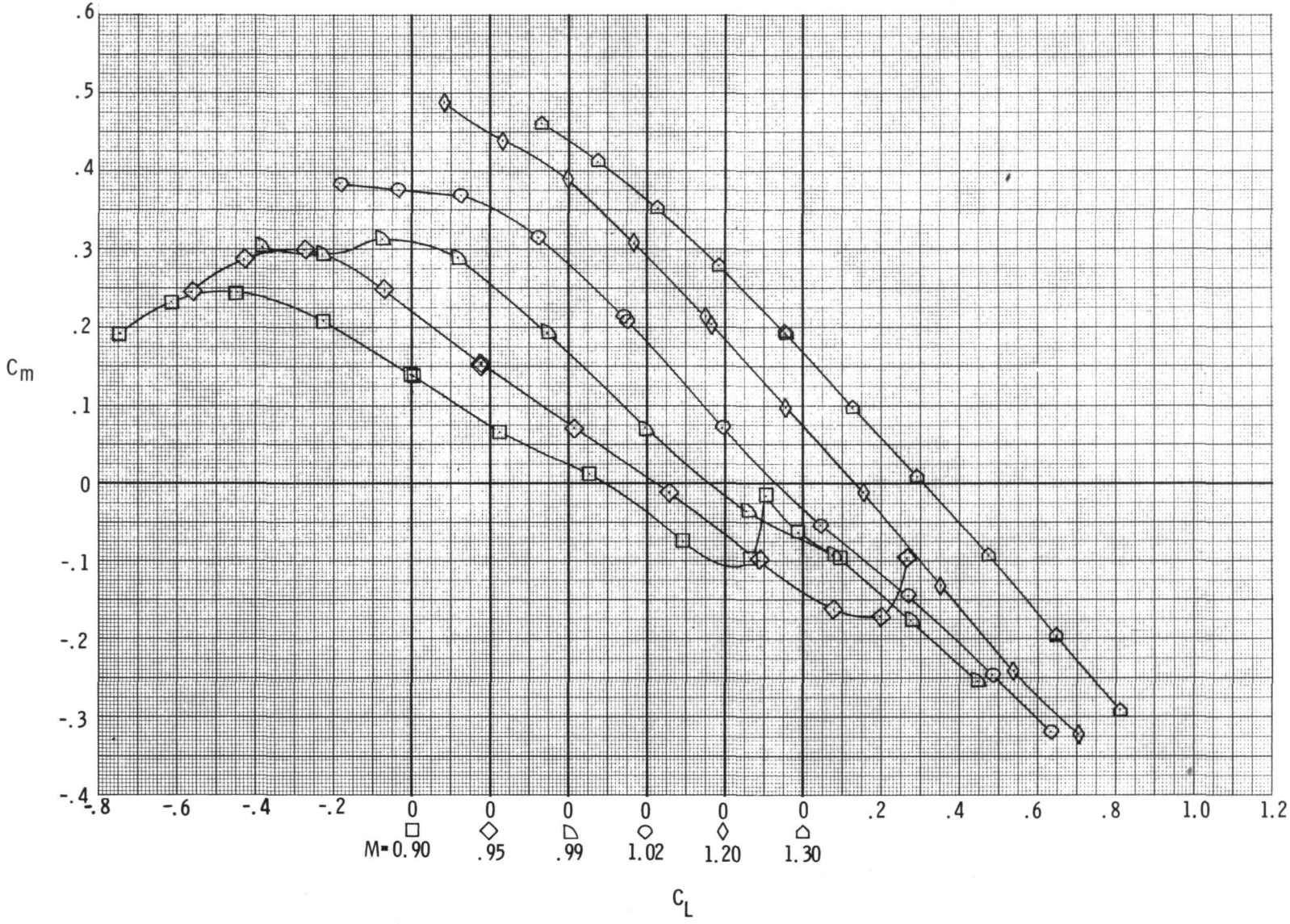

(e) $\delta_L = -5^o$.

Figure 21.- Continued.

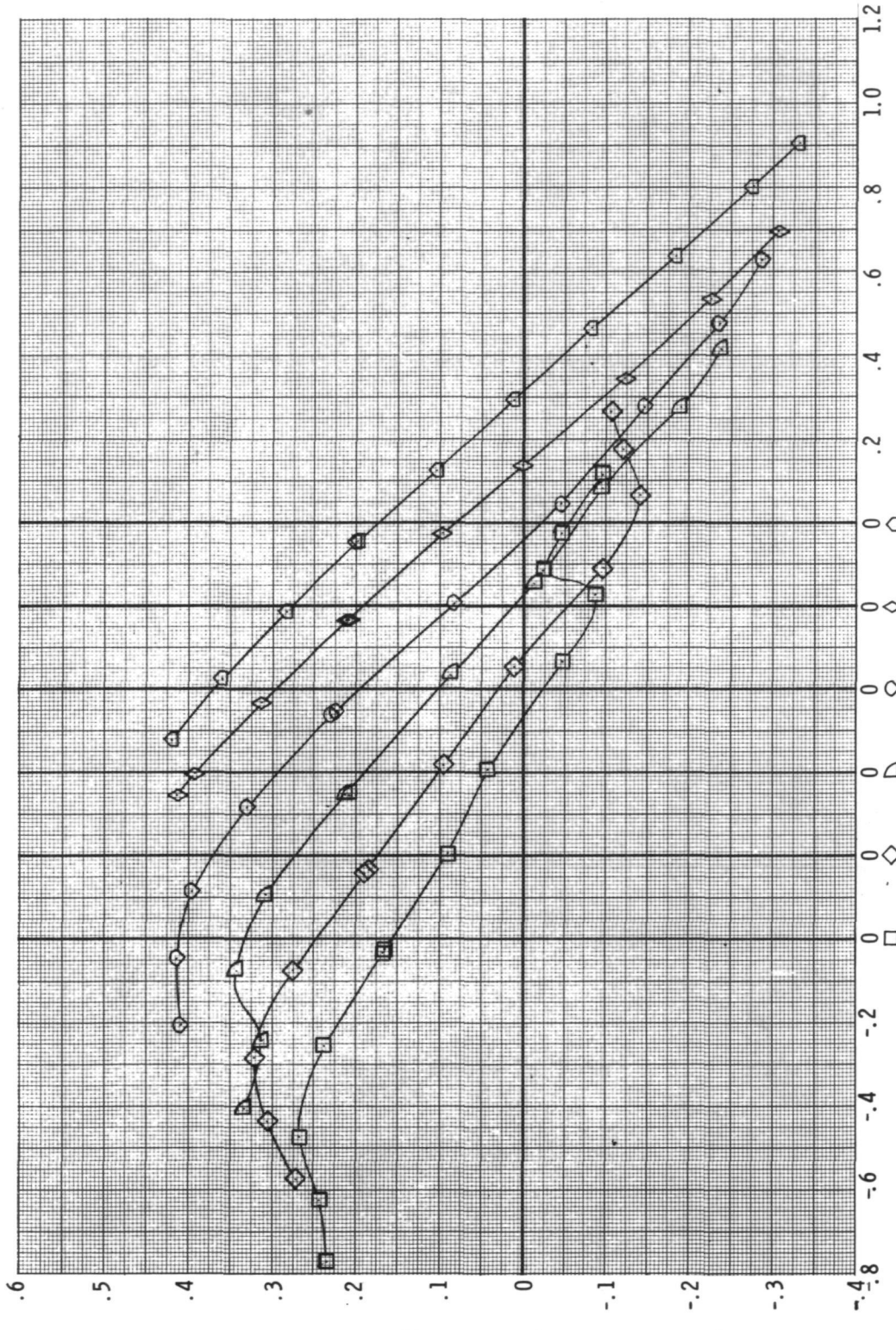

(f) $\delta_L = -10^\circ$.

Figure 21.- Continued.

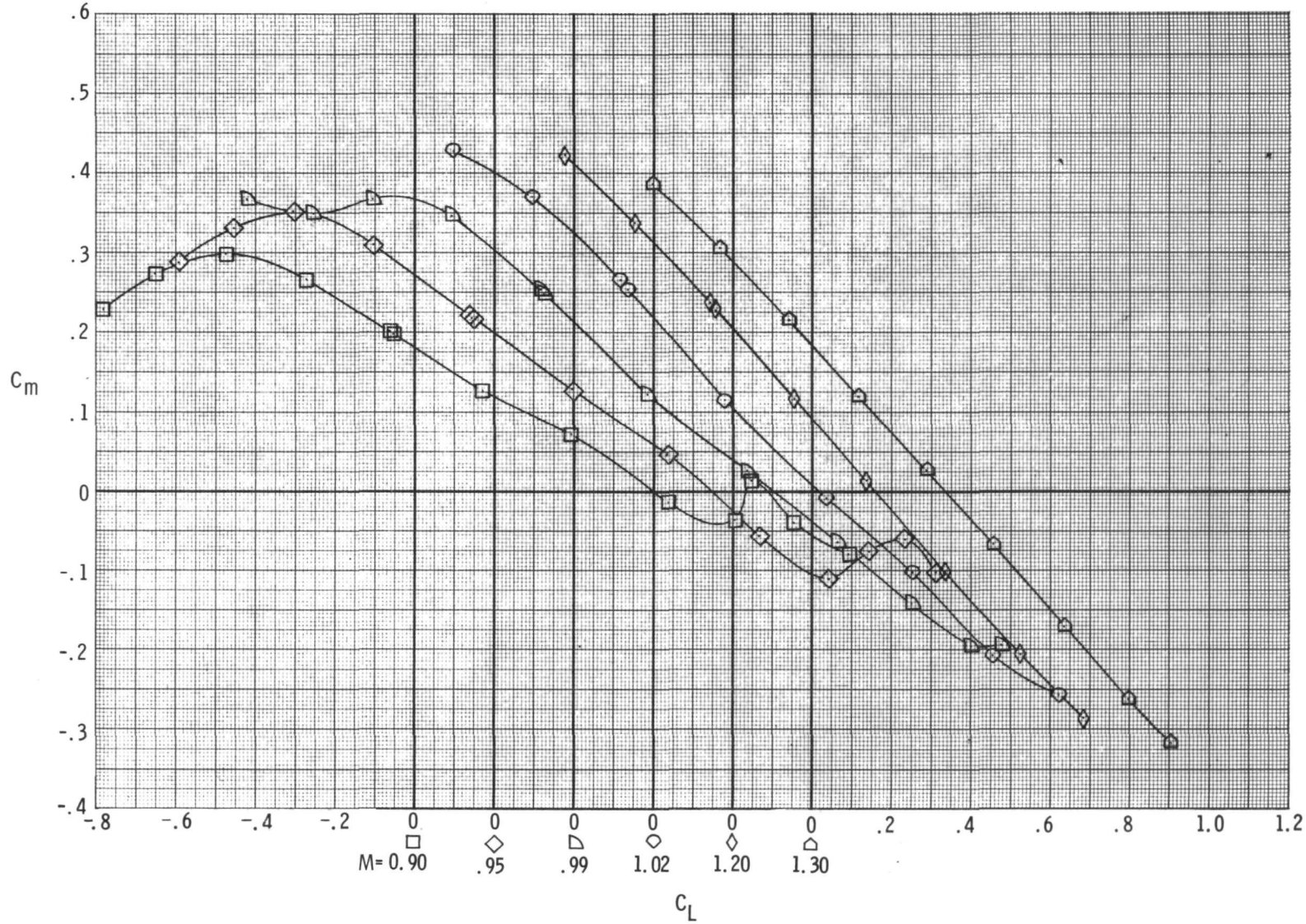

(g) $\delta_L = -15^o$.

Figure 21.- Concluded.

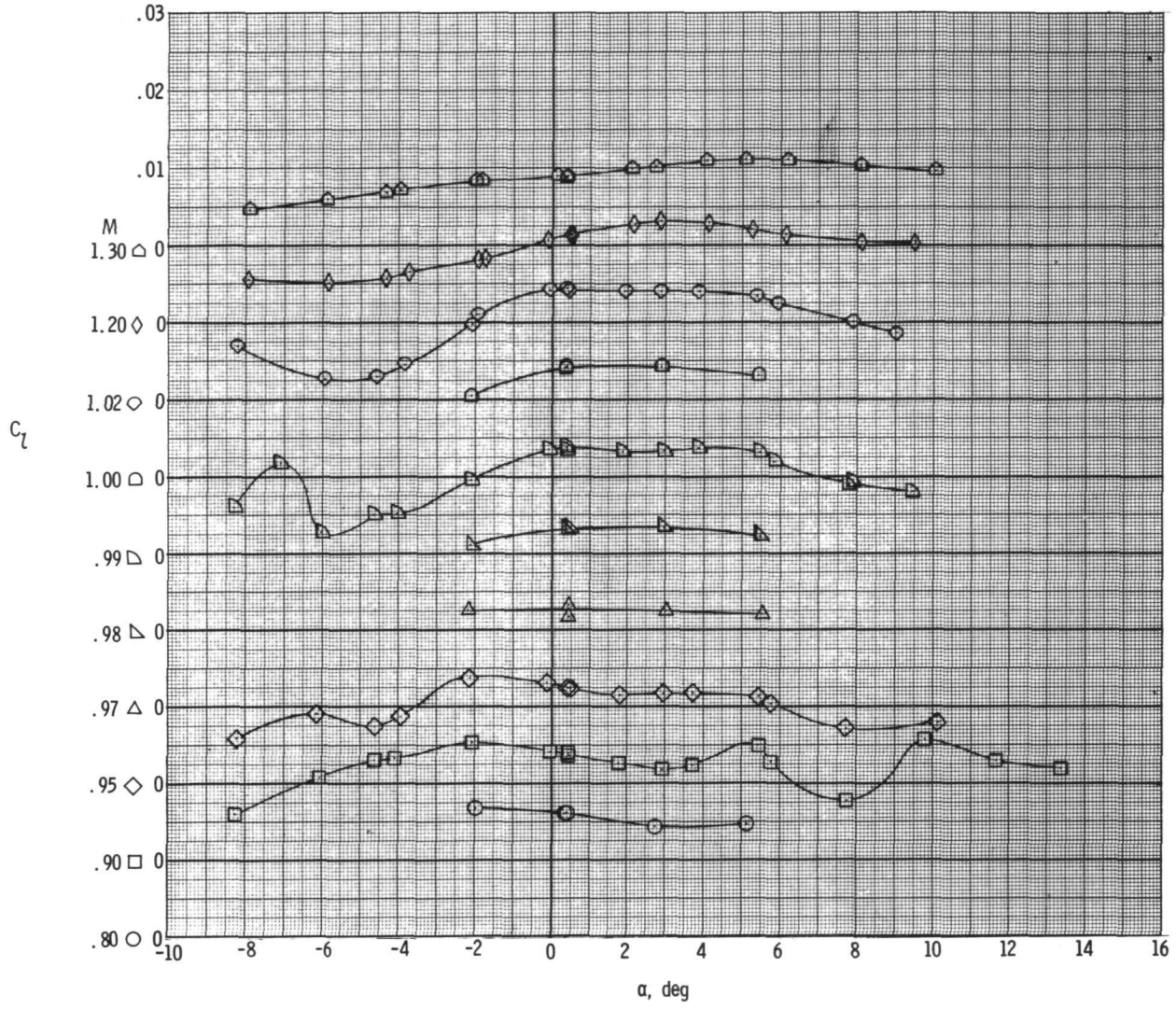

(a) $\delta_L = 15^o$.

Figure 22.- Variation of model rolling-moment coefficient with angle of attack for left aileron deflection. $\delta_h = -2.5^o$.

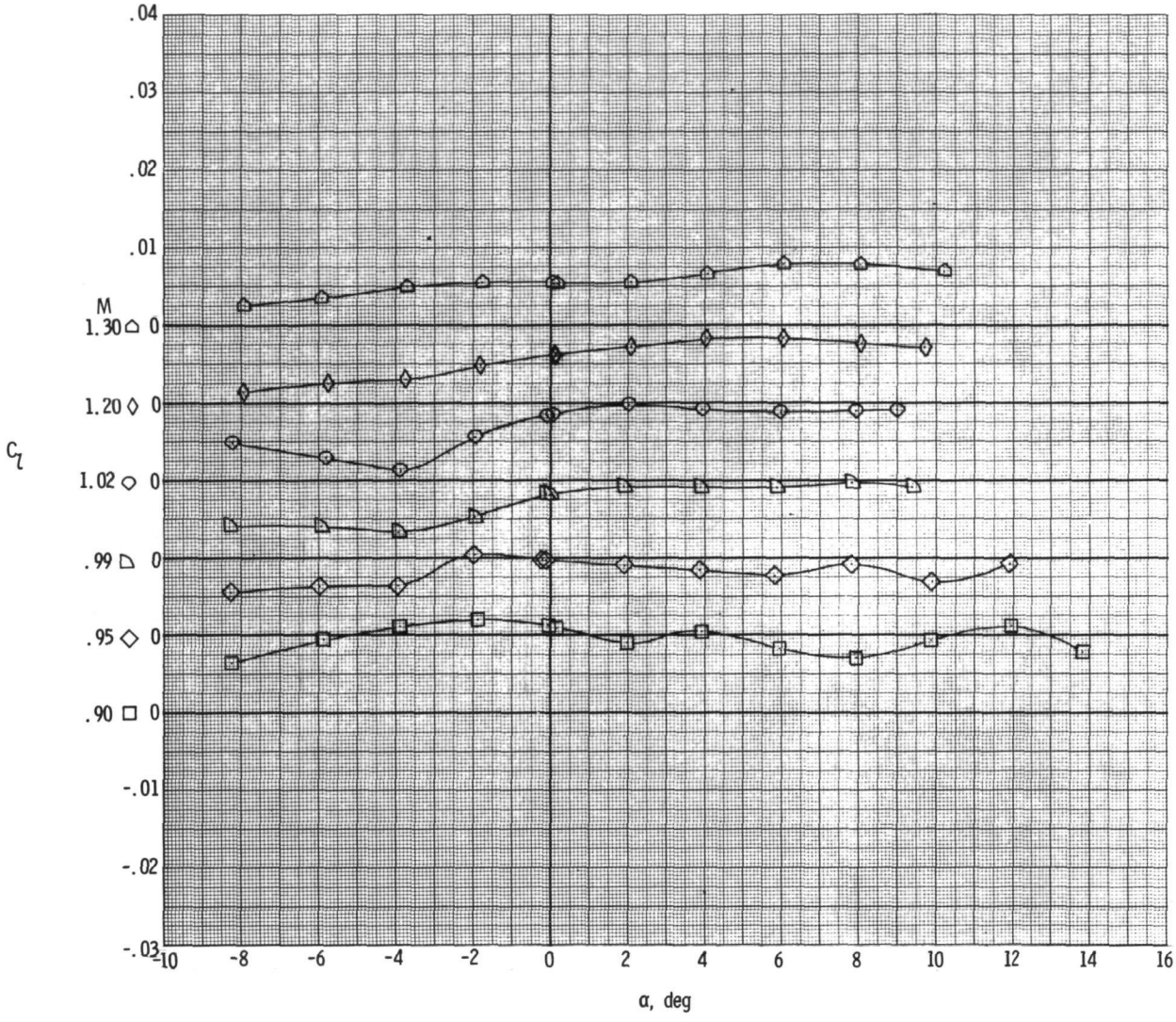

(b) $\delta_L = 10^o$.

Figure 22.- Continued.

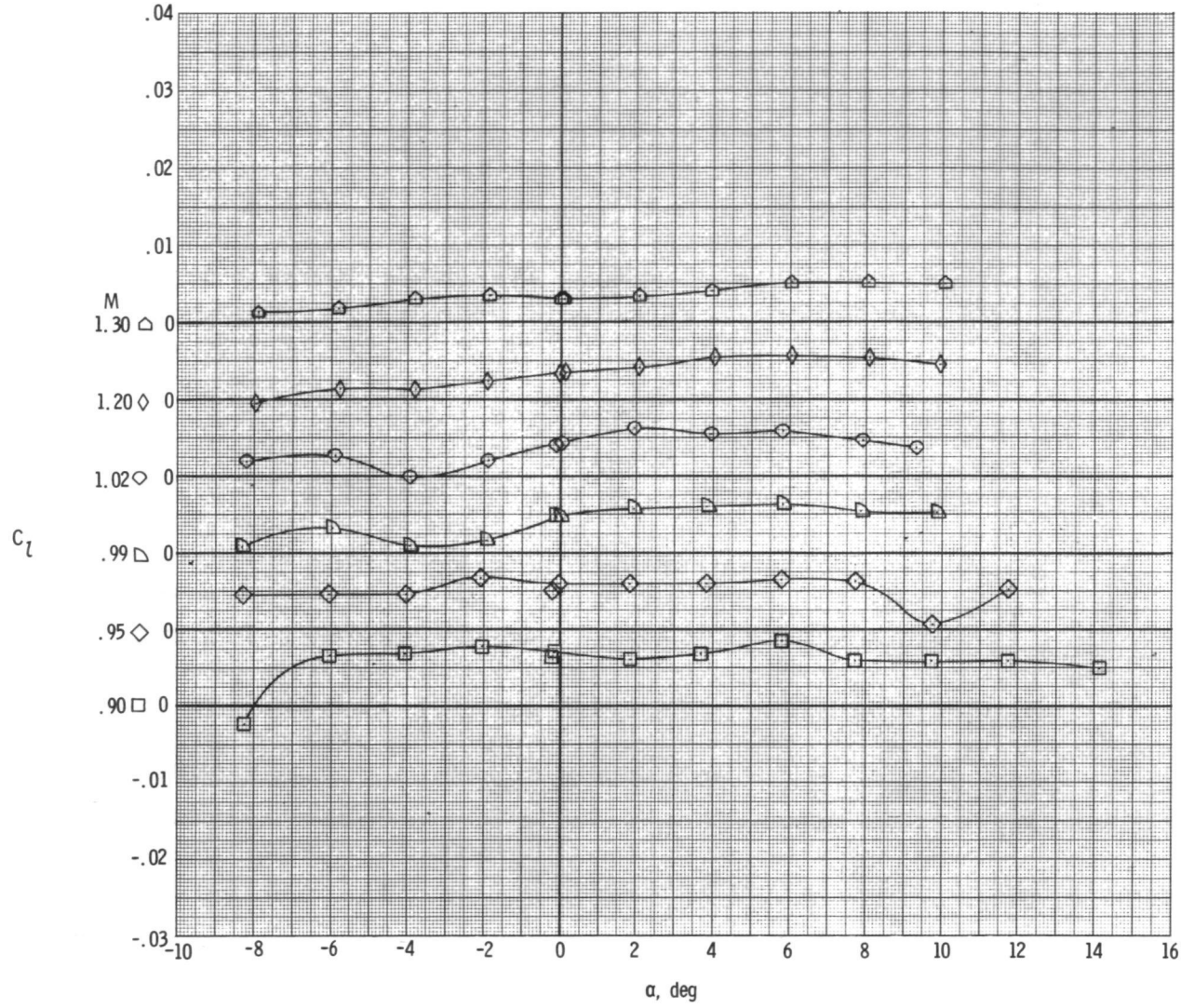

(c) $\delta_L = 5^o$.

Figure 22.- Continued.

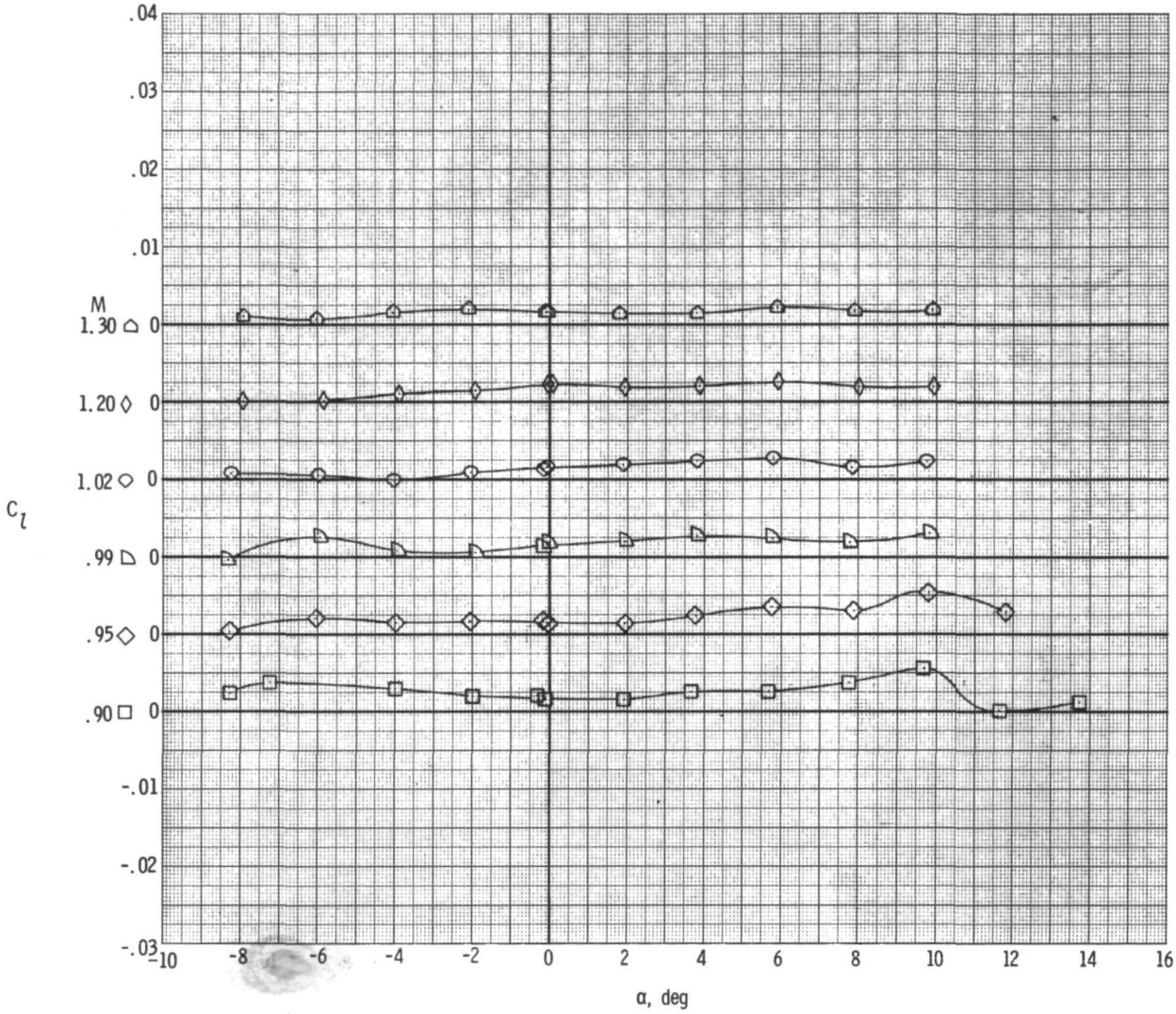

(d) $\delta_L = 0^o$.

Figure 22.- Continued.

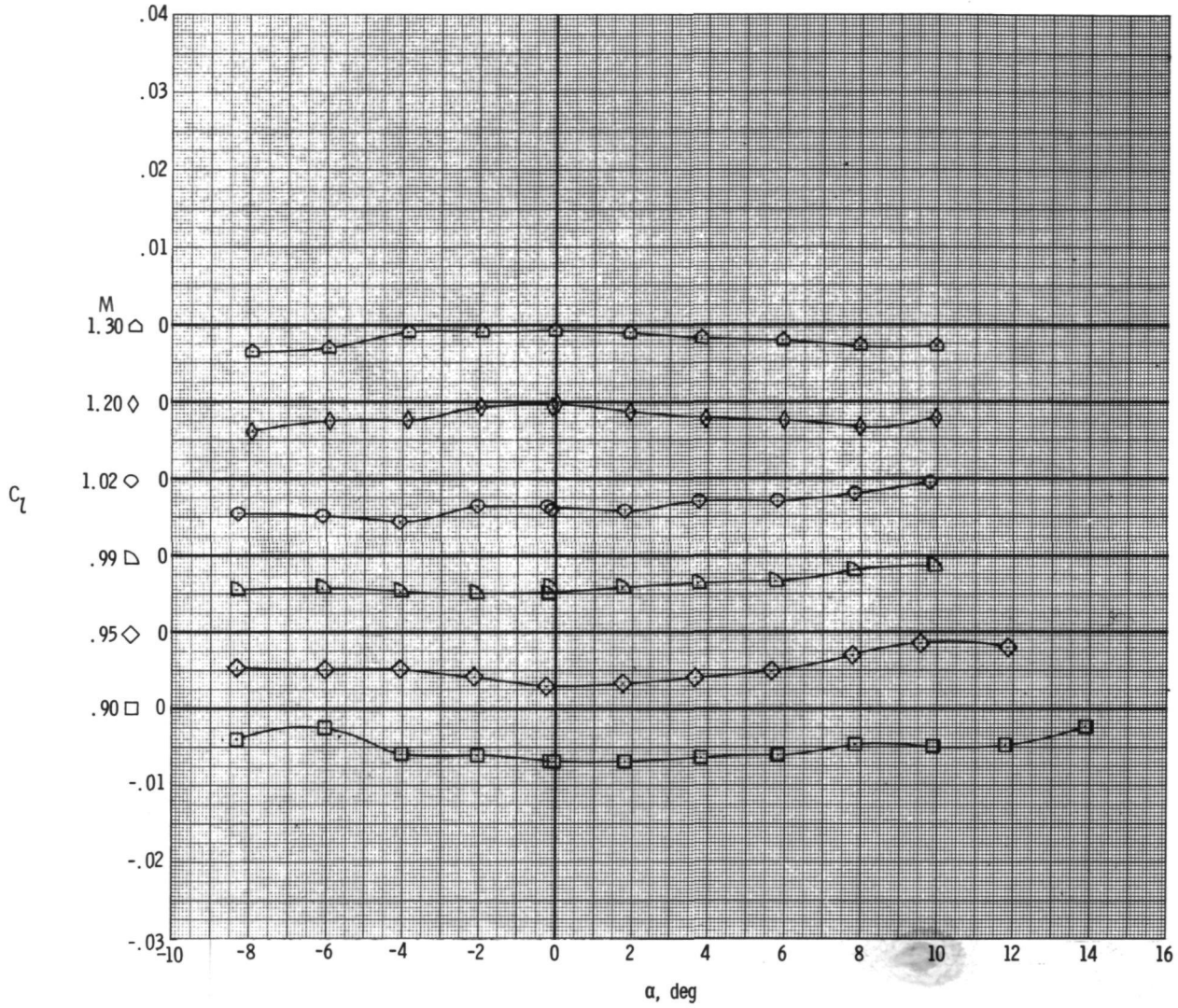

(e) $\delta_L = -5^o$.

Figure 22.- Continued.

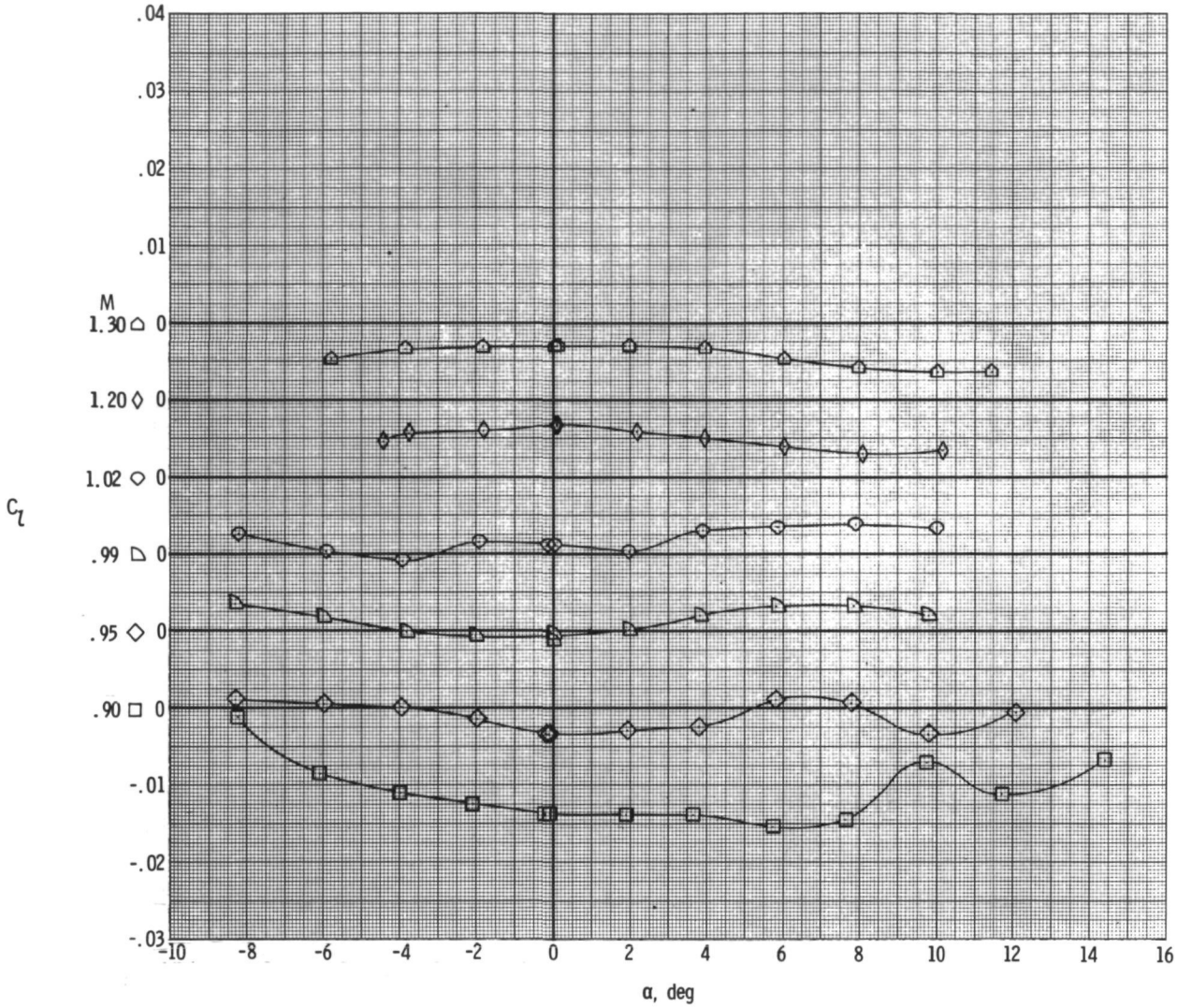

(f) $\delta_L = -10^o$.

Figure 22.- Continued.

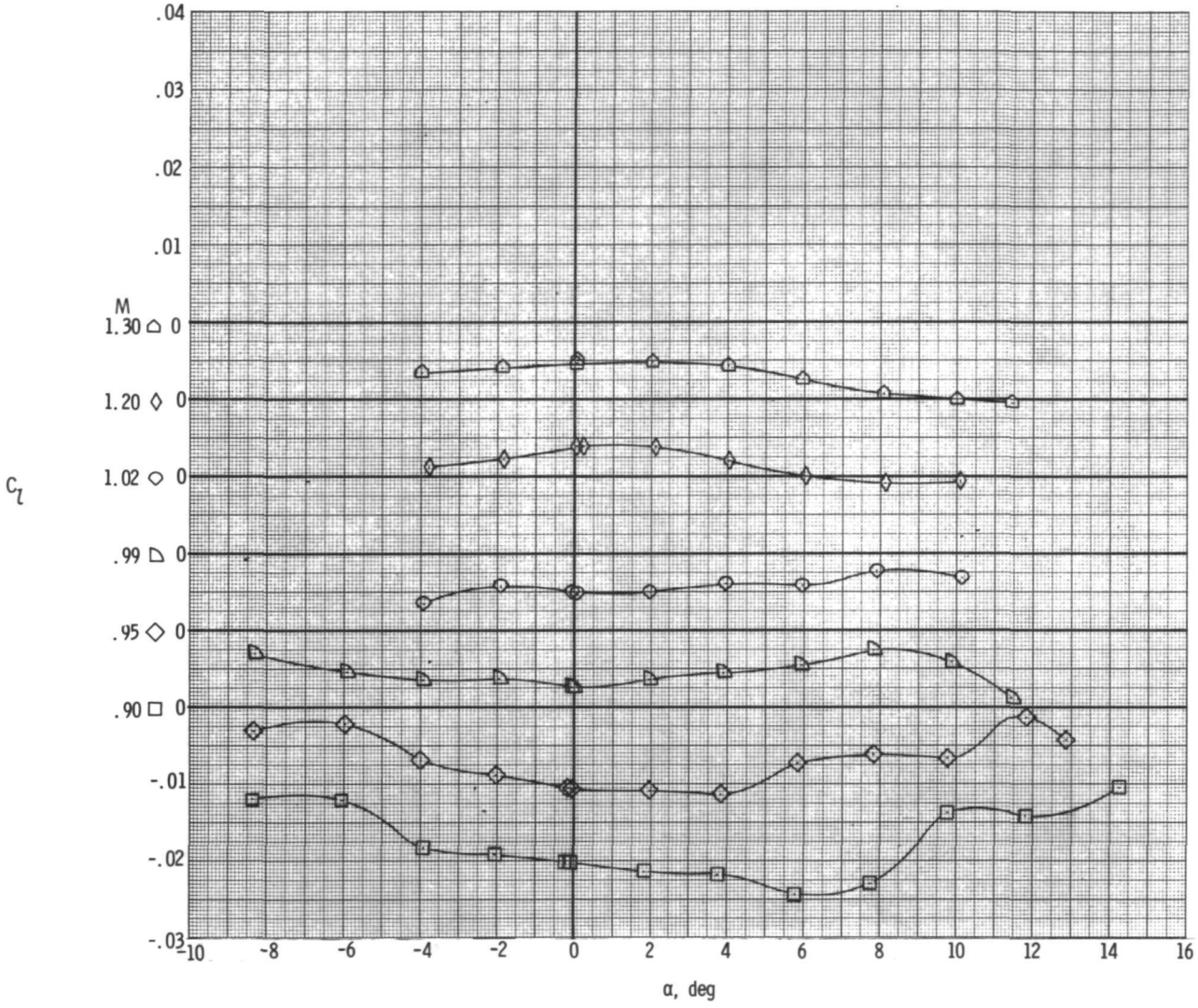

(g) $\delta_L = -15^o$.

Figure 22.- Concluded.

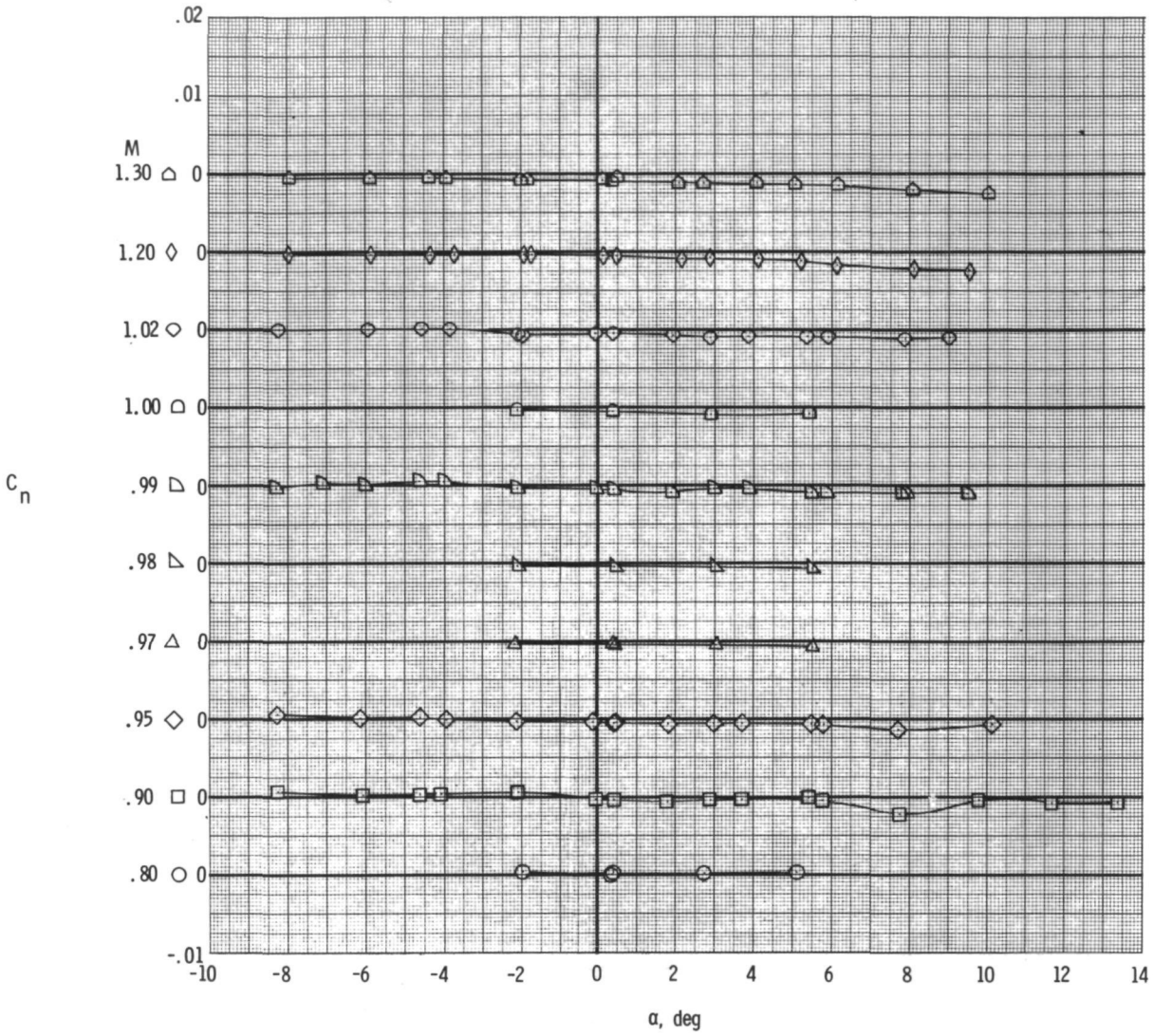

(a) $\delta_L = 15^o$.

Figure 23.- Variation of model yawing-moment coefficient with angle of attack for left aileron deflection. $\delta_h = -2.5^o$.

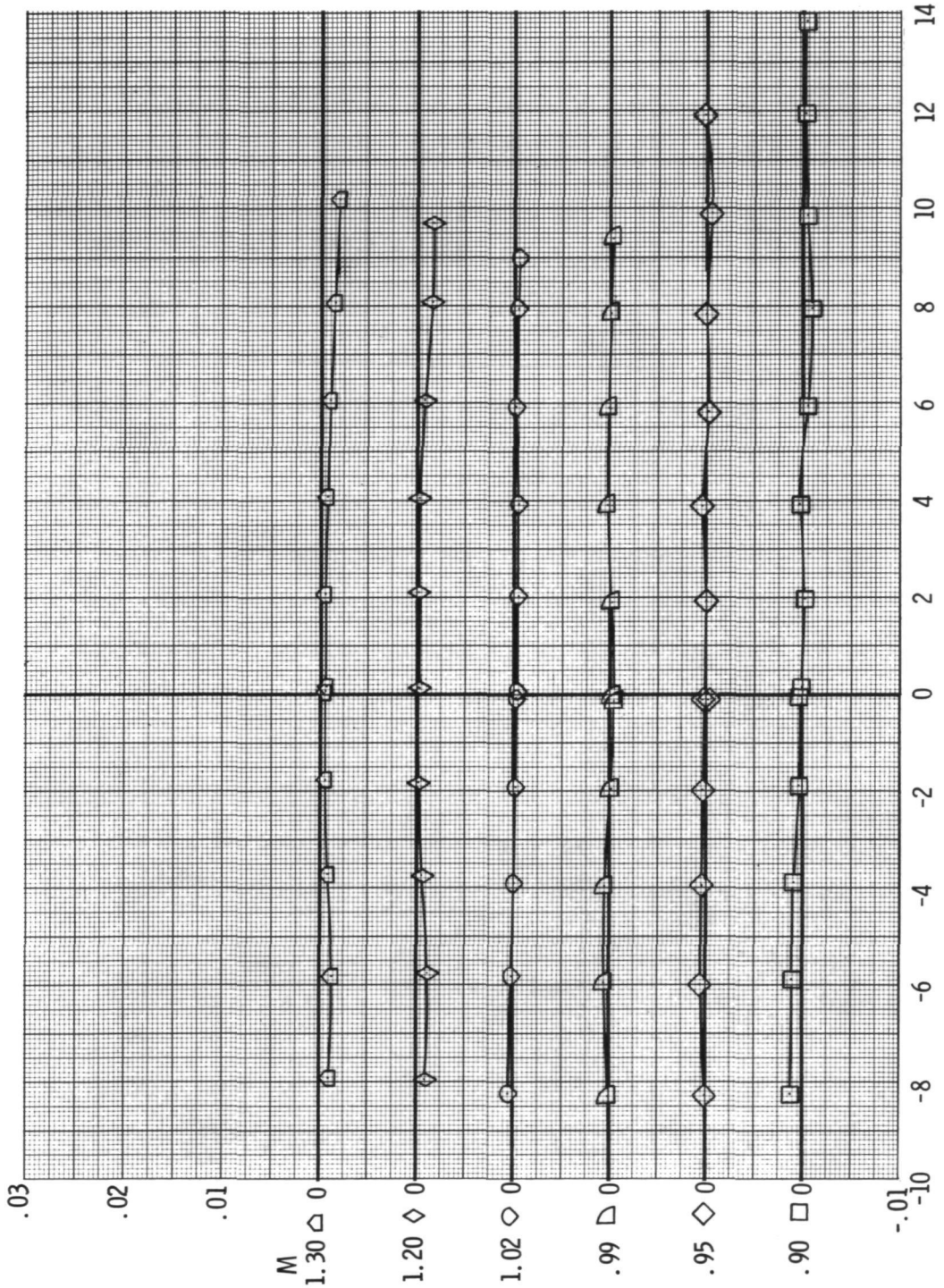

(b) $\delta_L = 10^o$.

Figure 23.- Continued.

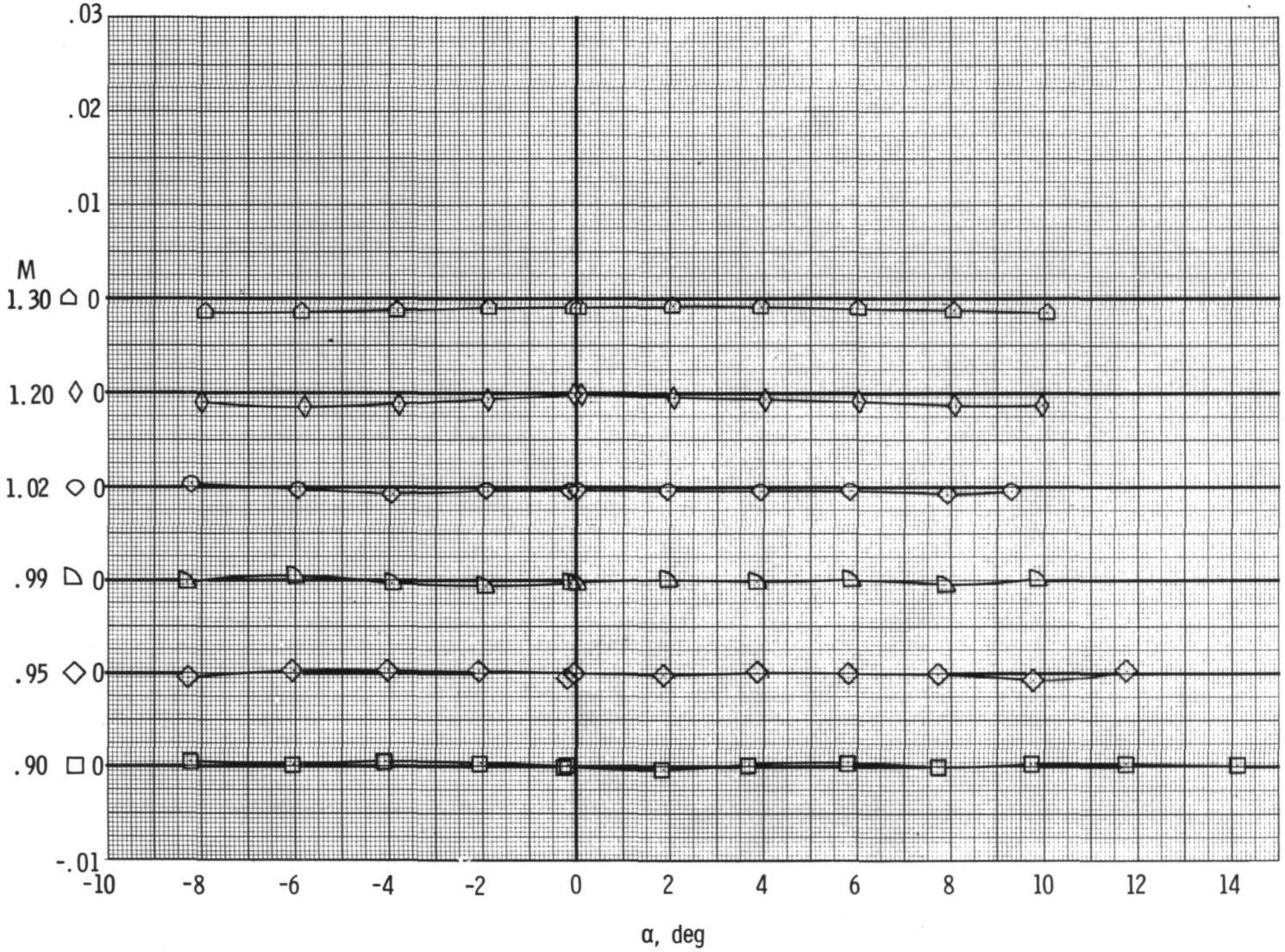

(c) $\delta_L = 5^o$.

Figure 23.- Continued.

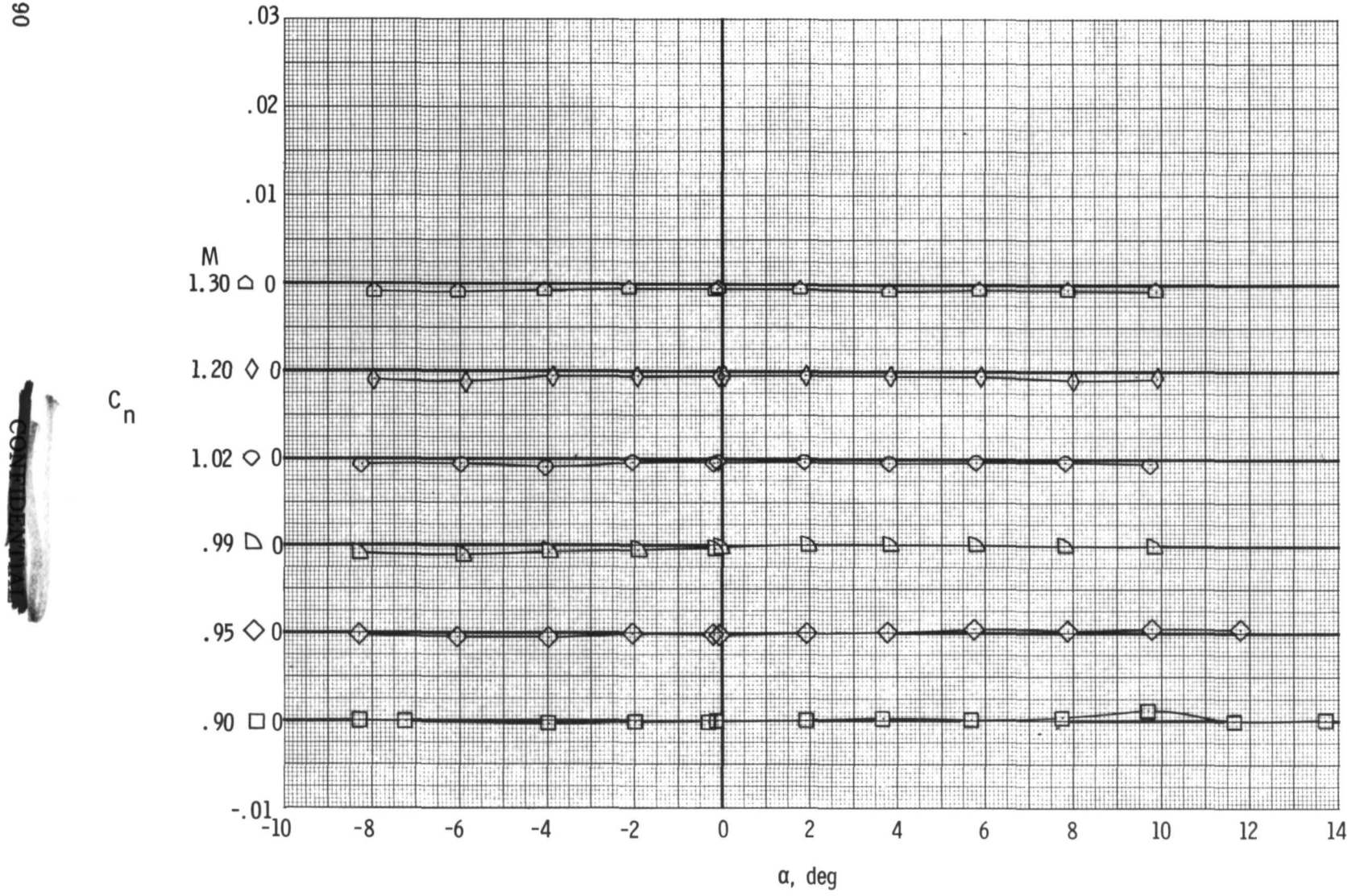

(d) $\delta_L = 0^o$.

Figure 23.- Continued.

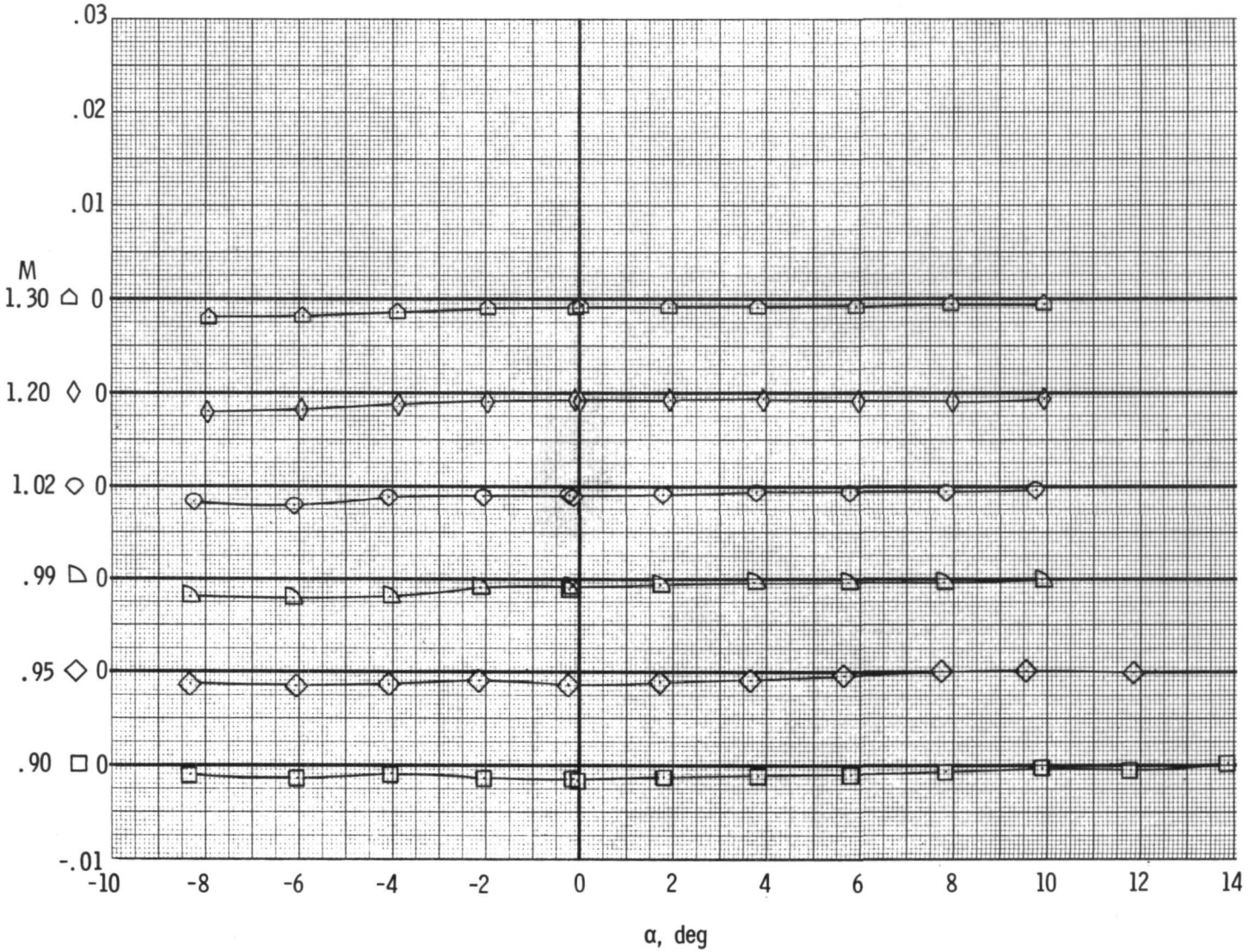

(e) $\delta_L = -5^o$.

Figure 23.- Continued.

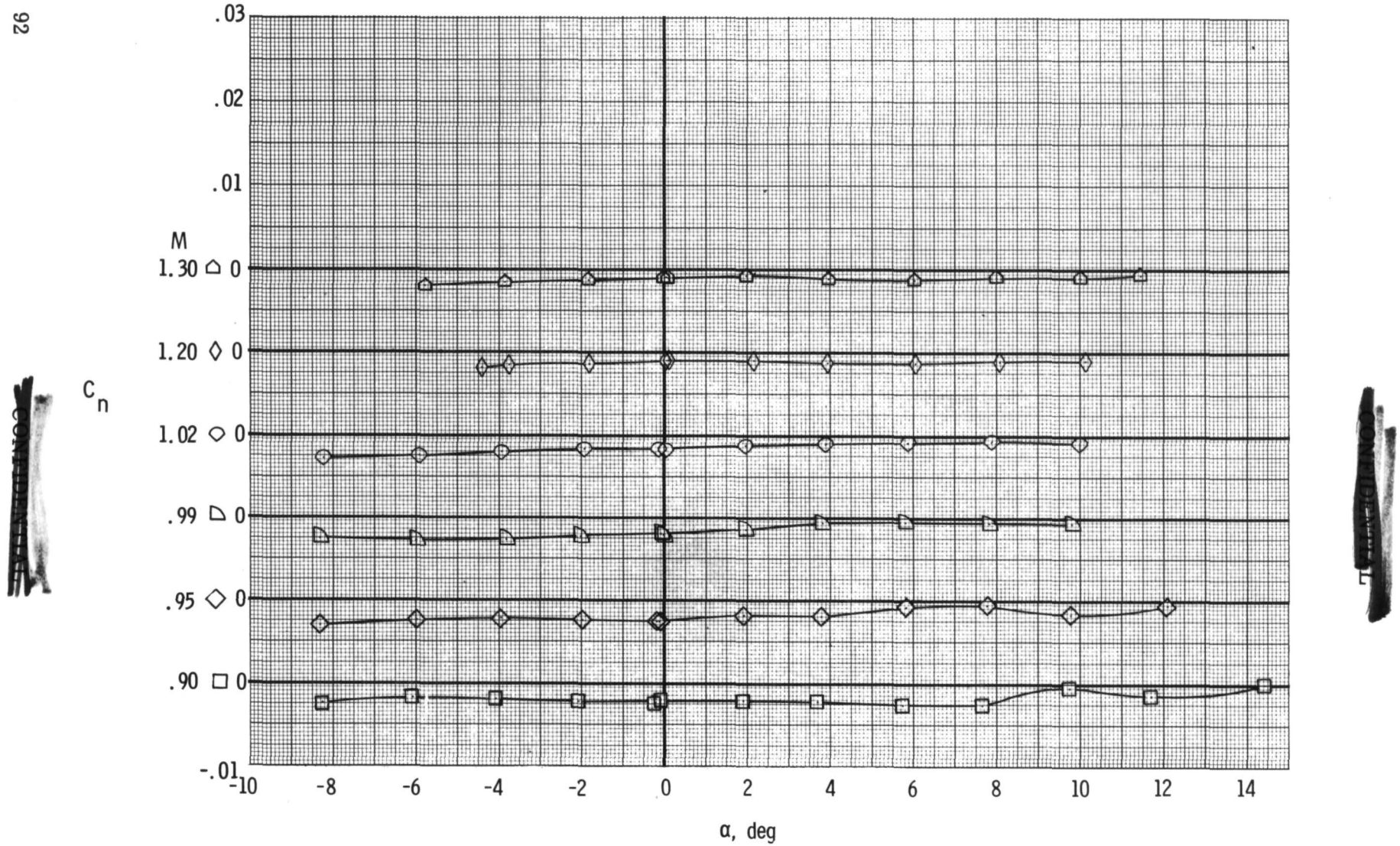

(f) $\delta_L = -10^o$.

Figure 23.- Continued.

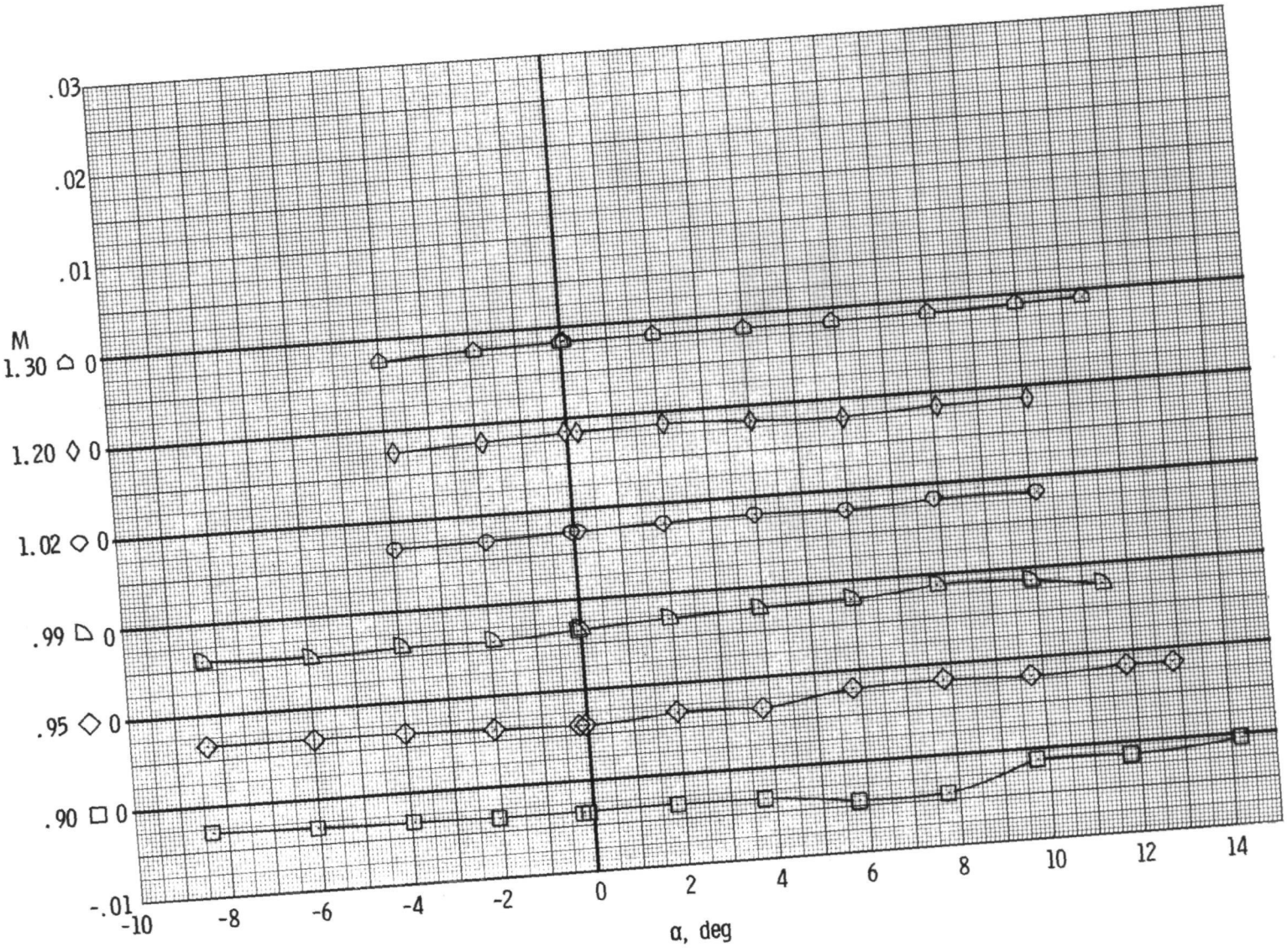

(g) $\delta_L = -15^o$.

Figure 23.- Concluded.

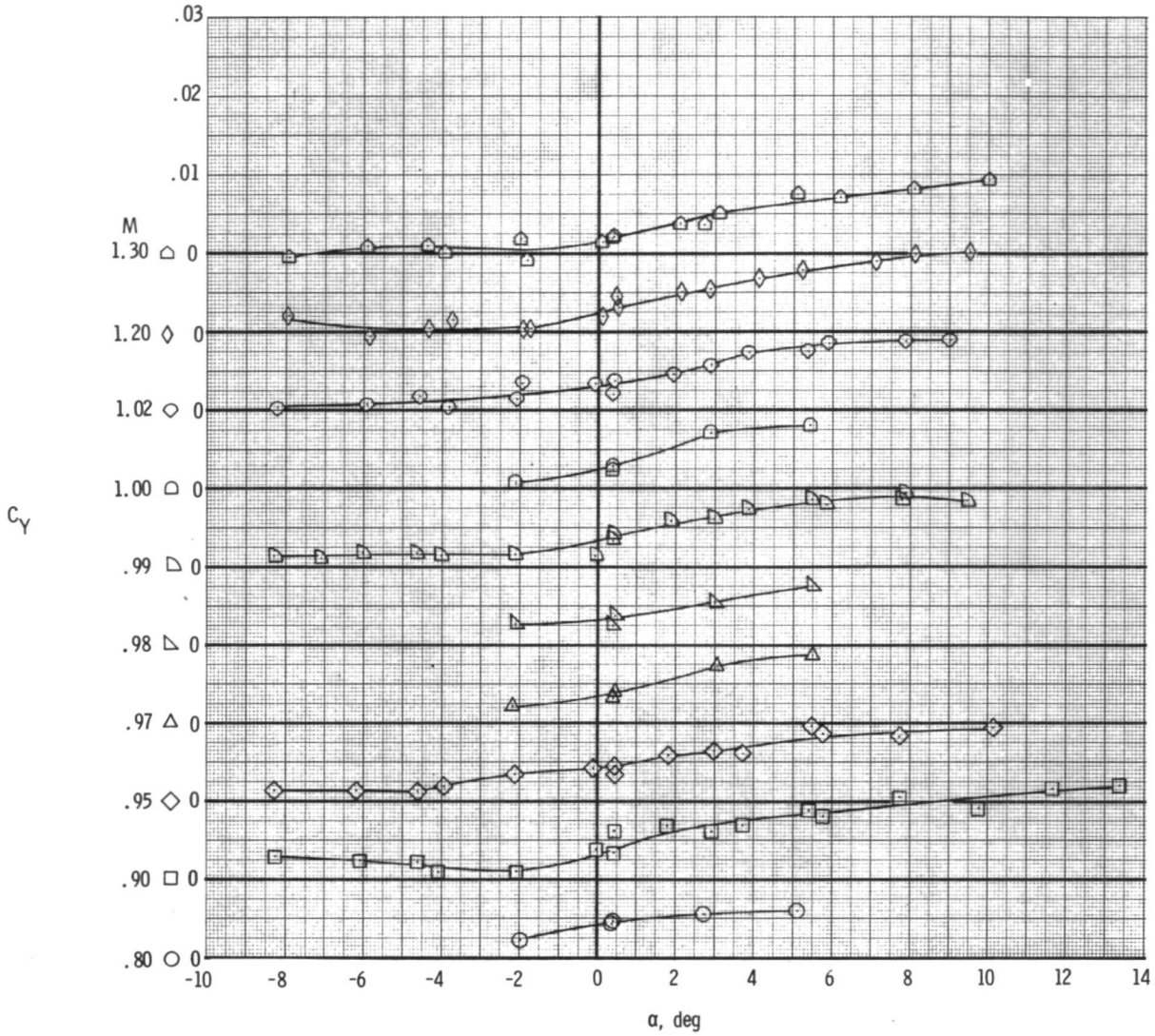

(a) $\delta_L = 15^o$.

Figure 24.- Variation of model side-force coefficient with angle of attack for left aileron deflection. $\delta_h = -2.5^o$.

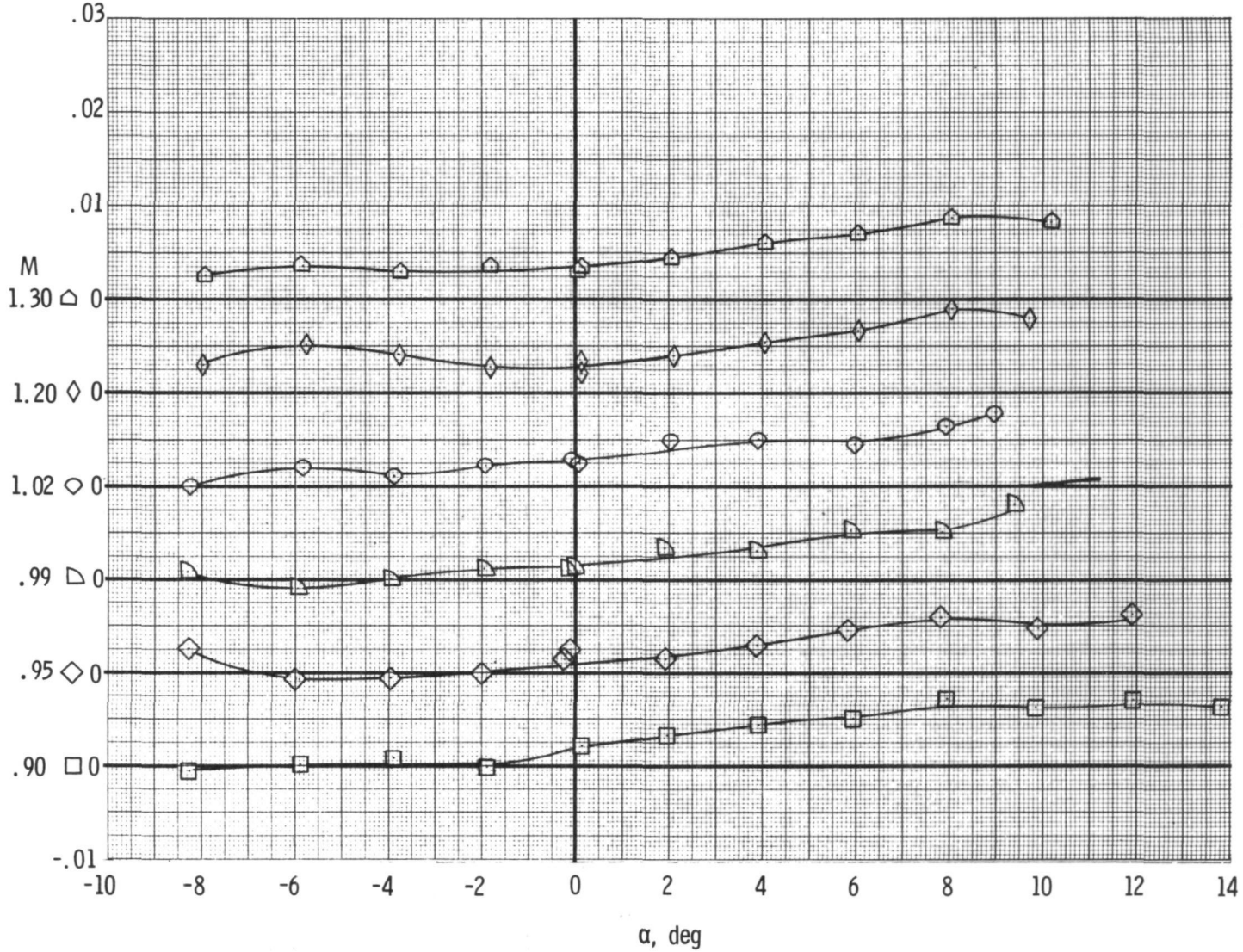

(b) $\delta_L = 10^o$.

Figure 24.- Continued.

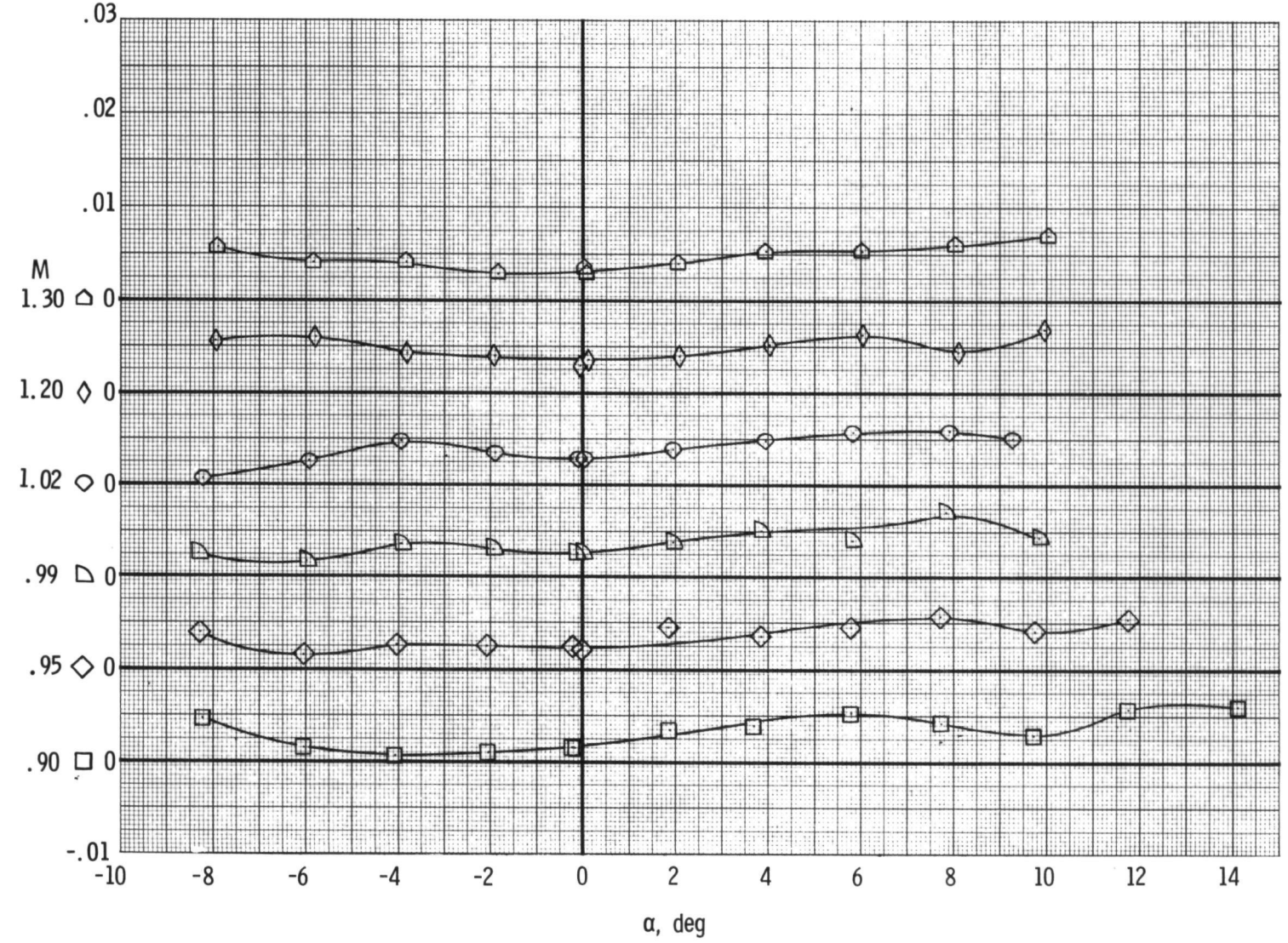

(c) $\delta_L = 5^o$.

Figure 24.- Continued.

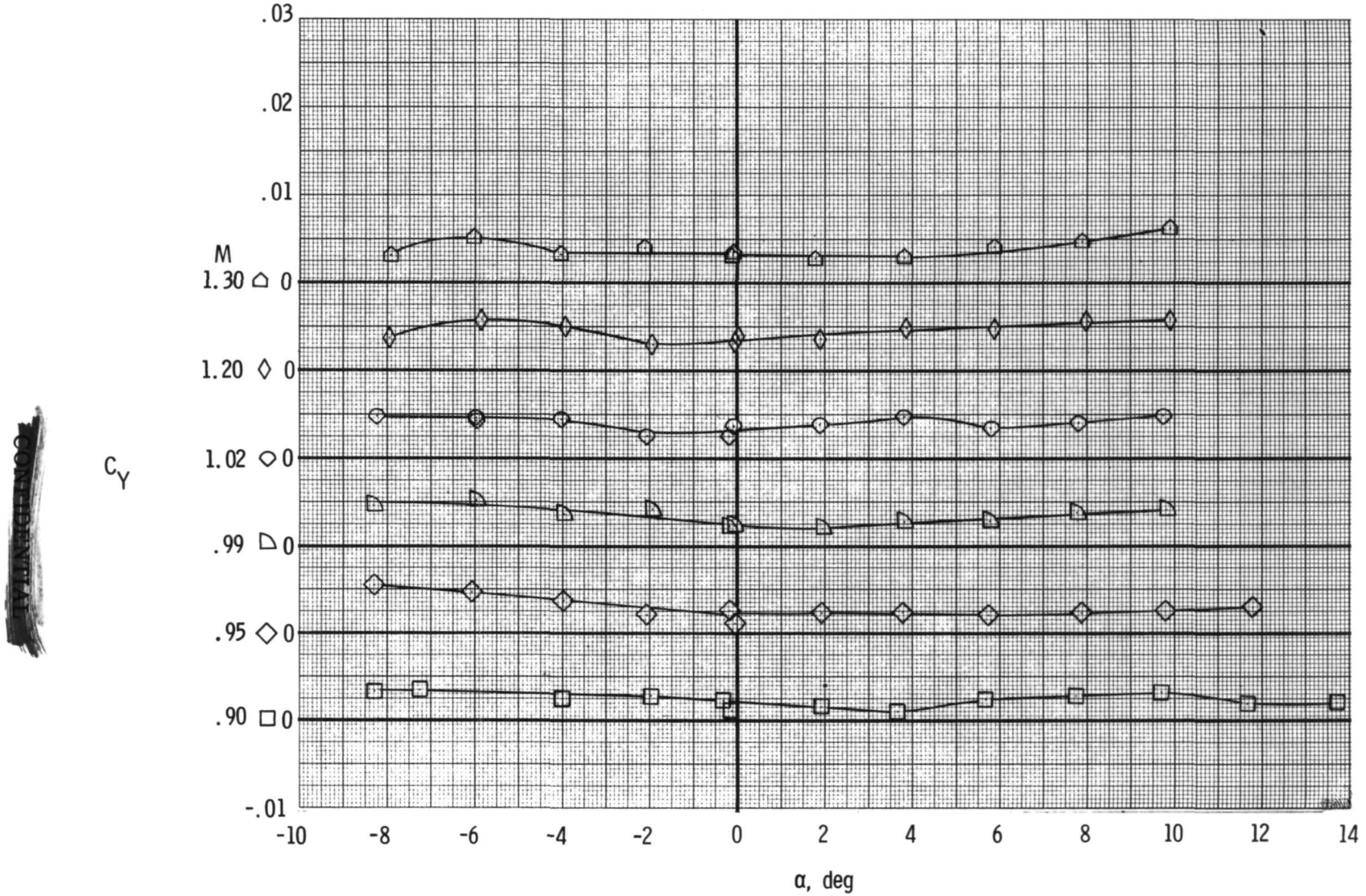

(d) $\delta_L = 0^o$.

Figure 24.- Continued.

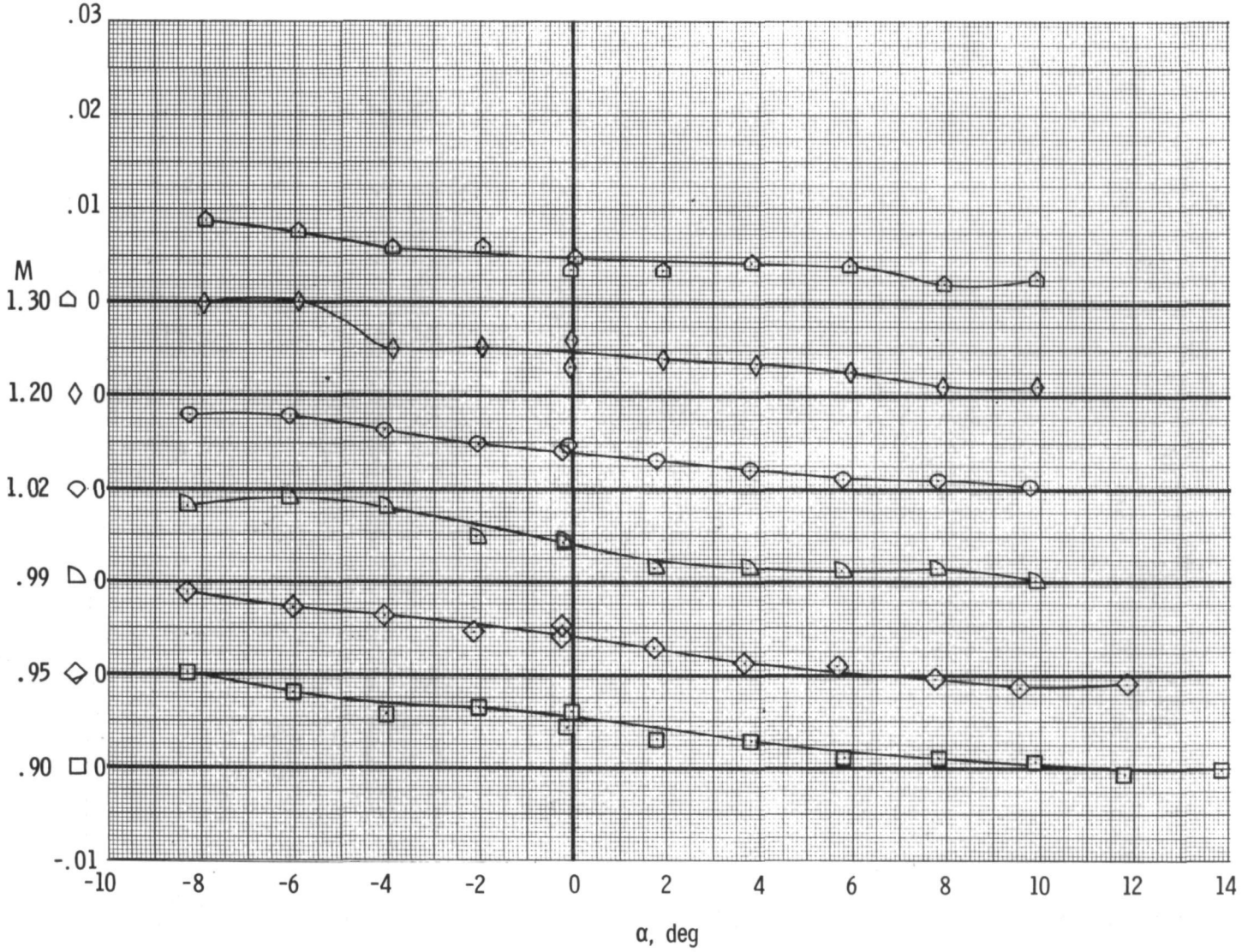

(e) $\delta_L = -5^o$.

Figure 24.- Continued.

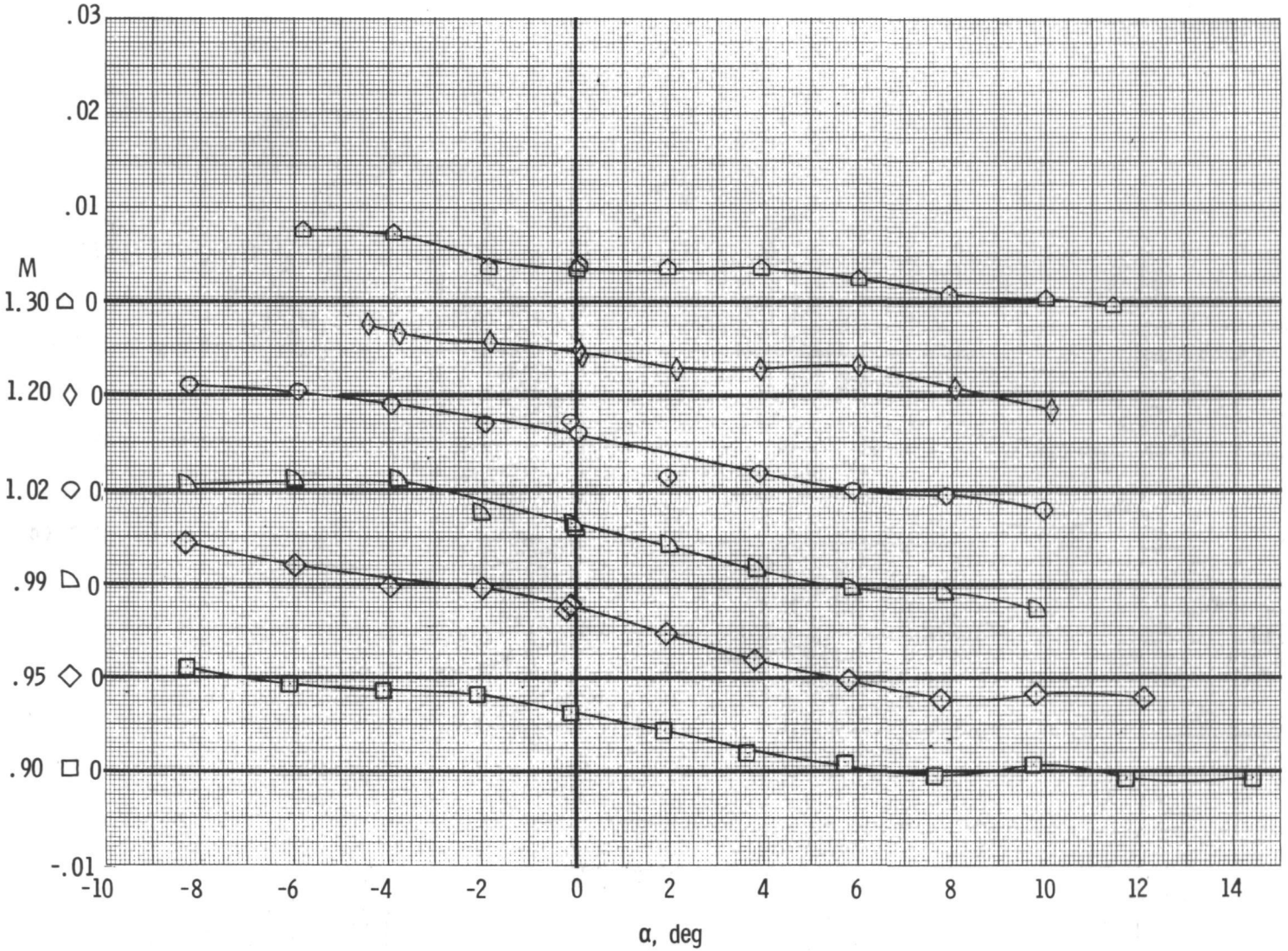

(f) $\delta_L = -10^o$.

Figure 24.- Continued.

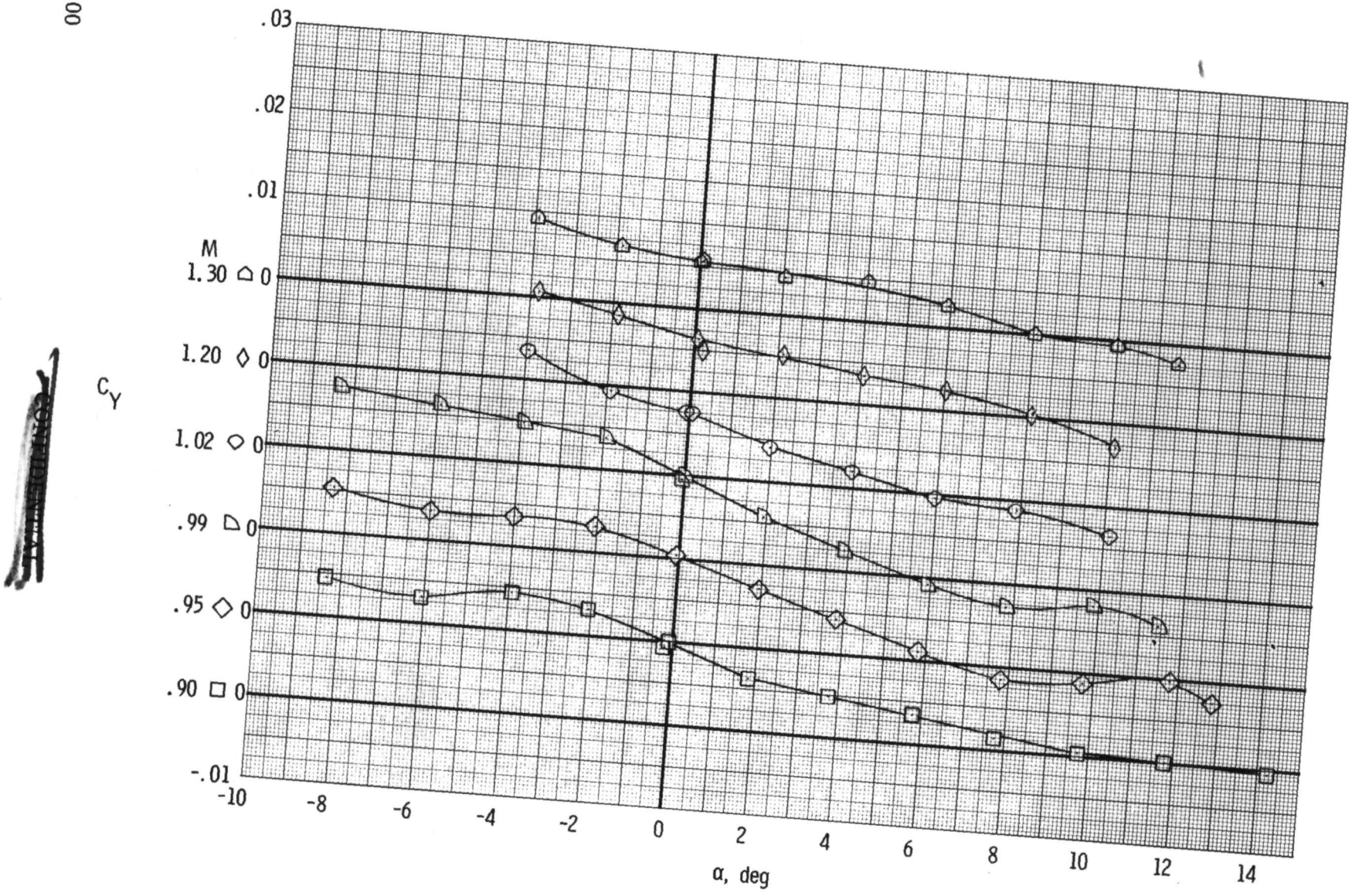

(g) $\delta_L = -15^\circ$.

Figure 24.- Concluded.

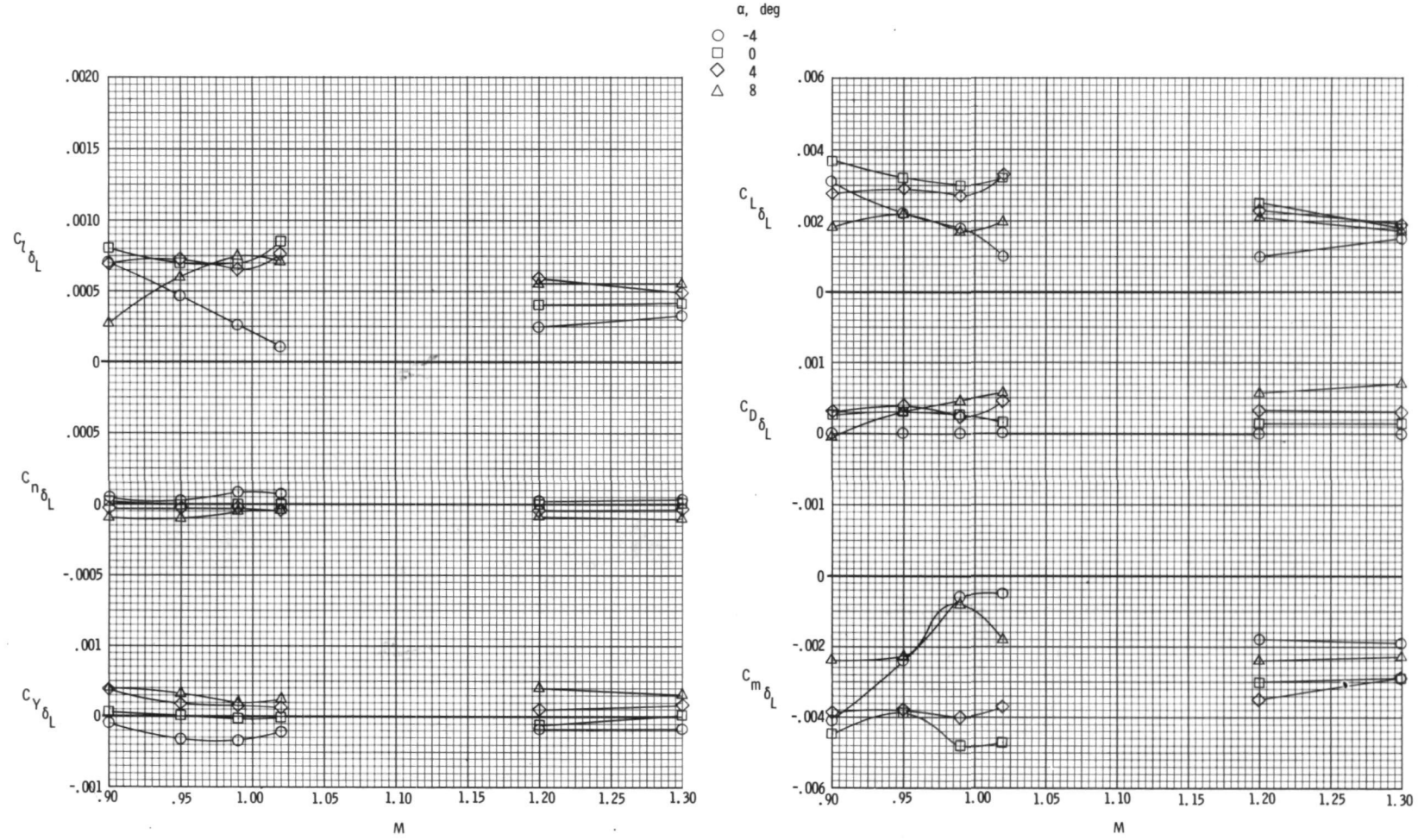

(a) Downward (positive) aileron deflection.

Figure 25.- Variation with Mach number of effect of left aileron deflection on model longitudinal and lateral aerodynamic coefficients. $\delta_h = -2.5^o$ and $\beta = 0^o$.

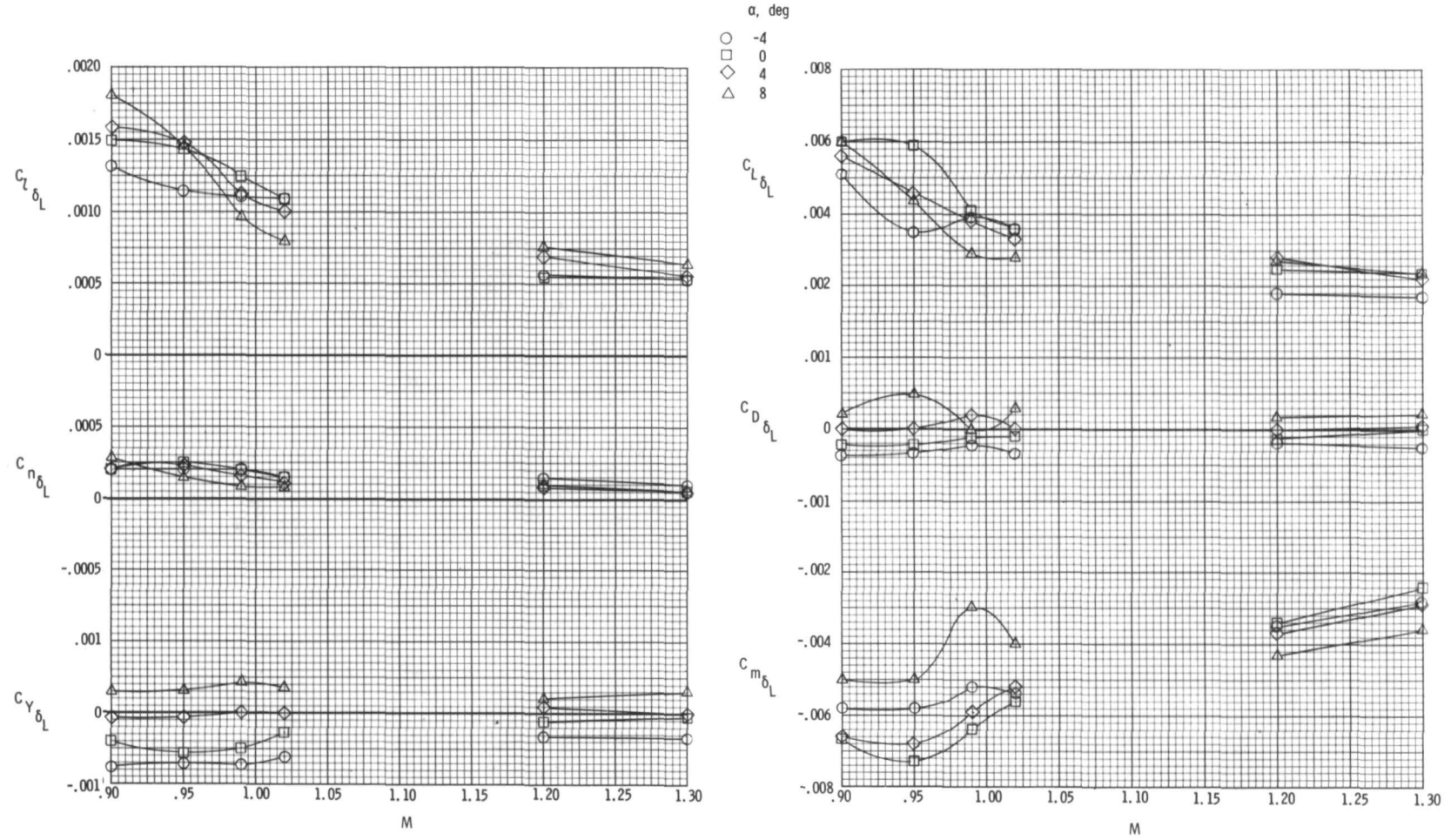

(b) Upward (negative) aileron deflection.

Figure 25.- Concluded.

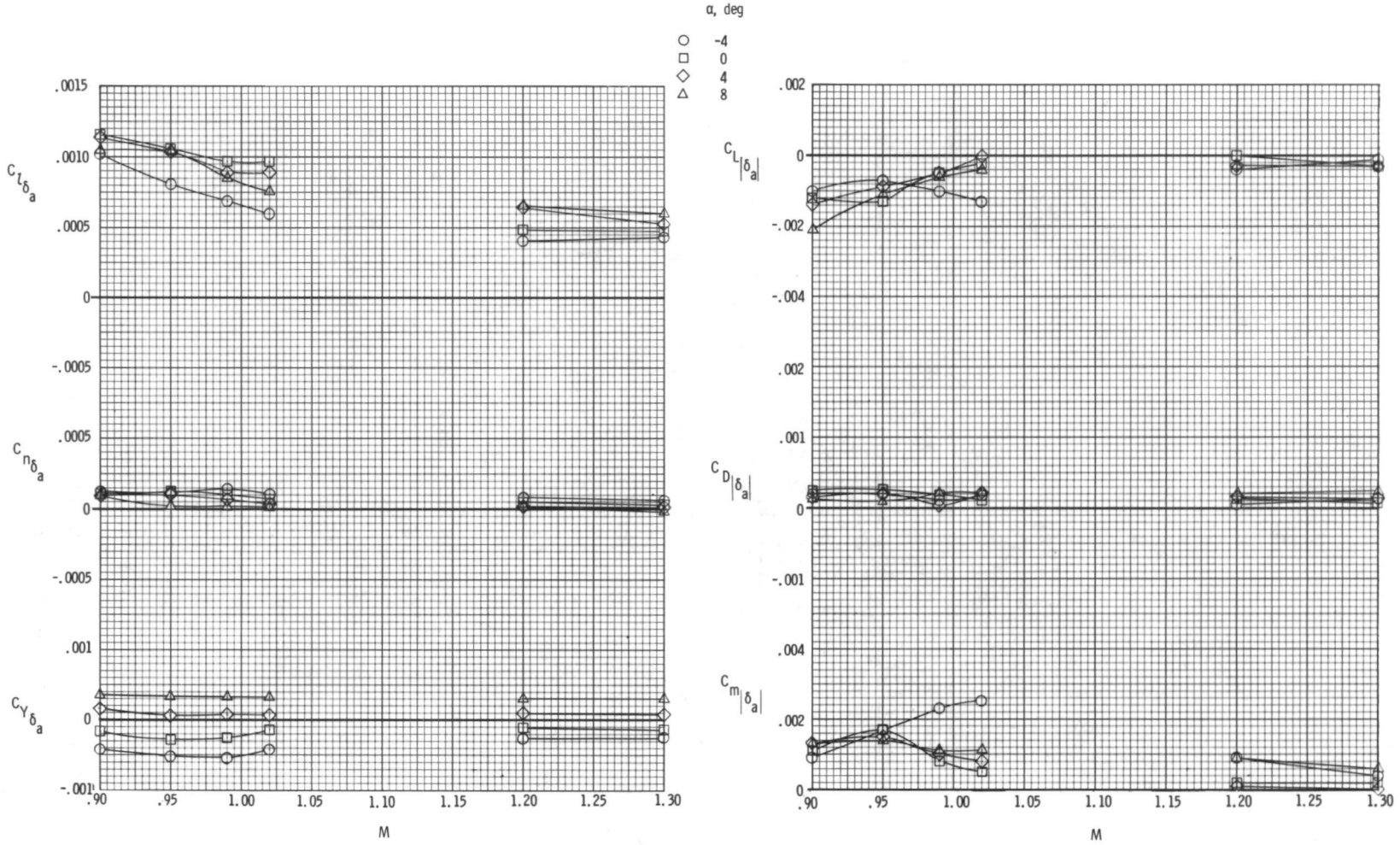

Figure 26.- Variation with Mach number of effect of differential aileron deflection on longitudinal and lateral aerodynamic coefficients. $\delta_h = -2.5^o$ and $\beta = 0^o$. $(|\delta_a|$ denote absolute value of δ_a used.$)$

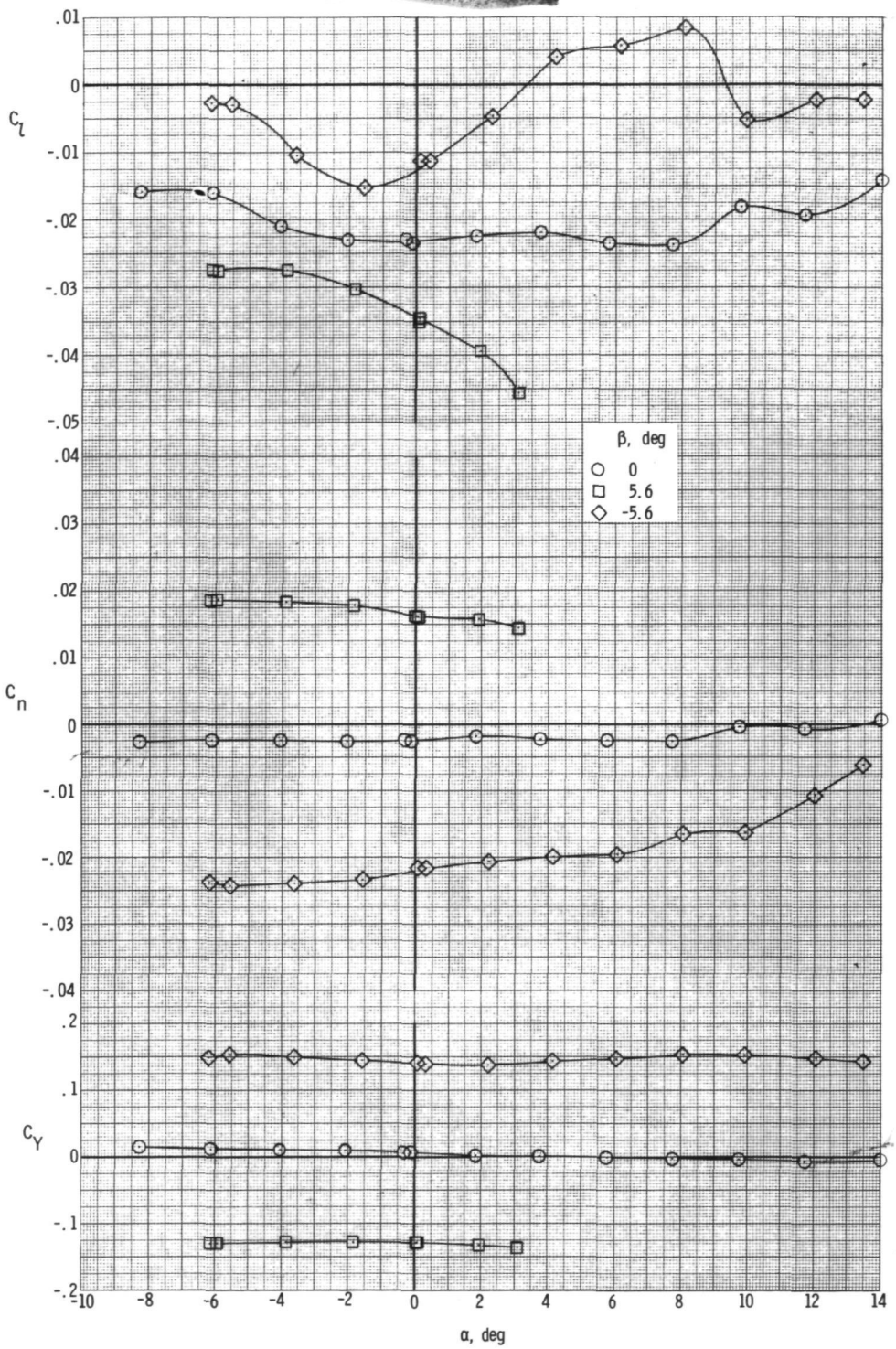

(a) M = 0.90.

Figure 27.- Variation of lateral aerodynamic coefficients with angle of attack for the model at three angles of sideslip with ailerons differentially deflected. $\delta_a = -20^o$ and $\delta_h = -2.5^o$.

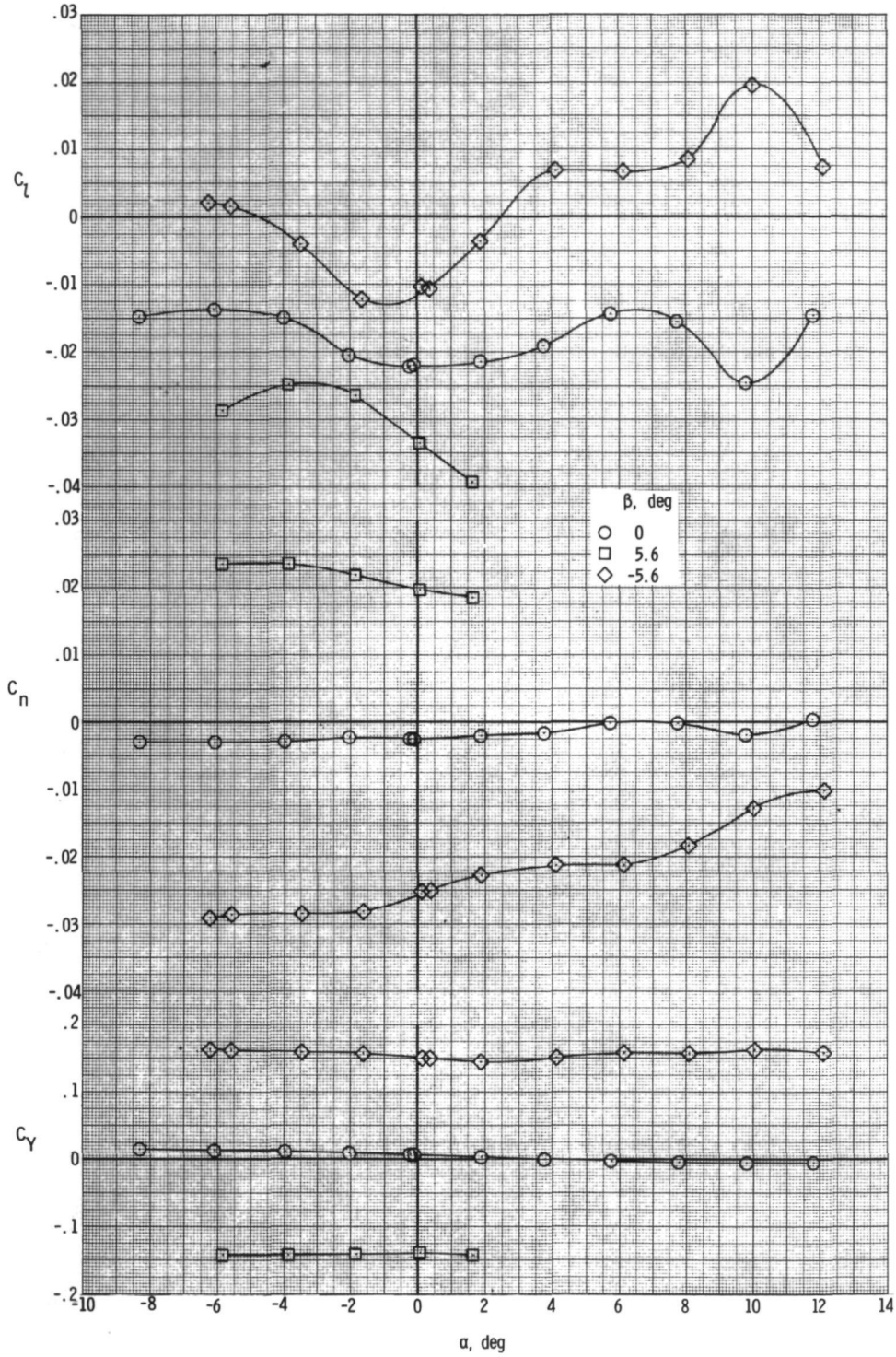

(b) M = 0.95.

Figure 27.- Continued.

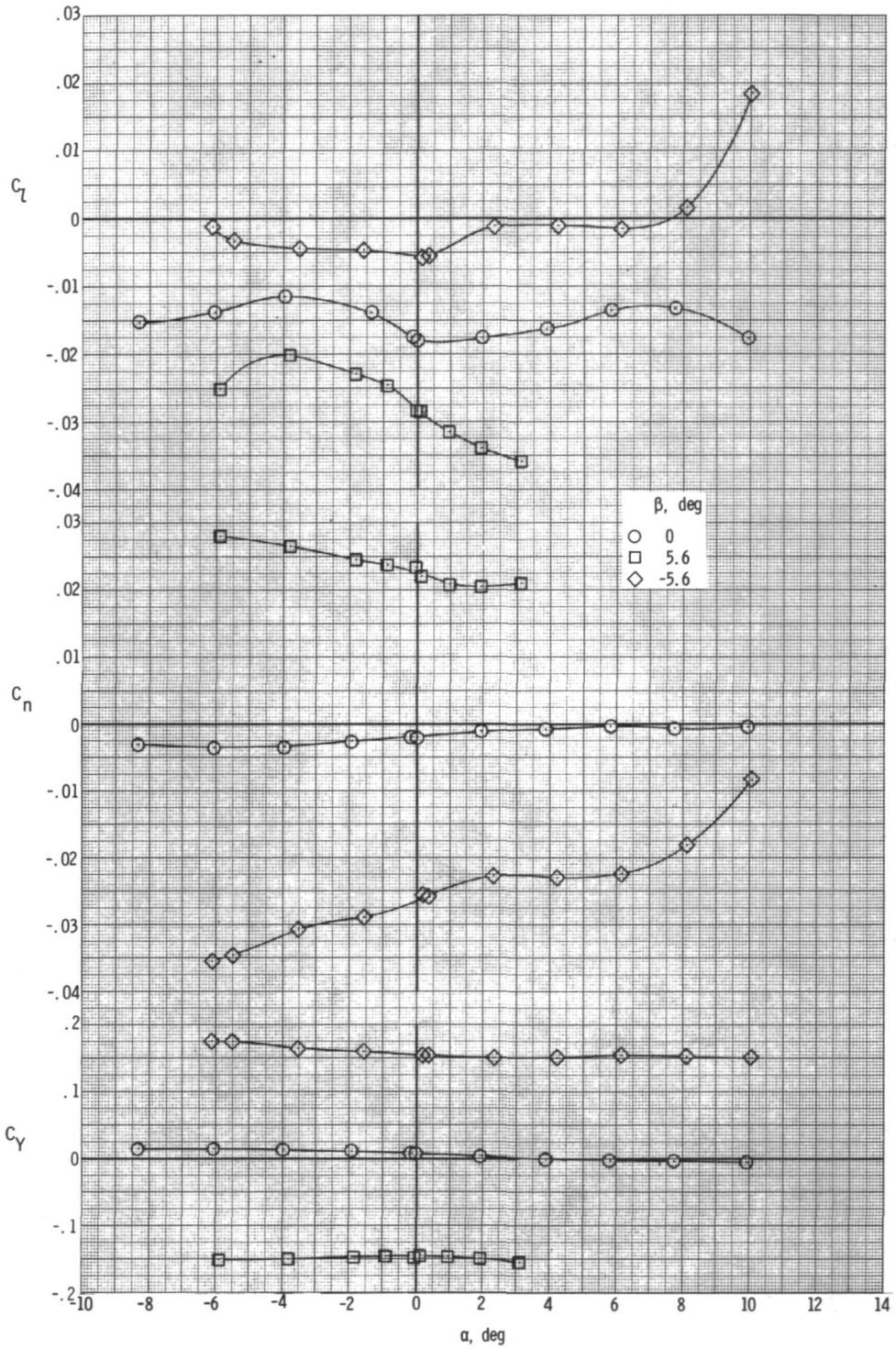

(c) M = 0.99.

Figure 27.- Continued.

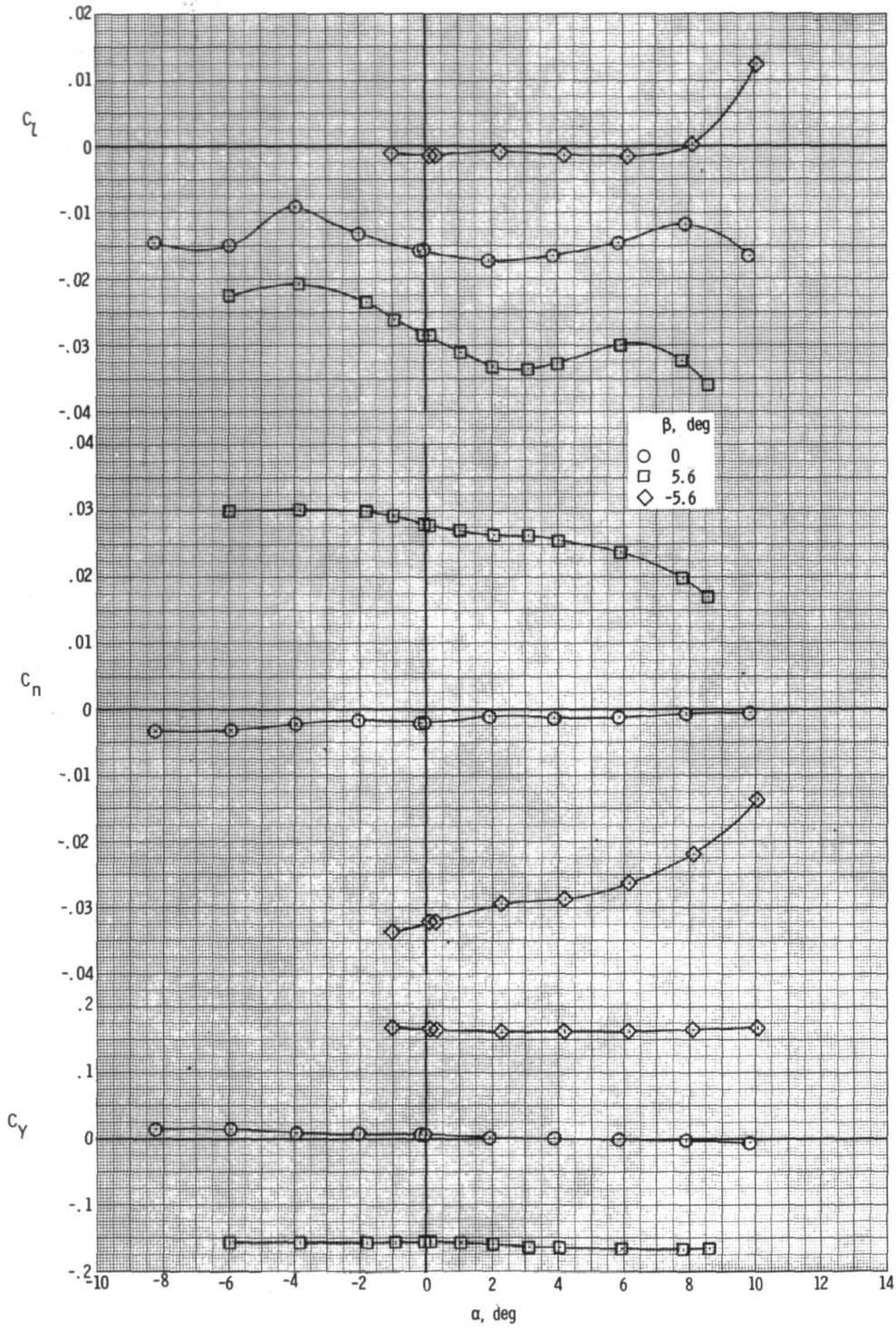

(d) M = 1.02.

Figure 27.- Continued.

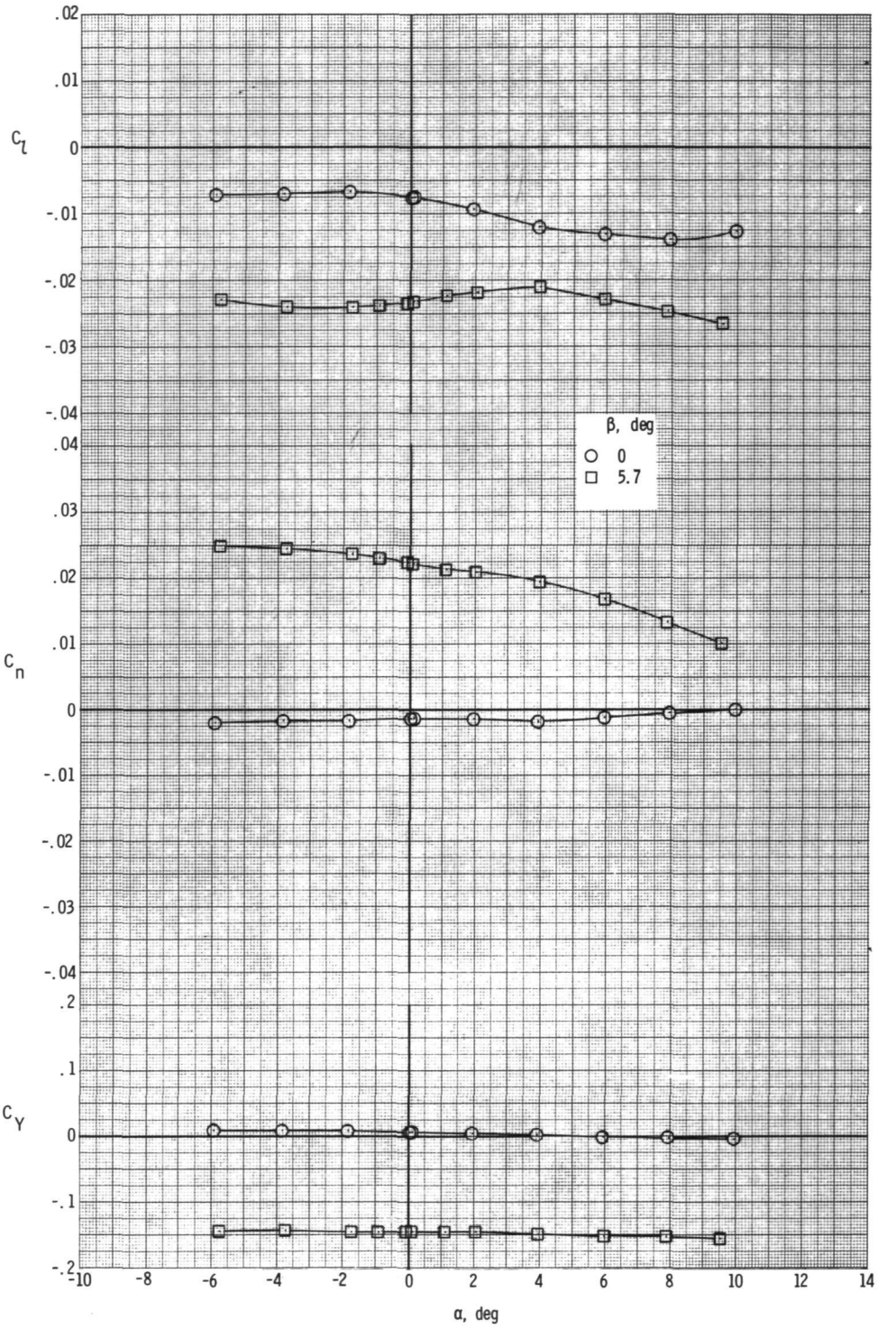

(e) M = 1.20.

Figure 27.- Continued.

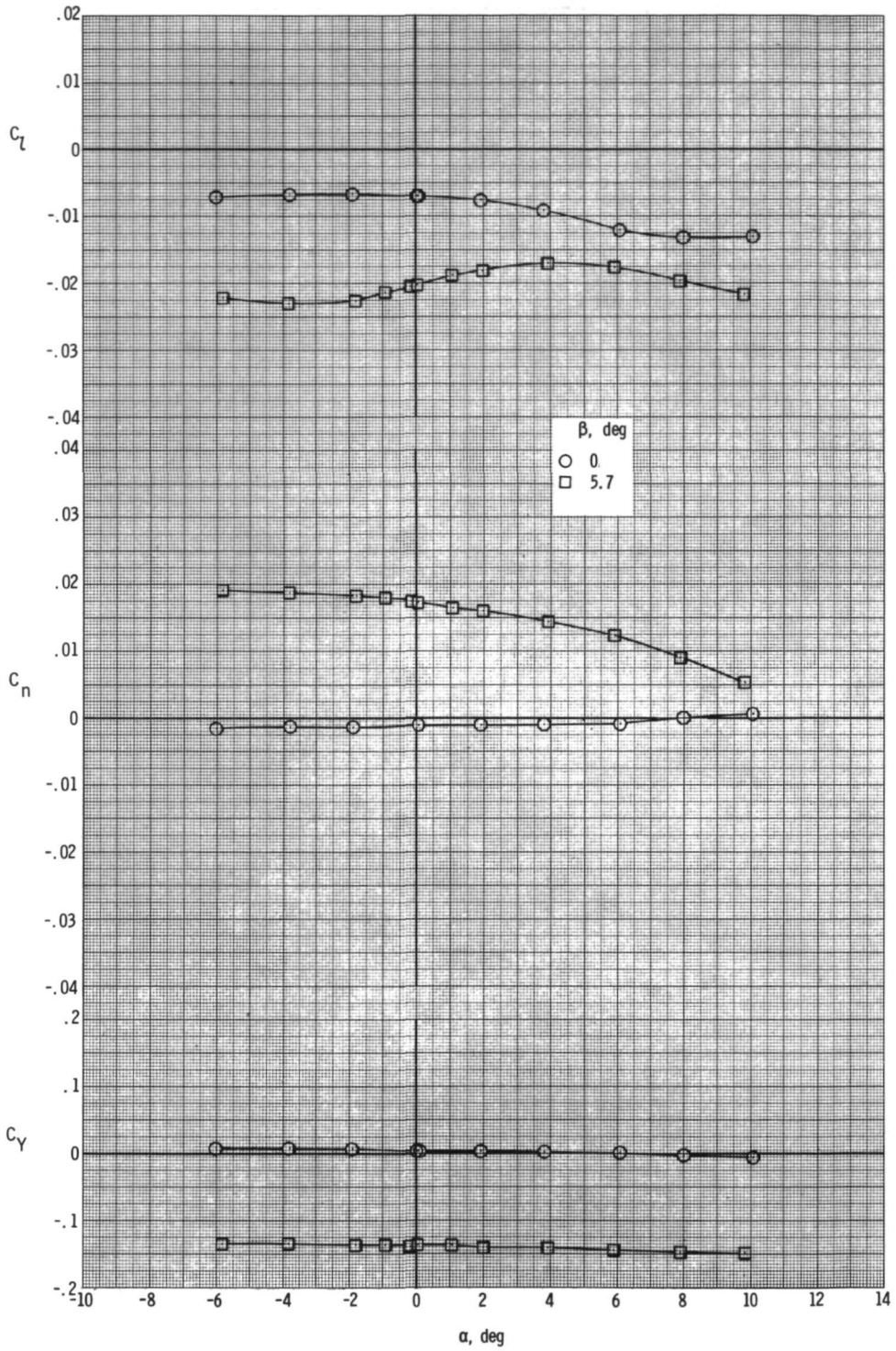

(f) M = 1.30.

Figure 27.- Concluded.

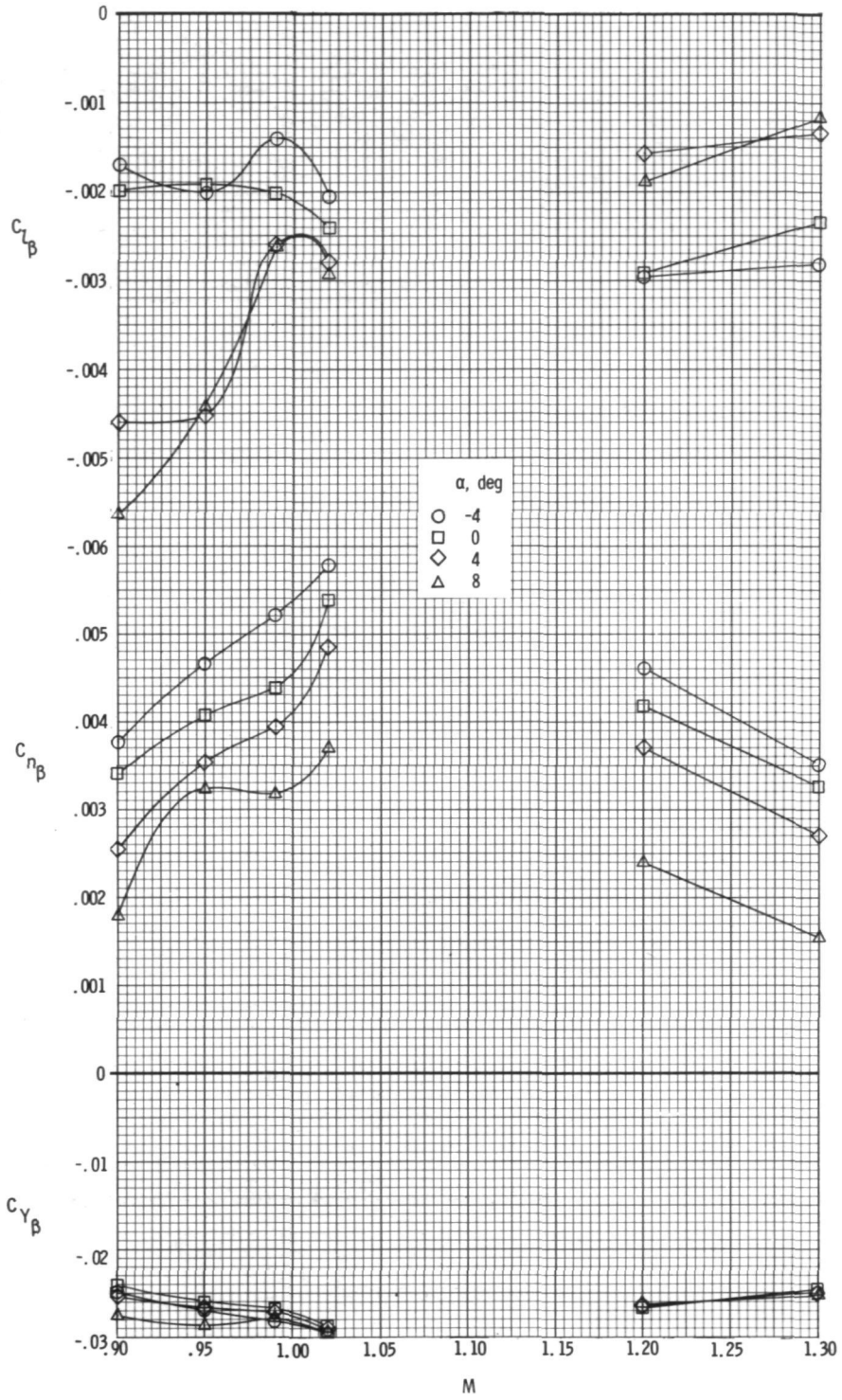

Figure 28.- Variation with Mach number of model lateral-directional stability characteristics at four angles of attack with ailerons deflected. $\delta_a = -20^o$ and $\delta_h = -2.5^o$.

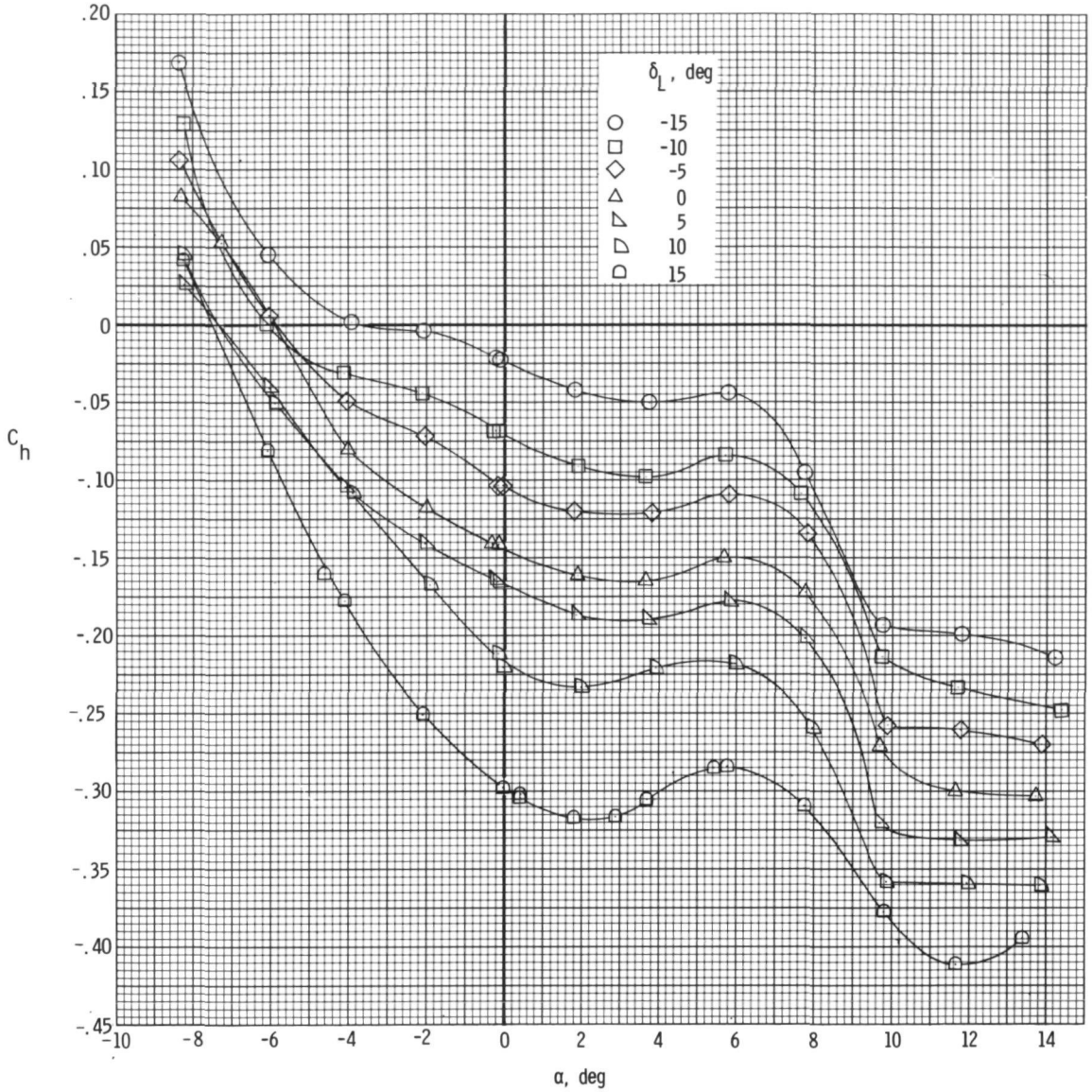

(a) M = 0.90.

Figure 29.- Variation of inboard aileron segment hinge-moment coefficient with model angle of attack.

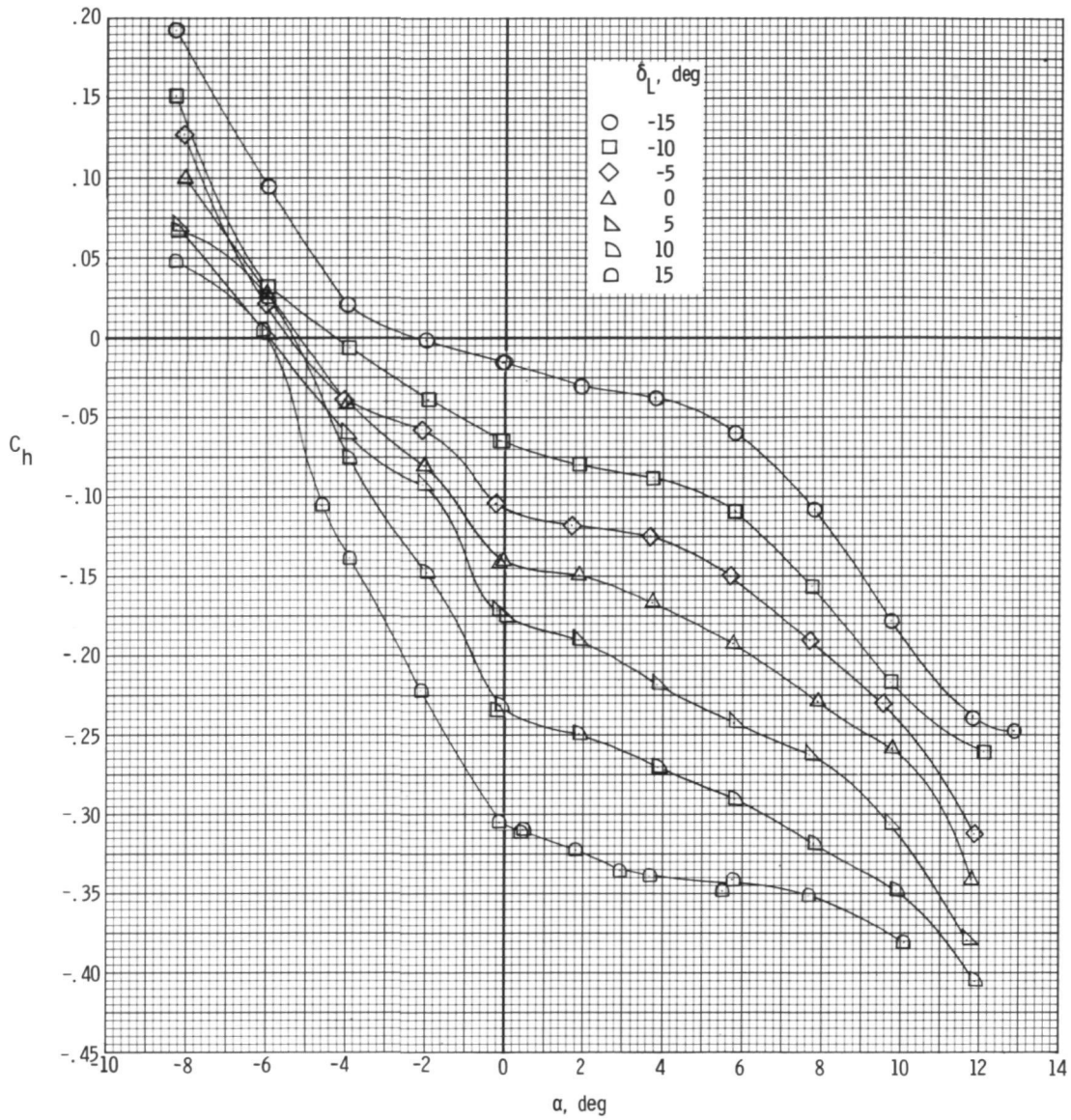

(b) M = 0.95.

Figure 29.- Continued.

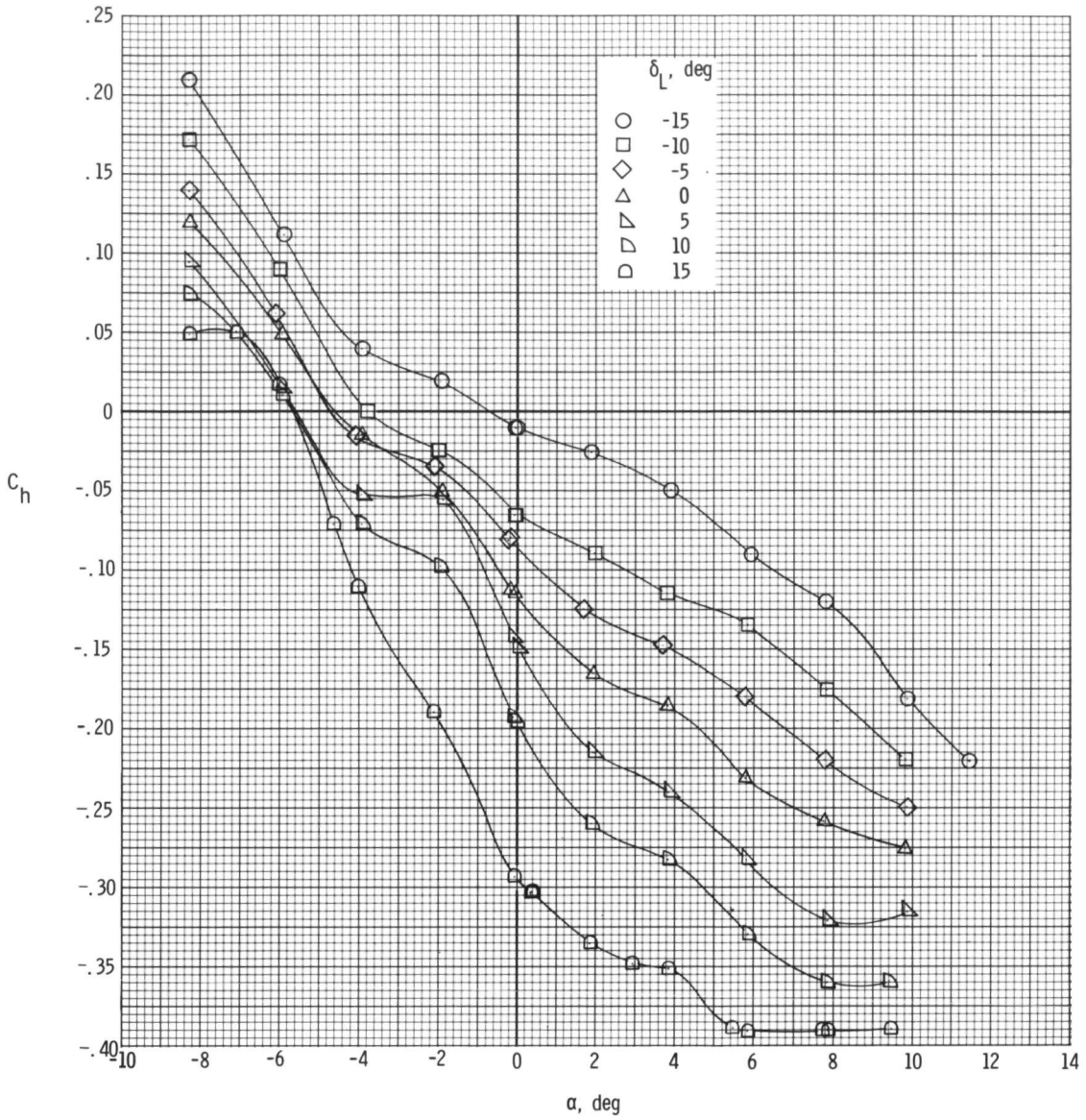

(c) M = 0.99.

Figure 29.- Continued.

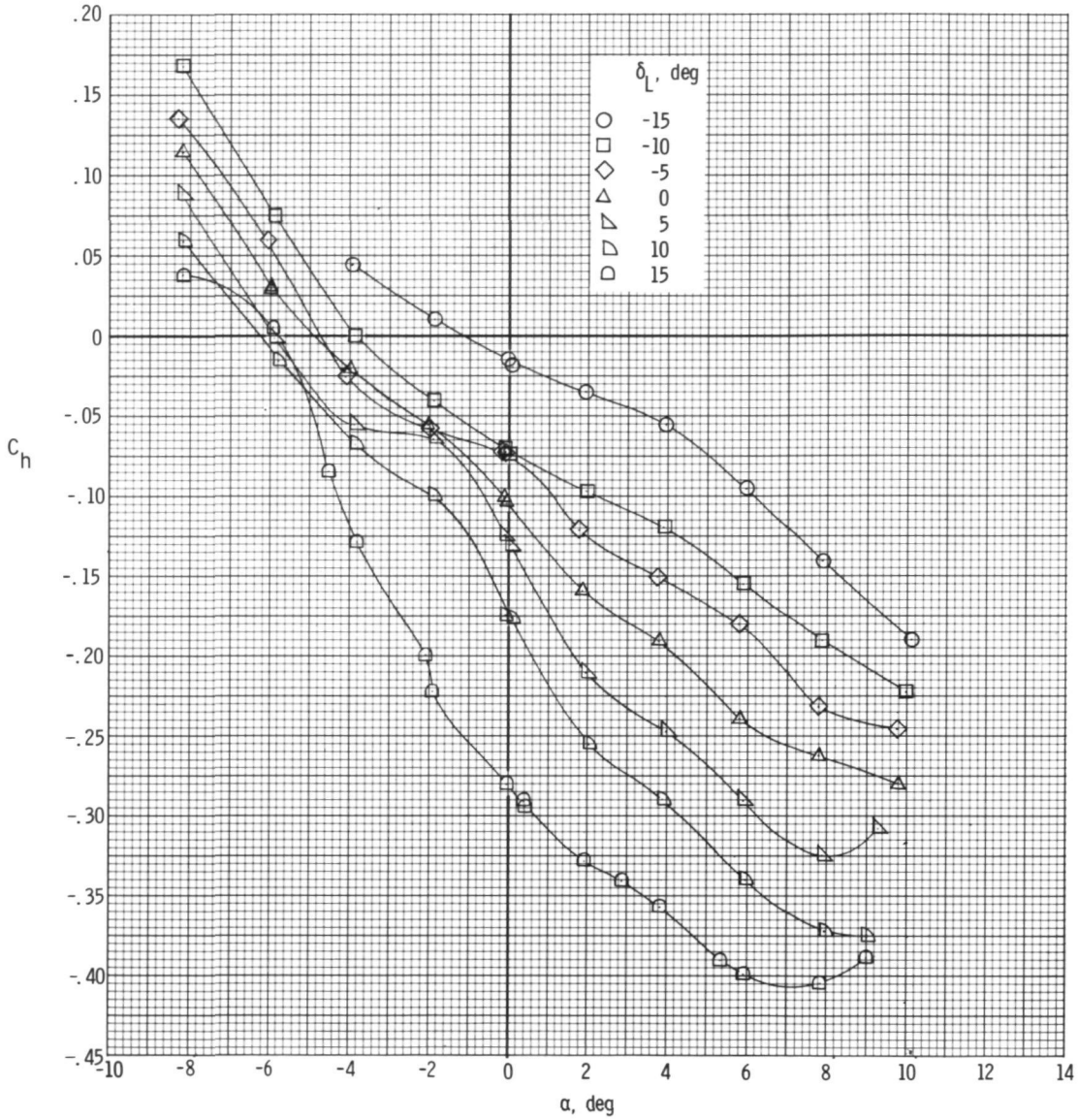

(d) M = 1.02.

Figure 29.- Continued.

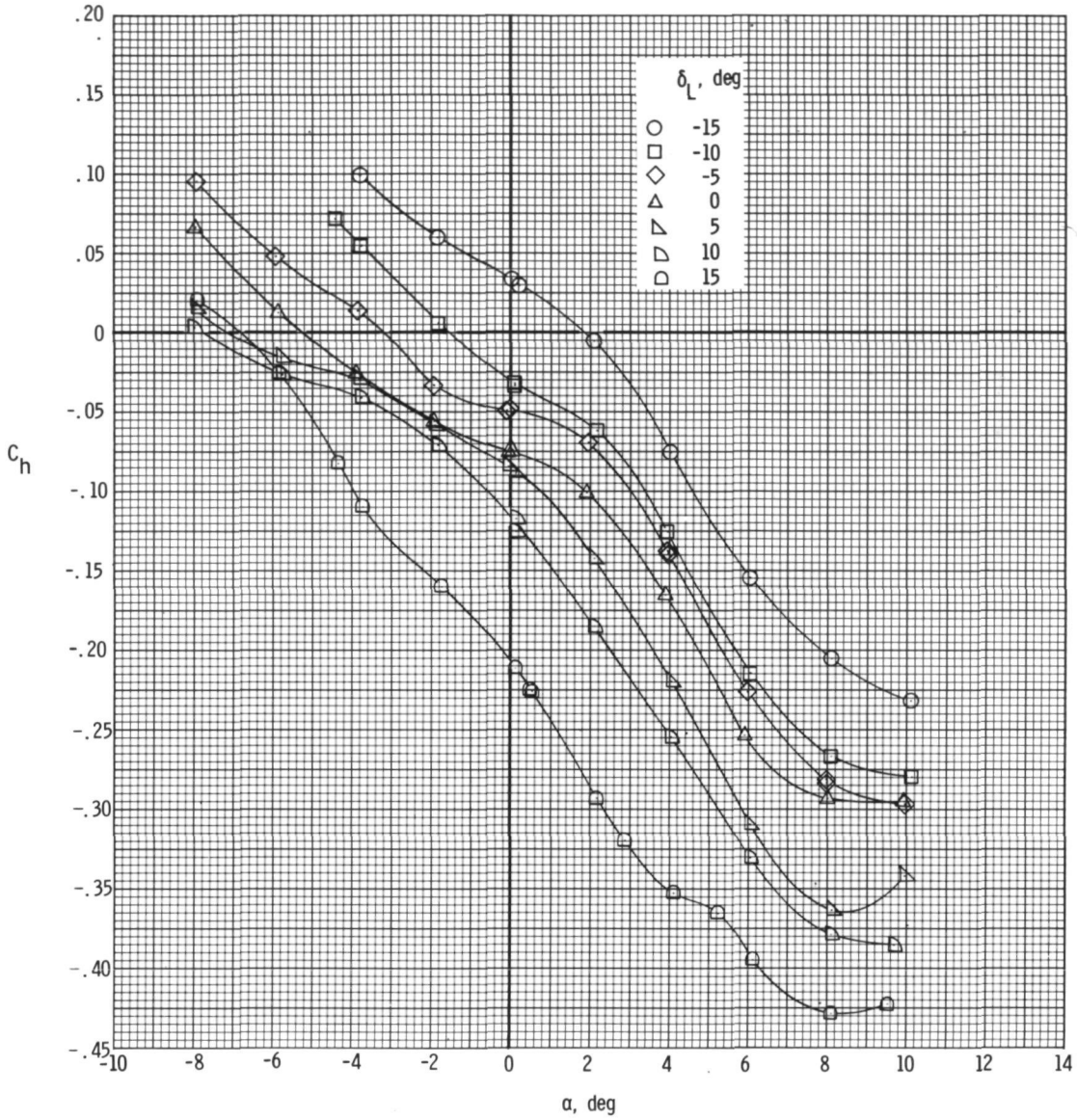

(e) M = 1.20.

Figure 29.- Continued.

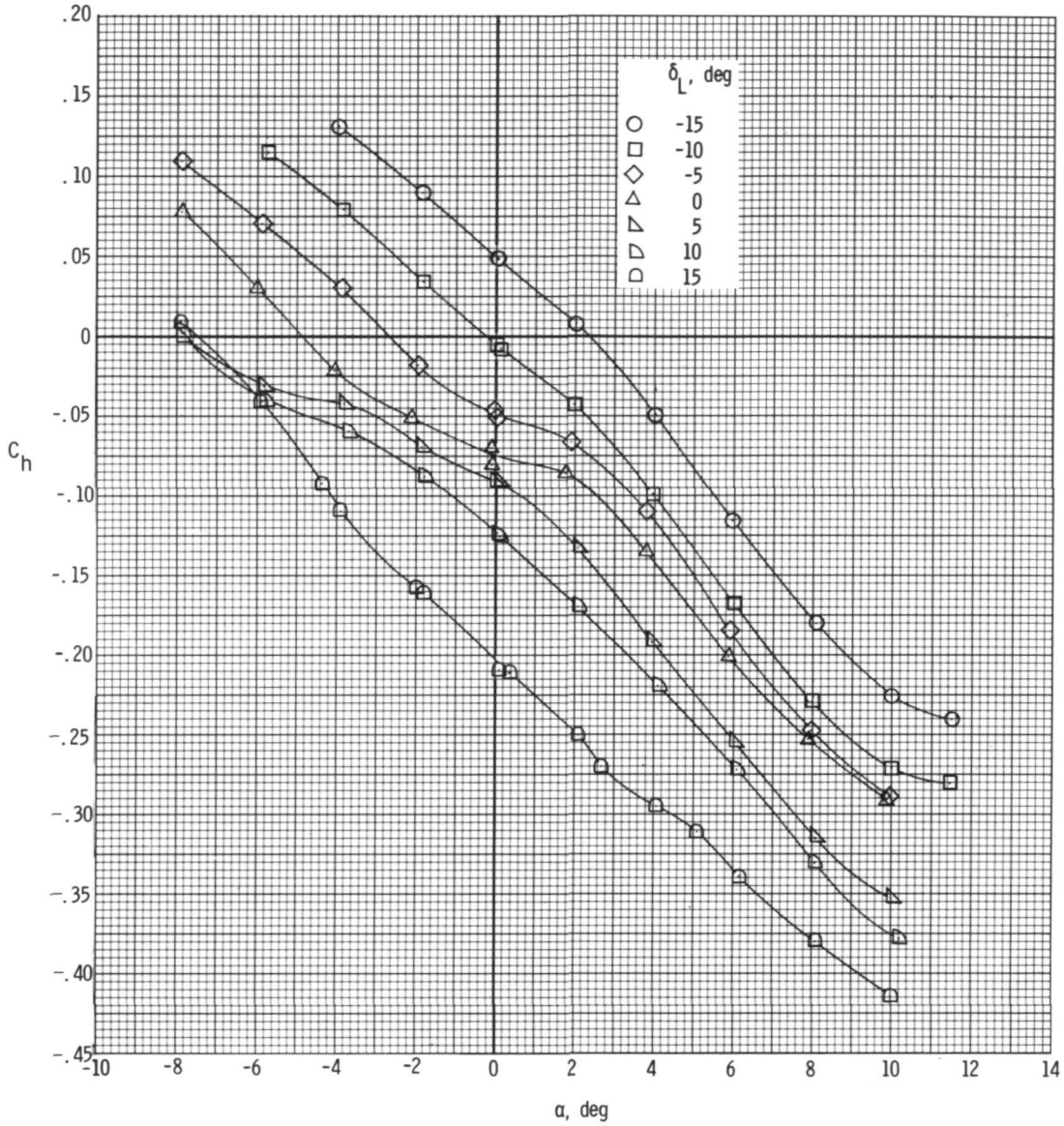

(f) M = 1.30.

Figure 29.- Concluded.

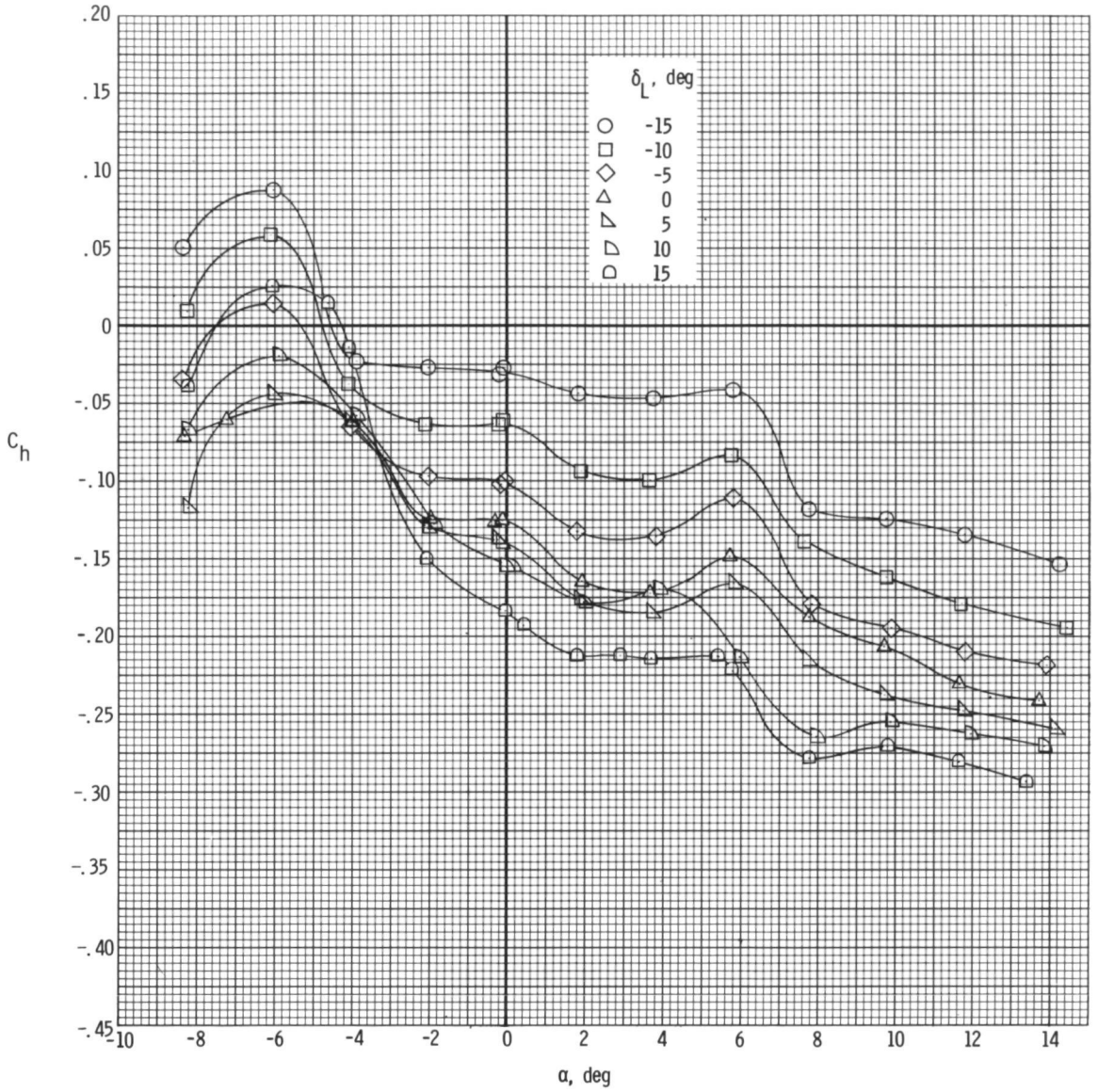

(a) M = 0.90.

Figure 30.- Variation of outboard aileron segment hinge-moment coefficient with model angle of attack.

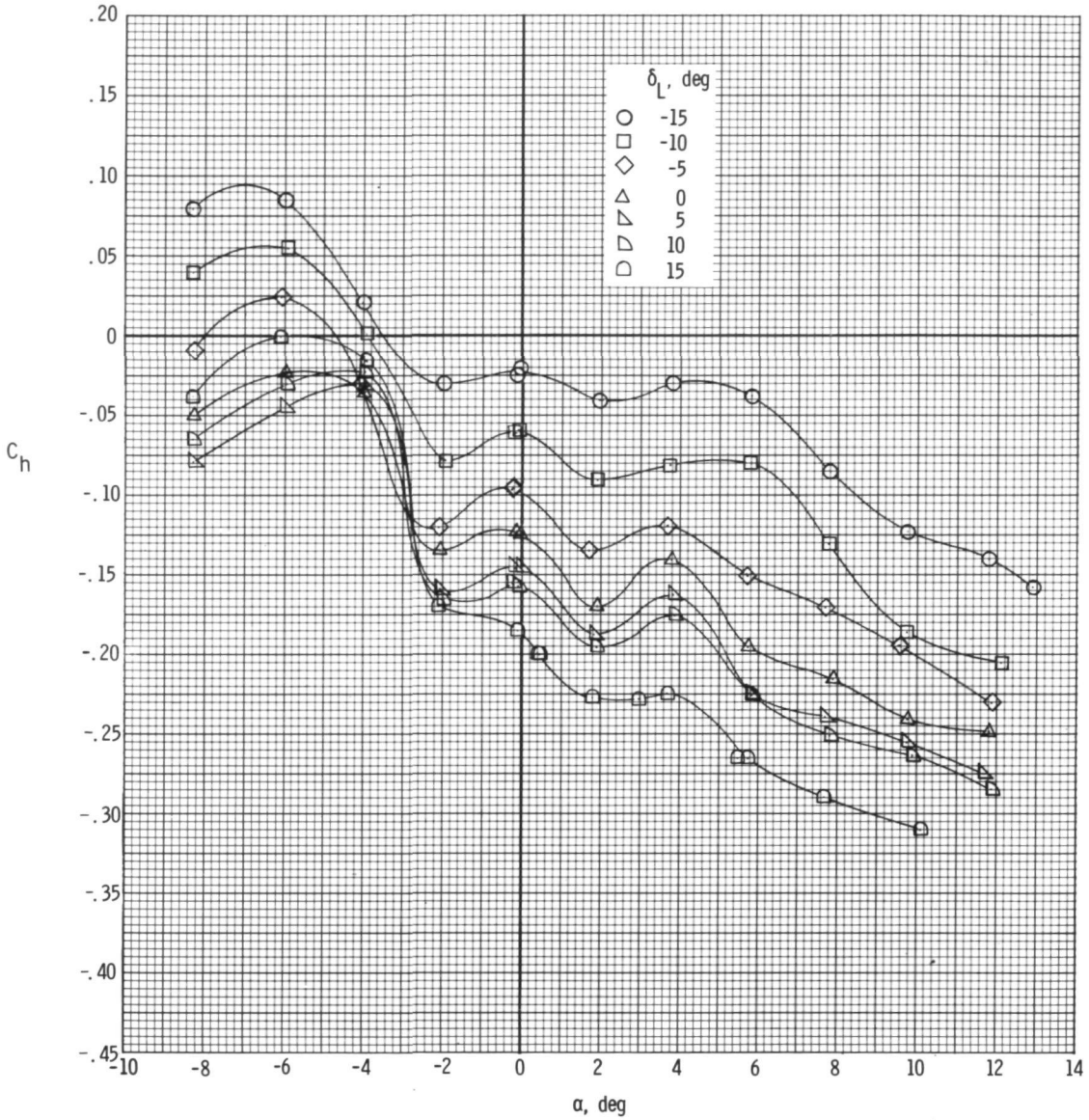

(b) M = 0.95.

Figure 30.- Continued.

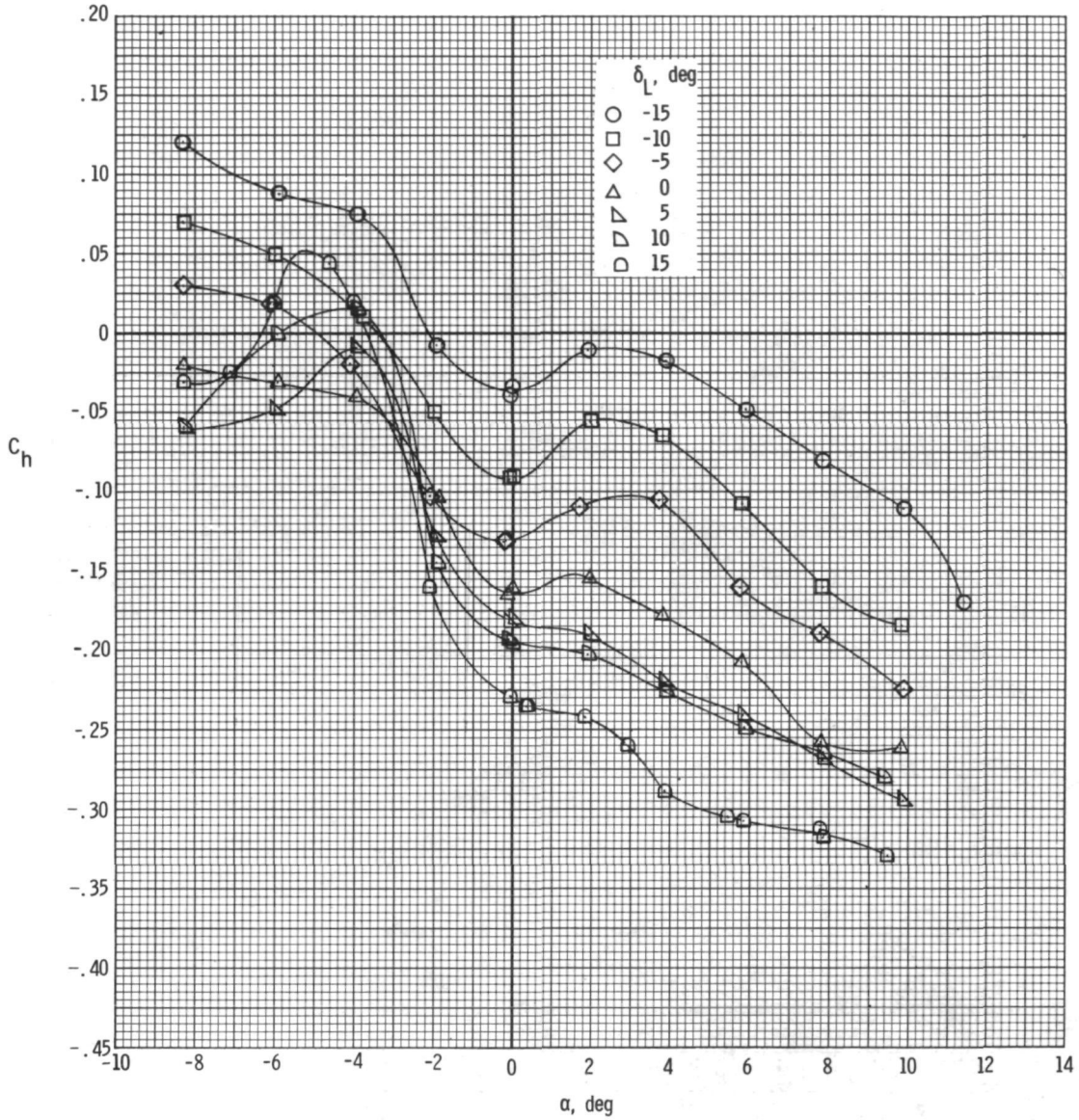

(c) M = 0.99.

Figure 30.- Continued.

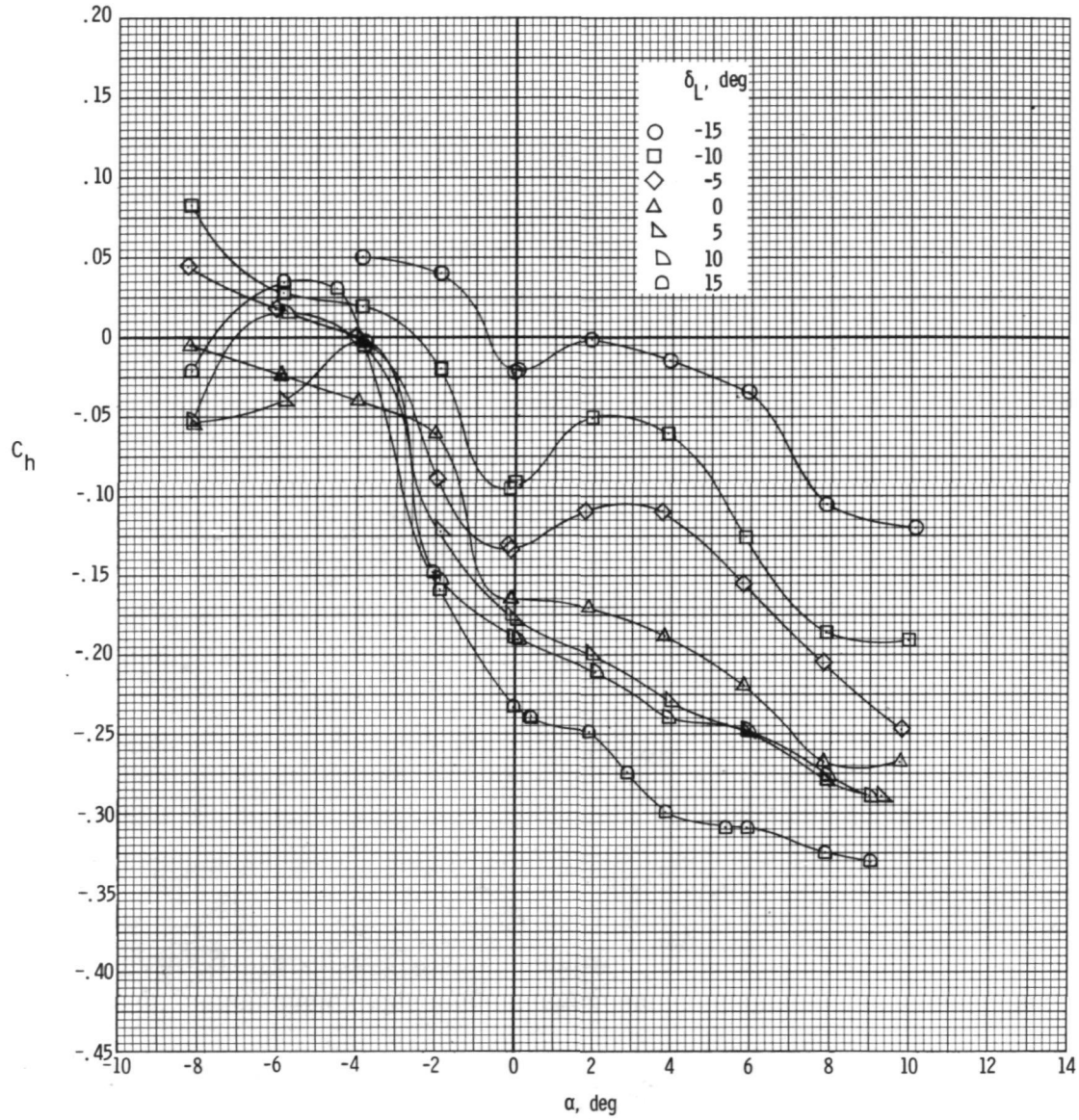

(d) M = 1.02.

Figure 30.- Continued.

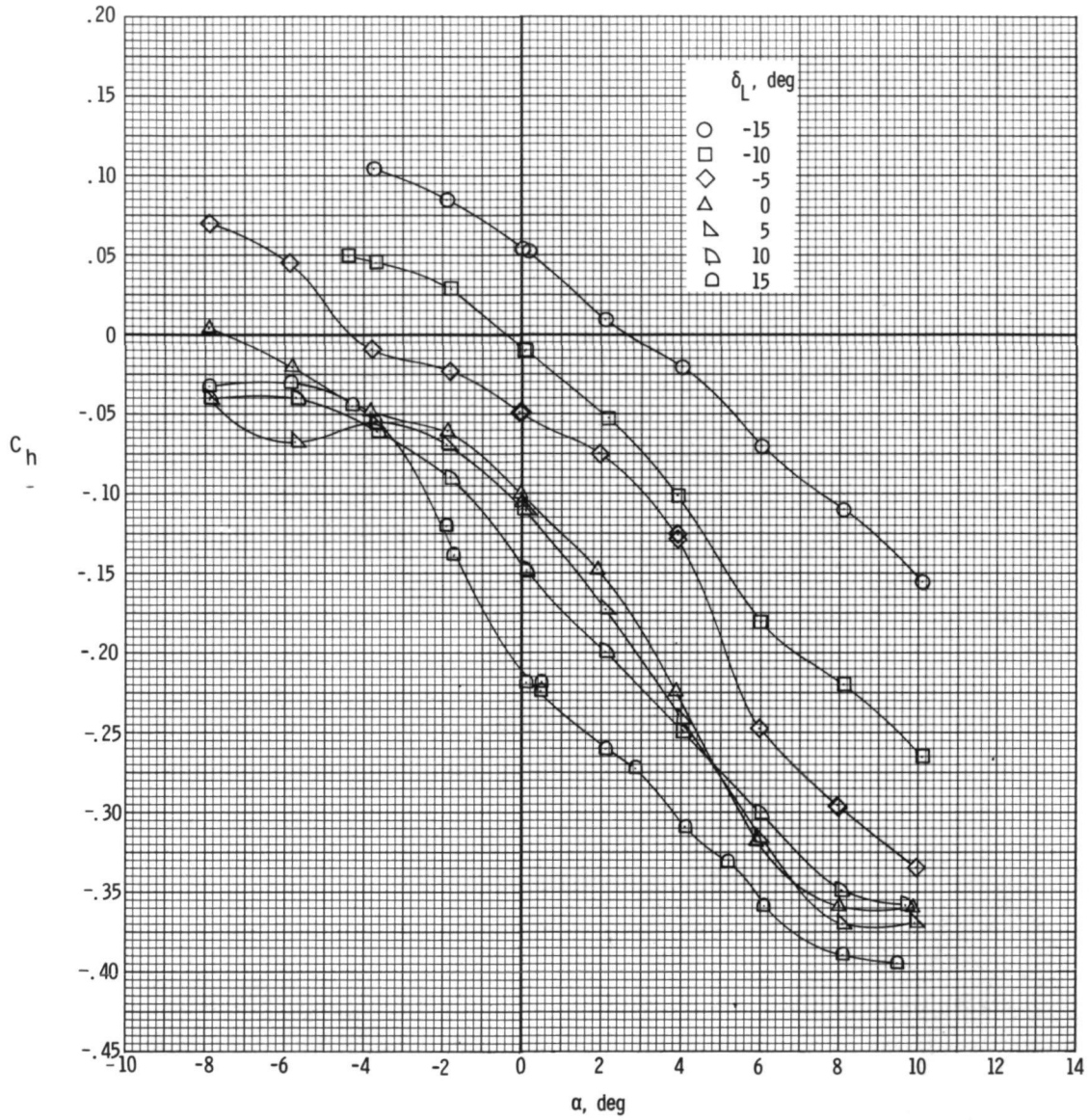

(e) M = 1.20.

Figure 30.- Continued.

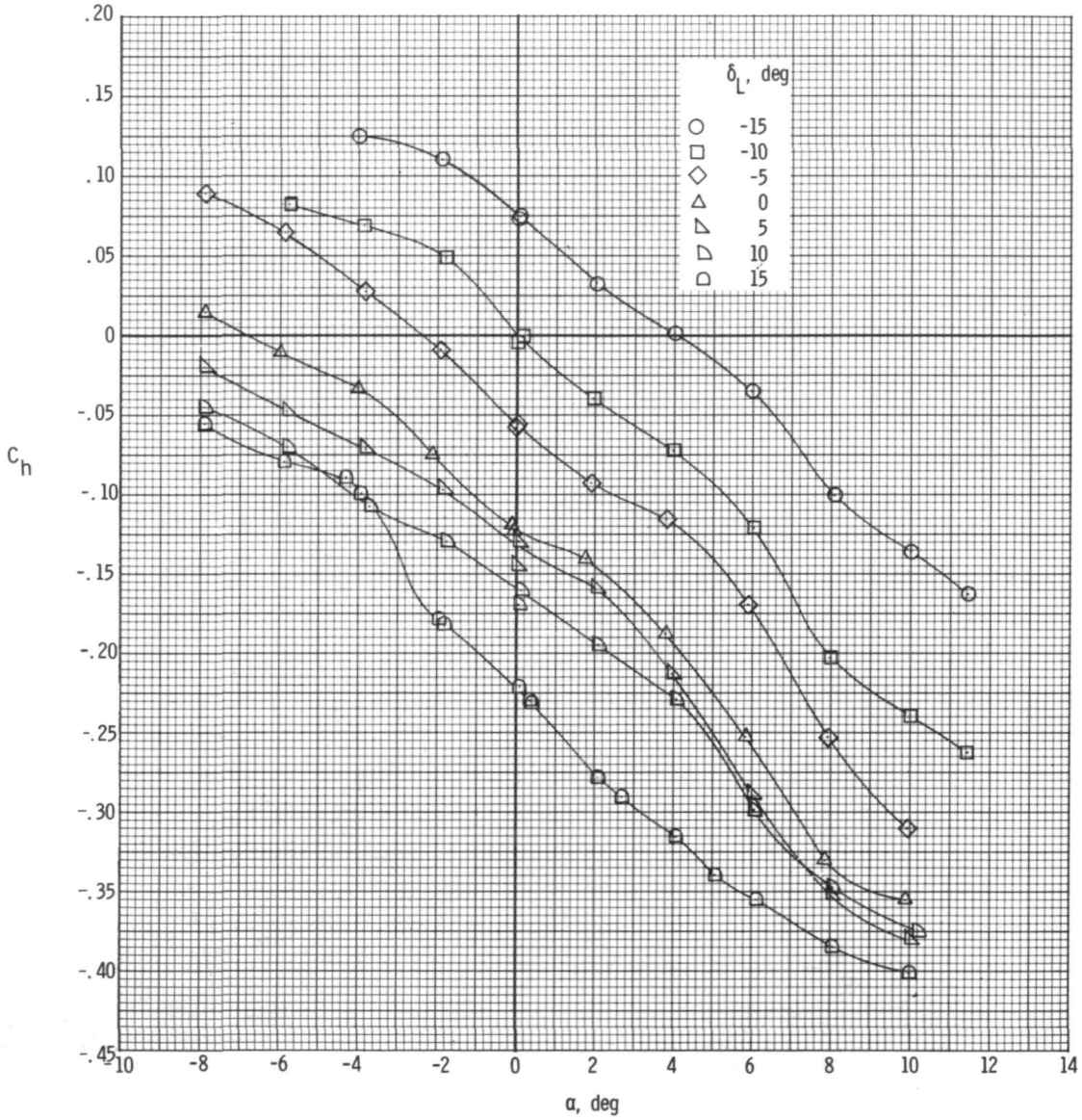

(f) M = 1.30.

Figure 30.- Concluded.

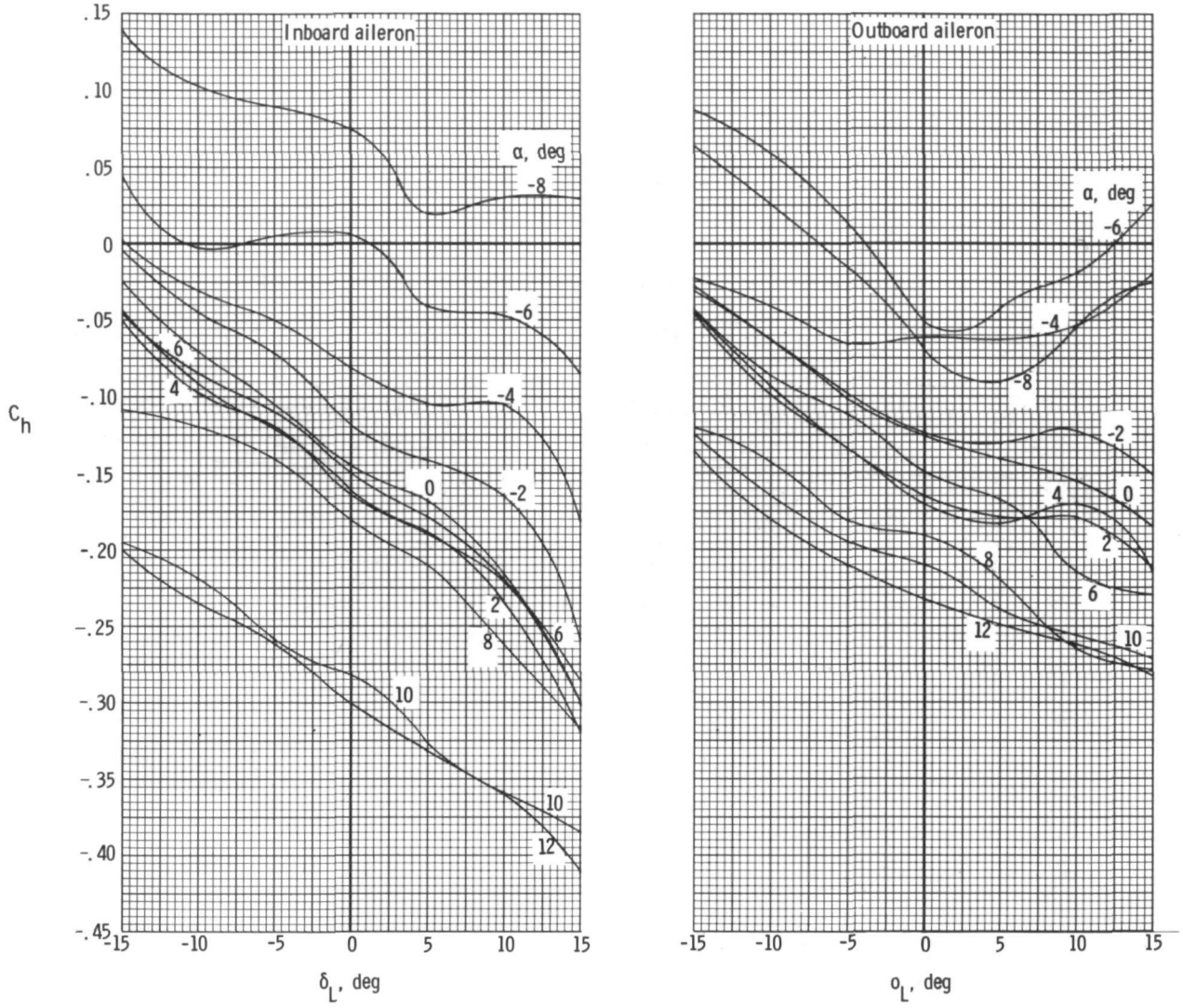

(a) M = 0.90.

Figure 31.- Variation of hinge-moment coefficient with aileron deflection angle for constant angles of attack.

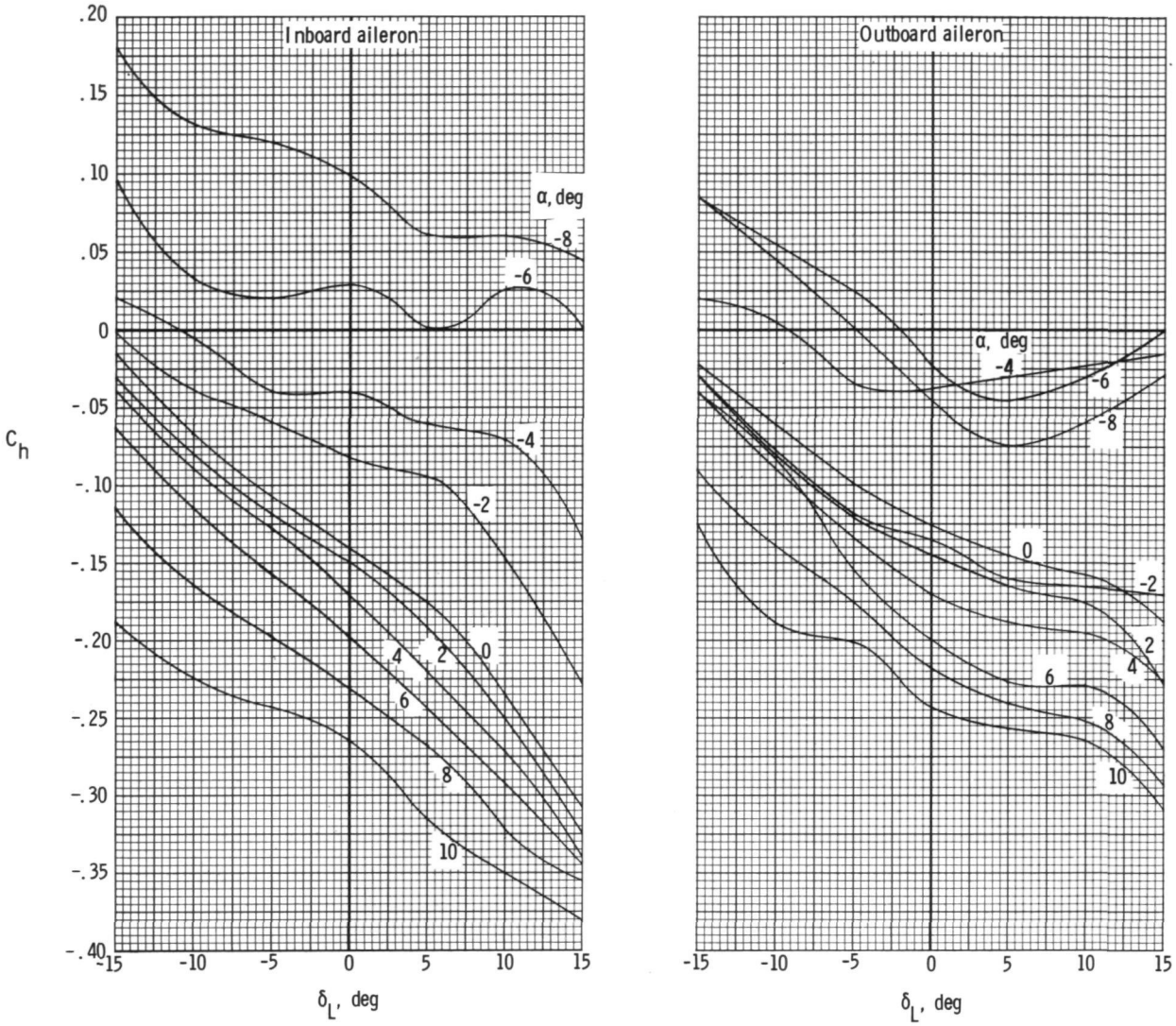

(b) M = 0.95.

Figure 31.- Continued.

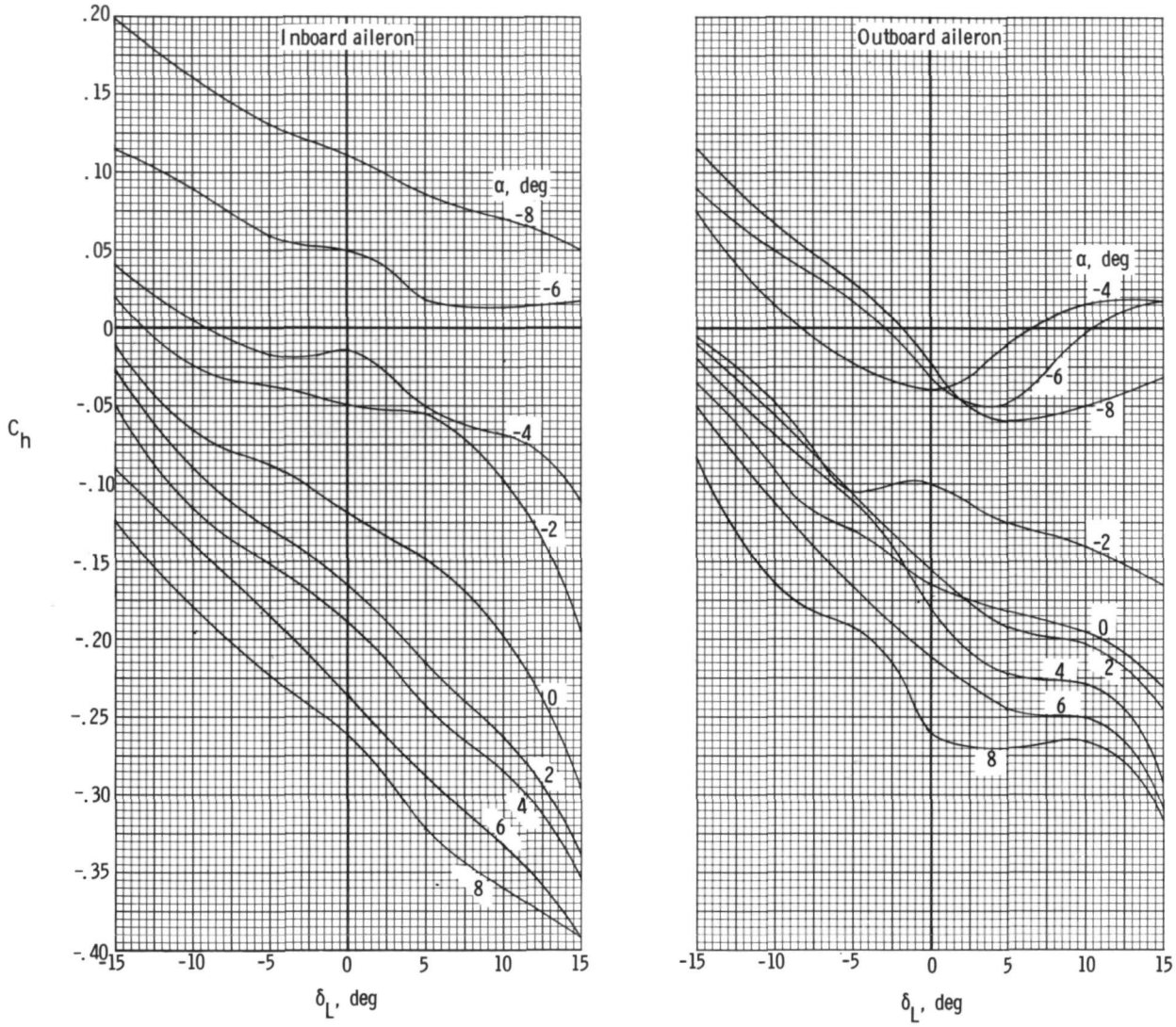

(c) M = 0.99.

Figure 31.- Continued.

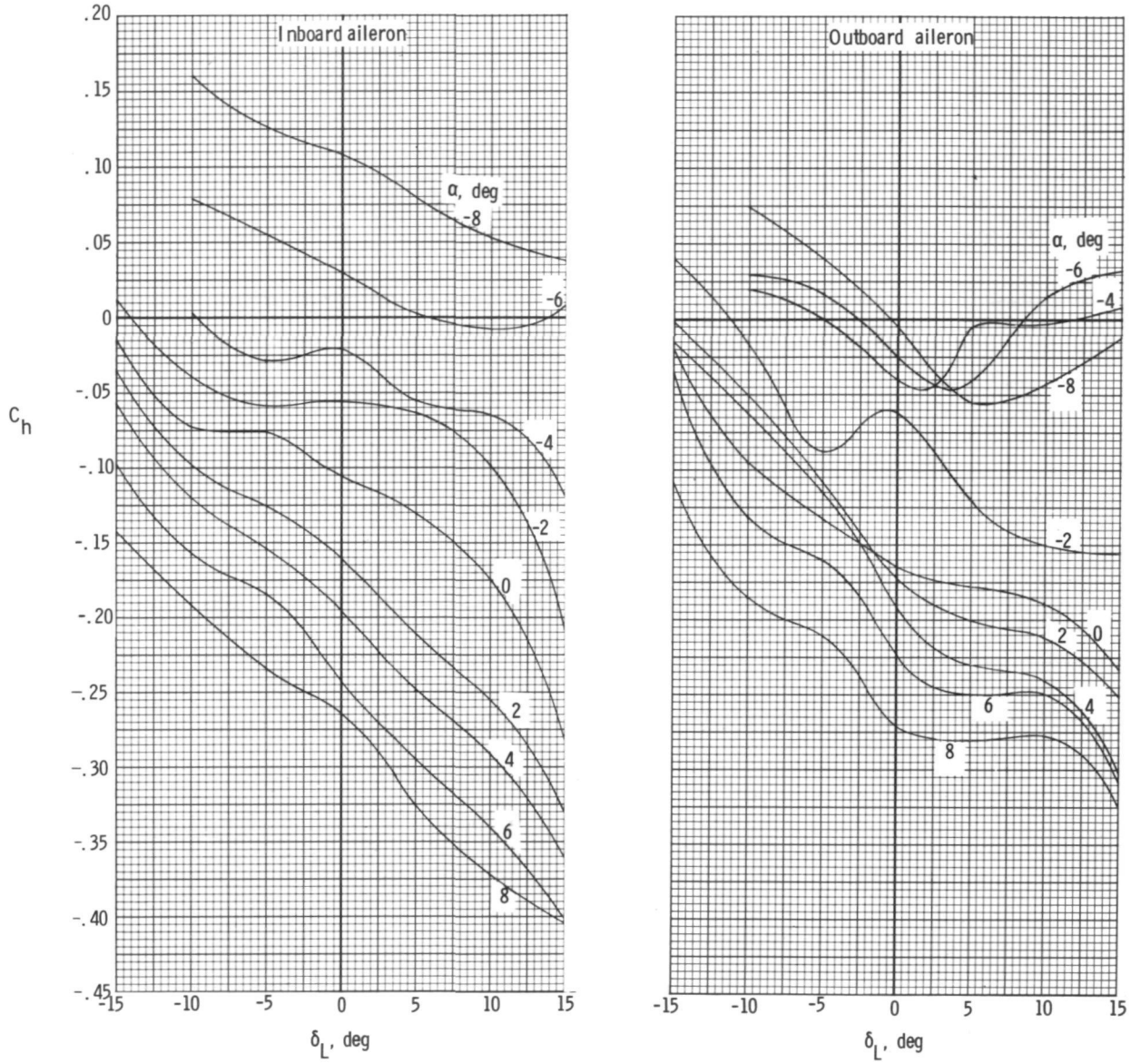

(d) M = 1.02.

Figure 31.- Continued.

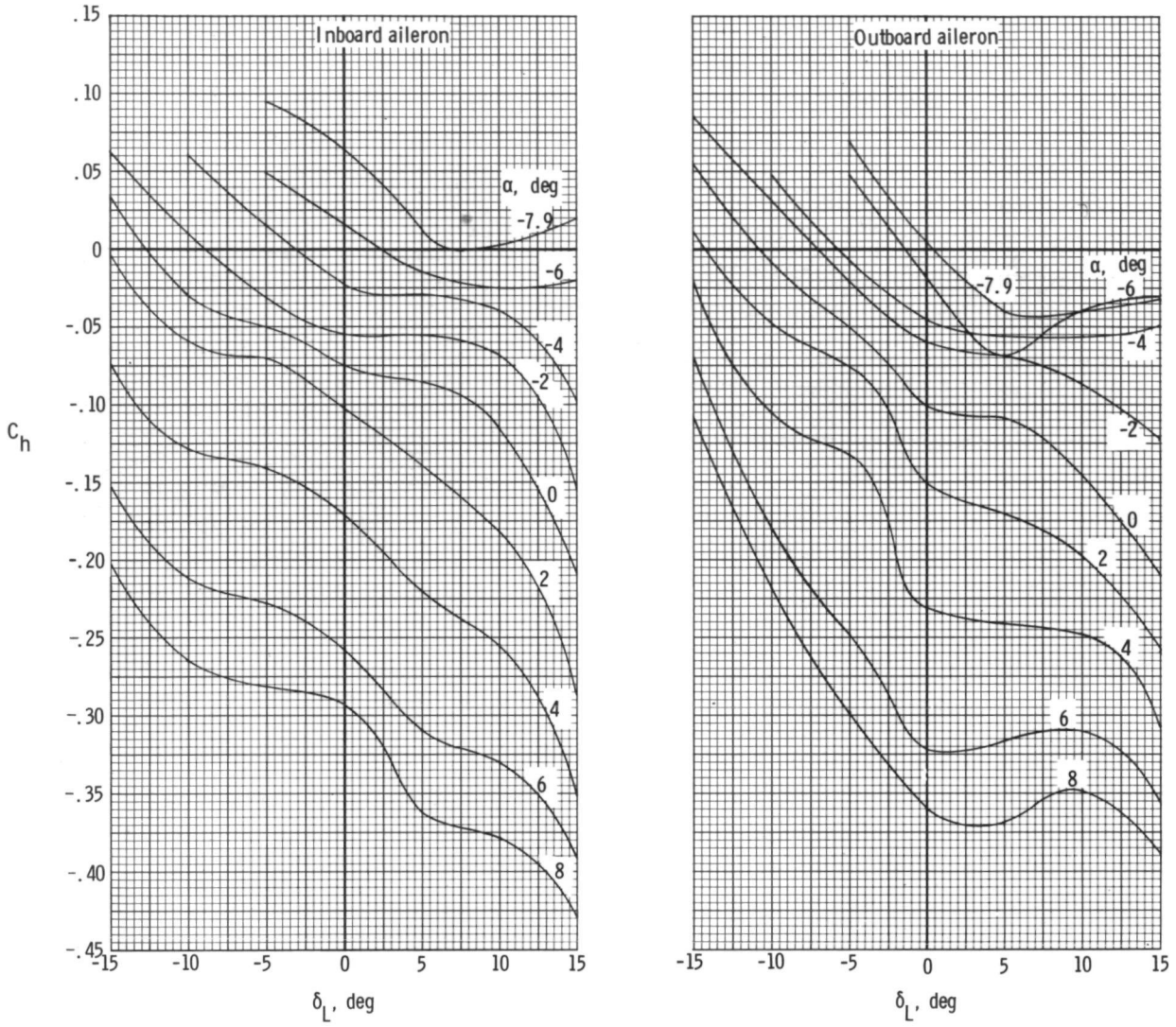

(e) M = 1.20.

Figure 31.- Continued.

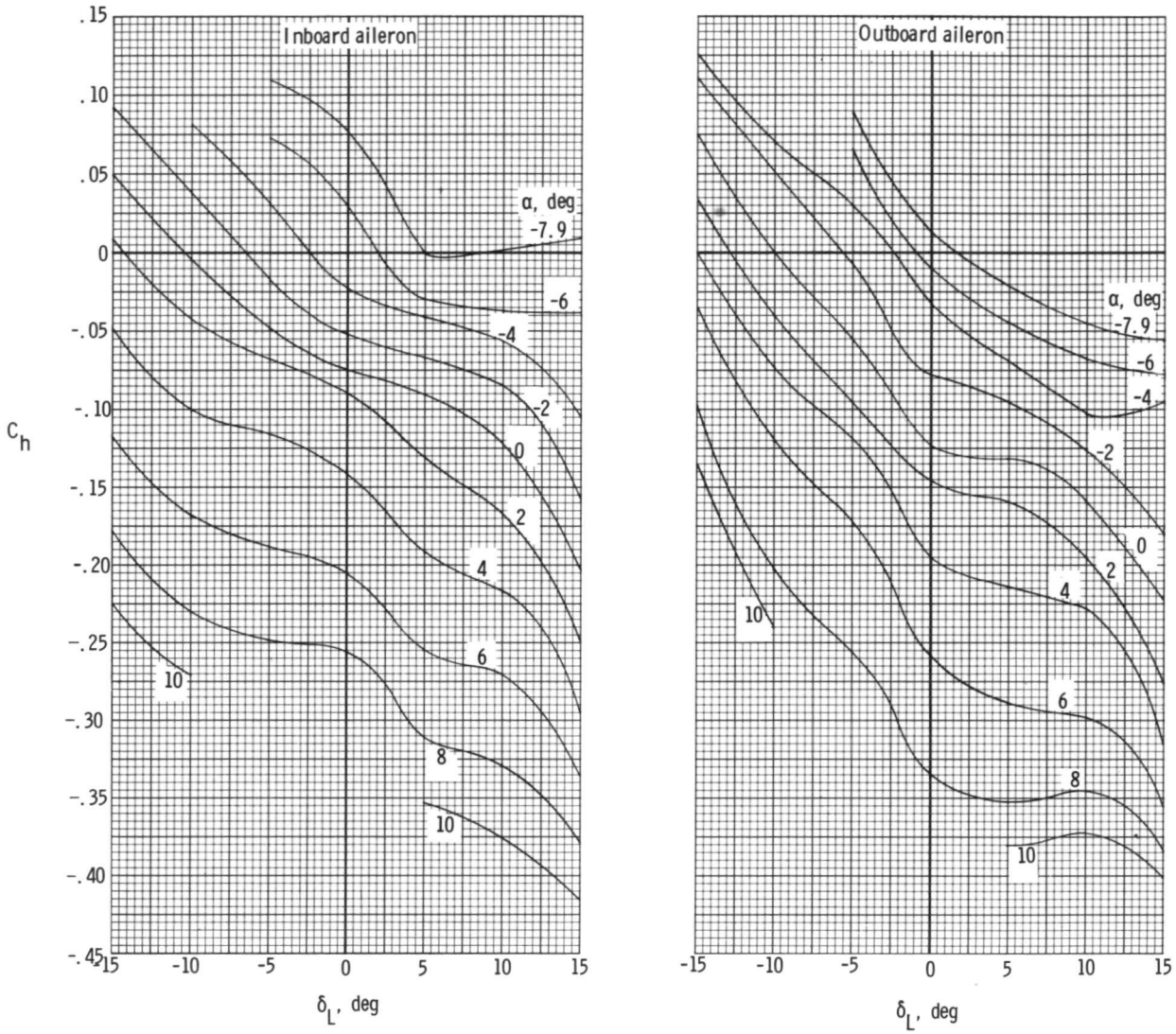

(f) M = 1.30.

Figure 31.- Concluded.

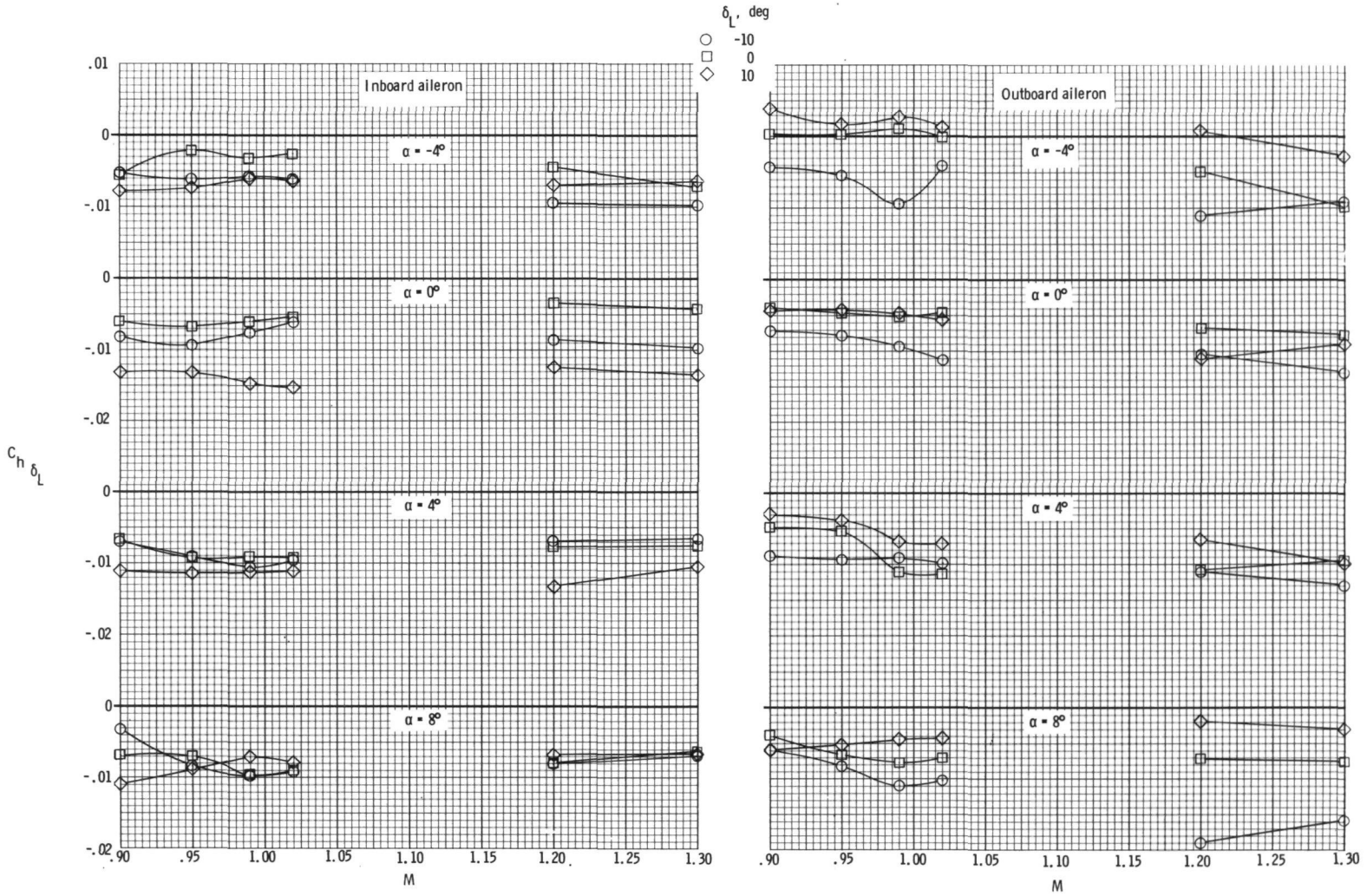

Figure 32.- Variation with Mach number of $C_{h_{\delta_L}}$ at constant angles of attack.

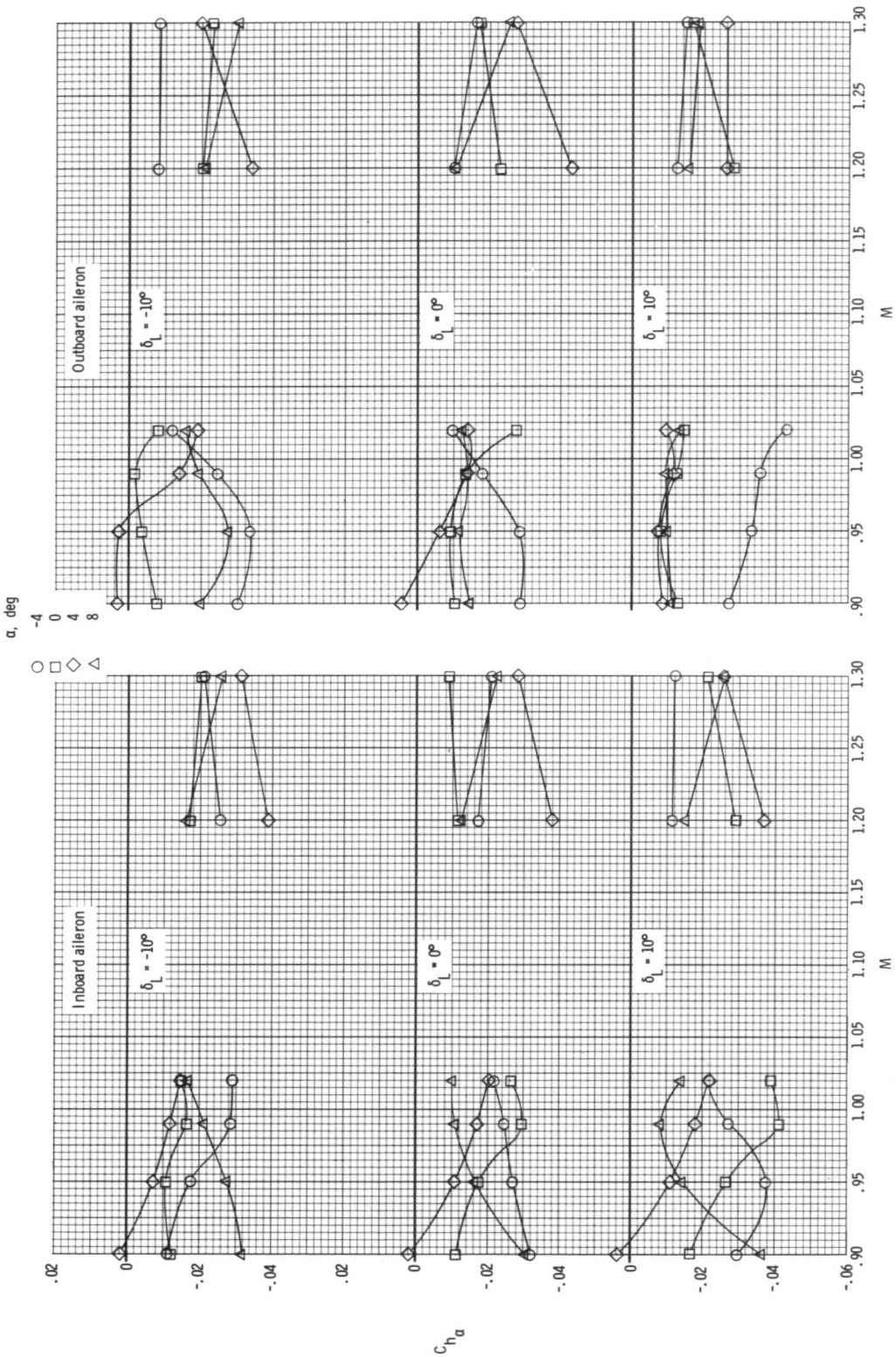

Figure 33.- Variation with Mach number of C_{h_α} at three aileron deflection angles.

"The aeronautical and space activities of the United States shall be conducted so as to contribute . . . to the expansion of human knowledge of phenomena in the atmosphere and space. The Administration shall provide for the widest practicable and appropriate dissemination of information concerning its activities and the results thereof."

—National Aeronautics and Space Act of 1958

NASA SCIENTIFIC AND TECHNICAL PUBLICATIONS

TECHNICAL REPORTS: Scientific and technical information considered important, complete, and a lasting contribution to existing knowledge.

TECHNICAL NOTES: Information less broad in scope but nevertheless of importance as a contribution to existing knowledge.

TECHNICAL MEMORANDUMS: Information receiving limited distribution because of preliminary data, security classification, or other reasons.

CONTRACTOR REPORTS: Scientific and technical information generated under a NASA contract or grant and considered an important contribution to existing knowledge.

TECHNICAL TRANSLATIONS: Information published in a foreign language considered to merit NASA distribution in English.

SPECIAL PUBLICATIONS: Information derived from or of value to NASA activities. Publications include conference proceedings, monographs, data compilations, handbooks, sourcebooks, and special bibliographies.

TECHNOLOGY UTILIZATION PUBLICATIONS: Information on technology used by NASA that may be of particular interest in commercial and other non-aerospace applications. Publications include Tech Briefs, Technology Utilization Reports, and Technology Surveys.

Details on the availability of these publications may be obtained from:

SCIENTIFIC AND TECHNICAL INFORMATION OFFICE

NATIONAL AERONAUTICS AND SPACE ADMINISTRATION

Washington, D.C. 20546